Field investigation and performance-based seismic design of rocking shallow foundations in cohesive soil

by

Keshab Sharma

A thesis in partial fulfillment of the requirements for the degree of

Doctor of Philosophy
in
Geotechnical Engineering

Department of Civil and Environmental Engineering
University of Alberta

Abstract

This research investigated the use of rocking shallow foundations in improving the seismic performance of soil-footing-structure systems. A series of lateral loading tests of large-scale rocking foundation systems in natural cohesive soil were conducted and a performance-based seismic design guide was developed with design examples.

A soil-footing-structure rocking system was fabricated for the present research. Two types of field tests of rocking foundations were performed in a cohesive soil in Edmonton, Canada: firstly by a quick release (snap-back) method and secondly by applying lateral cyclic loading. The loading direction, depth of embedment, and initial static factor of safety were systematically varied. The system consisted of a 1.5 m by 1.0 m concrete footing, steel column, and deck to simulate a prototype bridge system. The footing was intensively instrumented with strain gauges.

The first part of the field tests characterized the dynamic behaviour of the rocking system using snap-back tests. In total, 27 snap-back tests were conducted, where a variety of initial drift ratios were applied with a maximum value of 8.5%. The damping ratio observed during the oscillations after snap-back release of the shallow foundations ranged from 8 to 30%. Average measured period of the rocking system was elongated by approximately 235% comparing with the period of fixed-base structure. The rocking system on clay exhibited a good recentering ability, which is even better than on sand.

The second part of the field tests consisted of slow cyclic loadings along the axis of the footing at various drift ratios up to 7%. Twenty-four tests were conducted for foundations with varying initial factors of safety against the bearing failure, loading directions, rotation amplitudes, and embedment. Rocking foundations had the re-centering ability that resulted in less residual

rotations and showed non-degrading moment capacity. Rocking foundations were a good energy dissipater. The rocking-induced settlement increased with the cumulative footing rotation and decreased with the factor of safety for vertical bearing capacity. Footing's mechanical response was quantified from strain gauge readings. The footing remained elastic in tension, which then confirmed that the footing body may perform well in cyclic motion. The transient soil-footing contact areas were estimated with strain gauges and they agreed very well with the measured or calculated contact areas.

The third part of the field tests characterised the effects of lateral loading obliquity on the performance of rocking foundations. The rocking system was subjected to loading at an angle of 45° with respect to the footing axes. A method of estimating the rocking moment capacity of footing subjected to oblique loading was developed and validated by the present tests. Natural periods, damping ratio, re-centering ratio, settlement, and stiffness degradation during the tests were discussed and compared with the results from previous studies with orthogonal loading.

Lastly, a performance-based seismic design (PBSD) guide was proposed for the design of rocking shallow foundations. The empirical equations of normalized secant stiffness and damping ratio developed from present field tests were used as input to the PBSD guide. Additionally, rocking-induced settlement and residual drift were checked as performance indicators. An ordinary bridge composed of a column and a nonlinear rocking foundation was considered as an example and then the PBSD was applied to redesign the shallow foundation. Step-by-step design procedure was elaborated with two design examples assumed to be located in British Columbia and California. The design examples showed the feasibility of the PBSD method.

This Thesis Is Dedicated to

My Great Mother

Late Padma Sharma

Acknowledgment

I would like to extend my sincere gratitude to Dr. Lijun Deng for his wise and patient guidance, encouragement and assistance throughout my PhD study. I thank him for his seemingly infinite patience and care and for always being there when I needed him the most. He always provided me unflinching encouragement and support in various ways. He not only guides his students for their research but also take the students as his family members. I am thankful to Dr. Carlos Cruz Noguez for his feedback and comments during this study.

I truly appreciate the financial support of Natural Sciences and Engineering Research Council of Canada- Industrial Postgraduate Scholarship with the contribution from Almita Piling Inc. I would like to thank the technical support of Raymond Lee of Lafarge Canada Inc. (Edmonton) and Mobil Augers Research Ltd. Special thanks go to Benoit Trudeau and Dennis Lechot of Workonthat Structures for the assistance in performing the field tests. I am indebted to Yu Wei and Wenbo Zhang for helping with the instrumentation and laboratory tests.

I would like to thank Moira Guo for her kind help to set up the instrumentation for my research. I am also grateful for the immense support of a number of people in the department. Special thanks go to Weidong Li, Abel Sanchez Juncal, and Khagendra Belbase for there their companionship throughout the study. I would like to thank Ramesh Thapa and Mohan Acharya for their mentorship in Canada. You are very kind and cooperative.

I cannot finish without highlighting the never-ending support from my family who were always beside me in pursuing my unending education. I would to remind my grandfather and grandmother who taught me Nepali alphabet in candle light. This work is dedicated to my mother whose hard work in supporting my education encouraged me to accomplish this goal and gave me the strength I needed throughout my work. I am very grateful to my father who never

Table of Contents

List of Tables

List of Figures

1. Introduction

1.1   Background

Shallow foundation is commonly used to support building and short- to medium-span bridge structures worldwide. Even for long-span bridges in seismic zones, shallow foundations have been used where deep foundations are unfavorable due to various construction and economic factors. For an example, 2,252 m long Rion−Antirrion cable−stayed bridge in Greece was constructed with shallow foundation (Pecker 2003). The provisions of the shallow foundation have been adopted in the building and bridge codes of several countries (FHWA 2002; CFEM 2006; AASHTO 2011; CSA 2014). NCHRP (2010) reported that 17% of bridges in 39 states in the USA are supported by shallow foundations, including 30% in Washington and 25% in Nevada. Moreover, 6% and 3.75% of bridges that have shallow foundation are supported by clay in Washington and Nevada respectively. Siddiquee and Alam (2017) reported that shallow foundation comprised of 36.4% and 40.3% of single and flared column bridge system respectively in BC, Canada. Shallow foundation is also used in highly seismic countries such as Japan and New Zealand (Shirato et al. 2012; Pecker and Pender 2000).

In earthquake – prone zones, rocking shallow foundations have been observed to be a good mechanism of base isolation and energy dissipation during strong seismic events. After reviewing the past research and post-earthquake investigation, to fulfill the existing requirement for the ductile component, a rocking shallow foundation may have the following benefits:

1. Rocking foundation reduces the damage and prevents the structure from complete collapse.

2. The moments, shear forces and accelerations are significantly reduced in the superstructure when compared to a conventional structure fixed at the base.

3. Moment capacity of a rocking foundation is non-degrading, unlike conventional concrete components.

4. Bearing pressures increase during rocking and uplift lead to plastic deformation of soil around the footing, which is a source of hysteretic damping.

5. A footing designed for rocking significantly reduces the cost for footing.

Researchers have been conducting rocking foundation investigation using geotechnical centrifuge modeling and shake-table tests of small-scale models primarily in sand. Despite the progress, there is a lack of research in the field tests of rocking foundations and in the performance of rocking foundations in clay. In addition, the response of shallow foundation subjected to near-fault ground motion is poorly understood.

1.2 Problem statement and Objectives

The literature has suggested the benefits of rocking foundation. Most of present building and bridge design codes worldwide have added the provisions of soil nonlinearity i.e. rocking foundations. However, there are still a few important hurdles to full acceptance of rocking shallow foundations as a primary component of base isolation and energy dissipation. Following research gaps may be identified throughout the literature review:

1. Performance of rocking foundations from large-scale field testing is very limited.

2. Mechanical response of footing during rocking is not studied.

3. Performance of rocking foundations subject to skewed loads is not available.

4. A lack of simple and practical guideline for designing rocking shallow foundation.

The application of newly-developed seismic energy dissipaters such as base isolator, viscous dampers, and friction dampers is not affordable in many places of the world. The rocking shallow foundation could be developed as natural "fuse" limiting seismic load to the superstructure, allowing soil to yield under a shallow foundation and mobilization of the moment capacity of the footing. The engineering community has been continuously suggesting that quality experimental data should be obtained through field tests and simplified design guidelines based on field tests data should be developed. The general goal of the proposed research were to investigate the performance of rocking shallow foundations by carrying out field testing of large-scale systems on a natural soil deposit and develop a design guide based on field tests data. To achieve this goal, the specific objectives of the research are as follows:

1. Investigate the dynamic characteristics of the soil-foundation-structure system through the snap-back tests

2. Further understanding of soil-foundation interaction during rocking

3. Investigate the effects of static vertical factor of safety (FSv) on performance

4. Characterize settlement (or uplift), energy dissipation, stiffness degradation, and damping

5. Investigate the response of foundation subjected to skewed loads

6. Characterise the mechanical response of the footing during rocking

7. Investigate the change in soil properties due to rocking

8. Develop a performance-based seismic design guide for rocking shallow foundation using field test results

1.3   Research Methodology

1.3.1   Field Test

The test site is located at the University of Alberta farm located in central Edmonton, Alberta. The surficial deposits are glaciolacustrine sediments as a part of the glacial lake Edmonton deposits formed approximately 10,000 years ago. Though some site investigation reports of this site are available, detailed geotechnical investigation were performed to determine soil properties pre- and post-rocking. Site investigation consisted of Cone Penetration Tests prior to tests, Shelby tube sampling before and after field tests, and laboratory testing of undisturbed soil samples. Laboratory test program consisted of unconfined compressive strength (UCS), direct shear tests at a variety of normal stresses, Atterberg limits, and particle size analysis.

1.3.1.1   Cyclic Loading Test

Previous research has been predominantly focused on the performance of model foundations in sandy soils (Hakhamaneshi 2014; Sharma and Deng 2018). There are only few studies of rocking foundations embedded in cohesive soils including centrifuge testing (Algie 2011; Phipps et al. 2012; Hakhamaneshi 2014). However, these tests did not characterize the soil-footing behaviour such as stiffness degradation, damping, re-centering ratio, or residual settlement. A comprehensive characterization of rocking foundations in cohesive soils, particularly using field tests, and an investigation of footing and underlying soil response are imperatively needed. Because it is difficult to conduct dynamic loading tests in the field, an alternative is to use slow cyclic (i.e., quasi-static) loading (Gajan et al. 2005; Sharma and Deng 2018). Slow cyclic loadings for the performance assessment of structures are also recommended by ATC-24 (ATC 1992), FEMA-461 (FEMA 2007) and CSA (2014).

Two series of cyclic loading tests were carried out: orthogonal (i.e. aligned) and oblique cyclic loading test. In orthogonal tests, the cyclic loading was applied along the axial directions of rectangular footings whereas cyclic loading was applied at an angle of 45° with respect to the footing axes for oblique loading test. The previous research predominantly focused on the performance of rocking foundations subjected to orthogonal loading. However the seismic loading could be applied along any arbitrary lateral direction (i.e. oblique loads). The oblique loading results in biaxial moments and two-way eccentricity and rotation, which may complicate the performance evaluation. There is no prediction method for determining the moment capacity of obliquely loaded foundations. In addition, the plane of rotation, shape of footing contact area, and other performance indices are still poorly understood. Thus, a field test study of rocking foundations subjected to oblique loading is needed.

The rocking foundation system consisted of a rectangular reinforced-concrete (RC) spread footing, a steel tubular column, and RC slabs used as the superstructure weight. The system was adapted from a highway overpass bridge. In order to focus more on the specific research objectives without the complexities of comprehensive system behaviour (such as a bridge with multiple spans), an idealized single column bridge pier with deck mass supported by an isolated footing was considered in this research. The yield moment of the column was designed to be stronger than the rocking moment capacity of the footing and thus the rocking response would be mobilized. The rectangular footing stood on the ground surface or embedded in soil, representing an isolated footing supporting a structural assembly. Mounted to a strong reaction frame, a hydraulic jack exerts the lateral cyclic loading to the deck, analogous to the inertia force of the superstructure during earthquake shaking. Vertical factor of safety (FSv)

5

against the bearing failure, embedded depth of footing and loading direction were systematically varied during the field tests.

1.3.1.2   Snap-back Test

Previous studies (e.g. Algie 2011; Phips et al. 2012; Acikgoz et al. 2016; Salimath et al. 2017) showed that snap-back testing is an effective, simple approach to the soil-foundation-structure interaction (SFSI) research of systems subjected to pulse-like motions. Thus far, however, there has not been any comprehensive characterization of rocking foundation system using field snap-back tests. The objective of snap-back test is to investigate the nonlinear soil-footing interaction for rocking foundations and characterise the dynamic parameters of rocking systems, such as the equivalent stiffness, period elongation, and damping. The dynamic parameters of rocking system are needed for performance-based seismic design methodology.

The snap-back tests were conducted by pulling the structure over using chains attached to a quick release mechanism. As in cyclic tests, two series of snap-back tests were carried out: orthogonal and oblique. Chain with shackles was secured around the top of the deck on the north side of the structure and fastened to an excavator through a quick release mechanism. The excavator was used as an anchor point for the chains. At the desired rotation the device was released and the structure would rock in free vibration. An accelerometer was placed on the top of structure to measure the horizontal acceleration at the top of structure along the rocking direction.

1.3.2   Performance-based Seismic Design (PBSD)

The principle of rocking foundation has been adopted in the building and bridge codes of several countries (NZS 2004; FEMA 2005; NBCC 2010; AASHTO 2011; CSA 2014; EGBC 2018;

ASCE 2014). However, engineers are hesitant to use rocking foundations in design. This might be attributed to lack of specific design guidelines for rocking shallow foundation.

The provisions of PBSD have been accepted in several countries primarily limited to superstructures. In this regards, a simplified PBSD methodology for designing the rocking shallow foundation primarily for a simple bridge is proposed. This study develops empirical correlations to obtain the secant stiffness and hysteresis damping ratios of rocking foundations as an input to the proposed PBSD guide. The empirical equations of re-centering ratio and residual settlement obtained from field testing program of rocking foundation were adopted to check the performance in terms of residual drift and residual settlement.In this design procedure, a bridge system consisting of a rocking foundation, a damped elastic column, and a deck mass is integrated into a single-degree-of-freedom system for which the system damping and period are calculated. The PBSD methodology is further illustrated with two examples.

It is worthy to point out that rocking foundations can be adopted into multiple structural types, such as highway bridges, 1-story buildings, and multi-story buildings. The object of the present PBSD is ordinary highway overpass bridge for which the performance criteria are known.

1.4   Organization of Thesis

This thesis reports a portion of results in present studies. The thesis is outlined as follows:

Chapter 1: Background and scope of the research; organization of the thesis.

Chapter 2: Case histories of bridge and building damages in earthquakes; a literature review of the state-of-art research in rocking foundation; the role of rocking in current seismic design codes; a literature review of performance-based seismic design.

Chapter 3: Characterization of rocking shallow foundations on cohesive soil using field snap-back tests; effects of initial factor of safety against the bearing failure, initial drift amplitude, and snap-back directions on the dynamic properties of the rocking system are presented.

Chapter 4: Field testing of rocking foundations in cohesive soil: cyclic performance and footing mechanical response; moment capacity, damping, stiffness, settlement and re-centering capability etc. are quantified and compared to the published literature. Footing internal response during the rocking was characterised and presented.

Chapter 5: Effects of loading obliquity on field performance of rocking shallow foundations in cohesive soil; presents system performance indicators, such as moment capacity, damping, stiffness, settlement and re-centering capability of the system under oblique loading, and compares to the performance of footings subjected to orthogonal loading

Chapter 6: Performance-based seismic design (PBSD) for the rocking shallow foundations of ordinary bridges and presents a design procedure; uses an empirical relationship between the hysteresis damping vs. footing rotation, secant stiffness vs. footing rotation, and re-centering ratio vs. footing rotation developed using field test results; two design examples in details are presented.

Chapter 7: Summary and discussions; recommendations for future work.

2. Literature Review

This chapter provides an overview of the key research findings that are relevant to the proposed study. A literature review on the rocking shallow foundations is divided into three sections i.e. case studies, physical experiments, and numerical modeling, each section containing references relevant to its topic. In addition, a review of PBSD and application of rocking shallow foundation in practice is presented.

2.1   Case Studies

Many case studies from earthquakes showed that a number of structures resting on shallow foundation had escaped more severe damages by rocking on their footings. Many structures during 1952 Arvin-Tehachapi (California) earthquake (Housner 1956), 1960 Chili earthquake (Housner 1963), 1977 Tongan earthquake (Campbell et al. 1977), 1989 Loma Prieta earthquake (Elghazouli 2009), 1993 Hokkaido Nansei-Oki and 1995 Kobe earthquake (NEHRP 2004), 1999 Kocaeli earthquake (Gazetas et al. 2003), and 2011 Christchurch (Storie et al. 2014) had escaped more serious damages by rocking on their shallow footing. A number of tall, slender structures with shallow foundation survived the earthquake whereas more so-called stable structures were severely damaged (Kariuki 2016; Sharma and Deng, 2019a). However, structures mentioned above were not designed intentionally to rock about their base.

Figure 2.1a shows a case from 1995 Kobe earthquake where reinforced-concrete columns of elevated expressway suffered severe flexural damage due to formation of plastic hinge above the pile foundations. Figure 2.1a shows a good example of how a system with strong foundations and yielding columns can potentially fail when the demand on the columns exceed their capacity. The foundations were observed very intact and no sign of ground deformation or cracks were

noticed. Severe failures of elevated expressway as shown in Figure 2.1a shows the risk behind plastic hinging in the superstructure when the design earthquake is exceeded. However, Yashinsky and Karshenas (2003) observed interesting case rocking foundation at Pier 697 along the Route 3 of the elevated express way in Kobe. They reported that the foundation at Pier 697 was able to rock back and forth during the earthquake indicated by the disturbance to the surrounding soil as shown in Figure 2.2b, and there was no damage to the pier. They concluded that rocking foundation had protected the pier column by limiting the seismic forces to the pier.

Figure 2.1. (a) Elevated road collapsed due to plastic hinging in the superstructure and (b) undamaged Pier 697 on Route 3 as the shallow foundation rocked during the same earthquake (Yashinsky and Karshenas 2003).

Failure of the one-storey reinforced concrete building shown in Figure 2.2 occurred due to moderate excitation during 1999 indicates a very poor design for capacity. The foundation was very heavy as compared to the superstructure even though the soil was very stiff. The moment capacity of the footing was extremely high as compared to the yield moment capacity of column. The plastic hinge was formed at the end of column and brittle failure occurred immediately after the earthquake. The concept of rocking foundation is to avoid such a brittle failure and to reduce the cost of footing as well (Gazetas 2019).

Figure 2.2. Columns and foundations of the one-storey building collapsed during moderate earthquake, 1999 Athens earthquake (Gazetas 2019).
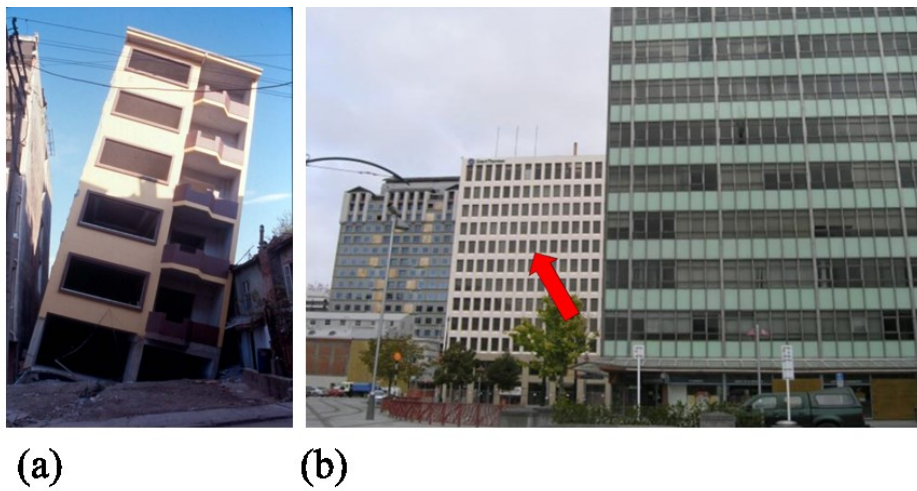
Figure 2.3. (a) Tilted buildings that suffered severe damages in shallow foundations but did not collapse during 1999 Kocaeli earthquake (source: Prof. R. W. Boulanger, UC Davis) and (b) building on a rocking foundation has excessive tilting in Christchurch (source: Prof. I. Towhata, University of Tokyo, Japan).

Figure 2.3a shows tilted buildings resting on shallow foundations that suffered bearing capacity failure in the 1999 Kocaeli earthquake. In spite of the yielding failure of soil beneath the

footing, the superstructures were able to sustain the seismic loads because of limited seismic force transmitted through the footing to the superstructure. Many multi-story buildings on shallow foundations in the city of Christchurch, New Zealand were found perform satisfactorily during the 2011 Christchurch earthquake as shown in Figure 2.3b (Storie et al. 2014, Kariuki 2016). There were a number of multi-story buildings on shallow foundations in the city of Christchurch, New Zealand that performed satisfactorily during the Christchurch Earthquake. Soil-foundation-structure interaction (SFSI) provides a possible explanation for the good performance of these buildings (Storie et al. 2014). Both buildings presented in Figure 2.3 highlight the safer failure mechanism when plastic hinging occurred in the soil beneath the footing. Recently, GEER (2017) also reported that a few buildings on rocking foundations suffered minor structural damage while fixed-based structures sustained severe damage during the M_w 7.1 Puebla-Mexico City earthquake in 2017.

2.2 Physical Test

2.2.1 Geotechnical Centrifuge Modeling Test

Ko et al. (2018a) conducted horizontal slow cyclic tests on an embedded shallow foundation model for three different slenderness ratios using centrifuge and studied the approximate distribution of soil reaction stress under the rocking foundation in sand, but the footing contact area was not derived from the measurement. They observed that contact area between the soil and foundation converges to the critical contact area, and the overturning moment converges to the non-degradable ultimate moment capacity of the foundation. Ko et al. (2018b) evaluated the cyclic and dynamic rocking behavior for embedded shallow foundation and observed that the moment vs. rotation behaviour of rocking foundation under slow cyclic and dynamic loads match fairly well.

Ilki and Fardis (2014), Kim et al (2015), and Liu et al (2012) conducted a series of centrifuge test to evaluate the seismic behavior of low-rise frame buildings, considering the yielding mechanisms of fuses and rocking shallow foundations. The foundation rocking dominated low rise building demonstrated its ability to protect the superstructure from seismic demands when compared to yielding mechanisms of fuses. Hakhamaneshi (2014) and Hakhamaneshi and Kutter (2016) investigated the effect of footing shape on the residual settlement and uplift, rocking stiffness, and re-centering. The moment vs. rotation behavior in these tests compare favorably to the proposed backbone curve in ASCE 41-13 guideline (ASCE 2014).
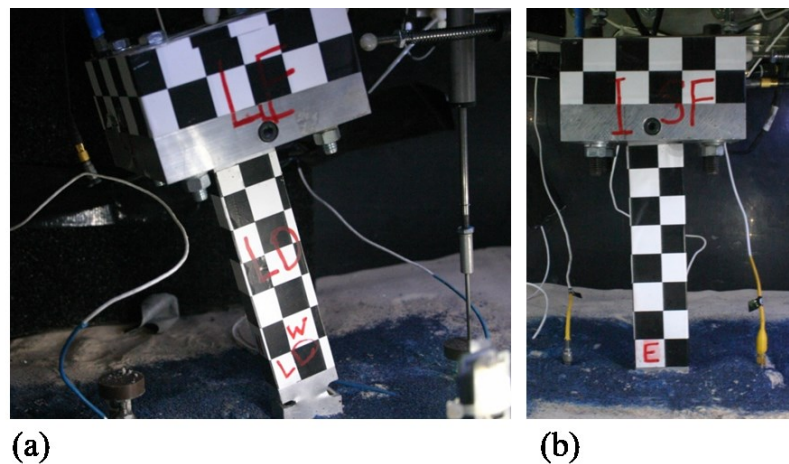
Figure 2.4. Centrifuge modeling (a) fixed base (hinging column) and (b) rocking foundation system (Deng et al. 2012a).

Researchers (Gajan et al. 2005, Kutter et al. 2006, Gajan and Kutter 2008, Deng et al. 2012a, Deng and Kutter 2012) have performed centrifuge testing on shallow rocking foundations in order to evaluate the dynamic response and energy dissipation of rocking foundations on soil. They found that rocking structures are less likely to tip over, even during major seismic events. They have shown that nonlinear soil-structure interaction effects can reduce residual rotations,

displacement demand on the structural components, and the collapse potential of structures. In general, they concluded that rocking systems are more stable and conventional methods are not appropriate for predicting their drift demands. Deng et al. (2012a) performed centrifuge experiments on two scaled-down bridge systems: Fixed base (hinging column) and rocking foundation system. Model with fixed base system sustained significant residual rotation and settlement as compared to rocking foundation as shown in Figure 2.4.

Gazetas and Apostolou (2004) and Loli et al. (2014) carried out a series of dynamic centrifuge tests on reduced scale models of a modern reinforced concrete (RC) bridge pier to investigate the rocking isolation. A variety of seismic ground motions were considered as excitations. They found that the rocking isolated pier has superior performance in comparison with the one designed conventionally. Seismic demand is reduced in terms of both inertial load and deck drift. They demonstrated that foundation uplifting has a self-centering potential, and soil yielding provides a particularly effective energy dissipation mechanism, exhibiting significant resistance to cumulative damage.

2.2.2 Shaking Table Test

Several series of shaking table tests have been performed on rocking shallow foundations sitting under column and shear wall with or without structural assembly. One of the first large-scale shaking table tests to investigate the rocking behaviour of shallow square footing (1 m^2) under lateral loading was conducted in the framework of TRISEE project (Negro et al. 2000, Faccioli et al. 2001). Paolucci et al. (2008) performed a series of large-scale shaking table and cyclic eccentric tests at Public Works Research Institute, Tsukuba, Japan. Maximum footing rotation was notably small (<3%). In all cases, the research showed that rocking isolation may increase

substantially the safety margins against collapse, even for the earthquake exceeding the design level.

Antonellis et al. (2014 a, b and 2015) conducted a series of shaking table test of a nearly full-scale bridge pier supported on 1.52-m^2 rocking shallow foundation. California Department of Transportation (Caltrans) funded this project to develop the guidelines for design of bridges supported on piers that rock on their foundations. The shaking table tests demonstrated the outstanding performance of highly under-designed rocking foundations against very strong seismic shaking with minimal residual drift ratios and settlement with no structural damage. The residual drift ratios were 0.1% and 0.3% under the design earthquake (DE) and maximum considered earthquake (MCE) level excitation.

Anastasopoulos et al. (2015) studied the seismic performance of an existing three-storey building, retrofitted through addition of shear walls by conducting a series of reduced scale shaking table tests. Despite the excellent performance of the rocking-isolated system, residual foundation rotations are not always negligible. Tsatsis and Anastasopoulos (2015) and Chiou et al. (2015) conducted shaking table tests on rocking dominated column-footing model to investigate the rocking effect on the dynamic behavior of a structure under seismic loading. They found that the rocking response of the footing could help to reduce the dynamic amplification effect of the model. Anastasopoulos et al. (2013) conducted a series of reduced-scale shaking table tests on a bridge pier to compare the performance of a rocking-isolated system to a pier foundation conventionally designed. A variety of shaking events, comprising real records and artificial motions of varying intensity were applied to both piers types to investigate the performance in successive earthquake events. It was found that rocking isolation is quite effective in reducing the inertia forces transmitted onto the superstructure. Due to soil

densification, the rate of settlement accumulation is found to decrease with repeating seismic excitations. Nevertheless, the rocking-isolated system survives overturning collapse, even when subjected to an earthquake that significantly exceeded the design earthquake.

2.2.3 Reduced-scale Laboratory Test

Bartlett (1976) and Weissing (1979) conducted 1g experiments by testing model footings (0.50m by 0.25m) subjected to slow cyclic and dynamic rocking on sand respectively. They found that significant energy dissipation and progressive settlement occurred during the rocking cycles. They both explained a rounding of the soil that occurs due to yielding beneath the foundation, which reduces the stiffness of the system and causes nonlinearity in moment-rotation behaviour. Anastasopoulos et al. (2012) investigated the rocking response of two reduced-scale slender SDOF structures and the effectiveness of shallow soil improvement stretching to various depths below the foundation. For large-intensity earthquakes that exceed the design limits, the performance of the rocking foundation system was proven advantageous, not only avoiding collapse but hardly suffering any inelastic structural deformation. Kokkali et al. (2014) compared centrifuge tests and equivalent 1g slow cyclic tests to explore the effects associated with the low confining stresses prevailing at 1g test conditions.

2.2.4 In-situ Field Test

Algie (2011) and Phipps (2013) conducted a series of field experiments on shallow foundations embedded in a cohesive soil deposits. The experiment structure used in Algie (2011) was excited by an eccentric mass shaker mounted on top of the frame supported by rocking shallow foundation. Phipps (2013 investigated the shallow footing under three different loading conditions i.e. free vibration, quasi-static cyclic loading and dynamic forced vibration test. Nevertheless, the maximum footing rotation was notably small (<3%) with very high initial

factor of safety (*FSv*) up to 54 in Algie (2011). Phipps et al. (2012) carried out several trials at one *FSv* against bearing failure. However, Algie (2011) and Phipps et al. (2012) did not characterize the key performance indicators such as the periods, recentering ratio, residual settlement of the footing, and change in soil properties. The results from Algie (2011) and Phips (2013) showed that rocking foundations produce highly nonlinear moment-rotation behaviour and a well-defined moment capacity. A very small portion of the soil was found to yield due to the large factor of safety. The static equation for the moment capacity compared well with the experimental results. The settlement that occurred during the strong shaking was minimal, encouraging for future design aspects of rocking foundations (Algie et al. 2010; Phipps et al. 2012). Algie (2011) used the pressure sensors attached on the underside of the foundation to get insight into soil-footing interaction; unfortunately, pressure sensor did not work during the tests.

Both Algie (2011) and Phipps et al. (2012) highlighted further need for field tests of rocking shallow foundations with different parameters including different types of natural soil deposits, embedded depth and loading directions.

2.2.5 Snap-back Test

A snap-back test is a comparatively short dynamic test, which allows the structure to rock at its natural frequency. Previous studies showed that snap-back testing is an effective and a simple tool to investigate the nonlinear behavior of shallow foundation subjected to near-fault ground motions (Salimath et al. 2017, Acikgoz et al. 2016, Acikgoz and DeJong 2014, Algie 2007). Pender et al. (2011), Algie (2007), Phipps et al. (2012) and Salimath et al. (2017) performed a series of snap-back tests to study the moment-rotation response of shallow foundations on natural soil deposits. The results showed that snap-back testing is an effective tool for obtaining insight into the nonlinear behavior and earthquake response of shallow foundations. However,

there is a lack of field tests data under different conditions such as rocking direction, initial amplitude, and the static factor of safety.

2.3   Numerical Modeling

This section describes numerical modeling and analytical analysis to predict the behaviour of rocking shallow foundations during earthquakes. Uncoupled springs, the Beam-on-Nonlinear-Winkler Foundation (BNWF) approach, Macro-element approach, and the continuum finite element approaches are some commonly used numerical modeling. In addition some analytical approach such as equivalent linear analysis, which is simple but can predict the rocking behaviour approximately, is found to be used more often.

Raychowdhury (2008) and Raychowdhury and Hutchinson (2009, 2011) performed extensive numerical simulations using the BNWF approach to study the effect of inelastic SFSI on the seismic response of shear wall-footing structure systems. It is observed that the moment demand transmitted to the base of the shear wall during an earthquake is reduced by 15 to 80% compared with that of a fixed-base configuration. In addition, for low-rise buildings energy dissipation is dominated by nonlinear footing sliding, whereas for medium and high-rise structures, footing rocking contributes more than 80% of the total dissipated energy. Antonellis and Panagiotou (2014) investigated the 3-D response of 6 RC bridges hypothetically located about 3 km from the Hayward fault, USA. They considered 3 types of column foundations: conventionally designed foundation (based on Caltrans seismic code), rocking pile foundation, and rocking shallow foundation. Conventionally designed bridges experienced substantial inelastic deformations and damage in the columns, whereas the bridges with rocking foundations resulted to negligible structural damage, a nominally elastic response and small residual deformations.

Deng et al. (2012b) developed numerical models of rocking and hinging systems, which confirmed the finding that it is easier to topple a hinging system than a rocking system if two systems are assigned with similar parameters. Kutter et al. (2006) attempted to analyze and identify the important parameters of nonlinear spring-type models used in BNWF approaches that would reasonably capture system response for performance-based design methodologies. The investigators implemented the BNWF model in the OpenSees platform to carry out the study. These BNWF models were used to simulate the centrifuge tests as well as experimental datasets from other researchers.

Gazetas et al. (2013) utilized theoretical results from nonlinear finite element analyses to develop a dimensionless expression and an accompanying chart for the equivalent-linear static stiffness considering various rocking foundation shapes.

Lu et al. (2016) developed a simplified nonlinear sway-rocking model to capture load displacement response of shallow foundations during strong earthquake events. Iwashita and Taniguchi (2000) undertook a 2-D nonlinear seismic analysis assuming uplift of foundation, for a building that had been observed to be lightly damaged during the 1995 Kobe earthquake. The result was small deformation similar to those observed on the ground. A similar analysis assuming restraining of the foundation showed damage much larger than actually observed. They pointed out that similar behaviour had also been observed in a hospital building in the 1971 San Fernando earthquake.

2.4   Performance-based Seismic Design

In the past, seismic design of structures was solely based on force based design. However, over the last two decades there has been an understanding that increasing strength may not actually reduce damage and increase safety (Qiu and Zhu 2017; Gaxiola-Camacho et al. 2017; Sil 2019;

Zhang and Alam 2019). This lead to develop a new design methodology called "performance-based seismic design (PBSD)". PBSD is assumed as a modern designing concept of seismic resistant structure to control the various form of displacements with in permissible limit (Surez and Kowalsky 2011; Sadan et al. 2013; Finn 2018, Sil 2019). In PBSD methodology, design criteria are expressed in terms of achieving stated performance level when the structure is subjected to design earthquake. PBSD not only addresses strength and performance limit, which are important features of design specifications, but it also facilitates designers and owners to make decisions about the seismic performance of structures by considering different earthquake scenario and different performance level such as immediate occupancy, life safety, collapse prevention after an earthquake. PBSD will help designers and owners to build structures with a more predictable and quantifiable performance during an earthquake even.

Although PBSD is rather well-established, extensively researched and has been practiced for years in the building engineering, its implementation is still sparse in the bridge and geotechnical engineering (Ataei et al. 2017; Finn 2018; Kramer 2019). Particularly for geotechnical engineering, use of PBSD in geotechnical earthquake engineering has increased greatly over the past few years (Finn 2018). PBSD is used for developing remediation strategies for embankment dams with foundations susceptible to liquefaction under design seismic loadings (Finn 2018; Kramer 2019). The use of PBSD methodology particularly for foundations for bridge and buildings are still limited.

Sil (2019) carried out the nonlinear analysis of six different reinforced concrete moment frames that were designed using two major seismic design methods as Force Based Design (FBD) and Direct Displacement Based Design (DDBD). He concluded that DDBD structure shows good performance over the structural parameters and achieved design exhibits better and safe

compared to FBD structures. Lu et al. (2016) proposed a PBSD method for flexible base multi-storey buildings considering soil–structure interaction by introducing various factors such as strength reduction factor and soil-structure-interaction (SSI) modification factor. Results showed that considering SSI can reduce up to 60% the strength and ductility demands of multi-storey buildings, especially those with small slenderness ratio and low ductility demand. Lu et al. (2016) presented direct displacement based PBSD for flexible-base structures subjected to pulse-like ground motions. Lu et al. (2016) developed various equations to estimate the system damping of the building with flexible-base structures to apply in the proposed PBSD method.

Algie (2011) and Deng et al. (2014) proposed a direct displacement-based design (DDBD) methodology, similar to PBSD methodology, for the seismic design of rocking shallow foundations for shear wall and ordinary bridges respectively. Both defined the design performance level of the structure in terms of maximum drift limits. Hysteresis damping due to soil nonlinearity was considered in the design. Both of them presented design examples with step by step design procedures and performed nonlinear analysis to verify the design carried out by following the proposed methodology.

PBSD has been recently adopted by many design guidelines (AASHTO 2011; CSA 2014; FHWA 2014; NZT 2014). AASHTO is working to develop guidelines for Performance-based seismic bridge design. PBSD was first introduced in Canadian Highway Bridge Design Code (CSA 2014) in 2014. CSA (2014) defined some performance levels and performance criteria for different types of bridges. Engineers and Geoscientists British Columbia has published a professional Practice Guidelines – Performance Based Seismic Design of Bridges in British Columbia (EGBC 2018) and proposed as supplement document for CSA (2014). National

Cooperative Highway Research Program, USA presented a comprehensive study and guideline for performance based seismic design of bridges (Marsh and Stringer 2013).

2.5   Compatible Foundation Design

One concern of rocking foundation systems is the potential for significant accumulation of settlement or residual rotations in poor soils. Allmond and Kutter (2014) and Ha et al. (2019) demonstrated the viability of unattached piles with no tensile connection to the footing to obtain the beneficial rocking mechanism preventing excessive settlement even in poor or liquefiable soil conditions (Figure 2.5). Allmond and Kutter (2014) investigated the seismic behaviour of unattached pile foundations in liquefiable sand by dynamic centrifuge tests and showed that the rocking behaviour depends on the pile arrangements. Both Allmond and Kutter (2014) and Ha et al. (2019) concluded that unattached piles can be used to minimize the excessive settlement of rocking shallow foundation in poor soils.
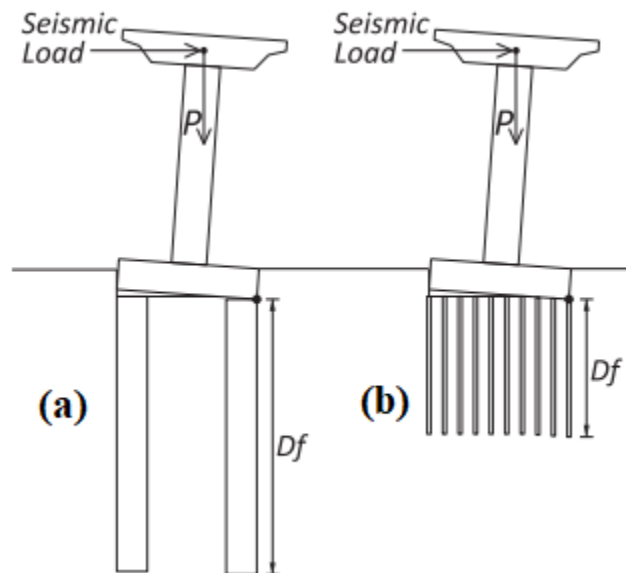
Figure 2.5. Rocking foundation schematic for (a) rocking foundation on piles and (b) rocking foundation on micropiles (Allmond and Kutter 2014).

Guan et al. (2018) carried out experiment on two model tests: one with a rocking pile foundation (detached pile cap), and the other with a conventional pile foundation (monolithic pile cap) and observed that compared to the conventional foundation, the rocking foundation resulted in much less damage in the piles, decreased the residual drift ratio by up to 88%, and retained nearly 60% of the initial stiffness following a maximum drift cycle of 6%.
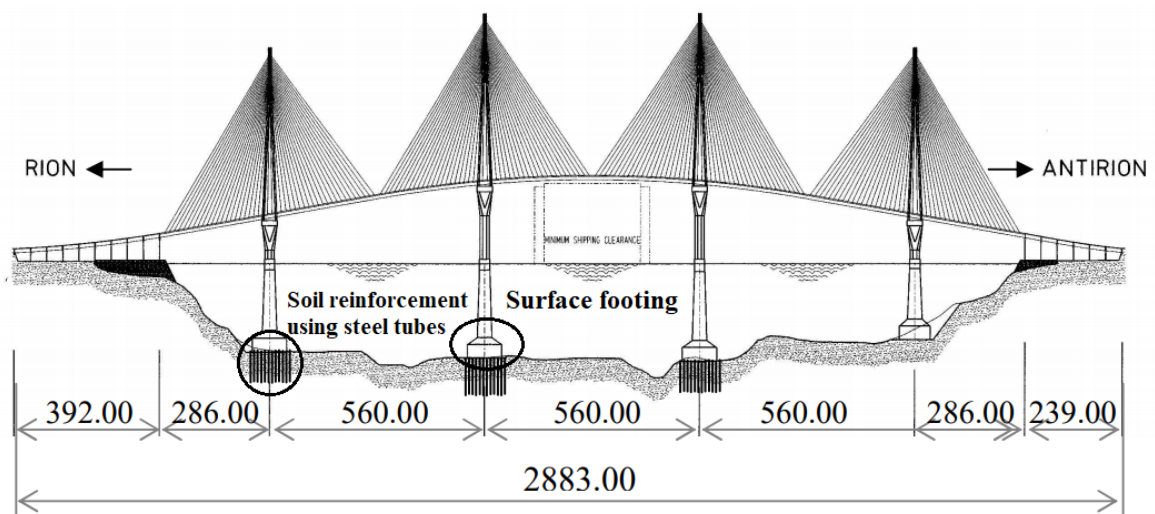
Figure 2.6. Bridge elevation, Rion Antirion multispan cable stayed bridge, Greece (Combault and Teyssandier 2005).

The concept of unattached piles to support the shallow foundation in poor soil is used in Rion Antirion multispan cable stayed bridge, Greece (Figure 2.6). Rion Antirion multispan cable stayed bridge (2,252 m long) is located in an exceptional environment which consists of deep water, deep soil strata consisting of weak alluvium and strong seismic activity with possible tectonic movements. Various foundation concepts such as piles foundations, deep embedded caissons and surface foundation had been investigated considering economy, constructability, and technical soundness. Due to the large seismic forces and weak soil conditions and, upper 25-30 m of the seabed subsoil of foundations were reinforced with steel tubes (inclusions) of 2 m diameter, 20 mm thick, driven at a regular spacing of 7 to 8 m underneath each pier base. The

steel tubes can work as micropiles. A 3-m thick, carefully gravel layer is properly leveled on top of the seabed and the shallow foundation was constructed on the top of gravel layer. The surface footing with some innovative ideas was found as a best option. Performance base design was carried out considering methodology was accepted. Several laboratory tests and numerical modeling were carried out. Nonlinearity of soil was accepted in the design and the equivalent damping ratios calculated from the hysteresis loops recorded during the centrifuge tests were considered in the design. The surface foundations was designed allowing for sliding, uplifting and partial mobilization of soil rupture mechanisms to resist the prescribed high levels of seismic excitation (Combault et al. 2005; Pecker 2006).

Saad et al. (2018) conducted an experimental study on the seismic performance of horizontally curved steel plate girder bridges with rocking shallow foundation allowed to uplift during seismic loading. A two-fifth scale, three-span highly curved bridge (Figure 2.7) was constructed on four shake tables and subjected to earthquake motions. Neoprene pads were placed beneath the footings instead of soil. It was observed that the rocking behaviour considerably limited the damage in the superstructure especially in columns and the residual displacement of the bridge under high earthquake intensities (i.e. applied motions were equivalent to 2.5 times the designed earthquake). The experiment showed that the bridges designed with rocking foundation system are less likely to topper even under the higher earthquake intensities. The experiments concluded that foundation rocking can provide a seismic isolation mechanism in which the ductility and acceleration demands imposed on structural components are greatly limited. Finally, they highlighted that a rocking system can be designed so that at high amplitude motions the rocking system becomes similar to a conventional fixed-based system.
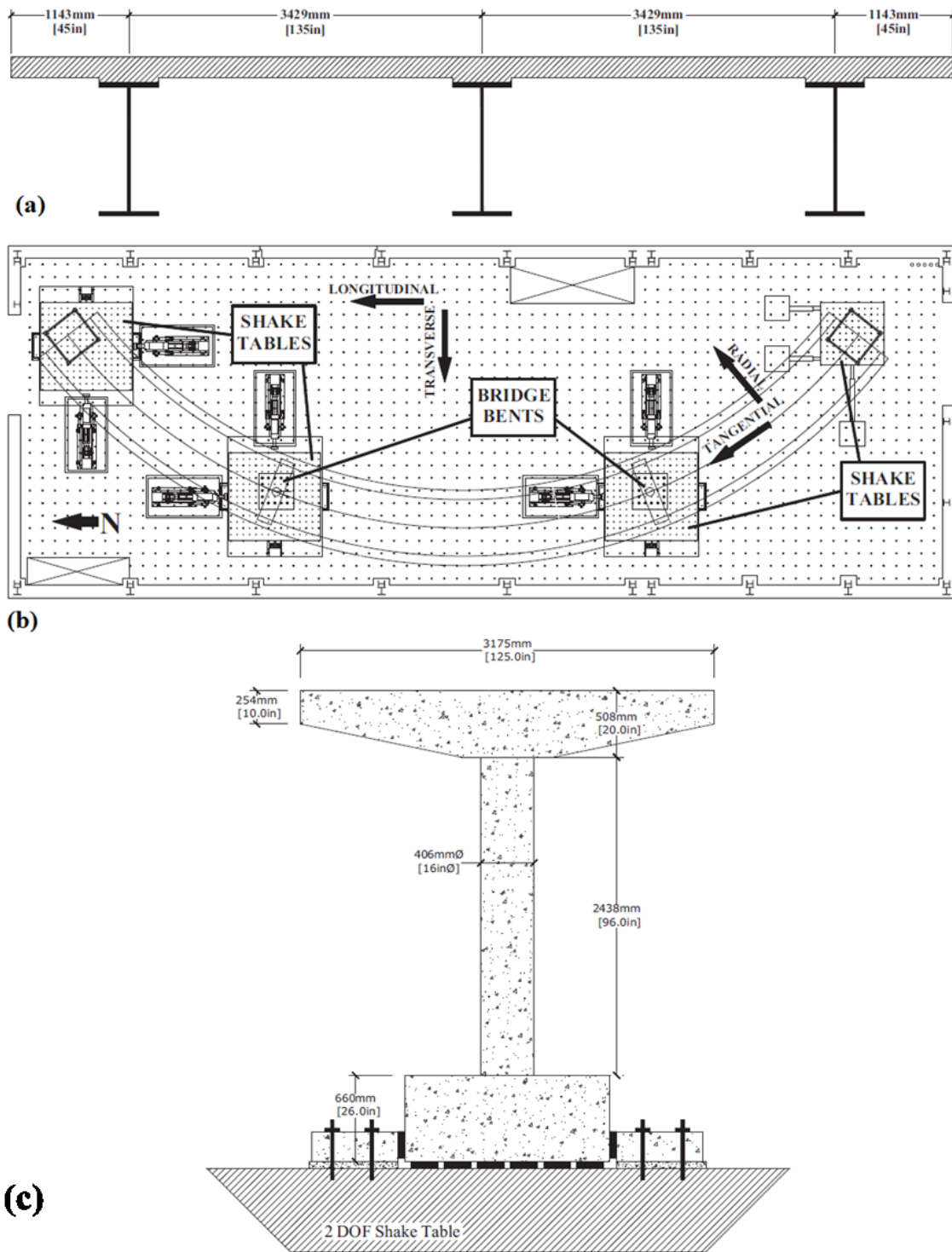
Figure 2.7. (a) Cross section of the prototype bridge (b) plan view of the laboratory including the bridge, and (c) experimental setup for the bridge bent on the shake table (Saad et al. 2018).

Gazetas et al. (2018) and Kourkoulis et al. (2012) investigated seismic performance of a two-story 2D frame structure founded on shallow footing. Another five-story 3D frame–shear-wall was considered by Gazetas et al. (2018). Both conventional and rocking foundations were considered to compare the seismic performance of the building frame. In case of building frame with conventional footing, plastic hinges firstly develop in the beams and subsequently at the base of all three columns, while soil under the footings remains practically elastic (Figure 2.8a). The frame eventually collapsed as it undergone excessive curvature ductility of the columns as shown in Figure 2.8b. Contrary to the frame with conventional footing, the frame with rocking footing withstands the shaking, with plastic hinging taking place only in the beams, leaving the columns intact. Plastic hinging developed beneath the footing as marked by red colour in Figure 2.8a. The residual rotation of the frame with rocking footing is almost zero as shown in Figure 2.8a, which might be attributed to re-centering characteristics of the rocking foundation.
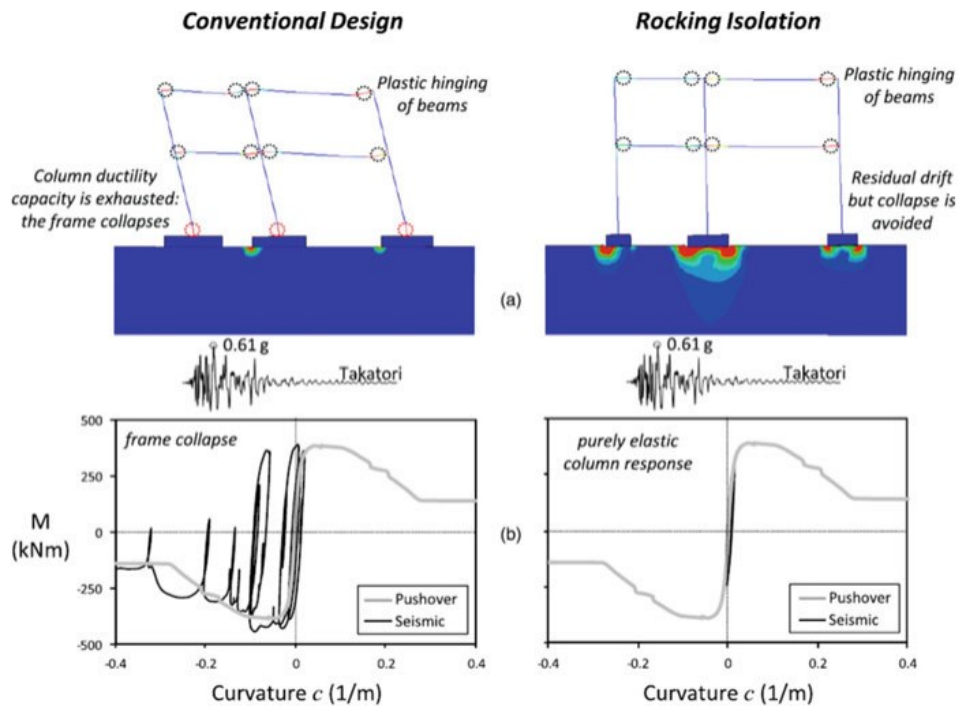
Figure 2.8. Comparison of performance of two alternatives (a) deformed mesh with plastic strain contours and (b) column moment-curvature response (Gazetas et al. 2018)

26

Liu et al. (2015a and b) carried out series of centrifuge testing to evaluate the seismic performance of low-rise frame-wall-foundation systems (Figure 2.9) under both cyclic and dynamic loading condition. Three types of frame-wall-foundation configurations were designed with variable strength between a shear wall and foundation: structural hinging dominated (SHD), foundation rocking dominated (FRD), and balanced design (BD) as shown in Figure 2.9. An OpenSees model was also develop to compare the performance of three configurations numerically. It was shown that the FRD system greatly reduced the superstructure drift demand due to footing rotation as compared to SHD system which exhibited significant peak transient and permanent deformation demand when excited by moderate and intense earthquake motion. A displacement based static pushover analysis using OpenSees, results a larger global strength and yield drift ratio for FRD system while the SHD system had lower capacity and yield drift ratio as well as showed similar strain-hardening behavior with conventional frame structures. The ductility demand of SHD was significantly greater than FRD. They concluded that the foundation rocking dominated building demonstrates its ability to protect the superstructure from seismic demands.
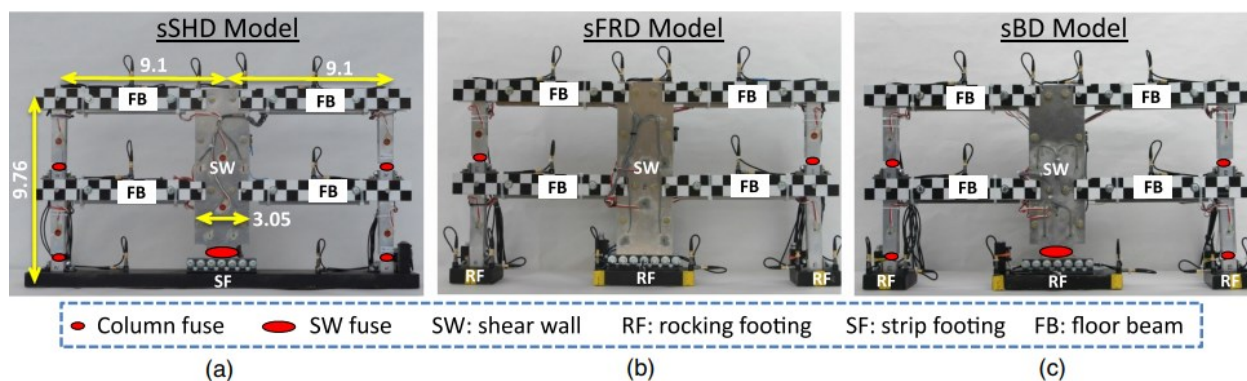
Figure 2.9. Constructed symmetric frame-wall-foundation models: (a) SHD, (b) FRD, and (c) BD. Note: fuse elements shown are designed to engage only post yield (Liu et al. 2015a).

Recentering post-tensioned (PT) connections have been investigated by numerous researchers as an alternative to fully restrained moment connections (Speicher et al. 2009). Barthes (2012) studied various possible connections for rocking column instead of designing earthquake resistant bridges with monolithic joints. He investigated several column configurations such as elastic column, modular and segmental column, unbonded post-tensioning (PT) cable and observed that the dissipative fuse in combination with a long unbonded post-tensioning (PT) cable as shown in Figure 2.10 proves to be effective for moderate to severe earthquake. Fuse with PT cable allows a column to resist a large earthquake with small rocking rotation. Barthes (2012) concluded that the fuse is designed properly; it can help to reduce the rocking rotations and enhance the stability of the structure. This concept can be used in rocking foundation too.
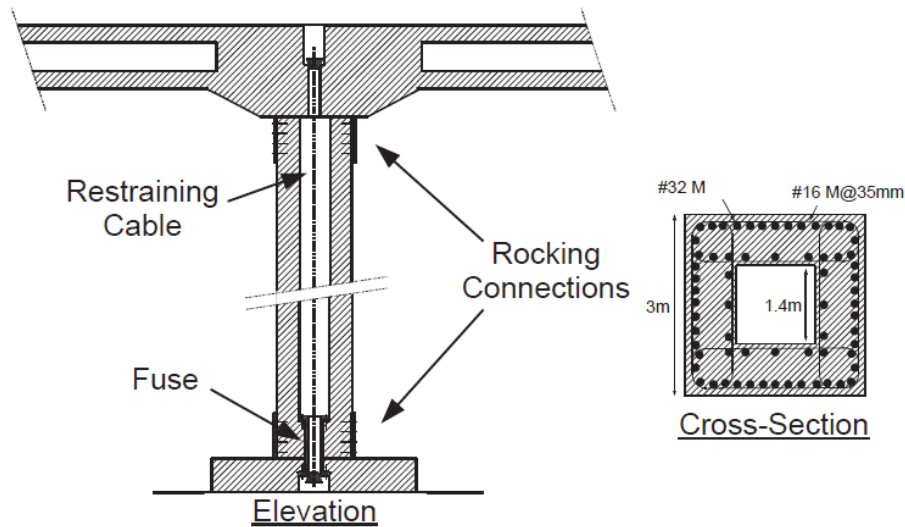
Figure 2.10. Drawing outline of the column connections with its footing and the superstructure (Barthes 2012).

Mitoulis and Rodriguez (2017) proposed a connection for segmental bridge construction (Figure 2.11) to provide cost-effective, low-damage bridge designs in seismic zone. This

connection itself can dissipate some amount of energy through bar yielding and provides recentering capabilities. This also reduces time to repair after the earthquake due to ease of replacement of the damaged components (Figure 2.11). This concept can be used in a bridge with rocking foundation with or without some modification.
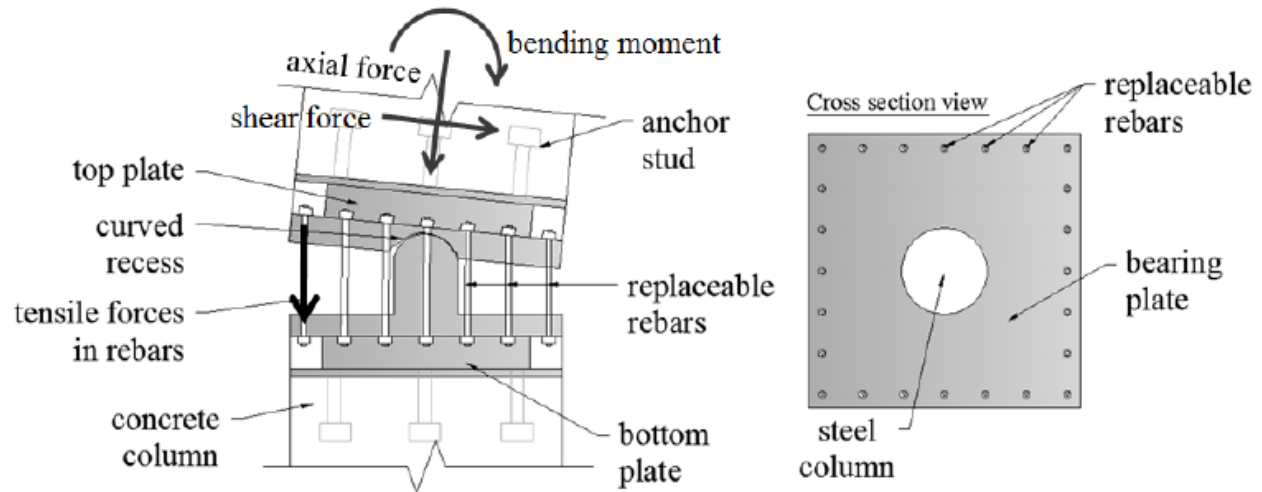
Figure 2.11. Elevation and plan view of the proposed seismic connection (Mitoulis and Rodriguez 2017).

The re-centering connection for rocking frame in the previous research was designed to concentrate all of the inelastic deformation into the tendons while the remainder of the connection stays elastic (Speicher et al. 2009). Speicher et al. (2009) carried out four experimental tests under cyclic loading to investigate the behavior and validate the performance of recentering connection with tendons. The tendons were made of superelastic nickel–titanium (NiTi) shape memory alloys. They observed that the re-centering connection worked well under the cyclic loading and showed re-centering behaviour even for 5% drift.

AASHTO and FHWA are encouraging prefabrication technology because of the many advantages for bridge owners, engineers, builders, and the traveling public (Ou et al. 2010).

Accelerated bridge construction (ABC) with segmental construction is a new paradigm used to expedite bridge construction by using new technologies, advanced planning, and improved and flexible detailing (Tazarv and Saiidi 2016). Application of ABC in high seismic areas, especially in columns and decks can be used for the bridge with rocking foundation (Mashal et al. 2014; Sideris et al. 2014; Zhao et al. 2018).

3. Characterization of Rocking Shallow Foundations on Cohesive Soil using Field Snap-back Tests[1]

Abstract

This paper presents a series of field snap-back experiments of a soil-footing-structure system equipped with rocking foundation on a cohesive soil. The objective was to investigate the nonlinear dynamic behaviour of the rocking system subjected to particularly pulse-like motions. During the snap-back tests, an initial drift ratio was applied to the deck, at a maximum of 8.5%, and then released using a quick release mechanism to enable the free vibration of the system. Effects of initial factor of safety against the bearing failure, initial drift amplitude, and snap-back directions on the dynamic properties of the rocking system were investigated. Test results show that the rocking moment versus footing rotation is highly nonlinear and the moment capacity can be well predicted on field cohesive soil. The shear capacity of footing did not significantly change with the number of trials or amplitude of initial drift. The damping ratio observed during the oscillations after snap-back release of the shallow foundations ranged from 8 to 30%. Average measured period of the rocking system was elongated by approximately 235% comparing with the period of fixed-base structure. An acceptably small residual settlement was observed even at a high cumulative rotation. The rocking system on clay exhibited a good recentering ability, which is even better than on sand. Finally, the increase in the density and shear strength of soil beneath the footing due to rocking cycles was observed.

3.1 Introduction

In conventional seismic design of foundations, the spread footing of a structure is usually assumed to be fixed. The footing uplift and rotation are precluded to prevent the superstructure from "overturning". With this design, the seismic energy is dissipated through damping and ductile action of the superstructure. This may lead to damage on the structure as a result of plastic hinge development in the superstructure, which is then susceptible to permanent drift or failure (Deng et al. 2012; Loli et al. 2014). Rocking shallow foundation is an innovative foundation design concept that allows the footing to rock nonlinearly during strong earthquake motions, as opposed to conventional "fixed-base" concept. The benefits of rocking shallow foundation have been suggested by the performance of several potentially unstable structures in major earthquakes (Housner 1963; NEHRP 2009; Storie et al. 2014).

To characterize the nonlinear soil-foundation-structure interaction (SFSI) of rocking systems, researchers have performed centrifuge tests (e.g., Gajan et al. 2005; Deng et al. 2012a; Loli et al. 2014; Hakhamaneshi and Kutter 2016) and scaled shaking table tests (Negro et al. 2000; Paolucci et al. 2008; Antonellis et al. 2015; Tsatsis and Anastasopoulos 2015) principally for foundations in sand. Seismic design provisions, such as FEMA 440 (FEMA 2005) and ASCE 41-13 (ASCE 2014), incorporate nonlinear SFSI (i.e. rocking) effects by considering an increased period and a modified damping. To use such concept, one design approach using the direct displacement-based methodology was proposed in Deng et al. (2014), for which the dynamic parameters of rocking systems, such as the equivalent stiffness, period elongation, and damping, may be required. Hence, it becomes critical to conduct comprehensive field investigation of the dynamic behaviour of full-scale rocking foundations, in addition to the scaled centrifuge or shake table tests.

As a type of dynamic test, a snap-back test simulates the free vibration of a structure after subjected to a pulse-like motion. During testing, a structure is pulled from its initial position, held still, and then released. Field snap-back testing may be more appropriate than slow cyclic testing for structures subjected to pulse-like motions (Pender et al. 2011). Tileylioglu et al. (2011) studied the dynamic stiffness and damping of the linear-elastic shallow foundation from a field forced-vibration test. Algie (2011) and Phipps et al. (2012) performed preliminary snap-back tests and characterized the rocking moment vs. rotation response of shallow foundations in the field on cohesive soils. Nevertheless, the maximum footing rotation was notably small (<3%) with very high initial factor of safety (FSv) up to 54 in Algie (2011). Phipps et al. (2012) carried out several trials at one FSv against bearing failure. However, Algie (2011) and Phipps et al. (2012) did not characterize the key performance indicators such as the periods, recentering ratio, residual settlement of the footing, and change in soil properties. Acikgoz et al. (2016) conducted laboratory snap-back tests of reduced-scale column to investigate the dynamic behavior of freely rocking flexible structures resting on an aluminum plate. These studies showed that snap-back testing is an effective, simple approach to the SFSI research of systems subjected to pulse-like motions. Thus far, however, there has not been any comprehensive characterization of rocking foundation system using field snap-back tests.

The present research characterized the dynamic behaviour of a soil-footing-structure system built upon a cohesive soil using field snap-back tests. The objective is to investigate the nonlinear soil-footing interaction for rocking foundations and compare the system performance with the performance of footings on sand based on small-scale testing approaches. The rocking foundation system consisted of a 1.5 m by 1.0 m concrete footing, steel column, and concrete deck to simulate a prototype single-degree-of-freedom (SDOF) system. The system is considered

a full-scale implementation of the rocking foundation concept. A geotechnical investigation was carried out to determine soil conditions before and after the snap-back tests. The initial *FSv* against bearing failure ranged from 5 to 20. Twenty-seven snap-back tests were conducted, where a variety of initial drift ratios were applied with a maximum value of 8.5%. This research investigated the effects of various parameters, such as vertical load on footings, initial drift ratio, and footing aspect ratio on rocking foundation capacities, dynamic parameters of the system, and the soil properties.
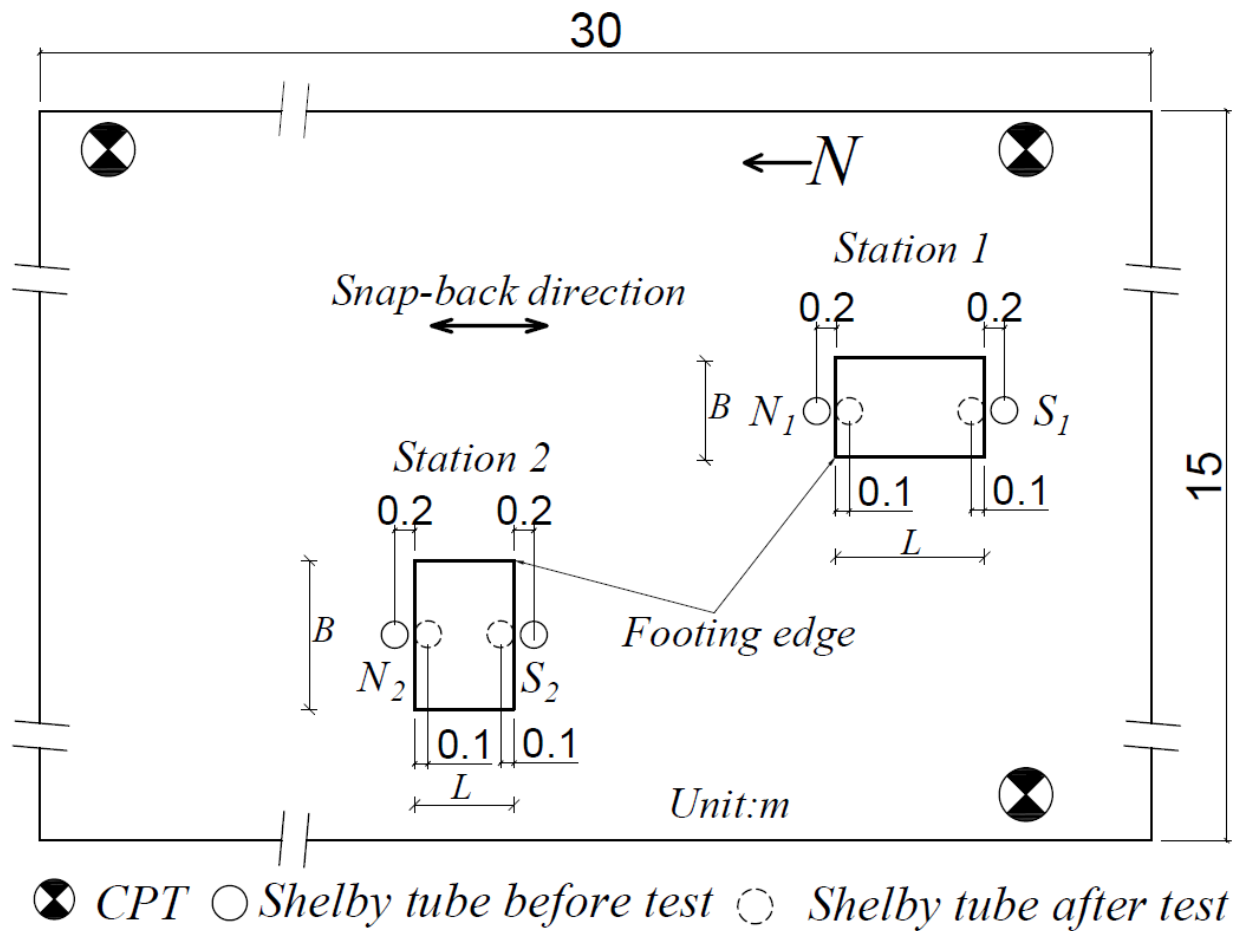
Figure 3.1. Field test layout with CPT and Shelby tube sampling locations.

3.2   Experimental Program

3.2.1   Subsurface Soil Characterization

A cohesive soil site, located on the university farm, was selected for the snap-back field tests of a rocking soil-footing-structure system. A geotechnical investigation was undertaken prior to the snap-back tests. Site investigation consisted of pre-test CPT, Shelby tube sampling before and after rocking tests, and laboratory testing of undisturbed soil samples. Figure 3.1 shows the test layout and locations of the CPT and Shelby tube sampling. Laboratory test programs were to determine the unconfined compressive strength (UCS), direct shear strength, Atterberg limits, and particle size distribution. The cone was pushed to a target depth of 4.0 m that is considered deeper than the influenced zone of footing (Figure 3.2). The depth of influenced zone under shallow a foundation is considered two times the footing length under the footing (3.0 m in this study). In addition to CPT tests, Shelby tube soil samples were collected from a depth of 0 m to 1.0 m from the base of the footing, before and immediately after a test sequence to evaluate the change in soil properties (Figure 3.1).

Figure 3.2 shows the correct tip resistance q_t, sleeve resistance f_s, shear strength s_u, and soil behavior type from CPT tests (Robertson and Cabal 2012). The upper layers were mostly soft to medium and fine grained. The lower layers were clay to silty clay or clayey silt to silty clay. The in-situ moisture content was slightly less than the plastic limit. The in-situ moisture content of the soil is about 30%, and plastic and liquid limit are about 35 and 75 respectively. The degree of saturation (S_r) of soil ranged from 86% to 91%. The soil in the site can be classified as elastic silt (MH) according to Unified Soil Classification System (USCS). Undrained shear strength (s_u) of undisturbed samples was measured using the UCS tests and direct shear tests under normal stresses ranging from 0 to 300 kPa. The strength, s_u, estimated

from CPT was about 70 to 85 kPa, down to 1 m depth from the footing base, which is consistent with s_u from the UCS tests, as shown in Figure 3.2. In direct shear tests, the specimen was sheared under a normal stress, in the range of the stresses experienced by the soil in the field during the tests. According to the sample depths and vertical load from structures, the representative in-situ normal stress may be 0 to 300 kPa. Values of s_u from direct shear tests ranged from 50 to 80 kPa under zero normal stress. The value of s_u increased with the applied normal stress, which is common as noted by Duncan et al. (2014) for unsaturated clay. However, when the normal stress exceeded 200 kPa, s_u remained almost independent of the normal stress.
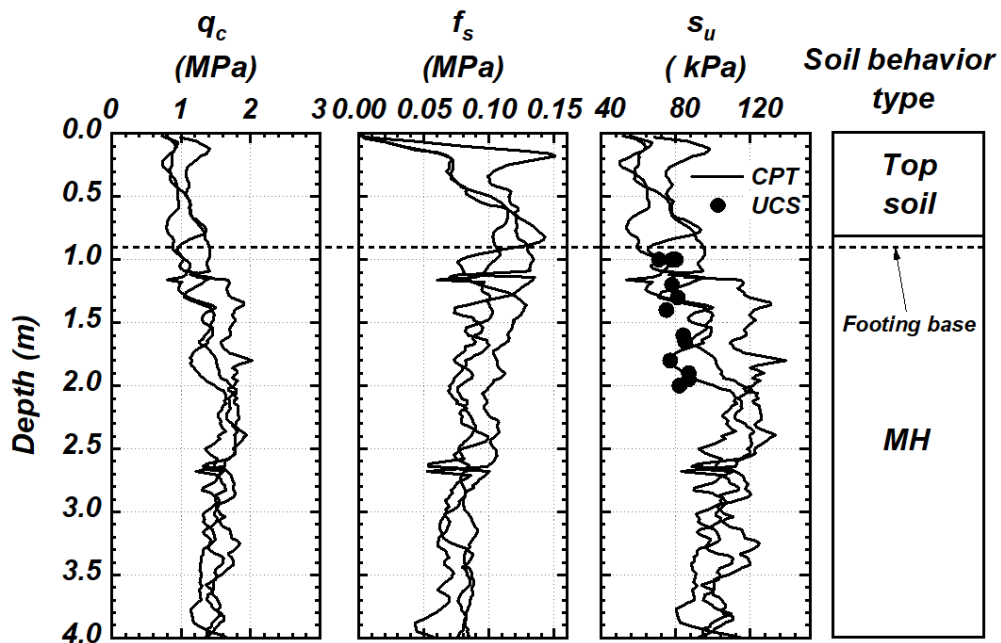
Figure 3.2. CPT profile of test site and soil behavior type.

3.2.2   Experimental Model

A SDOF system was designed for the snap-back tests. The system consisted of a rectangular reinforced-concrete (RC) spread footing, a square steel tubular column, and RC slabs used as the

superstructure weight (Figure 3.3a). Table 3.1 shows the key dimensions of elements and mechanical properties of the column. The first yield moment (M_{c_col}) of the column is designed to be stronger than the rocking moment capacity (M_{c_foot}) of the footing and thus the rocking response would be enabled. The value of M_{c_foot} is defined in Equation 3.1 (e.g., Gajan et al. 2005):

$$M_{c\_foot} = \frac{VL}{2}\left(1 - \frac{L_c}{L}\right) \qquad [3.1]$$

where V, L, and L_c are the vertical load, length of footing perpendicular to the axis of rocking and critical length of footing respectively. The term L_c represents the width of soil "plastic hinge" as the footing rotates about this critical area, defined in Equation 3.2:

$$L_c = \frac{V}{q_{bl}B} \qquad [3.2]$$

where B is the width of footing along the axis of rocking, and q_{bl} is the bearing capacity of soil under the critical contact area (A_c). The critical contact area (A_c) is the minimum footing area required to support the load from superstructure when the limit bearing capacity of the foundation soil is fully mobilized. An iterative process was carried out when estimating L_c because q_{bl} changes with both the L_c/B ratio and s_u within the influenced zone (assumed approximately $2L_c$ depth beneath the footing base) of A_c. Vertical stress beneath the footing was approximated at three depths (footing base, L_c, and $2L_c$) within the influenced zone and an average vertical stress beneath the footing was estimated using Simpson's method (Stoer and Bulirsch 1992). Figure 3.3b shows the concept of critical contact length and influenced zone. For simplicity, the s_u vs. σ (normal stress) relationship was used to interpolate s_u during the iterations. The average vertical stress beneath the footing was assumed as the normal stress in the soil beneath the critical contact area when estimating q_{bl}. The iterative process resulted in

37

compatible values of q_{bl} and L_c that satisfy Equation 3.2. Usually, four iterations were sufficient to reach q_{bl} convergence.
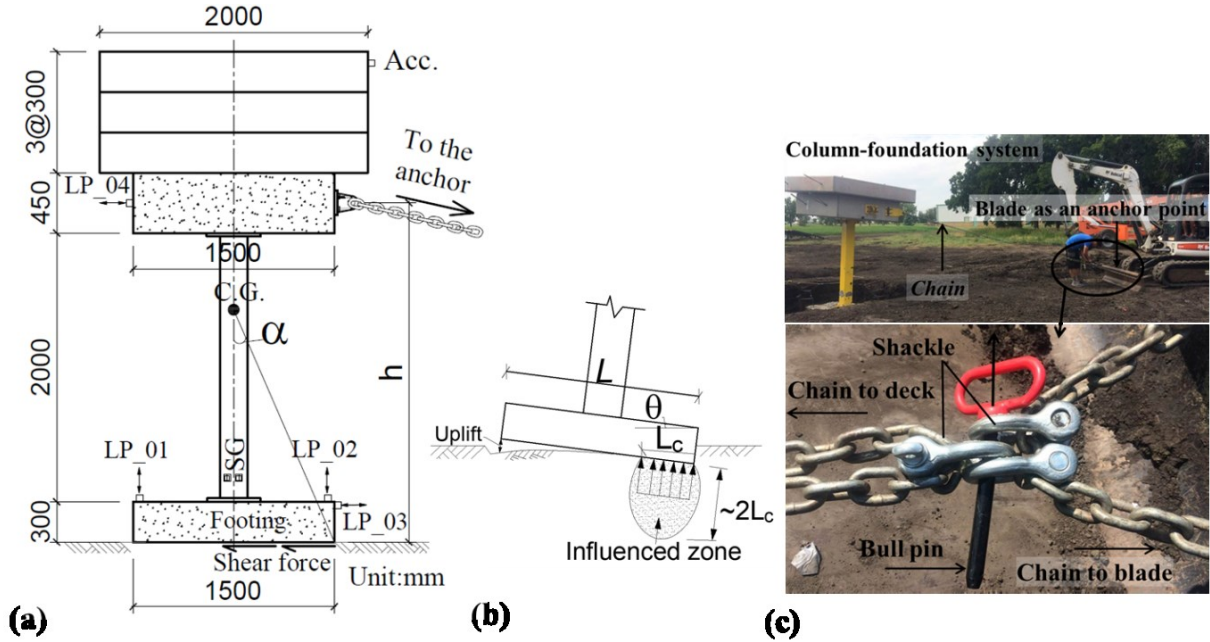
Figure 3.3. (a) Experimental setup, (b) concept of critical contact length and approximate influenced zone, and (c) the quick release mechanism. Acc.: Accelerometer, LP: Linear Potentiometer, SG: Strain Gauge, C.G.: Centre of gravity of system.

As shown in Figure 3.3a, a square steel tube (0.2 m by 0.2 m) is used as a column. The value of M_{c_col} is 113 kN-m, which is greater than M_{c_foot} that ranges from 17 kN-m to 79 kN-m in the present research. The bearing capacity equations by Terzaghi (1943) were adopted to determine the initial FS_V against the bearing failure. Consequently, the footing was 1.5 m long, 1.0 m wide and 0.3 m thick. The shallow foundations have an initial FS_V ranging from 5 to 20. When calculating the initial FS_V, s_u was also estimated considering the vertical stress within the influenced zone beneath the critical contact length (Figure 3.3b) due to the weight of the system.

To change the initial *FSv*, one to three RC concrete blocks were mounted on top of the deck, each weighing 28.17 kN.

Table 3.1. Properties of rocking foundation system

Component	Properties
Footing dimension	1.5 m × 1.0 m × 0.3 m
Height of column, h_{col} (m)	2.0
Steel tubular column section	0.2 m × 0.2 m
Column wall thickness (mm)	12.7
Column rigidity, EI (kN-m^2)	6,444
First yield moment, M_{y_col} (kN-m)	113

3.2.3 Instrumentation

Linear Potentiometers (LP) were attached to the foundation and column to measure the vertical and horizontal movement as shown in Figure 3.3a. An accelerometer was placed on the top of structure to measure the horizontal acceleration at the top of structure along the rocking direction (Figure 3.3a). The acceleration was used to calculate the lateral inertia force along the rocking direction and the force was further used to calculate the rocking moment at the base center of the footing. Axial force and bending moments in the column were measured by the strain gauges installed near the bottom of steel column.

3.2.4 Testing Procedure and Matrix

The snap-back tests were conducted by pulling the deck using chains attached to a quick release mechanism. The chain was fixed to the deck on the north side of the structure and fastened to an

excavator through a quick release mechanism as shown in Figure 3.3c. The excavator was used as a fixture point for the chains. At the desired drift ratio, the bull pin was pulled out and set the structure to rock. At each station, the test at high FSv and small drift ratio was carried out first. In total, 8 snap-back tests (in total 27 trials) were conducted at 2 stations. The system rocks about either the longitudinal or transverse axis to investigate the effect of footing aspect ratio, A_r ($=L/B$). The layout of the field tests is shown in Figure 3.1. Table 3.2 outlines the key parameters of the field tests including FSv, A/A_c, moment-to-shear ratio (i.e., M/H, where H is the shear force on the footing, Gajan et al. (2005)), A_r, and initial drift ratio (θ_i). Note that FSv and A/A_c may change slightly with the change in soil strength as the tests proceeded; however, it is difficult to estimate FSv and A/A_c of each trial. Each test is named as follows: the first character "F" stands for the free vibration, the second character stands for the loading direction where "L" for longitudinal and "T" for transverse, and the subsequent numbers stand for the test sequence. The maximum drift ratio before release was 8.5% (or 85 mrad. 1 mrad = 0.1%).

3.3   Test Results

3.3.1   Rocking Moment and Shear Capacities

Figure 3.4a shows the typical rocking moment vs. footing rotation curves for the test FL01 at base center of the footing, obtained during the application of static snap-back forces. It is apparent that there is a considerable nonlinearity in the moment-rotation curves and the rotational stiffness (k_θ) is degraded from one trial to the next during the early snap-backs. However, M_{c_foot} remained constant with the number of trials or amplitude of rotation (Figure 3.4a). The snap-backs leading to the largest drift (Trial 4) shows a decreased k_θ, likely as a consequence of soil rounding beneath the footing and the soil yielding under the edges of the

foundation from previous trials (Algie 2011). However, the rate of k_θ degradation decreases with

increase in number of trials. For example, in case of FLO1, k_θ remains relatively constant after 2-

3 trials as shown in Figure 3.4a. This might be attributed to damage and compaction of soil

during early trials (i.e. Trial 1 and 2) (Algie 2011). Rocking foundation progressively rounds the

soil, and this rounding causes a reduction in the contact length, results in nonlinearity and

stiffness reduction on the moment-rotation relationship. The soil compaction and yielding of soil

might change A/A_c for next trial, which is not exactly same as the initial A/A_c presented in Table

3.2. The effect of compaction or yielding of soil after each trial is not considered because it is

difficult to quantify.

Table 3.2. Snap-back field test matrix

Station	Test ID	Initial FSv	A/A_c	M/H	Aspect ratio, A_r[1]	Fixed-base period, T_{fixed} (sec)	Initial rotation of trials, θ_t (mrad)
1	FL01	19.7	17.8	1.68	1.5	0.289	30, 37, 49, 62
	FL02	11.0	10.1	2.83	1.5	0.460	28, 50, 63, 78
	FL03	7.6	7.1	3.03	1.5	0.617	29, 40, 45
	FL04	5.8	5.5	3.23	1.5	0.774	37, 41, 55
2	FT01	18.4	17.6	2.53	0.67	0.289	42, 69, 79, 85
	FT02	10.3	9.9	4.25	0.67	0.460	31, 57, 71
	FT03	7.1	6.8	4.55	0.67	0.617	39, 67, 76
	FT04	5.5	5.3	4.85	0.67	0.774	42, 49, 67

Note: 1. $A_r = L/B$, where L = length of the footing perpendicular to the axis of rocking and B = width of the footing along the axis of rocking.
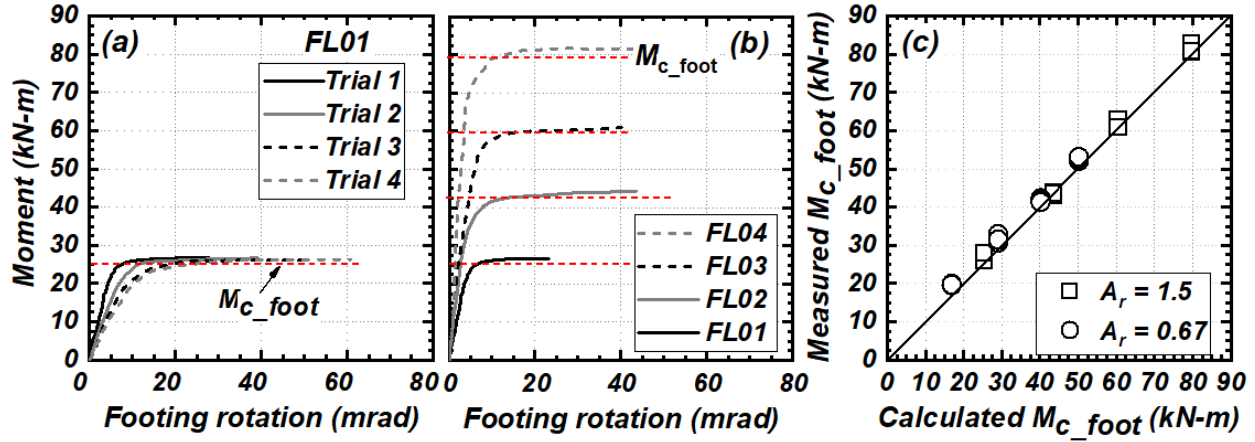
Figure 3.4. (a) Applied static rocking moment vs. footing rotation curves in snap-back stage for FL01, (b) moment-rotation in snap-back stage at different vertical loads for FL01-FL04 (first trial only), and (c) comparison of calculated and measured moment capacities for all tests in present study.

It is observed that Equation 3.1 works well for snap-back tests. The horizontal line in Figure 3.4a indicates the value of M_{c_foot} calculated using Equation 3.1. The calculated M_{c_foot} (25.3 kN-m) was very close to the measured M_{c_foot} (27 kN-m). Figure 3.4b shows that the initial stiffness of all snap-backs was almost same for the footing with various initial FSv as shown in Figure 3.4b. However, small increment of initial stiffness with increase in FSv was observed, which might be attributed to compaction of soil beneath the footing at lower FSv. The capacities of the snap-back curves imply the effects of vertical load on the structure; a greater vertical load corresponding to a greater M_{c_foot}. Figure 3.4c shows the relationship between calculated M_{c_foot} and measured M_{c_foot} for all trials in the present study. The measured M_{c_foot} is consistent with calculated M_{c_foot} irrespective of FSv or A_r. The result indicates that M_{c_foot} can be estimated reasonably well on a cohesive soil in the field.
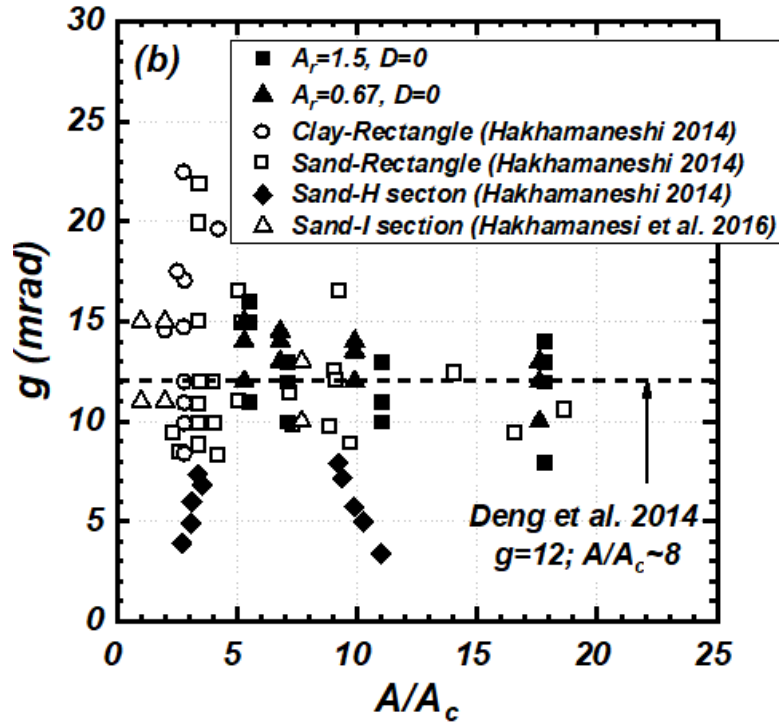
Figure 3.5. Observed relationship between footing rotation to mobilize moment capacity (g) and A/A_c.

The rotation angle (g) to mobilize the moment capacity of the footing is a crucial parameter in modeling the moment-rotation hysteresis behavior of rocking foundations. The values of g in the present study ranged from 8 to 17 mrad, although there is a considerable scatter as shown in Figure 3.5. Deng et al. (2014) recommended using $g = 0.012$ for design of rocking rectangular footings on sand when A/A_c is about 8. The value of g from Hakhamaneshi (2014) and Hakhamaneshi et al. (2016) are also plotted in Figure 3.5 for rectangular (on both sand and clay), H- and I-shaped (on sand) footings. No significant difference in g is observed between sand and clay. Except for some cases, it is seen that the estimate of $g = 0.012$ seems to be reasonable regardless of A_r and the soil type.

Figure 3.6 shows an example of the soil rounding along the loading direction observed after all tests in Station 2. The deformation of soil into the nonlinear range during rocking implies a source of energy dissipation for rocking system.
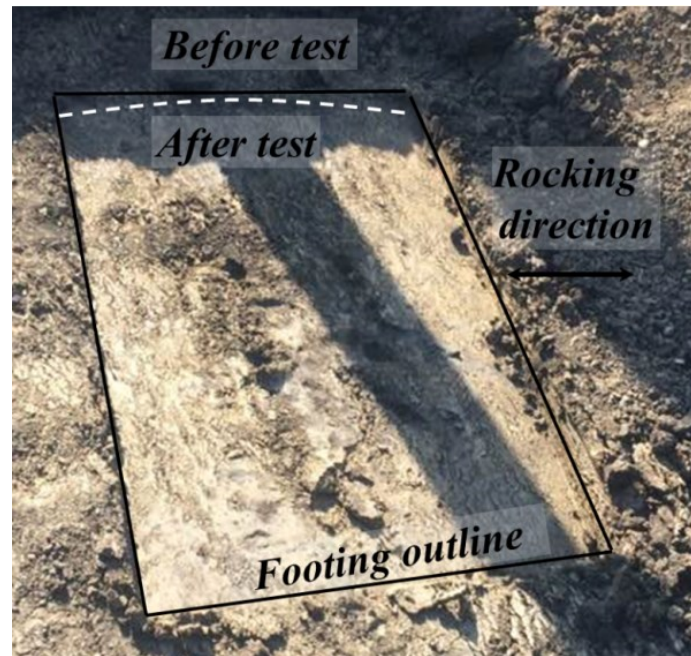
Figure 3.6. Observed rounding of soil beneath the footing after all tests in Station 2.

The curves of shear force (H) vs. sliding (s) normalized by L in snap-back stage are shown in Figure 3.7a. It is observed that the shear capacity (H_c) did not significantly change with the number of trials or amplitude of horizontal displacement. About 5% reduction in shear stiffness was observed with the number of trials or the amplitude of sliding. Similar pattern was observed for all tests. A sliding of 0.05% of footing length was mobilized when H_c was reached for FLO1 with FS_v 19.7. More noticeable s/L (0.18%) was observed after reaching H_c and at θ=62 mrad (Figure 3.7a), but in general the amplitude of s/L at higher rotation was small. This result indicates that such small sliding would likely be considered acceptable during a major seismic event.
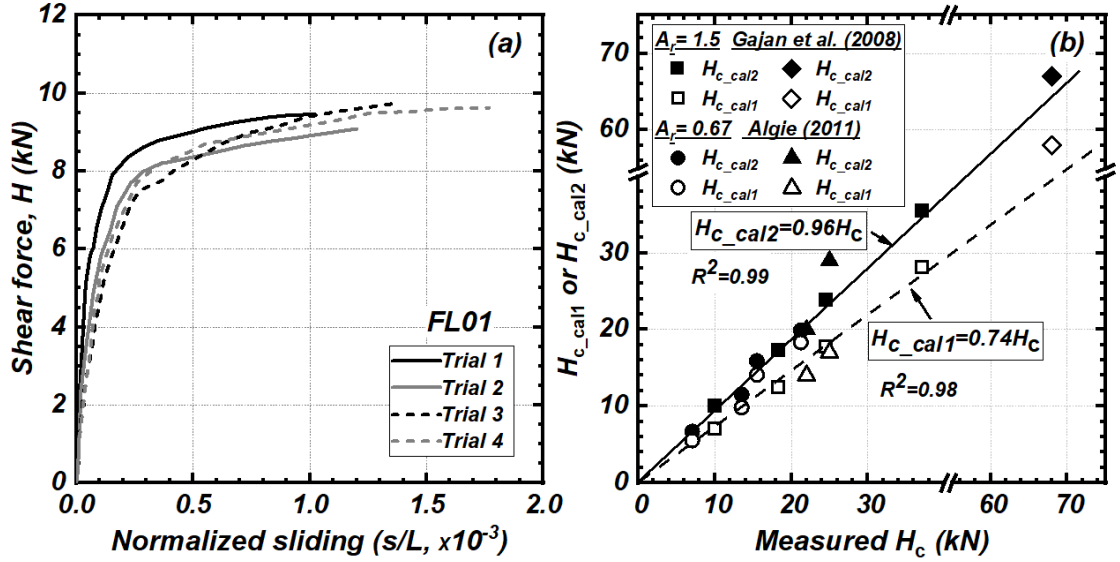
Figure 3.7. (a) Shear force vs. normalized sliding in pseudo-static snap-back stage for FL01 and

(b) comparison of measured shear capacities H_c and calculated capacities H_{c_cal1} and H_{c_cal2} from

all trials.

The shear failure capacity (H_c) is of interests to characterize the rocking foundation. We

estimated H_c using two approaches:

$$H_{c\_cal1} = L_c B s_u \hspace{3cm} [3.3a]$$

$$H_{c\_cal2} = \frac{M_{c\_foot}}{h} \hspace{3cm} [3.3b]$$

where h is the distance between the base center of the footing to the loading point on the deck

(Figure 3.3). Equation 3.3a assumes the soil-footing interface shear resistance to be s_u, whereas

Equation 3.3b is developed from the static equilibrium.

Figure 3.7b shows the relationship between the measured H_c, H_{c_cal1} and H_{c_cal2}. Several

data points from tests in clay (Algie 2011; Gajan et al. 2008) were also shown for comparison.

Note that H_{c_cal2} correlates well with H_c, as H_{c_cal2} equals $0.96H_c$ on average irrespective of the

footing aspect ratio. On the other hand, H_{c_cal1} equals $0.74H_c$ on average. Because the footing was

on the surface and the residual settlement at the end of tests was at mm scale, the passive earth

45

pressure and side resistance from the soil were shown insignificant. The discrepancy between H_c and H_{c_call} may possibly be attributed to the lateral component of soil resistance at the critical contact area when the footing attempted to plunge into the soil at an angle.
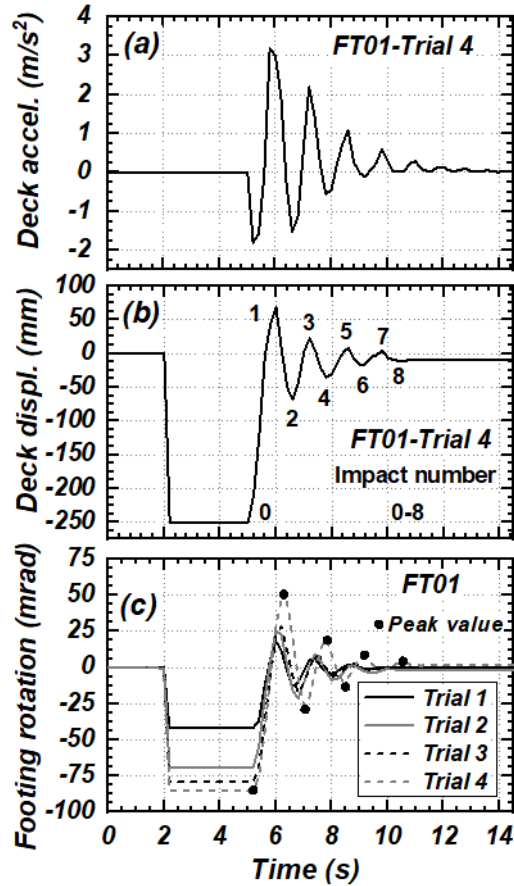
Figure 3.8. Typical time histories of (a) deck acceleration and (b) deck displacement, and (c) footing rotation for four trials in test FT01.

3.3.2 Damping and Energy Dissipation

Figure 3.8 shows typical time histories of deck acceleration, deck displacement, and footing rotation in test FT01. Throughout the snap-back tests, the rocking foundation only oscillated for 2 to 5 cycles before it came to rest, which indicates a high level of damping. Figures 3.8a and 3.8b show that the soil-footing interface can significantly decrease the deck acceleration pulses

46

while dissipating a significant amount of energy. The impact number (n, used in Algie 2011) was labelled in Figure 3.8b. The impact number, n is assumed "0" at the maximum initial displacement (Figure 3.8b). Then the peak on the opposite side after release corresponds to an impact number (n) of 1.

Figure 3.8c shows that a sequence of alternating footing uplift occurs after the structure was released from the initial position. The maximum vertical displacement of each uplift cycle reduced gradually. This is because of the energy dissipated when the footing impacted the soil beneath the footing. Note that the maximum footing rotation (similar to deck drift ratio) for snap-back is about 85 mrad, which is much greater than the allowable rotation in any building codes. The response shows a very small amount of permanent rotation when the dynamic response come to an end as shown in Figure 3.8c.
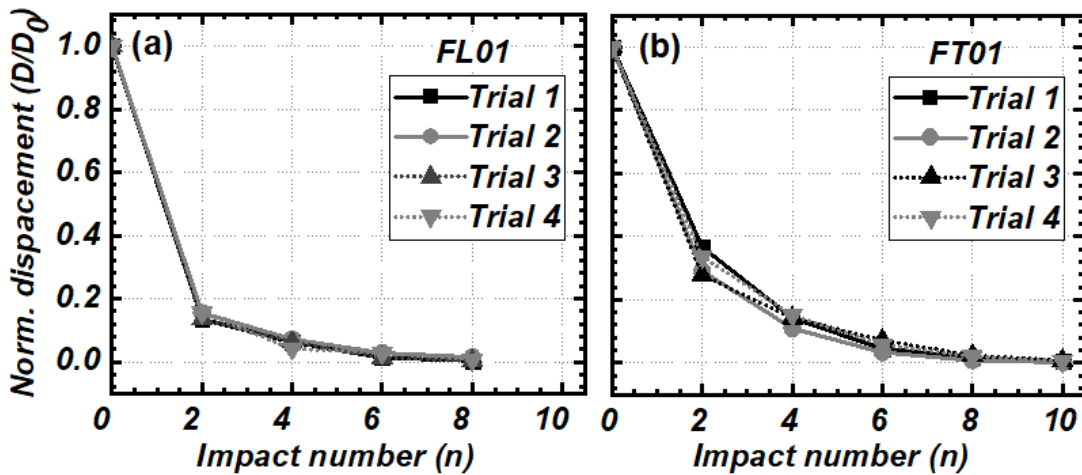
Figure 3.9. Normalized deck displacement with respect to impact number for the footing with A_r (a) 1.5 and (b) 0.67. (D_0 = initial deck displacement).

Figure 3.9 shows the deck displacement (D, i.e. drift) normalized by the initial deck displacement (D_0) with respect to n. It is seen that more than 80% of the initial displacement was lost during one complete cycle after release in FL01 (A_r=1.5) while this was about 65% for FT01

(A_r=0.67). This clearly indicates that the large amount of energy was dissipated during the first cycle of the motion. It is also seen that footing with a small A_r (Figure 3.9b) oscillated more cycles than the footing with a large A_r (Figure 3.9a), possibly because the soil-foundation flexibility increases as A_r decreases and this leads to more oscillation cycles. A similarity in the decaying amplitudes in all tests, irrespective of D_0, was observed in Figure 3.9. The results indicate that the energy dissipation at each impact for all trials was similar; however, some discrepancies were observed for FTO1 at impact number 2 and 4.
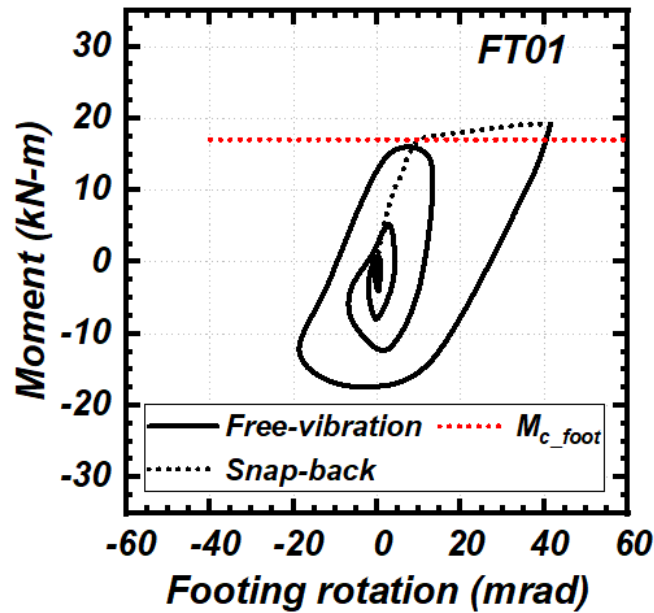
Figure 3.10. Typical moment vs. rotation relationship of shallow foundation with A_r=0.67.

Figure 3.10 shows a typical dynamic rocking moment vs. footing rotation curve together with the static snap-back moment vs. rotation. Data from strain gauges installed at the end of column was used to calculate the static moment while measured acceleration was used to calculate the dynamic moment at the base center of the footing. The comparison between the static and dynamic moment-rotation is reasonable as they have similar moment capacities. As shown in Figure 3.10, the moment-rotation curve is less "pinched" than the curves of footing

48

subjected to slow cyclic loads reported in previous studies (e.g., Gajan et al. 2005; Deng and

Kutter 2012) but is fairly similar to the curves subjected to dynamic loads (Deng et al. 2012a).

Out of various methods to calculate damping ratios (ξ), the method from the logarithmic

decrement (Chopra 2007) is useful in the snap-back tests, as expressed in Equation 3.4:

$$\xi = \frac{ln\left(\frac{\theta_1}{\theta_2}\right)}{2\pi} \qquad [3.4]$$

where θ_1 and θ_2 are the peaks (or valleys) of two adjacent cycles in the footing rotation histories.

Following Equation 3.4, the values of ξ for FT01 (Figure 3.8c) during the first cycle are

estimated to be 24%, 22%, 19%, and 16% for Trials 1 to 4, respectively. The decrease in ξ from

Trials 1 through to 4 is likely a consequence of the accumulation of permanent rounding

deformation in the soil beneath the foundation, such that the effective soil-footing contact length

of the foundation decreased as the cycle proceeded.
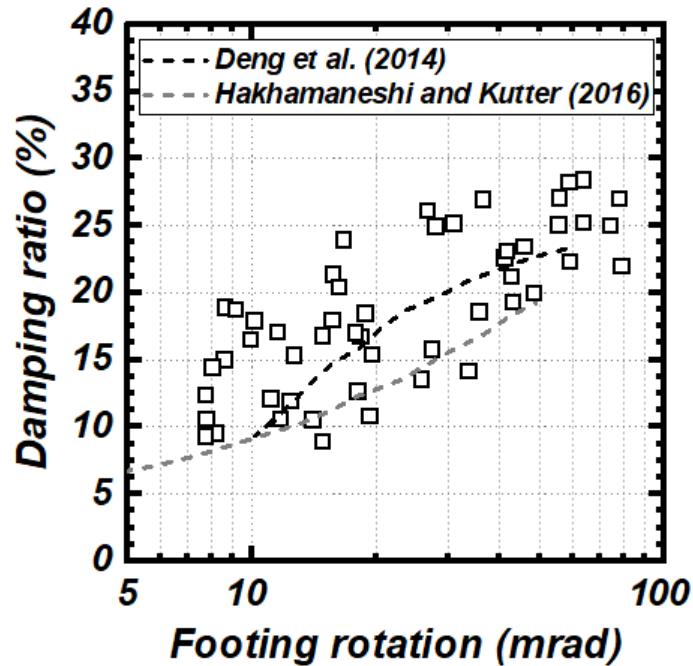
Figure 3.11. Damping ratio vs. footing rotation. Footing rotation is taken as the initial amplitude
of a considered cycle.

Figure 3.11 plots ξ vs. footing rotation (θ) from all snap-back tests using Equation 3.4, where θ was taken as the initial amplitude θ_l of a cycle (Equation 3.4). An important feature is the significant amplitude of ξ, ranging from 8% to 30%. This is promising in applications because it shows that the measured ξ is greater than ξ considered in many design guidelines (FEMA 2000; ASCE 2014). From the results, it is seen that ξ increases as θ increases, and reaches the maximum as θ reaches above 20 mrad. The damping ratio was relatively insensitive to θ for $\theta > 20$ mrad (Figure 3.11). Similarly, Gajan and Kutter (2008) and Algie (2011) reached a conclusion that any rotation greater than 2 mrad had significant damping and was insensitive to the amplitude of rotation. Figure 3.11 also compares the values of ξ with the trends from cyclic tests in sand (Deng et al. 2014; Hakhamaneshi and Kutter 2016). Deng et al. (2014) and Hakhamaneshi and Kutter (2016) showed that ξ increased the amplitude of footing rotation increased. The trend of ξ vs. θ for the footing on cohesive soils is similar with ξ on sand, although ξ on cohesive soil is greater than the damping observed on sand.

3.3.3   Natural Periods

Figure 3.12a shows the measured natural rocking periods (T_m) with respect to FSv. The period T_m is defined as the time required for the first full cycle of footing rotation. The measured T_m decreased with increasing FSv. For example, as FSv increased from 5.5 to 18.4 for the A_r=1.5 (i.e., vertical load changing from 120 to 35 kN), T_m decreased from 1.4 to 0.8 s (Figure 3.12a). This might be attributed to the decrease in mass of structure and the increase in rotational stiffness of the system as FSv increases. Similar trends are also observed for the A_r=0.67. As the first vibration mode (i.e. fundamental mode) is the most critical and dominant mode to rocking

(Acikgoz 2016; Vivek and Raychowdhury 2015), the period and damping corresponding to the first mode are considered in this research.
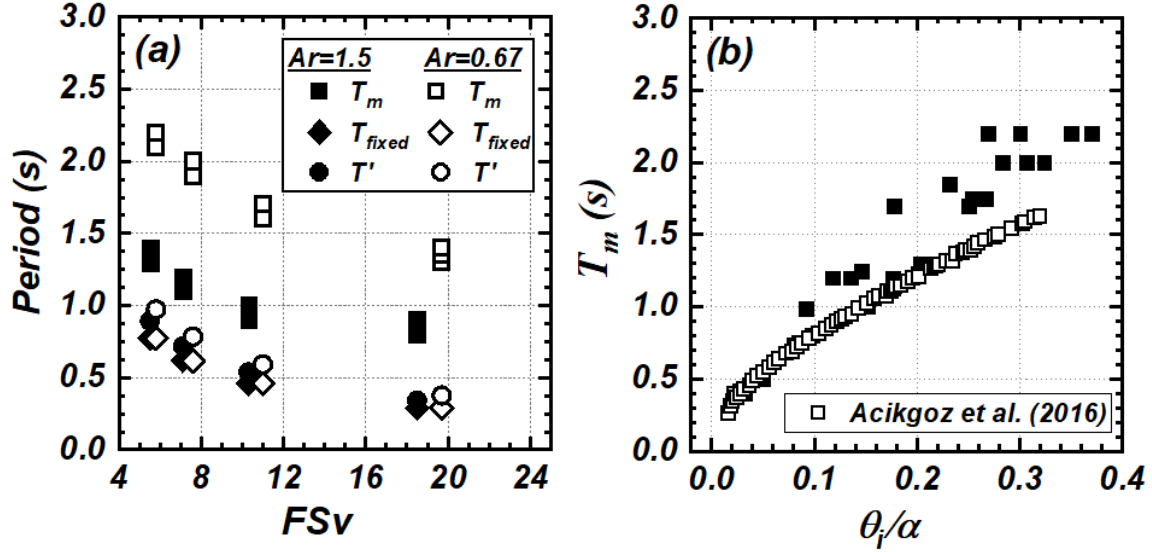
Figure 3.12. (a) Measured rocking period (T_m), fixed base period (T_{fixed}), and FEMA rocking period (T') vs. FSv for all tests and (b) relationship between the natural period and rocking amplitude for all tests.

The period-lengthening expression as per FEMA 440 (FEMA 2005) considering elasto-perfectly-plastic rocking model is defined in Equation 3.5:

$$\frac{T'}{T_{fixed}} = \sqrt{1 + \frac{K_{fixed}}{K_x} + \frac{K_{fixed} \cdot h_{cg}^2}{K_\theta}} \qquad [3.5]$$

where T_{fixed} and T' = fundamental periods of the fixed-base and flexible base structure, respectively; K_{fixed} = lateral stiffness of the fixed-base structure; K_x and K_θ = static stiffness in the horizontal and rocking mode, respectively, for both surface and embedded footings; and h_{cg} = height from the base of footing to the centre of gravity of the deck mass. K_{fixed} and T_{fixed} were calculated based on the mechanical properties of the model presented in Table 3.1. The static stiffnesses (K_x and K_θ) were computed by established principles recommended by FEMA 440

(FEMA 2005) and Gazetas (1991) using soil properties (i.e. shear modulus G and Poisson's ratio υ). The average G and υ for the soils beneath the foundation was estimated, considering s_u of the soil beneath footing, from established empirical relationships (Gazetas 1991).

Figure 3.12a compares the T_{fixed}, T' and T_m for fixed based system, elasto-perfectly-plastic rocking system and rocking foundation system respectively. The period considering the SFSI effects using Equation 3.5 was observed 15 to 20 % greater than T_{fixed} for the foundation with A_r=1.5 and 25 to 30 % for the foundation with A_r=0.67 (Figure 3.12a). The measured period (T_m) of the foundation with A_r=1.5 is 1.5 to 2.2 times greater than T' whereas the foundation with A_r=0.67 is 2.5 to 0.5 times greater than T' (Figure 3.12a). This confirms that rocking foundation can attribute to seismic resistance through an increase in damping and an elongation of natural period. This might be a reason that apparently unstable structures had survived major earthquakes because the entire structure rocked on its foundations (Browne 2006).

Figure 3.12b illustrates the relationship between rocking amplitude (θ_i/α) and T_m for all tests. The rocking amplitude is defined as the initial rotation (θ_i) of the structure normalized by α, which is the angle between the centre of gravity of the system to the bottom edge of the footing as shown in Figure 3.3a (Housner 1963). A rocking amplitude of 1 indicates a condition where the structure is on the verge of tipping over. Since the displacement demand is used in rocking foundation designs (Deng et al. 2014), exploring this relationship is useful in determining the period characteristics which govern the lateral response of the structure after the initiation of rocking. Acikgoz et al. (2016) conducted an experiment to investigate the free vibration response of a reduced scale rocking system resting on an aluminum plate. The relationship between θ_i/α and T_m of measured by Acikgoz et al. (2016) in the laboratory correlate fairly with the field test results when rocking amplitude is less than 0.25 as shown in Figure

3.12b. For θ_i/α greater than 0.25, T_m on clay is greater than the periods measured by Acikgoz et al. (2016) in the laboratory.
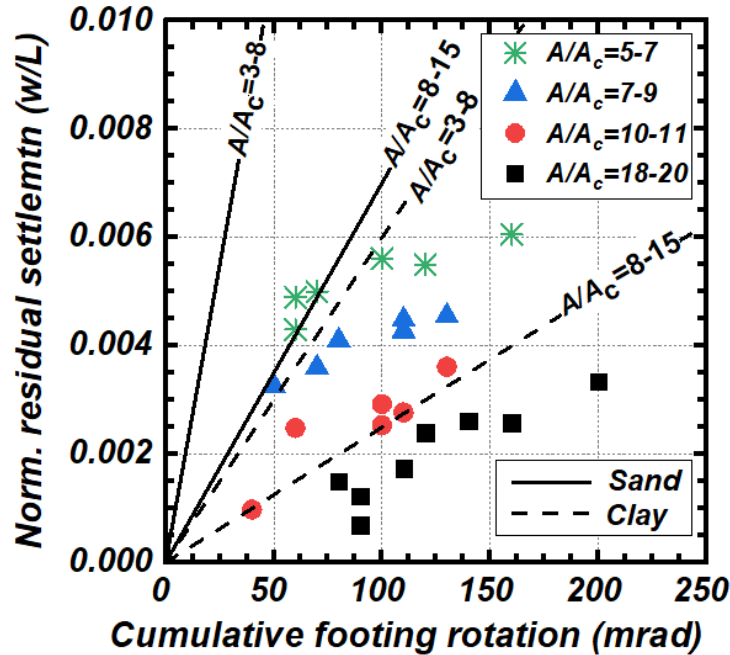
Figure 3.13. Normalized cumulative settlement vs. cumulative footing rotation correlation. Straight lines are adapted from Deng et al. (2012a) on sand and Hakhamaneshi (2014) on clay using centrifuge modeling.

3.3.4   Settlement and Recentering Ratio

The cumulative footing rotation and residual settlement (w) of the rocking footings as shown in Figure 3.13 were obtained using the method of Deng and Kutter (2012); the settlement (w) was then normalized by L. As shown in Figure 3.8c, using the footing's rotation time history, all the peak values greater than threshold rotation were identified. The absolute peak values of footing rotations were summed up to get the cumulative footing rotation. Rotations smaller than the threshold were not considered as these values may not cause any residual settlement or uplift. The threshold rotation was assumed as 1 mrad in this case. As the footing rocks, the contact area

between the soil and footing reduces and leads to limited localized bearing failure at the edge of footing that in turn leads to progressive settlement. Previous literature suggested that the settlement is significant if A/A_c ratio is small. If the A/A_c ratio is large (e.g., > 15), the settlements tend to be very small. Figure 3.13 shows that the settlement is always less than $0.01L$ even at cumulative footing rotations of 250 mrad. Such small settlements would be deemed acceptable during a major seismic event. The w/L vs. cumulative footing rotation is compared to previous centrifuge tests of rocking foundation on sand and clay by Deng et al. (2012a) and Hakhamaneshi (2014) in Figure 3.13. The residual settlements of the present tests on cohesive soil are similar to results of the centrifuge tests on clay for the same A/A_c group (Figure 3.13), while the residual settlements are much less on cohesive soil than on sand even for same A/A_c group. The similarity in the relationships for sand and clay indicate that the effect of changing soil type and scale of test can be reasonably accounted for through the effect on A/A_c.
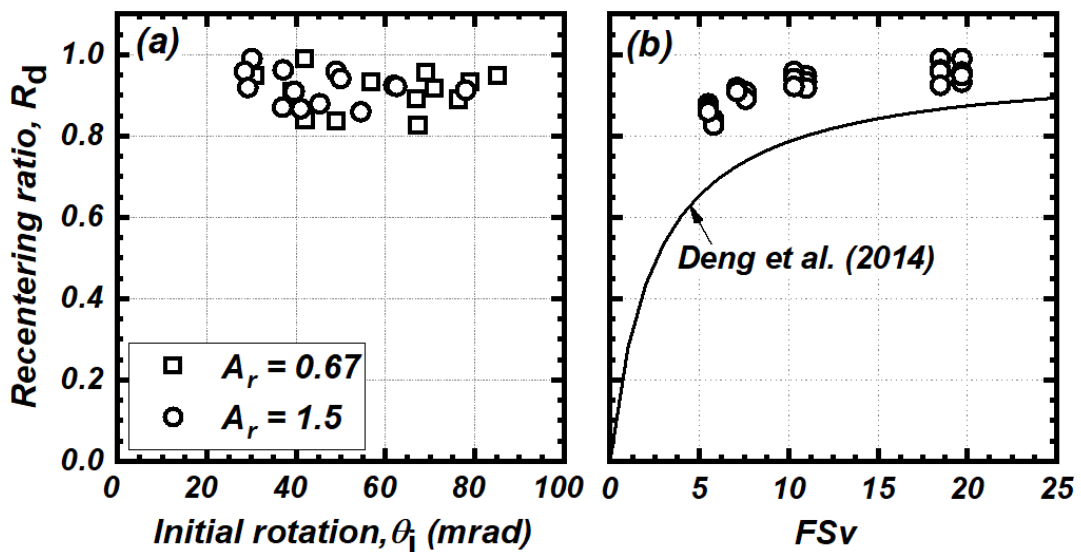
Figure 3.14. (a) Recentering ratio vs. initial rotation and (b) recentering ratio vs. *FSv*. The empirical curve obtained from Deng et al. (2014) was for rocking foundation in sand subjected to dynamic shaking.

54

Deng et al. (2014) quantified the recentering ability of a rocking system by the term "displacement recentering ratio (R_d)" which is defined as

$$R_d = 1 - \frac{\theta_{res}}{\theta_i} \qquad\qquad [3.6]$$

where θ_{res}= residual (or permanent) rotation of footing after structure comes to rest. An R_d value of 1.0 indicates a perfectly recentering system ($\theta_{res} = 0$).

Figure 3.14a depicts the variation of R_d with θ_i for all test. As can be seen from Figure 3.14a, for θ_i between 20 to 85 mrad, R_d is relatively high for all the tests irrespective of A_r of the foundation, indicating a good potential for the structure to return back to it's initial (center) position. Even though the maximum rotation (about 85 mrad) is much greater than allowable maximum rotation by current design codes (which is typically 20 mrad), rocking foundations possess a significant recentering ability.

Figure 3.14b shows the relationship between R_d and FSv along with the empirical trend developed by Deng et al. (2014) footings on sand. It appears that R_d increases with the FSv value and eventually converges to a constant value (≈ 1) which means the footing perfectly re-centers when FSv is very large. The R_d vs. FSv relationship of tests on clay follows the similar trend as the trend on sand. However, R_d on clay is greater than on sand, indicating a better recentering ability.

3.3.5 Effects of Rocking Foundation on Soil Properties

Figure 3.15 shows the distributions of ρ_t and s_u before and after all tests at Station 1. The increase in both ρ_t and s_u of soil is significant. It is seen that ρ_t of soil before tests was about 1.90 Mg/m^3 and was increased to about 1.92 Mg/m^3 after four tests at Station 1 (Figure 3.15). The average s_u of soil from UCS tests before the test was about 70 kPa, which was increased to

average s_u of 80 kPa at a shallow depth (<0.45 m) at Station 1 (Figure 3.15a). The increased

density and shear strength of soil after the experiments should be attributed to the soil

densification during the experiment. However, we have not observed obvious changes in either

ρ_t or s_u for soils deeper than approximately 0.45 m. The depth beneath the footing where the

increase in ρ_t and s_u was observed may be related to the influenced zone of the critical contact

area (refer to Figures 3.4b and 3.15). It is noted the depth where the soil properties changed

significantly equals approximately $2L_c$ of the case with the least FSv (L_c = 0.26 m in such case).
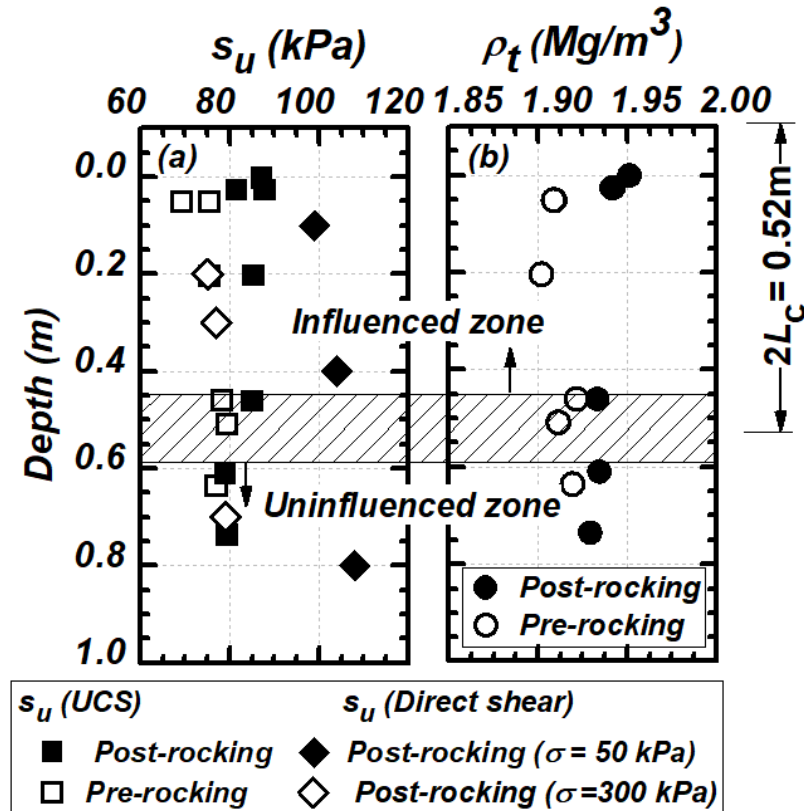
Figure 3.15. Soil properties before and after all tests in Station 1: (a) shear strength and (b) total

density. L_c= critical contact length of footing with the least FSv.

3.4   Conclusions

The nonlinear dynamic behaviour of a soil-footing-column-structure system designed with a rocking foundation was investigated using snap-back tests at a cohesive soil site. The following conclusions may be drawn.

1. The predicted rocking moment capacity correlated very well with the observed values. The footing rotation required to mobilize the moment capacity of footing on clay was investigated. An estimate of $g = 0.012$ rad appears reasonable.

2. The shear capacity of footing did not significantly change with the number of trials or amplitude of horizontal displacement. The maximum sliding observed was about 0.18% of footing length, which is very small in general. The shear capacity considering the soil-footing interface shear resistance underestimated the measured shear capacity by 26% and the shear capacity considering statics equilibrium correlated well with the measured values.

3. The damping ratio observed during the oscillations after snap-back release of the shallow foundations ranged from 8 to 30%. The damping ratio was insensitive to the amplitude of rotation when footing rotation exceeded 20 mrad, despite of scattered data. The trend of damping ratio with footing rotation on clay was observed slightly higher than footing on sand.

4. Average measured period of the rocking system was elongated by approximately 235% comparing with the period of fixed-base structure. The fundamental periods of the rocking system increase approximately linearly, as the initial FSv decreases.

5. The residual settlement was less than 1% of the length of the foundation even at a cumulative footing rotation of 250 mrad. As A/A_c increases, the residual settlement of the

footing reduces significantly. The settlement of footing on clay was much less than the values on sand given the similar A/A_c range.

6. The rocking system exhibited a good recentering ability. The recentering ability of a rocking system on clay is slightly better than on sand.

7. An increase in the density and shear strength beneath the critical contact area due to rocking cycles was observed. The depth of influence zone, where the soil properties changed significantly, was approximately $2L_c$.

4. Field Testing of Rocking Foundations in Cohesive Soil: Cyclic Performance and Footing Mechanical Response[2]

Abstract

This paper presents a field test program of a large-scale soil-footing-structure system designed with a rocking foundation in a cohesive soil, to examine the behaviour of the system and to provide case histories for possible performance-based seismic design of foundations. The rocking system was subjected to slow cyclic loadings at various drift ratios up to 7%. Twenty-four tests were conducted for foundations with varying initial factors of safety against the bearing failure, loading directions, rotation amplitudes, and embedment. A geotechnical investigation was carried out to determine soil properties before and after the experiments. The system performance indices, such as damping, stiffness, settlement and re-centering capability, were quantified and compared to the published literature. Field test results showed that the strength and unit weight of soils at footing edges were increased due to rocking, for the present cohesive soil. The rocking moment capacity increased slightly with the increasing soil strength. An empirical equation for the secant stiffness was developed. The rocking system on the cohesive soil exhibited superior performance in terms of small residual settlement and large re-centering capability. Footing's mechanical response was quantified using strain gauge readings. The footing remained elastic in tension; the transient soil-footing contact areas were estimated with strain gauges and they agreed very well with the measured or calculated contact areas.

4.1 Introduction

The dynamic performance of rocking shallow foundations has been investigated experimentally using centrifuge tests (e.g. Gajan et al. 2005; Deng and Kutter 2012; Ko et al. 2018a and 2018b; Pelekis et al. 2018), shake table tests (Paolucci et al. 2008; Shirato et al. 2008; Espinoza and Mahin 2008), and reduced-scale laboratory tests (Drosos et al. 2012; Anastasopoulos et al. 2012). In general it is suggested that rocking foundations can reduce the peak and residual deck drift and lower the demand on the column base shear and moment capacities, when compared to the principle of fixed-base foundation design. Previous studies have suggested that the soil-footing contact area is a crucial factor that restrains the seismic load demand on the superstructure. They have also shown that the performance, in terms of moment capacity and settlement, is strongly correlated to the ratio of the critical contact area to footing area. An improved estimate or direct observation of the contact area enhances not only the reliability of quantifying rocking foundation performance but also the confidence level in the use of rocking system, despite that there is a lack of research in the direct measurement or estimation of the contact area. Ko et al. (2018) studied the approximate distribution of soil reaction stress under the rocking foundation in sand using centrifuge modeling, but the contact area was not derived from the measurement.

The published literature has been predominantly focused on the performance of model foundations in sandy soils. There are only several studies of rocking foundations embedded in cohesive soils, such as centrifuge model tests (Hakhamaneshi 2014; Rosebrook 2001) and field tests (Algie 2011; Phipps 2013). Algie (2011) conducted a series of field experiment on shallow foundations, excited by an eccentric mass shaker mounted on top of the structures; nevertheless, the footing rotation was notably small (<0.8%) in Algie (2011) such that the nonlinear soil-footing interaction was barely observed. Phipps (2013) investigated a shallow footing in clay

under free vibration, quasi-static cyclic loading, and dynamic forced vibration test. The past field tests did not characterize the soil-footing behaviour such as damping, re-centering ratio, or residual settlement. In summary, a comprehensive characterization of rocking foundations in cohesive soils, particularly using field tests, and an investigation of footing and underlying soil response are imperatively needed for the further design principle (such as the performance-based design, Deng et al. 2014) of rocking foundations in cohesive soils. Because it is difficult to conduct dynamic loading tests in the field, an alternative is to use slow cyclic (i.e., quasi-static) loading. Gajan et al. (2005) conducted centrifuge testing on rocking foundation subjected to both slow cyclic and dynamic loading and concluded that slow cyclic test is appropriate for characterizing the moment-rotation behavior of a shallow foundation. Slow cyclic loadings for the performance assessment of structures are also recommended by ATC-24 (ATC 1992) and FEMA-461 (FEMA 2007).

In this study, a series of field tests of large-scale rocking shallow foundations on a natural cohesive soil was carried out. Slow cyclic loading in the lateral direction was applied. The first objective was to investigate the nonlinear soil-footing interaction for rocking foundations in cohesive soils, and the second was to study the effects of rocking on underlying soil properties and to examine the footing internal behaviour that provides an alternative approach to understand the progressive soil-footing contact area. Twenty-four tests were conducted for foundations with varying initial factors of safety against the bearing failure, loading directions, rotation amplitudes, and embedment. In-situ investigation and laboratory tests were performed to provide the pre- and post-rocking soil properties. The system performance indices, such as moment capacity, damping, stiffness, settlement and re-centering capability, were quantified and compared to the published literature. The changes in soil properties and the footing mechanical response were characterized.

61

The transient soil-footing contact areas were estimated using the strain gauge readings and compared to the measured or calculated values.
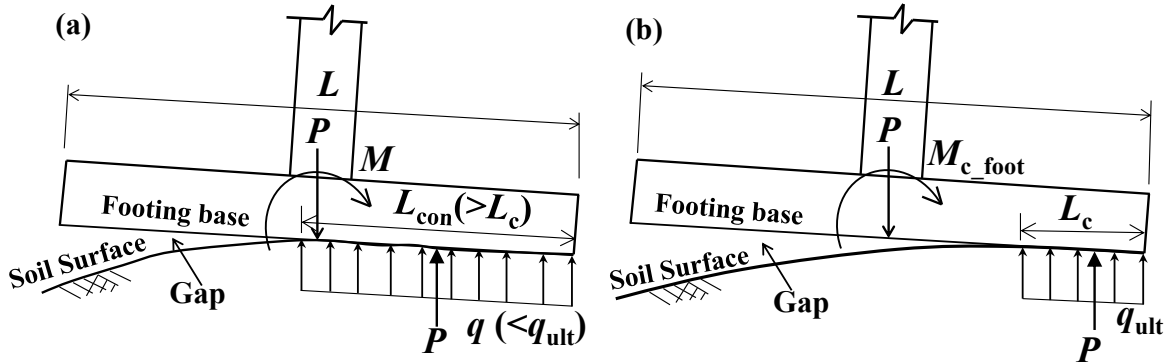
Figure 4.1 A schematic diagram for the concepts of foundation uplift (gap), transient contact length (L_{con}) and critical contact length (L_c): (a) foundation before reaching the moment capacity and (b) foundation at its moment capacity.

4.1.1 Rocking Moment Capacity and Contact Length

Figure 4.1 shows the soil-footing contact areas and the average soil reaction at two rotational stages, where L_{con} is the transient soil-footing contact length before a full mobilization of the soil's bearing capacity and L_c is the critical contact length when the underlying soil is at the verge of bearing failure. The rocking moment capacity (M_{c_foot}) when a footing rests on a critical area can be defined as:

$$M_{c\_foot} = \frac{PL}{2}\left(1 - \frac{L_c}{L}\right) \qquad [4.1]$$

where P is the total vertical load and L is the length of the footing along the direction of cyclic loading (Figure 4.1), and L_c can be estimated as:

$$L_c = \frac{P}{q_{ult}B} \qquad [4.2]$$

where B is the width of footing along the axis of rocking (note that B can be less or greater than L), and q_{ult} is the bearing capacity of soil under the critical contact area. As q_{ult} also depends on the aspect ratio L_c/B, an iterative process may be required to slightly improve the L_c estimation (Deng and Kutter 2012).
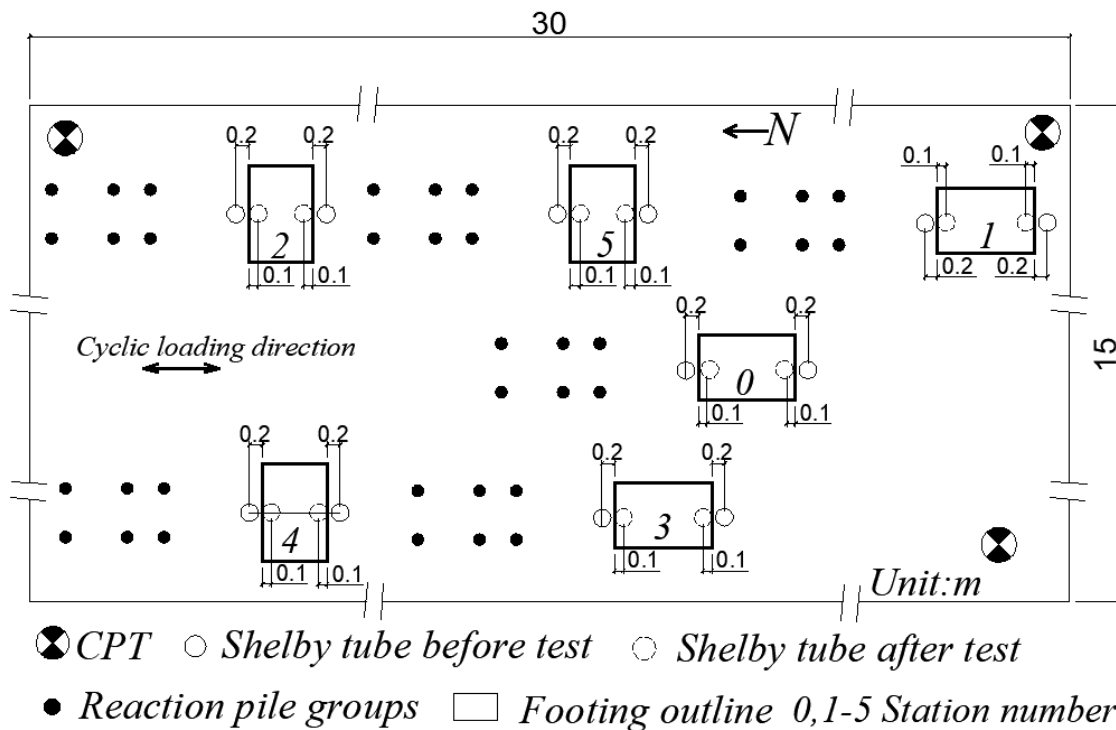
Figure 4.2 Field test layout with CPT and Shelby tube sampling locations.

4.2 Experimental Program

4.2.1 Pre- and Post-rocking Site Investigation

Figure 4.2 shows the layout of the test site located at the University of Alberta south campus farm, Edmonton, Canada. This site is composed of a layer of surface soil, underlain by cohesive soil. The soils at this site are mainly glaciolacustrine sediments as part of the Glacial Lake Edmonton. The program of site investigation included cone penetration tests (CPT), Shelby tube borehole sampling before and after field tests, and laboratory tests of undisturbed Shelby tube

samples. Laboratory test program was carried out to determine the unconfined compressive strength (UCS), undrained shear strength (s_u) using direct shear under various normal stresses, Atterberg limits, and physical properties. Three CPTs were conducted on the test site and four Shelby tube boreholes of 7.5 cm diameter were drilled at each footing station and soil samples were obtained. Out of four Shelby tube samples at each station, two were taken from just outside of footing to provide pre-rocking soils, and two inside the footing area after the tests. Figure 4.2 shows the layout of the CPT and Shelby tube sampling boreholes. The depth of CPT tests was 4.0 m that is considered sufficiently deep for the footing dimension in the present study. Shelby tube samples were obtained manually using a string of drill rod mounted to a mini crane, as deep as 1.0 m from the footing base.
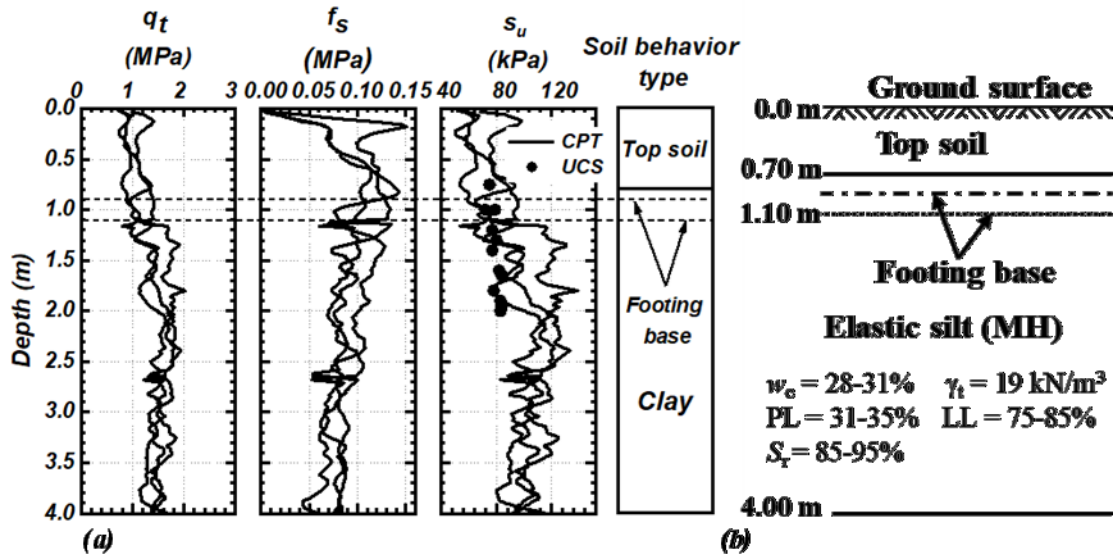
Figure 4.3. (a) CPT profile of test site with shear strengths from UCS tests, and (b) site stratigraphy and lab test results.

Figure 4.3a shows the tip resistance q_t, sleeve resistance f_s, and s_u. The strength s_u is estimated from CPT results using a cone factor of 14 (Robertson and Cabal 2012) based on prior experience with this site. The value of s_u is about 70 to 85 kPa to the depth 1 m from the footing

base. The in-situ moisture content (w = 30% on average) was close to or less than the plastic limit. The degree of saturation (S_r) ranged from 85% to 95% as shown in Figure 4.3b. Based on Unified Soil Classification System, the soil at the site can be classified as elastic silt (MH). The strength of undisturbed samples was measured using the unconfined compressive tests and direct shear tests under normal stresses ranging from 0 to 300 kPa. The direct shear test was performed without a membrane at a displacement rate of 1 mm/min, which is within the range of rate for undrained shearing (Liu and Evett, 1997). It is apparent that s_u from laboratory test results agree with the in-situ results (Figure 4.3a). The value of s_u from direct shear tests ranged from 50 to 80 kPa under zero normal stress as shown in Figure 4.4. At lower S_r (< 90%), the change in total stress may be taken by the effective stress and thus s_u increased with the applied normal stress. However, when the normal stress exceeded 200 kPa, s_u remained constant irrespective of the magnitude of normal stress (Figure 4.4), because the change in effective stress is not significant as S_r approaches 100%.
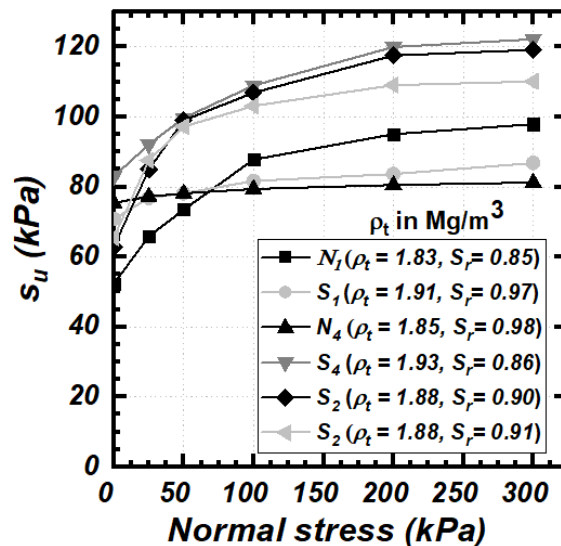
Figure 4.4. Strength of soil from direct shear tests under different normal stresses. Note: N and S represent North and South edge of footing; the number with N and S represents the footing station.

4.2.2 Design of Rocking Foundation System

The rocking foundation system consisted of a rectangular reinforced-concrete (RC) spread footing of 1.5 m by 1.0 m, a steel tubular column, and a varying number of RC slabs on the column used as the superstructure weight. The system is designed to simulate a pier from a generic highway overcrossing bridge (Figure 4.5). In order to avoid the complexities of system boundary conditions (such as a bridge with multiple spans), an idealized single-degree-of-freedom system supported by an isolated footing was considered. The footing was rested on the ground surface or embedded. A square steel tube (0.2 m by 0.2 m outer dimension, 12.7 mm wall thickness) is used as a column and designed for axial load, and bending and torsional moment. The rigidity (EI) of the column is 6.444 MN-m^2. The first yield moment of the column (113 kN-m) was designed to be greater than M_{c_foot} to enable rocking foundations.
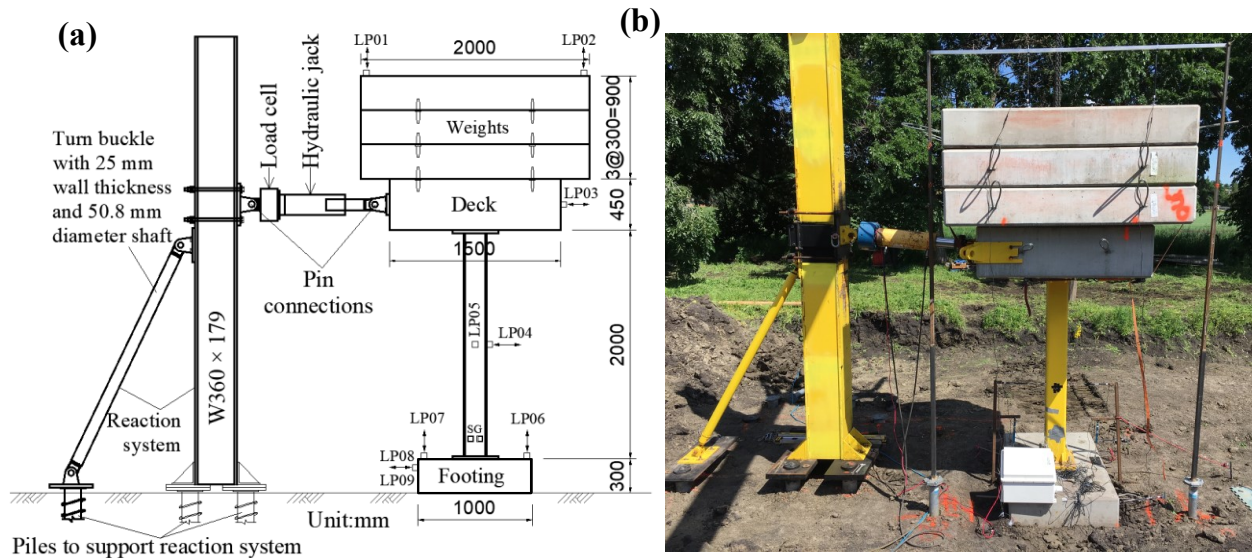
Figure 4.5. Setup of surface soil-footing-structure system: (a) drawing and (b) photo of test TS14.

The foundation design considered both the geotechnical capacity and structural reinforcement. The geotechnical design was the calculation of bearing capacity (CFEM 2006) to determine the footing dimension. In order to achieve various initial factors of safety (FSv) against the bearing failure, additional vertical loads from concrete slabs were added to the superstructure. Consequently, the footing was 1.5 m long, 1.0 m wide and 0.3 m thick. The shallow foundations had an initial FSv ranging from 4 to 25.
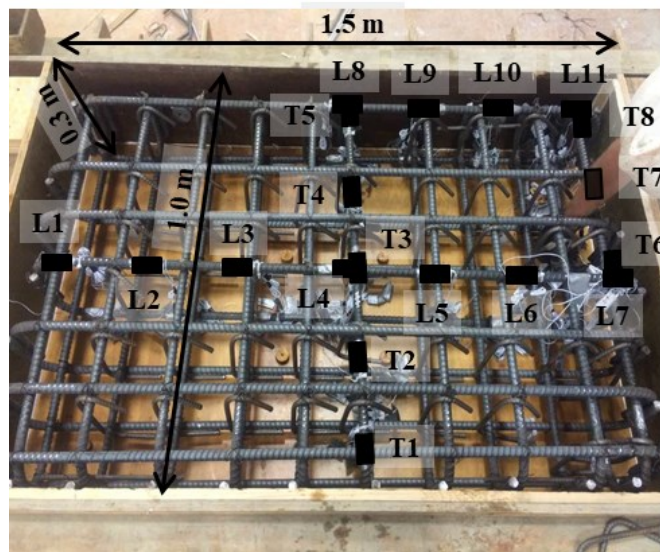
Figure 4.6. Reinforcement of the footing and locations of axial strain gauges stations.

Figure 4.6 shows the design of the footing reinforcement. The concrete for the footing slab had a compressive yield strength (f_c) of 60 MPa. The reinforcement ratio (ρ_{st}, ratio of the steel area to the gross cross-sectional area) required for the footing was calculated by taking into the shear force and bending moment acting in the footing according to the provision of CSA A23.3-14 (CSA 2014). The maximum bending moment in both directions was computed at critical sections of the footing that is considered as a cantilever beam. The rebar area is then computed for a rectangular section of width B or L, depending on the direction under consideration. The minimum ρ_{st} required for a concrete footing is 0.2% (CSA 2014). The as-built

ρ_{st} was about 6% in both directions, in order to limit the tensile strain in concrete within 100 $\mu\varepsilon$ approximately (CSA 2014) and to preclude tensile cracks in concrete during the cyclic loading. The longitudinal reinforcing was 7D20 bars top and bottom and the transverse reinforcement was 10D20 spaced at about 150 mm center to center (Figure 4.6). Single legged stirrups of D10 bars were used at an interval of about 150 mm as the shear reinforcement.

4.2.3   Instrumentation

Nine linear potentiometers of 200 mm stroke were used to measure the vertical and horizontal movement of the footing and deck. Potentiometers were attached to a steel frame that was anchored into the ground; the frame was not affected by the rocking system throughout the tests. A load cell was used to measure the force applied at the connection of the hydraulic jack and concrete deck (Figure 4.5); additionally, two full-bridge SG stations were attached at the base of column to measure the bending moment and shear force, respectively. All instruments were calibrated prior to the field test. The footing was intensively instrumented with SGs. Thirty-eight strain gauges were attached onto the top and bottom rebars of the footing. Figure 4.6 shows the locations of the SG stations that were wired to form full Wheatstone bridges. Three protective layers of coatings were applied: epoxy, thin rubber, and thick aluminum foil. The edge of the aluminum foil tape was sealed with rubber coating to prevent cement paste from entering the circuit. Due to the protective measures, only a few SGs were damaged during the entire course.

4.2.4   Test Setup and Cyclic Load Pattern

Figure 4.5a shows the test system setup with the reaction frame and hydraulic jack. The foundation was embedded in the clay after removing the top soil. In order to preclude the interaction between adjacent stations, the minimum spacing between two stations was kept more than 3 m (i.e. greater than 2L). The experimental program was designed so that the concrete deck

would be subjected to lateral cyclic loading using a double-hinged hydraulic jack mounted to the reaction frame (Figure 4.5b). The two hinges ensure that any unwanted moment or vertical force is precluded. The reaction column was supported by groups of screw micropiles and an inclined strut. The measured movement of the reaction system during the testing was less than 3 % of the drift of testing models.
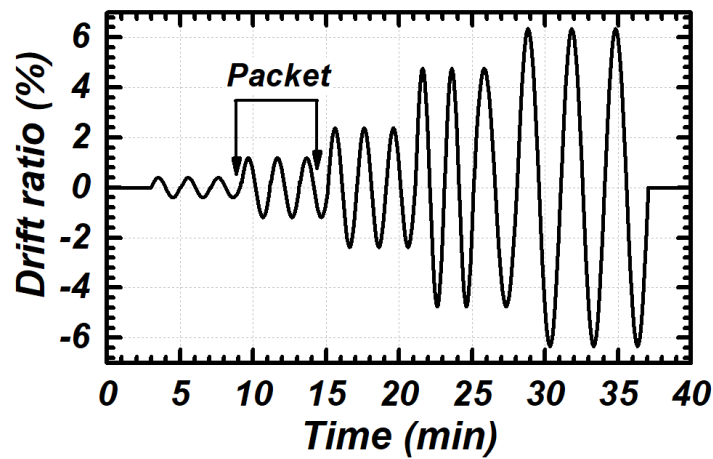
Figure 4.7. Typical histories of deck drift ratio. This is for tests at Station 4.

Cyclic loadings were carried out following the displacement-controlled method. The loading system was designed to produce rotational displacements to induce footing uplift on both sides as the load was reversed. The point of lateral load is 2.525 m above from the footing base. The cyclic loading consists of 4 to 5 packets, each of which contains 3 to 4 cycles of the same displacement amplitude. The drift ratio is defined as the ratio of deck's lateral displacement to the height between the footing base and deck. The maximum drift ratio was about 7%. The drift time histories are shown as the sinusoidal cycles (Figure 4.7). The amplitude, number of cycles and frequency may vary slightly, but they should have negligible effects on the test outcome. The average period of the cyclic loading was about 140 s that is sufficiently long to avoid the generation of an inertia force.

69

Table 4.1. Field test matrix

Station	Test ID	*Initial FSv*	L/L_c	D (m)	M_{c_foot} (kN-m)	A_r [1]
0	LS01	23.4	20.9	0	25.4	1.5
	LS02	13.0	11.8	0	44	1.5
	LS03	9.0	8.3	0	61.2	1.5
	LS04	6.9	6.4	0	76.9	1.5
1	LS11	19.7	18.4	0	25.2	1.5
	LS12	11.0	10.4	0	43.3	1.5
	LS13	7.6	7.3	0	59.7	1.5
	LS14	5.8	5.7	0	74.5	1.5
2	TS11	18.5	18.1	0	17.1	0.67
	TS12	10.3	10.2	0	29.7	0.67
	TS13	7.1	7.1	0	41.6	0.67
	TS14	5.5	5.5	0	52.6	0.67
3	LE11	20.3	23.9	0.5	29.1	1.5
	LE12	12.0	16.8	0.5	47.4	1.5
	LE13	8.4	9.9	0.5	64.3	1.5
	LE14	6.2	6.9	0.5	79.8	1.5
4	TE11	17.0	23.1	0.5	19.6	0.67
	TE12	10.1	15.1	0.5	32.2	0.67
	TE13	7.4	9.6	0.5	44.0	0.67
	TE14	5.3	6.3	0.5	55.1	0.67
5	TS21	17.2	17.6	0	17.0	0.67
	TS22	9.6	9.9	0	29.6	0.67
	TS23	6.7	6.9	0	41.3	0.67
	TS24	5.1	5.3	0	52.1	0.67

Note: 1. $A_r = L/B$, where L is the length along the direction of cyclic loading and B is the length perpendicular to the direction of loading.

The lateral load measured from the load cell, confirmed by the SG readings at the column base, was used to calculate the applied rocking moment on the footing; the P-Δ effect was also considered when calculating the moment. The values of FSv, embedded depth (D), and loading direction were systematically varied during the field tests. Table 4.1 outlines the key parameters of the field tests including FSv, D, calculated M_{c_foot}, and footing aspect ratio A_r (defined as L/B).

4.3   Test Results: Performance of Rocking Foundation

This section presents the effects of rocking foundations on soil properties and quantifies the performance of rocking foundations subjected to cyclic loading.

4.3.1   Effects of Rocking on Soil Properties

Figure 4.8 shows the measured total unit weight (γ_t) and s_u of soil beneath the footing before and after the tests at Stations 1 and 2. It is seen that the average γ_t before tests was about 19.0 kN/m^3 and then was increased to about 19.8 kN/m^3 after four tests at Stations 1 and 2 (Figure 4.8). The average s_u (from UCS tests) of soil before the test was about 75 kPa, and it was increased to an average of 88 kPa at shallow depth (<0.5 m) at Stations 1 and 2. In fact a similar increase in both γ_t and s_u of soil is also pronounced at all other stations (Figure 4.2). On the other hand, the changes in either γ_t or s_u for soils deeper than approximately 0.5 m was not obviously noticeable. The depth beneath the footing where the increase in γ_t and s_u was observed may be related to the zone influenced (considering a stress bulb) by the vertical stress on the soil-footing contact area. The depth of influenced zone in the present study is approximately equal to two times L_c (where L_c = 0.26 m) for the case with the least A/A_c (i.e. greatest L_c) at all stations (Figure 4.8). The normal stress on the critical contact area increased γ_t and s_u of underlying soil within the influenced zone and induced the settlement. Note that the soil under the footing has S_r of 85 to

71

98%; should the soil be saturated, the strength increment may be smaller and the footing settlement may be further reduced.
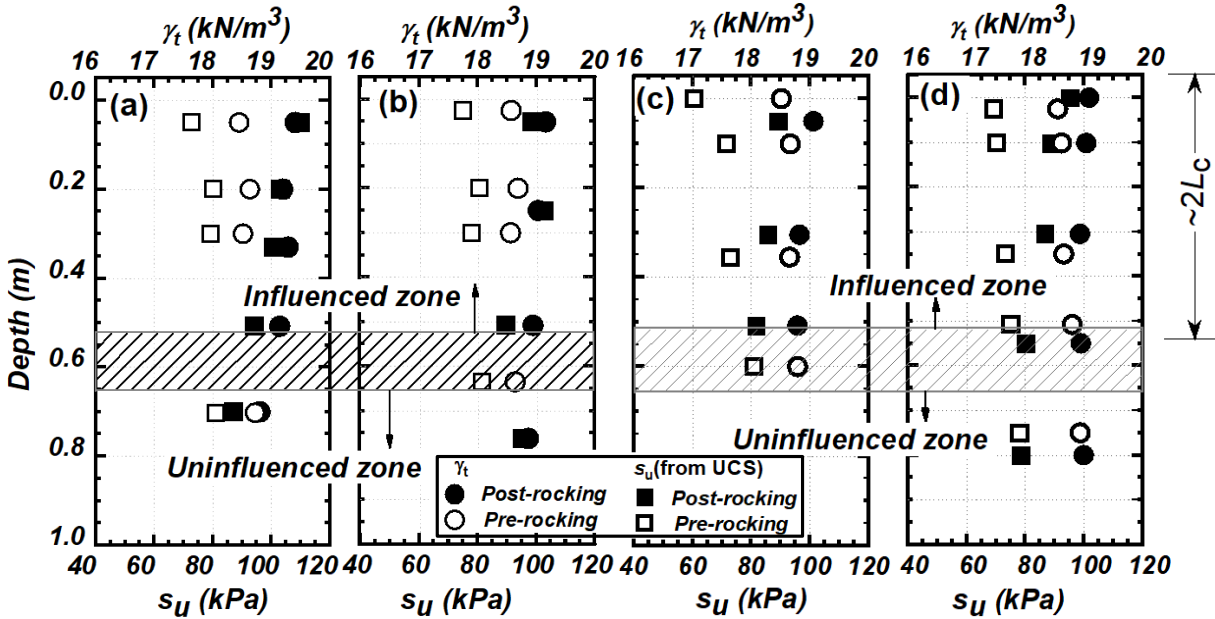
Figure 4.8. Unit weight and shear strength of Shelby tube samples before and after the test at: (a) Station 1: North, (b) Station 1: South, (c) Station 2: South, and (d) Station 2: North.

4.3.2 Moment-Rotation and Settlement-Sliding Correlations

Figure 4.9 shows the typical rocking moment vs. footing rotation (θ), shear force vs. sliding, settlement (w) vs. footing rotation, and settlement (w) vs. sliding relationships at the base center of the footing, using the test LS11 as an example. The rocking moment vs. rotation loops display a "pinched", S-shaped hysteresis as shown in Figure 4.9a. The dashes lines in Figure 4.9a show the estimated M_{c_foot} using the initial FSv based on the initial s_u values. It is seen that the moment vs. rotation relationship is highly nonlinear and encloses a large area, indicating that a significant amount of energy has been dissipated due to the soil-footing interaction (Figure 4.9a).

The rocking moment vs. rotation curves showed that a rocking foundation on cohesive soils has non-degrading M_{c_foot}, which was also observed for foundations in sands; in fact, M_{c_foot}

72

showed an increasing trend with the number of cycles, possibly due to the strengthening of soils and the penetration of the footing edge. The observed M_{c_foot} matched the predicted M_{c_foot} very well. The moment vs. rotation curves shows a sign of directivity, meaning that the maximum moment at the positive side was slightly greater than the counterpart at the negative side. The directivity was possibly caused by the penetration of footing edge into the ground at the positive side. The penetration provided a lateral soil resistance (in addition to the vertical resistance q_{ult}) to the footing, reduced the footing sliding (see Figure 4.9b), and increased the maximum moment resistance.
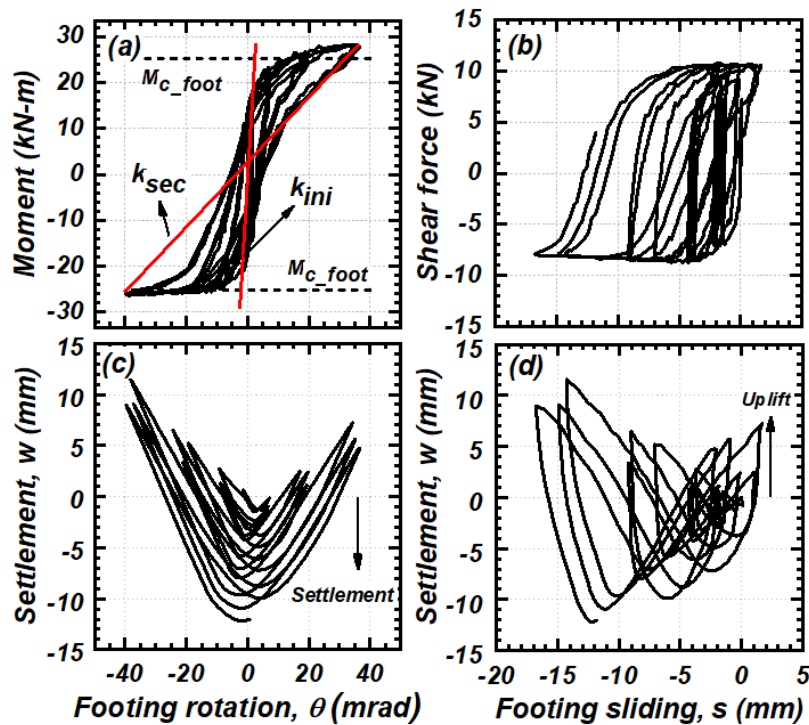
Figure 4.9. Results of test LS11: (a) moment vs. rotation, (b) shear force vs. footing sliding, (c) settlement vs. footing rotation, and (d) settlement vs. sliding.

The shear force vs. sliding curves (Figure 4.9b) show a negligible degradation in the horizontal shear capacity or in the stiffness with the number of cycles or amplitude of lateral

73

displacement. The amplitude of sliding increases with the increasing amplitude of rotation or number of cycles. However, sliding was also observed to remain relatively unchanged until the shear capacity was reached, at which point the footing began to slide. The amplitude of sliding increases with the amplitude of rotation or number of loading cycles. The sliding behavior of the footing showed a biased movement toward one side which is attributed to the initial direction of the subjected cyclic displacement. The sliding appeared to be significant in this test LS11 on surface; however, sliding could be effectively mitigated with embedment or shear keys.

The settlement (w) vs. footing rotation curve shown in Figures 4.9c illustrates the re-entering behaviour for rocking foundations on the stiff clay. The troughs of the curves show the amount of permanent vertical deformation accumulated with cycles. The residual settlement (w_r) was observed to increase with the increasing amplitude or number of cycles.

The formation of a gap on one side of the footing results in the yielding of the soil on the other side of the footing and a decreasing L_{con}, when the rotation is significantly large (Figure 4.9c and 9d). These gaps, in addition to the soil yielding under a changing contact area, contributed to the nonlinear moment-rotation relationship and the degradation of rotational stiffness. The coupling behaviour of the sliding and uplift of the footing and the closure of gap upon loading can be seen in the settlement-sliding relationship in Figure 4.9d.

4.3.3 Effect of Footing Aspect Ratio and Embedment

Figure 4.10 shows the moment vs. rotation and normalized settlement vs. rotation relationship at the base center point of the footing for three tests (LE11, TS11 and TE11) to illustrate the effects of embedment depth D and footing aspect ratio A_r. The footing with higher A_r (LS11 in Figure 4.9 and LE11 in Figure 4.10a) exhibited higher initial rocking stiffness (k_{ini}) and M_{c_foot} than the footing with lower A_r (TS11 and TE11 Figure 4.10b and 4.10c). This is reasonable because k_{ini} is

proportional to L^3 (FEMA 2000) and M_{c_foot} is proportional to L. The moment vs. rotation relations with higher A_r (LS11 and LE11 in Figure 4.10) display more pronounced S-shaped hysteresis. On the contrary, the hysteresis loops of the tests TS11 (Figure 4.10b) and TE11 (Figure 4.10c) with smaller A_r are less pinched and not S-shaped hysteresis curves and the unloading stiffness is nearly linear.
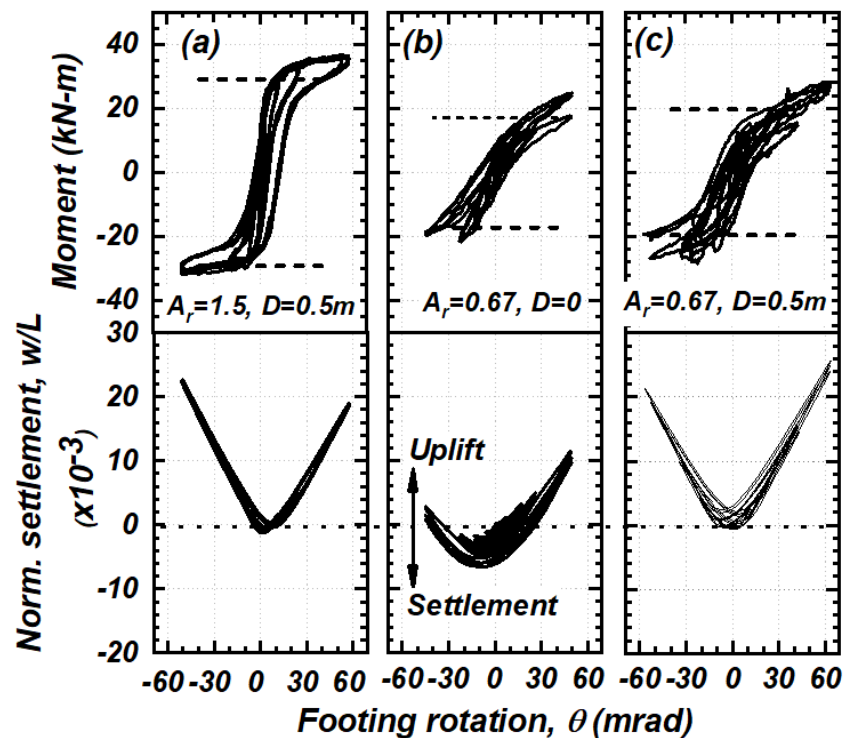
Figure 4.10. Relationship between moment, settlement and rotation for different embedded depth and aspect ratios (a) LE11, (b) TS11, and (c) TE11.

The embedded footing exhibited more uplift and less permanent settlement (as shown in Figures 4.10a and 4.10c). For all field tests, the settlement of embedded footings was noticeably less than the surface footings irrespective of A_r. This was attributed to the backfilled soil flowing into the gap formed during rocking or the dilatancy of the soil (Antonellis et al. 2015; Hakhamaneshi and Kutter 2016).

4.3.4   Measured and Calculated Moment Capacity

Figure 4.11 shows the results of measured M_{c_foot} vs. A/A_c, where M_{c_foot} is the maximum measured moment of all packets for each test ID. In Figure 4.11, M_{c_foot} is normalized by $PL/2$, where $PL/2$ represents the rocking moment to mobilize the uplift on a rigid interface, to eliminate the effect of weight and footing dimension. The solid curve in Figure 4.11 is the calculated M_{c_foot} derived from Equation 4.1.
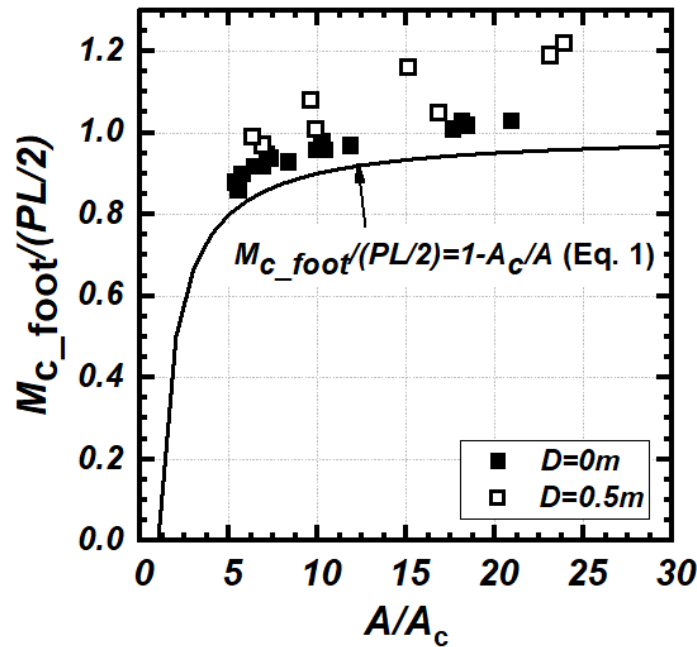
Figure 4.11. Measured and theoretical normalized M_{c_foot} vs. A/A_c.

It is shown that the measured M_{c_foot} follows the same trend as the calculated M_{c_foot} irrespective of FS_V, D and A_r, which indicates that M_{c_foot} can be reasonably estimated in cohesive soils. Moreover, the measured M_{c_foot}, particularly for the embedded footings, are greater than the estimated values. We think that a primary reason for the discrepancy is the increasing s_u underneath the footing as more cycles were applied. This increased A/A_c and should have elevated the estimated $M_{c\_foot}/(PL/2)$ curve closer to 1.0; however, such s_u increment was

not considered in the estimation based on Equation 4.1. Other reasons for the discrepancy may be the side friction on footing edges and passive earth pressure on the footing, which both make the measured M_{c_foot} greater than the estimation.
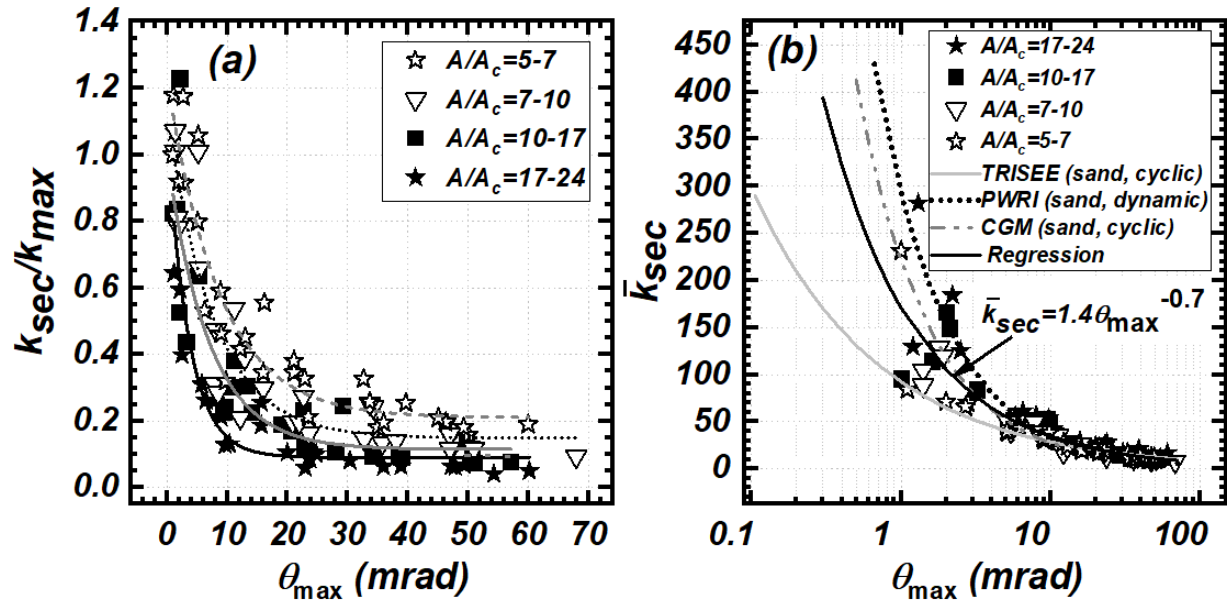
Figure 4.12. (a) Rotational stiffness degradation versus maximum footing rotation and (b) normalized rocking stiffness degradation compared to results from the literature (Chatzigogos et al. 2011). Note: $\overline{k}_{sec}$ is defined in Equation 4.4.

4.3.5   Stiffness Degradation

Figure 4.12a shows the progress of secant stiffness ($k_{sec} = M_{max}/\theta_{max}$) vs. the maximum footing rotation (θ_{max}). In order to develop a rotational stiffness reduction trend that occurs as results of foundation rocking, k_{sec} was normalized by a theoretical maximum stiffness (k_{max}) at each rotational increment. The value of θ_{max} is equal to the maximum footing rotation at each drift packet applied to the deck. The theoretical maximum stiffness (k_{max}) was estimated using Equation 4.3 (Gazetas 1991):

$$k_{max} = \frac{G}{1-\nu} I^{0.75} \left[3 \left(\frac{L}{B} \right)^{0.15} \right] \beta \qquad\qquad [4.3]$$

where G is the shear modulus estimated from s_u and soil plasticity, ν (=0.5) is the Poisson's ratio, I is the area moment of inertia about the centroidal axis of the footing, and β is an embedment factor (Gazetas 1991).

At the beginning of yielding for the tests with A/A_c ranging from 5 to 7, the measured k_{sec} is around 40% k_{max}; at the largest rotation, k_{sec} is 20% k_{max} (Figure 4.12a). The rotational stiffness at θ_{max} of the tests with A/A_c ranging from 17 to 24 is about 6% k_{max}. The results show that k_{sec}/k_{max} ratio decreases as A/A_c increases. Figure 4.12a also shows that the rate of k_{sec} degradation is increased as A/A_c increased.

Since the vertical load (P) on the foundation and L are not the same for all tests, the reduction of k_{sec}/k_{ini} is dependent on the value of A/A_c (Figure 4.12a). In order to eliminate the effects of P and L, the normalized stiffness $\bar{k}_{sec}$ can be introduced, as defined in Equation 4.4:

$$\bar{k}_{sec} = \frac{M_{max}}{\theta_{max}PL} = \frac{k_{sec}}{PL} \qquad\qquad [4.4]$$

where M_{max} is the maximum rocking moment at θ_{max} during a half load cycle. Figure 4.12b shows $\bar{k}_{sec}$ vs. θ_{max} curves for all tests. After the normalization, it is observed that the $\bar{k}_{sec}$ distribution becomes much more condensed and is almost unique at greater θ_{max} regardless of the A/A_c ratio or loading direction. This unique relationship of $\bar{k}_{sec}$ vs. θ_{max} is important when developing the design principle of rocking foundation, because the secant stiffness is a critical index in the displacement-based design for a rocking foundation. The best estimate of $\bar{k}_{sec}$ vs. θ_{max} correlation of the present study is obtained as follows:

$$\bar{k}_{sec} = 1.4\theta_{max}^{-0.7} \qquad\qquad [4.5]$$

which may be practically useful in predicting the equivalent period of the soil-footing-structure system. The present $\bar{k}_{sec}$ vs. θ_{max} results are compared to previous results from TRISEE, CGM and PWRI programs (as summarized in Chatzigogos et al. 2011). The TRISEE and CGM programs consisted of cyclic loading tests of small-scale model footing on sand (Negro et al. 2000) and cyclic loading tests of footing on sand in centrifuge testing (Gajan and Kutter 2008; Deng et al. 2012a) respectively; the PWRI tests comprised of the shaking table test of rocking foundation on sand (Paolucci et al. 2008; Shirato et al. 2008). Figure 4.12b shows that $\bar{k}_{sec}$ from different tests converge to a small bandwidth at relatively large θ_{max} irrespective of soil types and test methods. The stiffness degradation trend from the present field tests lies between k'_{sec} degradation trend of PWRI and TRISEE.

4.3.6 Damping Ratio and Energy Dissipation

The equivalent damping ratio (ξ) during the cyclic loading is calculated using Equation 4.6:

$$\xi = \frac{1}{4\pi}\frac{E_{\text{Diss}}}{\frac{1}{2}M_{max}\theta_{max}} \qquad [4.6]$$

where E_{Diss} is the dissipated energy in a hysteresis cycle (Gajan and Kutter 2008).

Figures 4.13a to 4.13d show the measured ξ vs. θ results to investigate the effect of A/A_c, A_r and D on ξ. The value of ξ is about 8 to 40% for all tests as shown in Figures 13a-13d. It is clearly seen that ξ increases as A/A_c decreases. Embedded footing exhibits slightly greater ξ than the surface footing (Figures 4.13a-4.13d). No significant relationship between A_r and ξ is observed (Figures 4.13a-4.13d). This might be attributed to the skinny moment-rotation hysteretic loops at the higher amplitude of rotation as shown in Figures 4.9-4.10.

The values of ξ are compared to previous experiment results in sand (summarized by Chatzigogos et al. 2011) in Figure 4.13e. A significant scatter is shown for ξ when footing

rotation is greater than 10 mrad except in the case of TRISEE where ξ increases with the increasing rotation. For $\theta > 10$ mrad, ξ ranges from 8 to 40% and shows a constant relation with the amplitude of the imposed rotation.
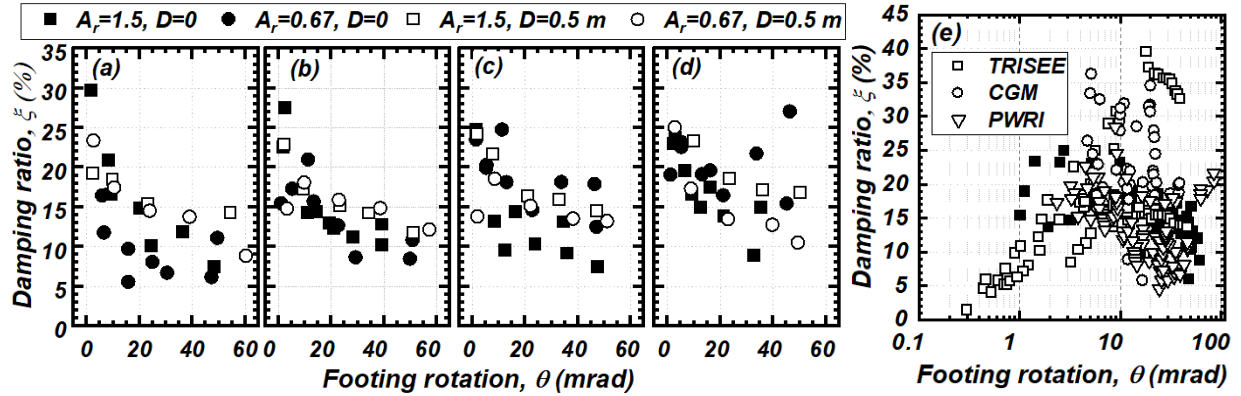
Figure 4.13. (a) Equivalent damping ratio versus amplitude of rotation for all tests with different A/A_c ranges: (a) 17-24, (b) 10-17, (c) 7-10 and (d) 5-7, and (e) equivalent damping ratio versus footing rotation comparison with the results from TRISEE, CGM and PWRI.
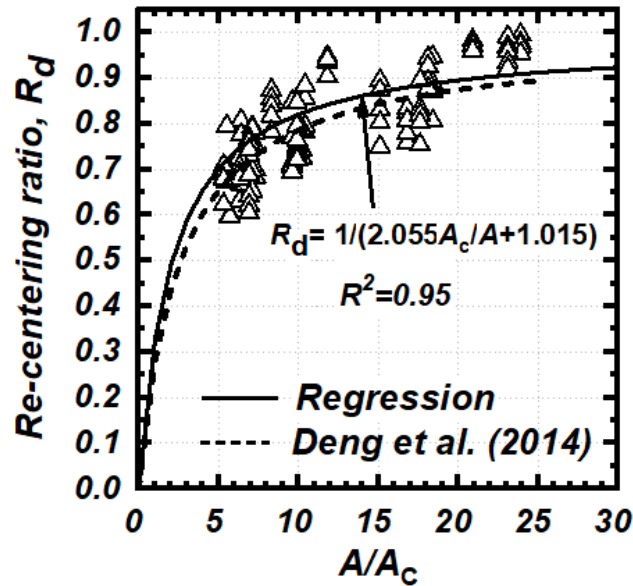
Figure 4.14. Effect of A/A_c on re-centering ratio.

4.3.7 Re-centering Ratio

An ideal soil-structure system should have the ability to re-center at the end of loading. To assess the re-centering performance, Deng et al. (2014) defined the re-centering ratio of rocking foundations as:

$$R_\mathrm{d} = 1 - \frac{\theta_\mathrm{res}}{\theta_\mathrm{max}} \qquad [4.7]$$

where θ_res is the residual foot rotation at zero rocking moment. The re-centering mechanism of a rocking footing is largely a result of the gap closure when the moment is released. An R_d value of 1.0 indicates a perfectly re-centering system ($\theta_\mathrm{res} = 0$).

Figure 4.14 depicts the distribution of R_d vs. A/A_c, since R_d was observed closely related to A/A_c in the present and past research. In the present study, R_d was obtained at zero moment condition after each packet (i.e. three full cycles at a given drift ratio). As shown in Figure 4.14, R_d is relatively high, ranges from 0.6 to 1.0, for all the tests regardless the loading direction. The results imply a good potential for the rocking structure to return to its initial (center) position given a reasonably high FSv in cohesive soils. Note that the re-centering ratio depends on the amplitude of rotation, where R_d tends to decrease as the rotation demand increases. However, for the rectangular footing with A_r 1.5 and 0.66, R_d greater than 65% can be acceptable for Life Safety level performance (ASCE 2014; Hakhamaneshi et al. 2016). This indicates that despite the large θ_max (up to 7%) during the tests, θ_res may still be acceptable, due to the re-centering characteristic of the rocking foundations. The empirical equation of R_d vs. A/A_c curve obtained from the present research is regressed as follows:

$$R_d = \frac{1}{2.055\frac{A_c}{A}+1.015} \qquad [4.8]$$

The equation is deemed appropriate for practical use given that the coefficient of determination (R^2) of Equation 4.8 is 0.95. Figure 4.14 compares the R_d vs. A/A_c curve in the present study to the curve for footings on sand in centrifuge testing (Deng et al. 2014, cyclic loading). It is shown that the curves in clay and sand follow a similar trend. However, R_d in clay is slightly greater than in sand, indicating a slightly better re-centering ability for foundations built in clay.

4.3.8 Residual Settlement

Figures 4.15a to 4.15b show the results of w_r/L vs. cumulative footing rotation (θ_{cum}), where the residual settlement (w_r) was obtained after 4 packets of 3 to 4 cycles of similar drift amplitude to a drift ratio up to 7%. The value of w_r was obtained at zero rotation condition after each cyclic packet. The settlement was calculated for all FSv at each station. The cumulative footing rotation was obtained using the method elaborated in Deng et al. (2012a) and Hakhamaneshi and Kutter (2016). In general, it is shown that the w_r/L vs. θ_{cum} results are approximately linear. The results show that residual settlements can be significant if A/A_c is small. If A/A_c is large (e.g., > 10), w_r appeared to be very small even at θ_{cum} of 400 mrad, which is seldom reached during a strong motion. In addition, it is seen that w_r/L of surface footing is always smaller than 3.0% even at θ_{cum} of 400 mrad (Figure 4.15a). The value of w_r/L of the embedded footing is minimal (< 1%) even under the lowest A/A_c and at θ_{cum} of 350 mrad (Figure 4.15b). This might be attributed to the soil collapsing from the backfill into the gap formed during rocking; the collapsed soil was observed after removing the footing. This is promising for rocking foundations on cohesive soils, since it indicates that the residual settlement may not be a major concern during a real earthquake.

Because w_r/L is shown to be linearly related to θ_{cum}, the dynamic settlement coefficient (C_{sett}) can be defined as $w_r/(L\theta_{cum})$ to provide the best estimates of the measured results. Figures 4.15a and 4.15b show the linear correlations of w/L vs. θ_{cum} as the best estimates of each A/A_c

group and labels the definition of C_{sett}. The fit line (w/L vs. θ_{cum}) for sand indicated by the straight lines in the graph encloses most of the data points from A/A_c groups.
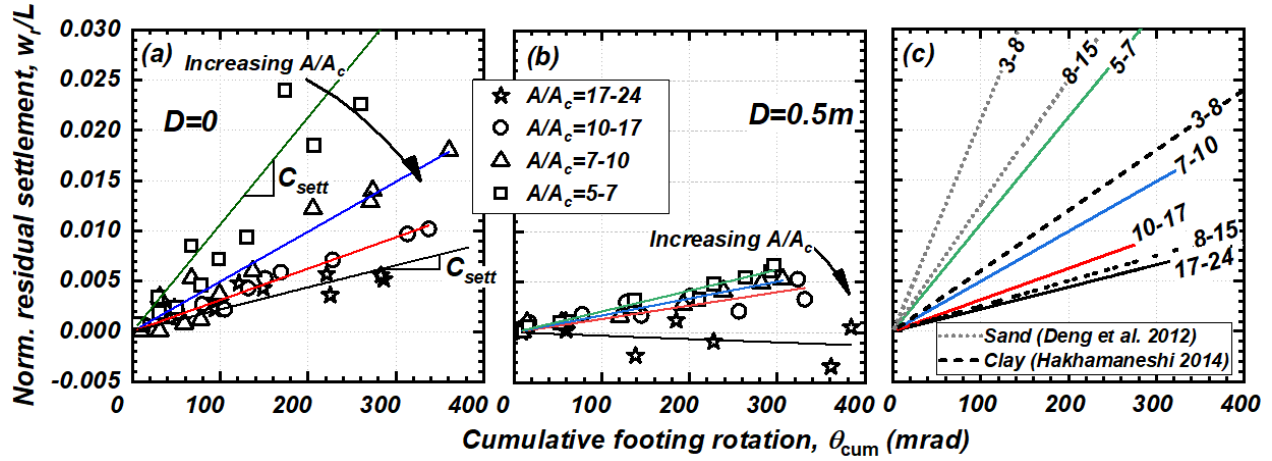
Figure 4.15. Normalized residual settlement vs. cumulative footing rotation of the footings, grouped into different A/A_c ratios (a) $D = 0$, (b) $D = 0.5$ m, and (c) w_r vs. θ_{cum} relations in published literature.

Table 4.2. Summary of settlement coefficient C_{sett}

		Present study		Deng et al. (2014)	Hakhamaneshi (2014)
Soil type		Clay, $s_u = 75\text{-}85$ kPa		Sand, $D_r = 73$ %	Clay, $s_u = 59$ kPa
Test type		Field, cyclic		Centrifuge, dynamic and cyclic	Centrifuge, cyclic
Embedment, D (m)		0	0.5	0.5	0
A/A_c	17~24	0.021	-0.003	N.A.	N.A.
	10~17	0.032	0.014	N.A.	0.025
	7~10	0.05	0.017	0.07	N.A.
	5~7	0.105	0.023	0.22	0.06

Table 4.2 summarises C_{sett} from all tests grouped into four ranges of A/A_c and previous experiments (Deng et al. 2012a; Hakhamaneshi and Kutter 2016). Deng et al. (2012a) and Hakhamaneshi and Kutter (2016) consisted of cyclic loading tests of footing on sand and clay respectively in centrifuge testing. The value of C_{sett} for the embedded footing is significantly less than that for surface footing under identical loading condition. Negative C_{sett} (i.e. residual uplift) for the footing with lower A/A_c ratio was observed due to the relatively "soft" backfill. The residual settlements of the present tests on clay are similar to results of the centrifuge tests on clay for the same A/A_c group (Figure 4.15c), but were less than the footings in sand. Moreover, the similarity in the relationships for sand and clay indicate that the effect of changing soil type can be reasonably accounted for through the effect of A/A_c.

4.4   Test Results: Footing Mechanical Response

The readings of SG stations in the footing were analysed to examine the footing mechanical response. The transient contact length was estimated from the SG readings and this method was validated by the actual tape measurements during cyclic loading tests.

4.4.1   Distribution of Normal Strain

Figure 4.16 shows the cross-sectional view of footing at a certain rotation angle (e.g. $\theta = 30$ mrad), free body diagram (FBD) of a footing segment (in Figure 4.16a), and typical time histories of normal strain (ε) measured by the SGs on top and bottom rebars (Figures 4.16b to 4.16c). Figure 4.16 presents the results of test LS12 for example. The patterns of the strain time histories were aligned very well with the applied lateral loads. The strain reached the peak, when the lateral loading was applied towards the SG location and reached the peak. During the reversal loading, the strain decreased to zero when the footing section at the SG location detached from

the ground. The maximum tensile ε along the loading direction recorded under the least FSv (i.e.

maximum moment at the base of footing) was 80 $\mu\varepsilon$ (= 80E-6). This shows that the

reinforcement design worked well to restrain the maximum strain below 100 $\mu\varepsilon$; indeed no

cracks were developed on the footing at end of all field tests. The normal strain in the transverse

direction was observed nearly zero and thus confirms the negligible load in the transverse

direction.
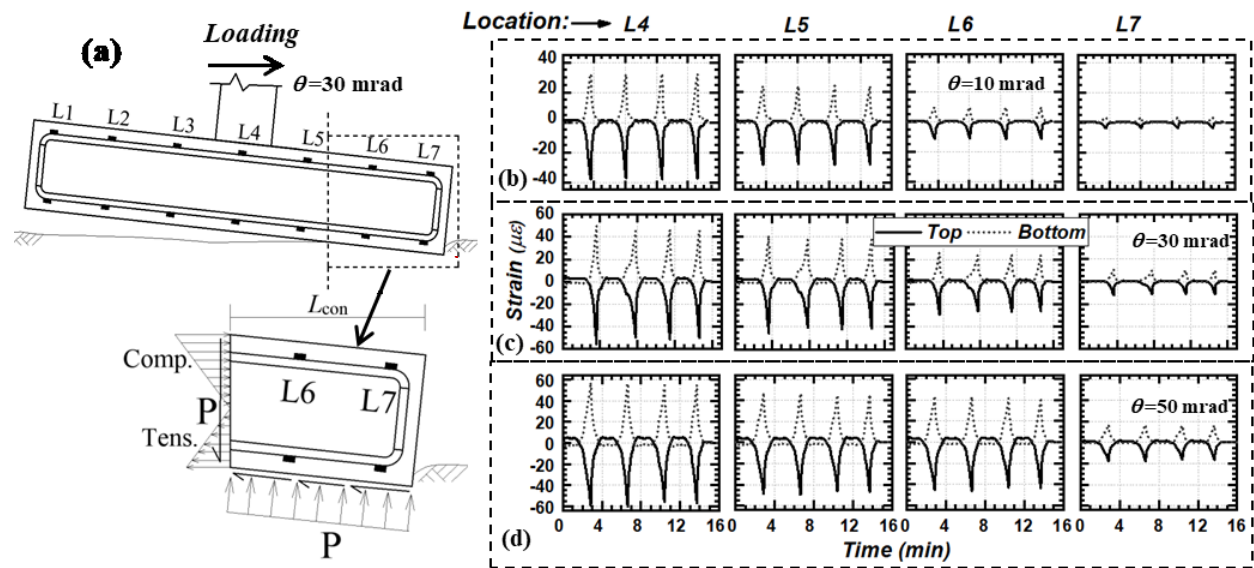
Figure 4.16. (a) Cross-sectional view of the footing in test LS12 (A_r=1.5) at θ = 30 mrad and the

stresses on the cut-off footing segment; (b) to (d) strain time histories for a cyclic packet in test

LS12 at θ = 10, 30 and 50 mrad, respectively.

The footing rotations corresponding to the strain distribution shown in Figures 4.16b to

4.16d are 10, 30, and 50 mrad, respectively. The normal strain distributions are used in this study

to estimate the transient contact area (i.e., range of L_{con}). As shown in the FBD (Figure 4.16a),

the increment between normal strains at two adjacent SG stations should be minimum, if two SG

stations are detached from the soil because there is no soil shear resistance along the uplift zone.

Therefore, the left edge of transient contact area should be within the SG stations where a sharp change in the normal strain occurred (e.g., between stations L6 and L7 in Figure 4.16d). Figures 4.16b to 4.16d indicate the L_{con} ranges and the decrease of L_{con} as the footing rotation increased, although the exact value of L_{con} is not attainable due to the limited number of SG stations.

4.4.2 Footing Normal Force and Transient Contact Area

Throughout the experiment of surface footings, L_{con} was manually logged using a tape measure when the footing reached the peak rotation of each cyclic packet. Figure 4.17 shows the strain distribution in the footing, using the example of LS12 at θ of 50 mrad; in addition, the shaded area shows the contact area based on the measured L_{con}. Note that the left edge of the measured contact area falls within the zone where the SG readings change sharply, which validates the prior method of using SG readings to estimate L_{con} range. In addition, it is observed that □ in the central array, particularly near the column (L4), were greater than □ measured near the footing edge (L8) because of the stress concentration near the column. The strains at the top and bottom rebars may not be equal as a result of the effect of soil shear stress under the footing.
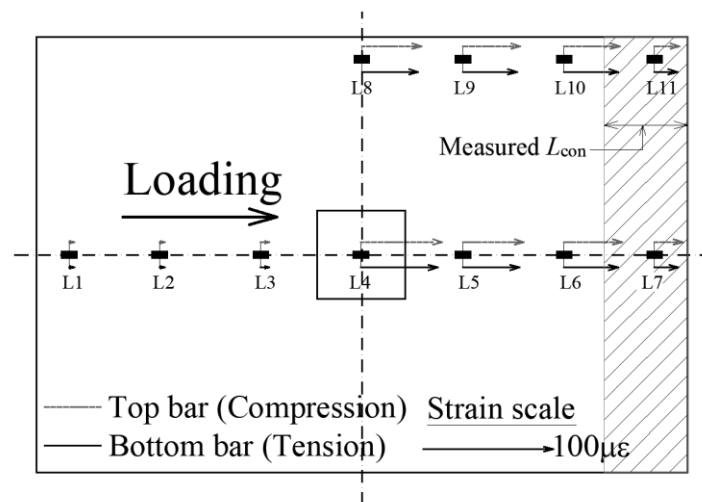
Figure 4.17. Typical strain distributions in the footing at θ = 50 mrad for test LS12. The shaded area is the measured transient contact area.

86
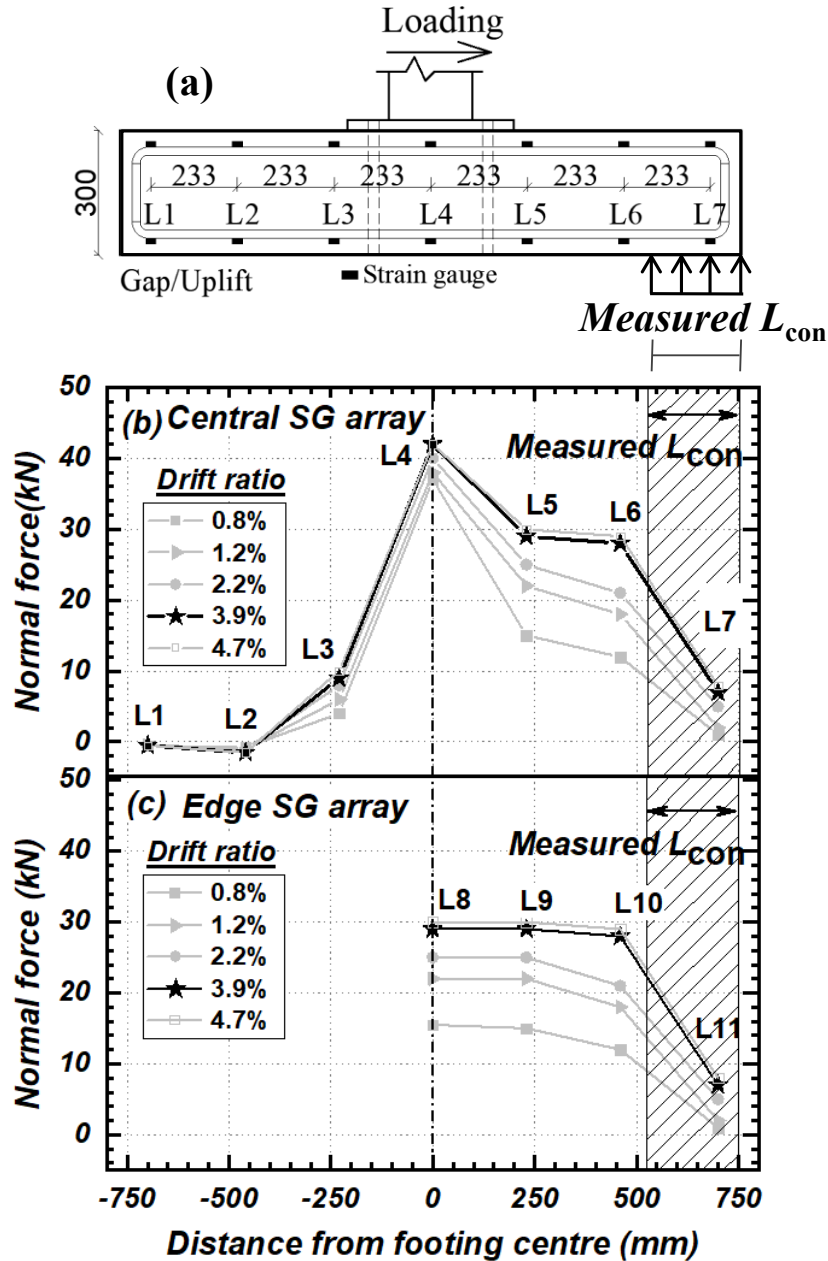
Figure 4.18. (a) Cross-sectional view of footing along loading direction; (b) normal force distribution calculated from central SG array for test LS04; and (c) normal force distribution calculated from edge SG array for LS04.

Figure 4.18 shows the distribution of normal forces along the central and edge SG arrays, for the test LS04 for each cyclic packet applied to the deck. The normal force is calculated from the top and bottom strains (Figure 4.18a) and the cross-sectional area at the SG station along the

transverse direction. It is noted that the normal forces along the edge and central array may not be identical because of the stress concentration near the column. In Figure 4.18b, we take the distribution at the drift ratio of 3.9% for example. The normal force at L5 and L6 is almost the same but there was a sharp change from L6 to L7; this indicates the footing segments from L1 to L6 were detached and the edge of the contact area should be between L6 and L7. In Figure 4.19c, the edge of the contact area should be between L10 and L11 following the same principle. The postulated contact areas are further confirmed by the measured L_{con}, shown as the shades in Figures 4.18b and 4.18c.
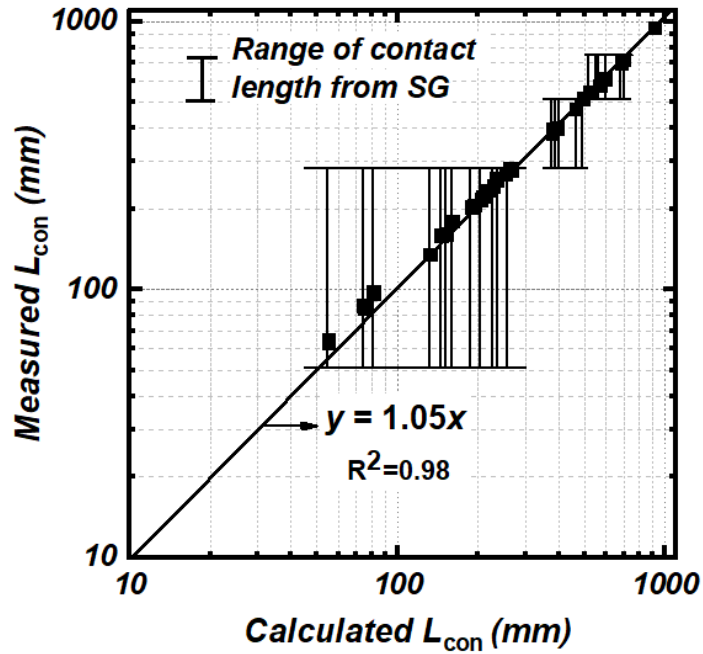
Figure 4.19. Calculated vs. measured L_{con}. The error bars show the range of L_{con} estimated from SG readings.

Figure 4.19 compares the calculated L_{con} to the measured L_{con} at the peak of each drift packet and also shows the SG-based range of L_{con} using error bars. For all surface footings, the calculated L_{con} is the transient contact length using Equation 4.9, derived from Equation 4.1:

$$L_{con} = L\left(1 - \frac{2M}{PL}\right) \qquad\qquad [4.9]$$

where M is the transient rocking moment.

As shown in Figure 4.19, the calculated L_{con} correlates linearly with the measured Lcon. On average, the measured L_{con} was observed about 5% greater than the calculated L_{con}. This small difference might be attributed to the inevitable error in the measurement of L_{con} during the field test. In addition, both the calculated and measured L_{con} fell within the ranges of contact length estimated from SG readings using the method above. The comparison validates the method of estimating the transient soil-footing contact area using SG readings.

4.5   Conclusions

Results from a series of field tests on surface and embedded rocking footings in cohesive soils are presented. The following conclusions may be drawn:

1. An increase in the unit weight and shear strength beneath the footing edges due to rocking cycles was observed. The influence depth was approximately two times the critical contact length of the footing.

2. The calculated M_{c_foot} agreed very well with the experimental results. The value of M_{c_foot} increased slightly with the number of cycles, possibly due to the increasing strength of soils in the critical contact area.

3. A rotational stiffness reduction curve was established for the rocking system on the clay. The normalized stiffness is almost unique at large footing rotation regardless of the A/A_c ratio, soil types, or test condition. The normalized stiffness vs. footing rotation equation is proposed for foundations in clay and may be useful for practice.

4. The damping ratio based on the moment-rotation hysteresis curve ranged from 8 to 40%. The damping ratio generally decreases as the amplitude of footing rotation increases.

5. The value of w_r was less than 3% of the footing length even at θ_{cum} of 350 mrad. As A/A_c increases, w_r reduces significantly. Footings with A/A_c greater than 10 showed negligible w_r. The settlement of footing on clay was less than the values on sand given the similar A/A_c range.

6. The rocking system exhibited a good re-centering ability. The correlation of re-centering ratio vs. A/A_c was developed. The re-centering ability of a rocking system on clay is slightly better than that of a footing on sand.

7. The footing remained elastic during rocking. The transient soil-footing contact length can be estimated with the mechanical response of footing based on the SG readings. The method suggests that the edge of the transient contact area should fall within the SG stations where there was a sharp change in the strain or normal force. Measured L_{con} agreed very well with the calculated L_{con} and confirmed the validity of the SG-based estimation method.

5. Effects of Loading Obliquity on Field Performance of Rocking Shallow Foundations in Cohesive Soil[3]

Abstract

This paper presents a field study of obliquely-loaded rocking shallow foundations resting on cohesive soil. Lateral snap-back and cyclic loading tests at an oblique angle of 45° with respect to the footing axes were carried. During the snap-back tests, an initial drift ratio was applied to the deck and then the system was released to enable the free vibration. The cyclic loading consists of 5 packets of which each contain 3 to 4 cycles of similar displacement amplitude. The rocking system consisted of a 1.5 m by 1.0 m concrete footing, column, and deck. The factors of safety against bearing failure were varied from 4 to 20. The system primarily rocked in plane. The moment capacities about footing axes deviated from the calculated values at the orthogonal loading conditions. A method of estimating the rocking moment capacity of footing subjected to oblique loading was developed and validated by the present tests. Natural periods, damping ratio, re-centering ratio, settlement, and stiffness degradation during the tests were discussed and compared with the results from previous studies with orthogonal loading. A method of calculating the critical contact area, observed approximately triangular, was developed based on the bearing capacity theory with two-way eccentricity.

5.1 Introduction

The benefits of a rocking shallow foundation for earthquake-resistance design have been extensively studied in recent years primarily using centrifuge model or shaking table testing

---

[3] A version of this chapter was in review as: Sharma, K. and Deng, L. 2019c. Effects of Loading Obliquity on Field Performance of Rocking Shallow Foundations in Cohesive Soil. Geotechnique.

(Gajan et al. 2005; Sakellaraki and Kawashima 2006; Apostolou et al. 2007; Paolucci et al. 2008; Deng et al. 2012a; Gelagoti et al. 2012; Antonellis and Panagiotou 2014; Kim et al. 2015; Ko et al. 2018). These studies revealed that a rocking foundation, as a base isolation mechanism, significantly reduces the peak deck drift, peak acceleration on the deck, and the column base shear and moment when compared to the fixed-base design principle. To investigate the field behaviour, Sharma and Deng (2019a and b) conducted a series of large-scale field experiment of rocking systems subjected to snap-back and cyclic loads in the orthogonal directions in a cohesive soil and concluded that rocking foundations can perform satisfactorily well in this soil type. In addition, earthquake case studies demonstrated that shallow foundations may have avoided severe damage on building structures by rocking about the footing, with some settlement and residual inclination (PWRI 1997; Yashinksy and Karshenas 2003; Phipps et al. 2012); case studies have shown that uplift and nonlinear soil-footing interaction to some degree is inevitable during major seismic events.

The previous research predominantly focused on the performance of rocking foundations subjected to orthogonal conditions in which the cyclic loading or dynamic shaking had been applied along the axial directions of rectangular footings. In reality, however, the seismic loading could be applied along any arbitrary lateral direction (i.e. oblique loads). Espinoza (2011) carried out the shake table test of a single bridge pier resting on an elastomeric pad under multidirectional excitations along the footing axes; however, the elastomeric pad may not resemble the soil's nonlinearity properly. Thus far there has not been any research toward the seismic behaviour of rocking foundations subjected to oblique loads, particularly at the field scale. The oblique loading results in biaxial moments and two-way eccentricity and rotation, which may complicate the performance evaluation. There is no prediction method for

determining the moment capacity of obliquely loaded foundations. In addition, the plane of rotation, shape of contact area, and other performance indices are still yet to be characterised. Thus, a field test study of rocking foundations subjected to oblique loading is needed.

The present paper characterises the effects of lateral loading obliquity on the performance of rocking foundations in a cohesive soil in the field. Field tests of rocking foundations subjected to loading at an angle of 45° with respect to the footing axes were carried out. Owing to the limitation of field test equipment, the angle of 45° was chosen to serve as a case study. The rocking system consisted of a 1.5 m by 1.0 m concrete footing, elastic steel column, and concrete deck to simulate a prototype single-degree-of-freedom (SDOF) system. Snap-back loading and slow cyclic loading were applied to the rocking system to resemble the different earthquake load patterns. Thirty six snap-back and eight cyclic loading tests were conducted for foundations with varying factors of safety (FSv) against bearing failure without any eccentricity, rotation amplitudes, and embedment. The value of FSv ranged from 4 to 20. In-situ investigation and laboratory soil tests were performed to characterise the soil before and after the rocking tests. This paper presents system performance indicators, such as moment capacity, damping, stiffness, settlement and re-centering capability, and compares to the performance of footings subjected to orthogonal loading.

5.2   Background

5.2.1   Shallow Foundations with Two-way Eccentricity

The ultimate bearing capacity of footings subjected to zero or one way eccentricity, when the soil-footing contact area is rectangular, is well documented in the literature (e.g. Meyerhof 1965; CFEM 2006). Oblique lateral loading causes biaxial moments (M_x and M_y) and eccentricity in both directions (Figure 5.1a). Meyerhof (1953) conducted laboratory tests of model footings on

clay and sand under two-way eccentricity and concluded that the contact area was no more rectangular. Highter and Anders (1985) developed an analytical method to estimate the shape and size of the soil-footing contact area under two-way eccentricity. When $e_L/L \geq 1/6$ and $e_B/B \geq 1/6$, where e_L and e_B are the eccentricities along L and B direction (Figure 5.1b), the contact area is triangular. The dimensions of the contact area (A_{c_ob}) for footing subjected oblique loading can be calculated using Equation 5.1 (Highter and Anders 1985; Das 2016):

$$A_{c\_ob} = \frac{1}{2}B_1 L_1 \qquad\qquad [5.1a]$$

where $\qquad L_1 = L\left(1.5 - \frac{3e_L}{L}\right)$ and $B_1 = B\left(1.5 - \frac{3e_B}{B}\right) \qquad [5.1b]$

and $\qquad e_L = \frac{M_y}{Q_u}$ and $e_B = \frac{M_x}{Q_u} \qquad\qquad [5.1c]$

where Q_u (kN) is the ultimate capacity of the footing without any eccentricity.
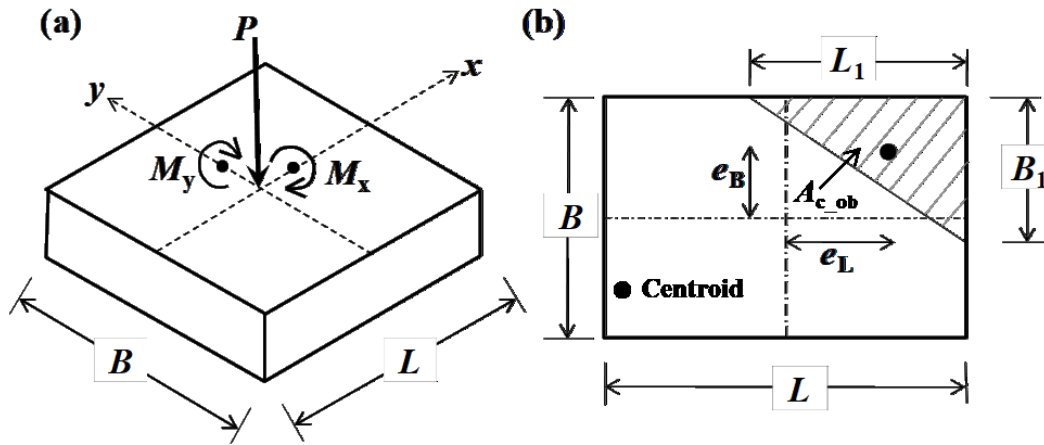
Figure 5.1. (a) Foundation with biaxial moment and two-way eccentricity, and (b) contact area for the case of $e_L/L \geq 1/6$ and $e_B/B \geq 1/6$.

In order to estimate the bearing capacity (q_u, kPa) of the footing with oblique loading (i.e. two-way eccentricity), A_{c_ob} is treated as an equivalent rectangular footing ($B' \times L'$, assumed no eccentricity), where the effective length L' is the greater of B_1 and L_1 and the effective width B' is

equal to A'/L'. Using conventional footing capacity theories (CFEM 2006), q_u is calculated for the area $B'×L'$ at zero eccentricity condition.

5.2.2 Rocking Foundations Subjected to Orthogonal Loading

When a lateral load is applied to a rocking system, an overturning moment will develop and the contact area will decrease. The critical contact area (A_c) is the minimum area when the bearing capacity of underlying soil is fully mobilized. The moment capacity (M_{c_foot}) of a footing subjected to orthogonal loading is estimated with Equation 5.2 (e.g., Gajan et al. 2005):

$$M_{c\_foot} = \frac{VL}{2}\left(1 - \frac{A_c}{A}\right), \quad \text{for orthogonal loading} \qquad [5.2]$$

where V and A are the total vertical load on the soil and the total footing area, respectively. The value of A_c can be calculated with an iterative process (Deng and Kutter 2012).

5.3   Experimental Program

5.3.1   Site Investigation

The field loading tests were carried out at a cohesive soil site, located on the university farm in Edmonton, Alberta. A comprehensive geotechnical investigation was undertaken prior to the tests to characterise the soil properties. Site investigation consisted of cone penetration tests (CPT), Shelby tube sampling before and after field tests, and laboratory testing of undisturbed soil samples. Test layout, CPT locations, and Shelby tube sampling locations are shown in Figure 5.2. Laboratory test program consisted of the unconfined compressive strength (UCS), undrained shear strength (s_u) using direct shear under various normal stresses, Atterberg limits, and physical properties. The critical soil properties are followed: $s_u = 65 - 75$ kPa, USCS classification MH, water content $= 28 - 32\%$, plastic limit $= 35.6$, liquid limit $= 89.0$. Detailed characterization and results of subsurface soil are presented in Sharma and Deng (2019 a and b).
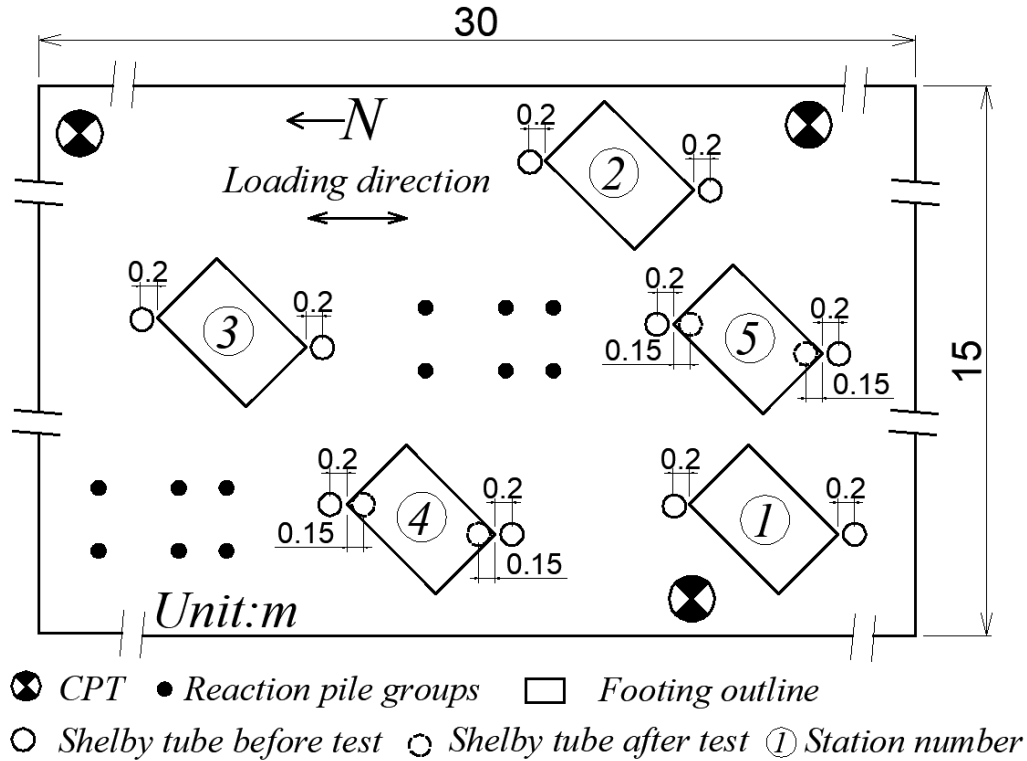
Figure 5.2. Field test layout with CPT and Shelby tube sampling locations (N: 53.498385°, E: -113.532628°).

5.3.2 Rocking Foundation System

A SDOF system was considered for the study. The system consisted of a rectangular reinforced-concrete (RC) spread footing, a steel tubular column, and RC slabs used as the superstructure weight (Figures 5.3). The height of the steel tubular column is 2.0 m, and the column has an outer dimension of 0.2 m by 0.2 m and a thickness of 12.7 mm. The column rigidity (*EI*) is 6.444 MN-m^2. The first yield moment (M_{c_col}, 113 kN-m) of the column is designed to be greater than M_{c_foot} in footing axial directions, and therefore the rocking response would be enabled.

The bearing capacity of soil considering zero eccentricity was calculated using CFEM (2006) equations. In order to achieve various *FSv*, three concrete slabs could be added to the superstructure. Consequently, the footing was 1.5 m long, 1.0 m wide and 0.3 m thick. The

rocking systems had *FSv* values ranging from 4 to 20 in the present tests. As the foundation flexibility factor (which defines the rigidity of footing with respect to the rigidity of soil beneath the footing) was equal to 78, the footing was perfectly rigid (Brown 1969). The footing was heavily reinforced with steel rebars according to CSA A23.3-14 (CSA 2014). The reinforcement ratio was about 6% in both axial directions in order to preclude tensile cracks in concrete during the cyclic loading. The longitudinal and transverse reinforcement consisted of 7D20 bars top and bottom and the 10D20 respectively spaced at about 150 mm center to center.
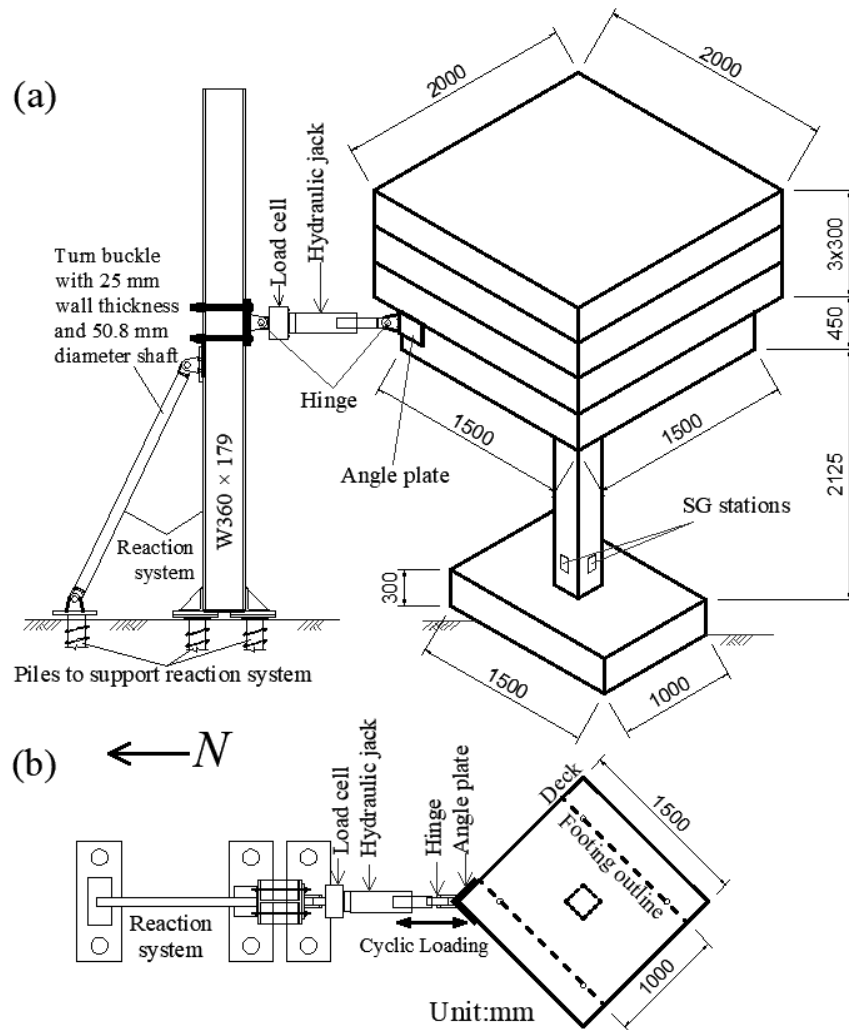
Figure 5.3. Schematic of the experimental model in oblique cyclic loading tests: (a) a semi-3D view and (b) top view.

5.3.3 Instrumentation

Linear potentiometers of 200 mm stroke were used to measure the vertical and horizontal movement of the footing and deck. Accelerometer was used to measure the acceleration of the deck mass for all snap-back tests. A load cell was used to measure the force applied at the connection of the hydraulic jack and concrete deck (Figure 5.3); additionally, two full-bridge strain gauge (SG) stations were attached at the base of column to measure the two-way bending moments (Figure 5.3a). The footing was intensively instrumented with SGs. Thirty-eight SG stations were attached onto the top and bottom rebars of the footing to monitor the normal strain in the footing. The SG's inside the footing were intended to assist in estimating the transient soil-footing contact area during the cyclic loading tests.
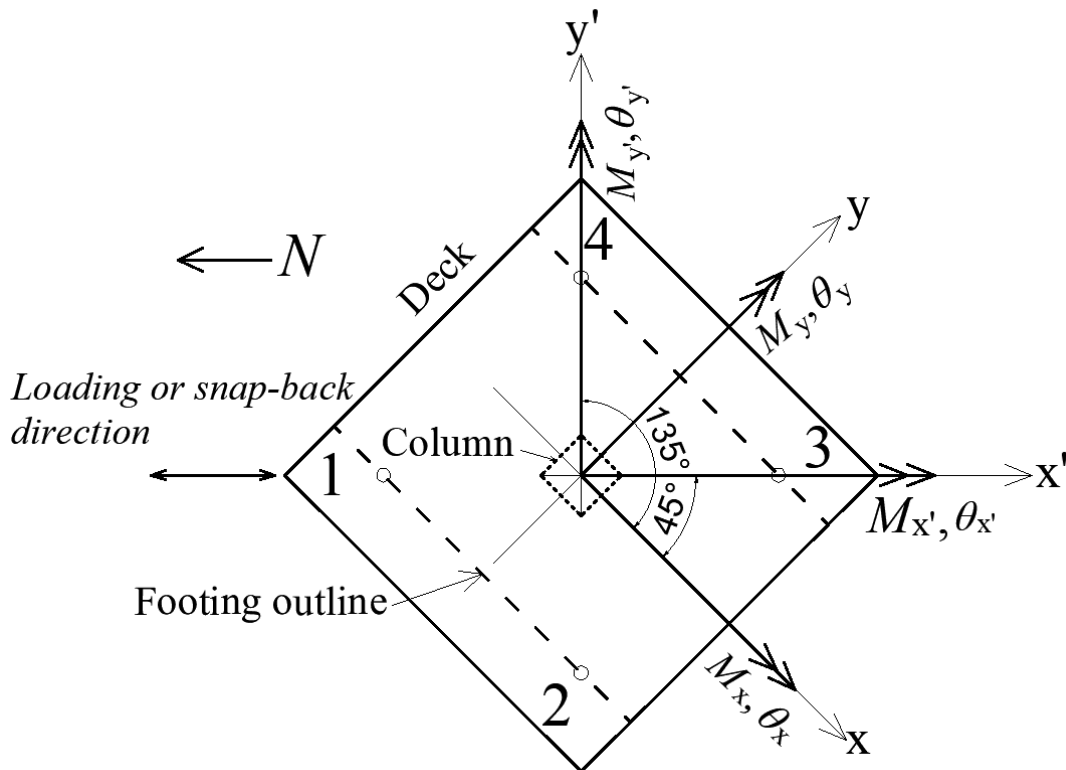
Figure 5.4. Definition of Cartesian coordinate system.

5.3.4 Snap-back Testing Procedure

The rocking foundation system was subjected to snap-back tests to investigate the dynamic soil-structure properties, because the testing simulates the free vibration of a structure after subjected to a pulse-like motion (Pender et al. 2011). Figure 5.2 shows the layout of the snap-back tests. Figure 5.4 defines the Cartesian coordinate system. The x and y axes are along the axis of the footing respectively, and the x' axis is along the loading direction. The directions of a moment (M) and footing rotation (θ) are labelled as a double arrow. The snap-back tests were conducted by pulling the deck at an angle of 45° (i.e., x' axis in Figure 5.4) with respect to the footing axis, using chains attached to a quick release mechanism. There were two reasons for considering an oblique angle of 45°. First, the system loaded at this angle serves as a case study; and secondly, the angle plate (Figure 5.3) was fabricated to enable the loading at 45° only.

At each station, the test at great FSv and small drift ratio was carried out first. In total, 36 trials of snap-back tests were conducted at 3 stations with different FSv, as listed in Table 5.1. The tests were duplicated and the accelerations along x', x and y axes were measured at Stations 1, 2 and 3 respectively. Each test is assigned a code as follows: the first character "O" stands for the oblique loading, the second character "F" for the free vibration, the first number (i.e. third character) for the station number and the second number for the test sequence. The initial rotation of footing ($\theta_{y'i}$) of each trial is shown in Table 5.1. The maximum drift ratio before release was 7.0% (or 70 mrad. 1 mrad = 0.1%).

Table 5.1. Snap-back test matrix

Station	Test ID	*FSv* without eccentricity	Fixed-base period, T_{fixed} (s)	Initial rotation of trials, θ_{yi} (mrad)
	OF11	19.7	0.289	30, 37, 49
	OF12	11.0	0.460	25, 51, 67
1	OF13	7.6	0.617	30, 40, 65
	OF14	5.8	0.774	18, 39, 59
	OF21	19.1	0.289	25, 39, 59
	OF22	10.5	0.460	20, 50, 67
2	OF23	7.1	0.617	29, 45, 65
	OF24	5.2	0.774	23, 43, 69
	OF31	19.5	0.289	20, 39, 59
	OF32	10.8	0.460	28, 45, 70
3	OF33	7.4	0.617	22, 41, 63
	OF34	5.5	0.774	29, 43, 68

5.3.5 Cyclic Load Testing Procedure

Cyclic loadings were carried out following the displacement-controlled method. Figure 5.3 shows the test system setup. The oblique load was applied at an angle of 45°. The experimental setup was designed so that the load can be applied at the corner of the concrete deck using a double-hinged hydraulic jack mounted to the reaction frame (Figure 5.5). The two hinges were used to avoid any unwanted moment or vertical force component. The reaction system was supported by groups of screw piles and an inclined strut (Figure 5.5). It was assumed that the

primary movement of the deck was in the direction of the load, i.e. along x' axis. However, some movement may be out of plane along y' axis. The out-of-plane movement was also measured.
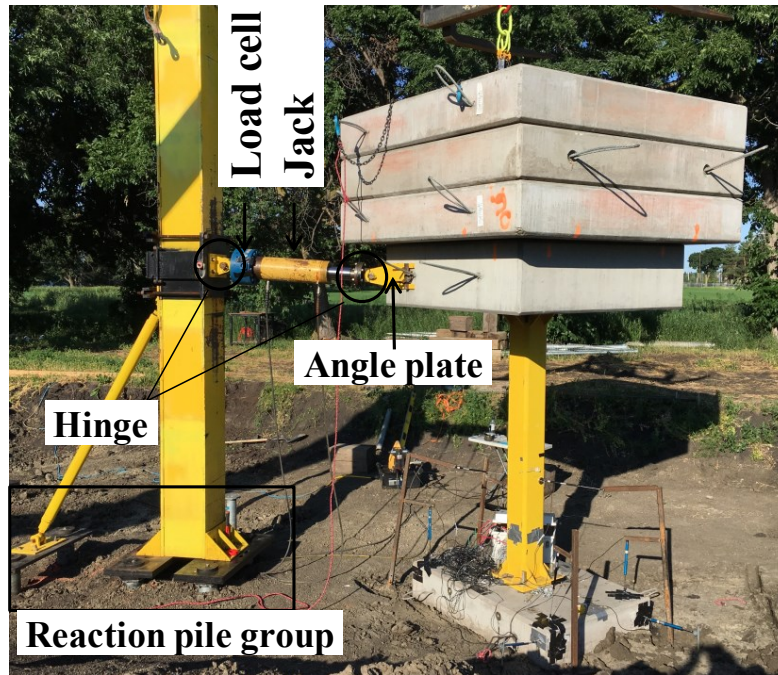
Figure 5.5. Field test setup (for test OS44).

The loading system was designed to produce rotational displacements to induce footing uplift on both sides as the load was reversed. Lateral cyclic tests were performed by loading the structure at a height 2.525 m above from the footing base. The cyclic loading consists of 4 to 5 packets, each of which contains 3 to 4 cycles of the same displacement amplitude, at a maximum drift ratio of about 7.0%. The typical drift time histories are shown as the sinusoidal cycles (Figure 5.6). The amplitude, number of cycles and frequency may vary slightly. The average period of the cyclic loading was about 140 s that is sufficiently long to avoid the generation of an inertia force. The embedment depth of footing (D) and FSv were systematically varied during the field tests for cyclic loading test. Table 5.2 outlines the key parameters of the field tests including the FSv, D, and moment capacity about x (i.e. M_{c_footx}) and y (i.e. M_{c_footy}) axes. The values of

M_{c_footx} and M_{c_footy} were calculated using Equation 5.2 considering orthogonal loading. The first character the test ID "O" stands for Oblique, the second for the footing condition where "S" for surface footing and "E" for embedded footing, and the first number (i.e. third character) is the station number and the second number is the test sequence.
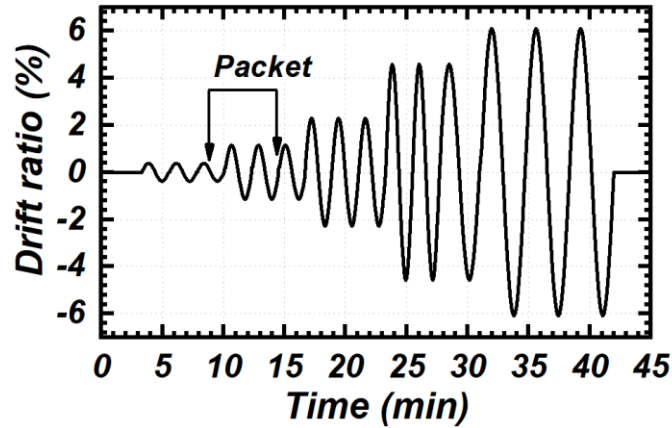
Figure 5.6. Typical time history of the drift ratio along x' axis under oblique cyclic load.

Table 5.2. Cyclic loading test matrix

Station	Test ID	FSv without eccentricity	D (m)	M_{c_footy} (kN-m)	M_{c_footx} (kN-m)
4	OS41	16.0	0	24.5	15.5
	OS42	8.9	0	41.8	27.8
	OS43	6.2	0	56.6	37.5
	OS44	4.7	0	69.39	45.8
5	OE51	19.5	0.5	28.5	16.9
	OE52	10.9	0.5	43.8	29.3
	OE53	7.5	0.5	64.3	40.5
	OE54	5.8	0.5	74.8	48.5

5.4 Results of Snap-back Tests

Figure 5.7a shows the typical relationship between the processed acceleration $a_{x'}$ (along the x' axis) and $a_{y'}$ of the deck of test OF11, which were calculated using Equation 5.3:

$$a_{x'} = a_x \cos{(45°)} + a_y \sin{(45°)}, \text{ in-plane acceleration} \qquad [5.3a]$$

$$a_{y'} = a_y \cos{(45°)} - a_x \sin{(45°)}, \text{ out-of-plane acceleration} \qquad [5.3b]$$

where a_x and a_y are the measured accelerations of the deck along x and y axes respectively.
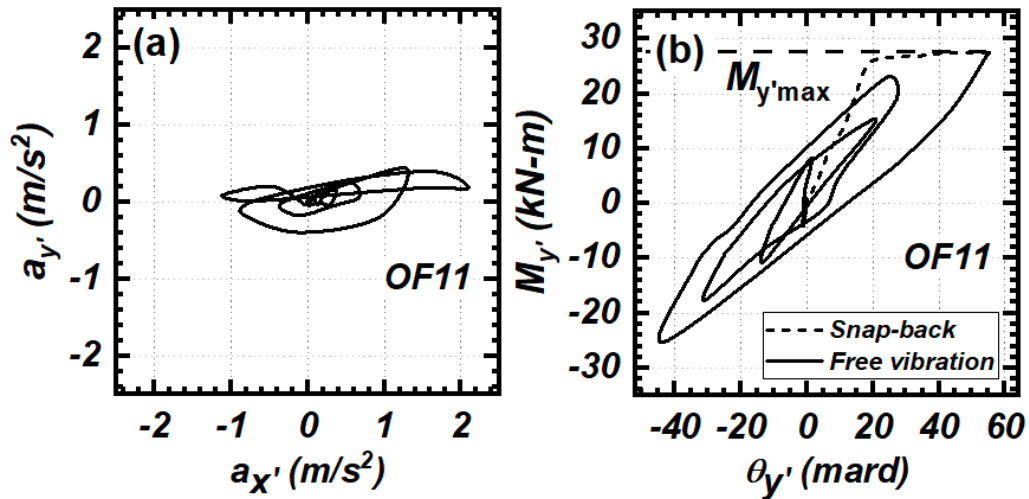
Figure 5.7. Results of test OF11: (a) relationship between processed $a_{x'}$ and $a_{y'}$ during snap-back test and (b) hysteresis of moment vs. footing rotation.

The maximum $a_{x'}$ was about 2.1 m/s², whereas maximum $a_{y'}$ was only about 0.5 m/s². It is seen that $a_{x'}$ is significantly greater than $a_{y'}$, which suggests that the system vibration is primarily in-plane along the x' loading direction. The pattern of motion during other snap-back tests at all stations was observed very similar to the pattern shown in Figure 5.7a.

Figure 5.7b shows the curves of rocking moment ($M_{y'}$) vs. footing rotation ($\theta_{y'}$) during the static snap-back and dynamic free-vibration stages. The rocking moment and footing rotation measured about x' and y' axes were calculated as follows:

103

$$M_{y'} = M_y \cos\ (45°) + M_x \sin\ (45°), \text{in-plane moment} \qquad [5.4a]$$

$$M_{x'} = M_y \sin\ (45°) - M_x \cos\ (45°), \text{out-of-plane moment} \qquad [5.4b]$$

$$\theta_{y'} = \theta_y \cos\ (45°) + \theta_x \sin\ (45°), \text{in-plane rotation} \qquad [5.5a]$$

$$\theta_{x'} = \theta_y \sin\ (45°) - \theta_x \cos\ (45°), \text{out-of-plane rotation} \qquad [5.5b]$$

where M_x, M_y, θ_x, and θ_y are the measured rocking moment and footing rotation about its respective axis. Equation 5.5 is based on the principle of vector analysis of rigid body rotations; it is noted that Equation 5.5 is valid only at a small rotation (Hibbeler 2015).

The dash line in Figure 5.7b is for the snap-back loading stage. A comparison between the static and dynamic moment vs. rotation curves shows similar moment capacities of the rocking footing. Figure 5.7b shows how the moment and rotation decreases with cycles. The moment vs. rotation curve encloses large areas in hysteresis loops, indicating that a considerable amount of energy is dissipated at the soil-footing interface. Figure 5.7b also shows that the residual footing rotation was almost negligible after 3 full cycles, suggesting that the footing exhibits a strong re-centering ability. The calculated $M_{x'}$ vs. $\theta_{x'}$ curves were not shown, because they did not render any meaningful pattern due to small amplitudes.

Figure 5.8 shows typical time histories of deck acceleration $a_{x'}$, deck displacement $d_{x'}$ and footing rotation $\theta_{y'}$ in test OF13 with FSv 7.6, where $\theta_{y'}$ was calculated using Equation 5.5a. It was observed that the rocking foundation only oscillated 3 to 5 cycles before it stopped, which indicates a high level of damping. The typical time histories show that the soil-footing interface can significantly decay the deck acceleration while dissipating a significant amount of energy. The curves of snap-back tests showed a very small amount of permanent rotation when the

dynamic response diminished even though the initial rotation was very high as shown in Figure 5.8c.
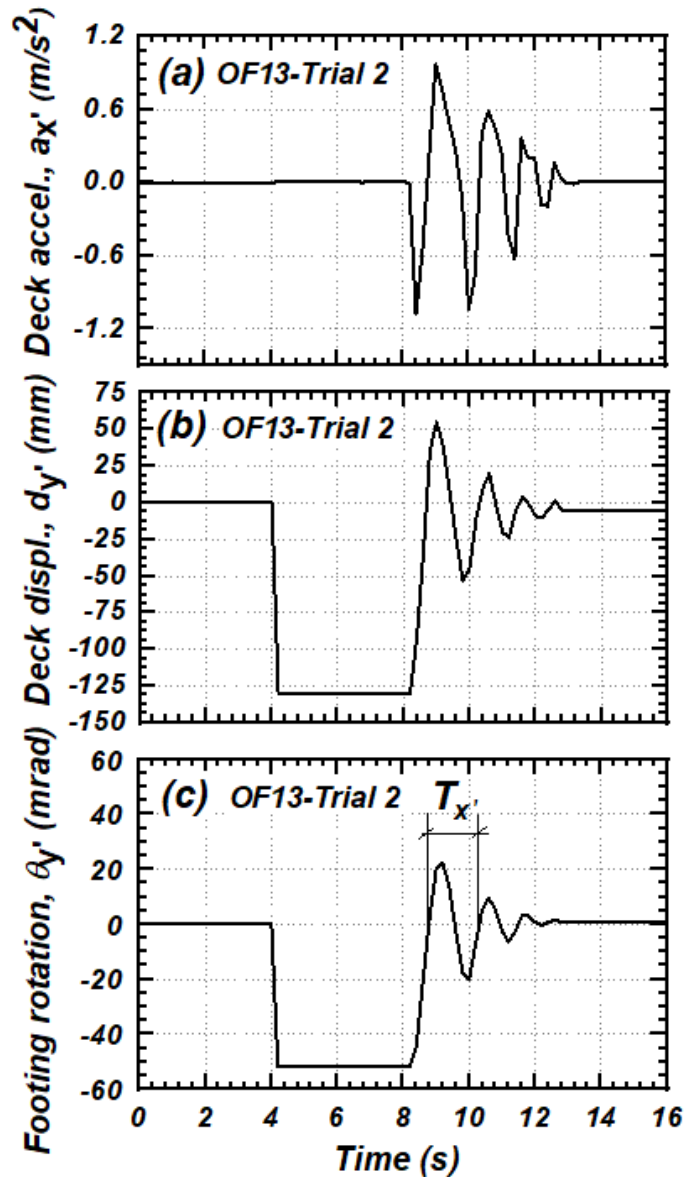
Figure 5.8. Time histories of deck motion and footing rotation in test OF13.

The natural period ($T_{x'}$) of the soil-footing-structure system can be defined as the time required for the first full cycle of footing rotation, as labeled in Figure 5.8c. Following this definition, Figure 5.9 compares the measured T_x, T_y, to $T_{x'}$, where T_x and T_y are the periods along

x and *y* axes respectively when the structure was pulled back along the footing axes. Results of T_x and T_y were obtained from Sharma and Deng (2019b). As in Figure 5.9, the measured T decreased with increasing *FSv* irrespective of rocking axis. The reduction of T was caused by the increase in *FSv* and perhaps the decrease in rotational stiffness of the system as *FSv* decreases. The value of $T_{x'}$ lies in between T_x and T_y, given similar *FSv*, because the critical contact length during oblique loading was also between the counterparts during orthogonal loading; a wider footing has greater resistance to displacement and a shorter period (Espinoza 2011). In addition, it is shown that $T_{x'}$ slightly increased with increasing $\theta_{y'i}$ for a given *FSv* at the same station, which was due to the greater amplitude of vibration as also observed in (Chopra and Yim 1985; Housner 1963). The fixed-base fundamental periods (T_{fixed}) of the structures are given in Table 5.1. The measured $T_{y'}$ was observed 2 to 4 times T_{fixed}, and similar trends are also observed for the system rocking about orthogonal axes. The lengthening of period due to rocking foundation will significantly alter the seismic response of a system and often leads to an advantageous reduction in the system acceleration or displacement (Browne 2006).
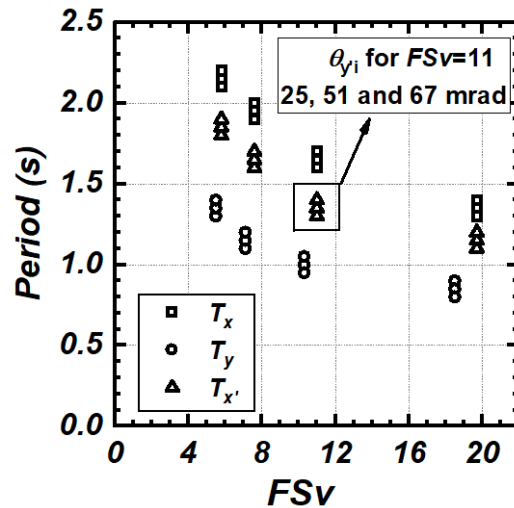
Figure 5.9. (a) Measured rocking period for all tests when structure was pulled back along *x* axis (T_x), *y* axis (T_y) and *x'* axis ($T_{x'}$). T_x and T_y are from Sharma and Deng (2019b).

106

5.5 Results of Cyclic Loading Tests

In this section, the moment vs. rotation, stiffness degradation, damping, re-centering ratio, and residual settlement will be computed and explained.
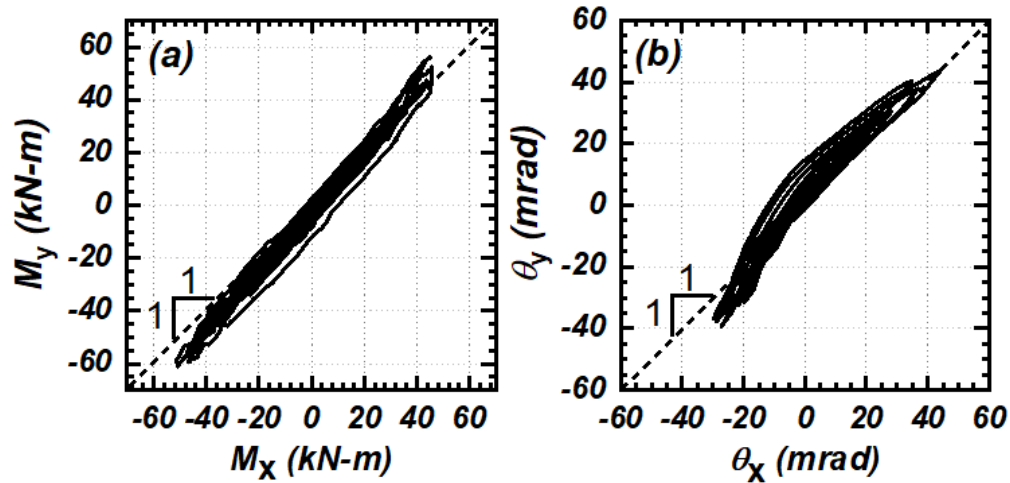
Figure 5.10. Results of test OE53: (a) measured M_y vs. M_x and (b) measured footing rotation θ_y vs. θ_x.

5.5.1 Moment vs. Rotation and Settlement vs. Rotation Correlations

Figure 5.10 shows the relationship between the moment and rotation at the base center of the footing measured for OE53. The measured M_x and M_y are observed to be fairly linear (Figure 5.10a). At the beginning, M_x and M_y were almost equal but with an increase in the number of cycles and amplitude of moment, M_y became greater than M_x, although the curves still remained linear. The reason is that the footing has greater rocking capacity about y axis than about x axis, owing to the difference in footing length. The measured θ_x and θ_y (Figure 5.10b) also shows a very linear relation and the ratio is almost 1:1. It implies that the footing rotation (a vector resultant of θ_x and θ_y) is primarily about the y' axis; in other words, the lateral displacement of

107

system is primarily in-plane along the x' axis (loading direction). The in-plane observation is consistent with that in the snap-back tests.
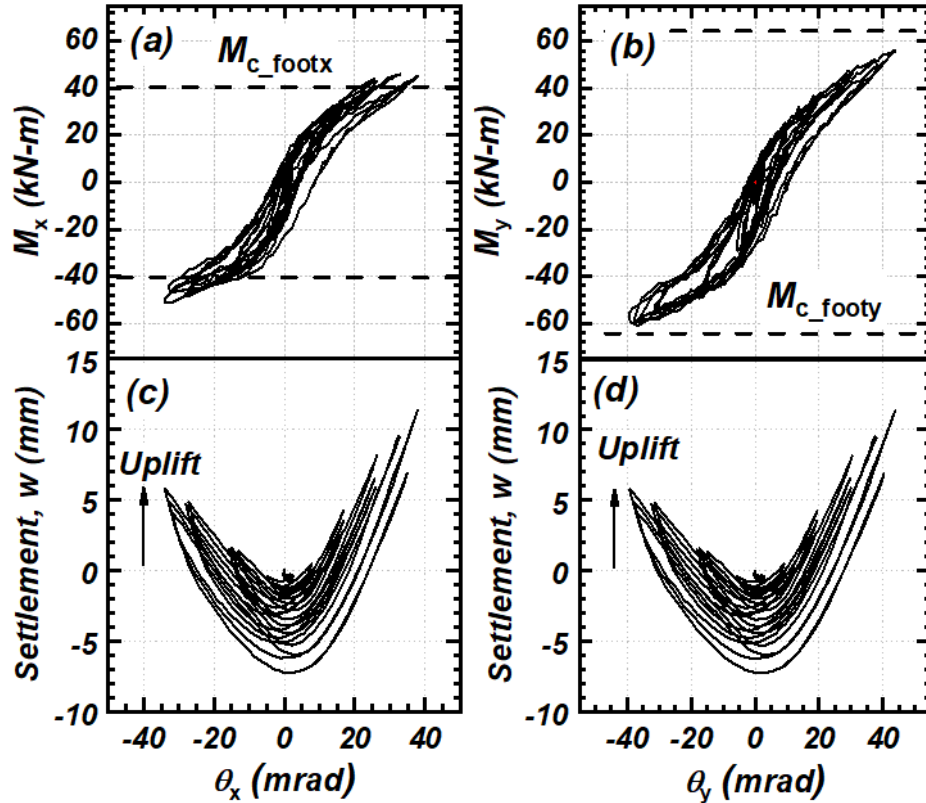
Figure 5.11. Results of test OE53 (a) measured M_x vs. θ_x (b) measured M_y vs. θ_y, (c) w vs. θ_x, and (d) w vs. θ_y. M_{c_footx} and M_{c_footy}: estimated moment capacity of footing subjected to orthogonal loading.

Figure 5.11 shows the curves of rocking moment vs. footing rotation and settlement (w) vs. footing rotation, using the test OE53 as an example. For comparison, the dash lines in Figure 5.11 represent M_{c_footx} and M_{c_footy} calculated with Equation 5.2. It is shown that M_x exceeded M_{c_footx} whereas M_y was yet to reach M_{c_footy} although the footing rotations were very large. It is likely that the moment capacities during oblique tests are coupled; if the capacity about one axis is decreased from the orthogonal capacity then the capacity about another axis will be increased

from the orthogonal counterpart. Figures 5.11c and 5.11d show the settlement vs. rotation curves about x and y axes respectively, which illustrate the re-entering behaviour for rocking foundations and also the considerable residual settlement (w_r).
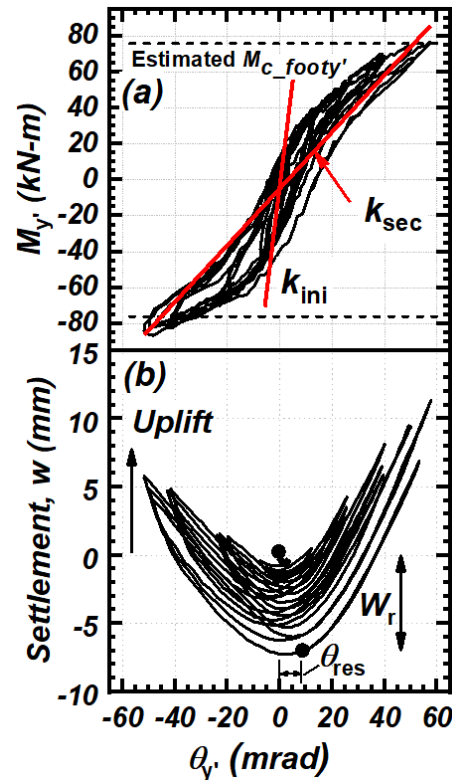
Figure 5.12. (a) Calculated moment ($M_{y'}$) vs. rotation ($\theta_{y'}$) and (b) settlement (w) vs. rotation ($\theta_{y'}$) for test OE53. All results were derived from the measurement.

Figure 5.12 shows the curves of $M_{y'}$ vs. $\theta_{y'}$ and w vs. $\theta_{y'}$ at the base center of the footing in test OE53. The values of $M_{y'}$ and $\theta_{y'}$ were calculated using Equations 5.4 and 5.5 respectively. The $M_{y'}$ vs. $\theta_{y'}$ curve shows that a rocking foundation on cohesive soils has non-degrading moment capacity irrespective of the loading direction, which was also observed for orthogonal loading of foundations in both cohesive soil and sands (Deng and Kutter 2012; Sharma and Deng

109

2019a); in fact, $M_{y'}$ slightly increased with the number of cycles, possibly due to the strengthening of soils.

The settlement (w) vs. footing rotation ($\theta_{y'}$) curve shown in Figures 5.12b illustrates the re-entering behaviour of rocking foundations in this clay. The troughs of the curves show the amount of permanent vertical deformation accumulated with cycles. The residual settlement (w_r) was observed to increase with the increasing amplitude and number of cycles, which is similar to the observation of previous studies on orthogonal loading in both cohesive soil and sand (2014; Sharma and Deng 2019a).

Table 5.3. Summary of measured and estimated results of cyclic tests

Test ID	$(M_{x'}/M_{y'})_{max}$ (%)	$(\theta_{x'}/\theta_{y'})_{max}$ (%)	Estimated q_u (kPa)	Estimated A_{c_ob} (m^2)	Measured m (mm)	Estimated n (mm)
OS41	12.0	11.5	399	0.068	163	834
OS42	6.0	9.3	401	0.12	262	916
OS43	7.0	9.9	403	0.167	314	1064
OS44	6.0	7.6	404	0.213	354	1203
OE51	15.0	13.4	456	0.061		
OE52	13.2	11.9	457	0.104	Not measured or	
OE53	12.5	11.7	459	0.148	estimated	
OE54	8.0	9.4	460	0.203		

Note: q_u = bearing capacity of critical contact area A_{c_ob}

Table 5.3 summarizes the maximum $M_{x'}/M_{y'}$ ratio measured for all cyclic loading tests. The maximum $M_{x'}/M_{y'}$ ranges from 6 to 15%, which implies that the rocking moment is primarily in-plane. In addition, the maximum $\theta_{x'}/\theta_{y'}$ ratio in Table 5.3 varied throughout the tests but in general was considered small, which confirms the in-plane rotation observation. Although cyclic tests were conducted with care, $\theta_{x'}$ could still take place perhaps due to misalignment of loading direction or uneven soil reaction stress.
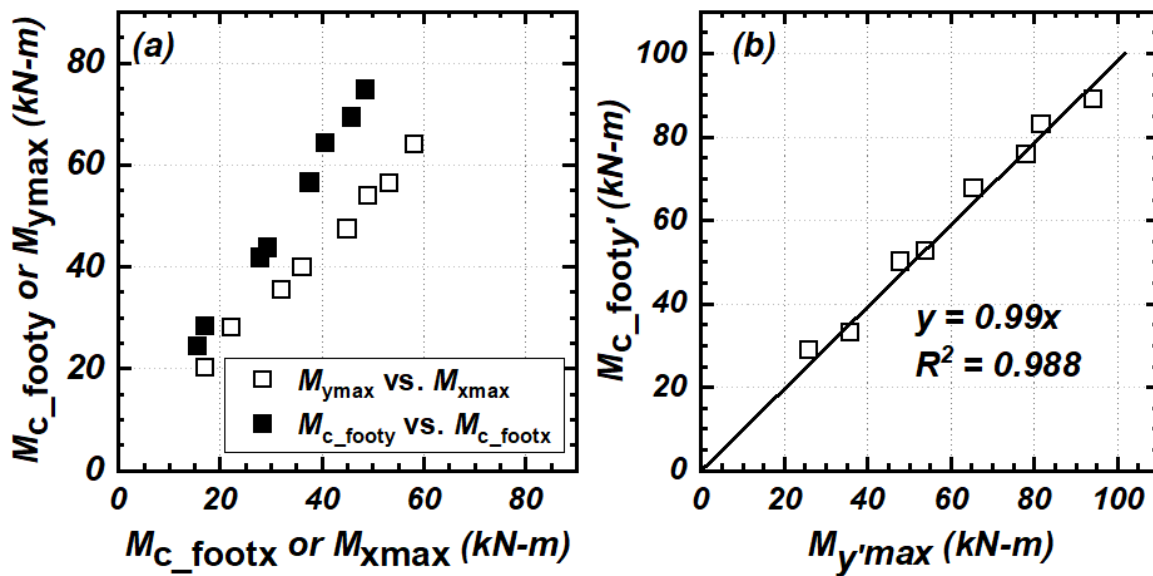
Figure 5.13. Summary of results of all cyclic loading tests: (a) comparison of moment capacities about x and y axes and (b) estimated $M_{c\_footy'}$ vs. measured $M_{y'max}$. $M_{c\_footy'}$: resultant of M_{c_footx} and M_{c_footy}; $M_{y'max}$: resultant of M_{xmax} and M_{ymax}.

The dash lines in Figure 5.12a show the estimated moment capacity of footing about y' axis, $M_{c\_footy'}$ (= M_{c_footy} cos45° + M_{c_footx} sin45°, which essentially follows Equation 5.4). The estimated $M_{c\_footy'}$ agrees very well with the maximum $M_{y'}$ in this test. This may suggest a new valid method of estimating the capacity of rocking foundations subjected to oblique loading, although the obliquity has altered the orthogonal capacities. To verify the new method, Figure

111

5.13a compares the measured M_{xmax} and M_{ymax} with the estimated M_{c_footx} and M_{c_footy}, where M_{xmax} and M_{ymax} were the maximum moment about x and y axes for all tests, and M_{c_footx} and M_{c_footy} were calculated using Equation 5.2. In Figure 5.13a, each data point represents the capacities at one FSv. Similar to the observation in Figure 5.11, moment capacities are altered by the oblique loading. It appears that M_{xmax} is greater than M_{c_footx} but M_{ymax} is less than M_{c_footy}; this must be related to changes in "critical contact length" along x or y axes during oblique loading. On the other hand, Figure 5.13a suggests that the resultants of moment capacity components are nearly equal. Figure 5.13b compares $M_{y'max}$ (a resultant of M_{xmax} and M_{ymax}) with the estimated $M_{c\_footy'}$ (a resultant of M_{c_footx} and M_{c_footy}). Clearly, the measured $M_{y'max}$ correlates very well with the estimated $M_{c\_foot'}$ on the 1:1 line.

As the method for estimating $M_{c\_footy'}$ is valid for the present tests at an oblique angle of 45°, a general equation may be recommended to estimate the capacity of the footing at any oblique angle as Equation 5.6:

$$M_{c\_foot\alpha} = M_{c\_footy} \cos (\alpha) + M_{c\_footx} \sin (\alpha), \qquad \text{for } 0 \leq \alpha \leq 90° \qquad [5.6]$$

where α is the oblique angle with respect to the x axis of footing.

5.5.2   Stiffness Degradation and Damping

Figure 5.14a shows the progress of secant stiffness ($k_{sec} = M_{y'max}/\theta_{y'max}$) vs. the maximum footing rotation ($\theta_{y'max}$). The secant stiffness is normalized by the initial stiffness (k_{ini}), which is the slope of the linear portion of the moment vs. rotation curve, and $\theta_{y'max}$ is at each drift packet applied to the deck. A mean stiffness reduction trend was computed for each level of rotation for all tests. The mean stiffness reduction trend is important when developing the design principle of rocking foundation, because the secant stiffness is a critical index in the displacement-based design for a

rocking foundation. The best estimate of stiffness degradation vs. $\theta_{y'max}$ correlation of the present study is obtained as follows:

$$\frac{k_{sec}}{k_{ini}} = a\theta_{y'max}{}^{b} = 0.013\theta_{y'max}{}^{-0.681} \qquad\qquad [5.7]$$

The stiffness reduction trend of the obliquely loaded foundation is similar to the trend of foundation under orthogonal loading (Sharma and Deng 2017), where the fitting parameters are: $a = 0.0157$ and $b = -0.503$.
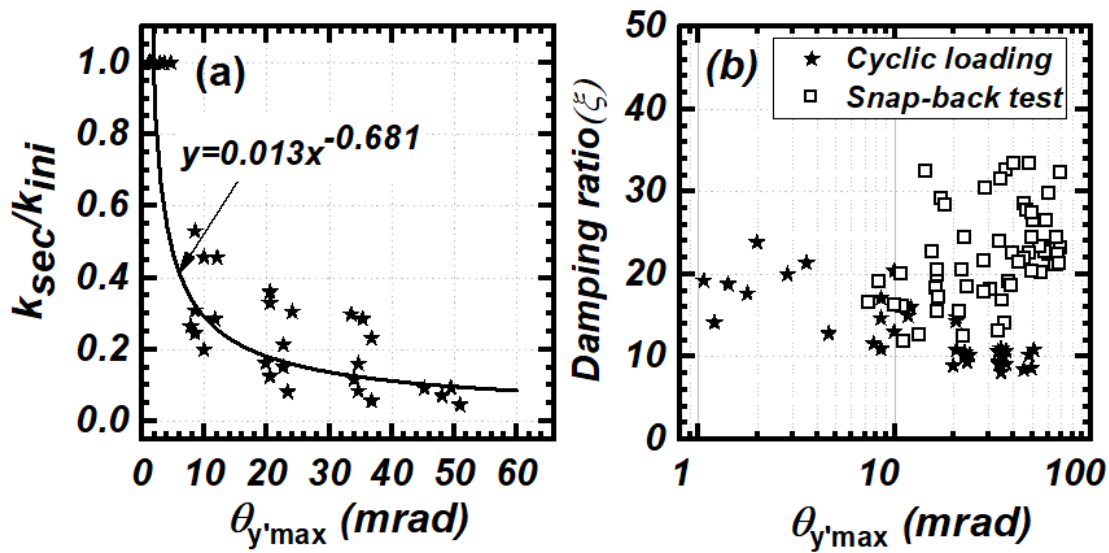
Figure 5.14. (a) Rotational stiffness degradation vs. maximum footing rotation, and (b) damping ratio vs. maximum footing rotation.

Figure 5.14b shows the relationship between damping ratio (ξ) and $\theta_{y'max}$, for both test types. For snap-back tests, the damping ratios of the rocking system were estimated from the decay of the deck drift after releasing the structure from the desired drift ratio (Chopra 2007). Out of various methods, the logarithmic decrement (Chopra 2007) was used to calculate the "viscous" damping ratio in the snap-back tests. For cyclic tests, the equivalent damping ratio was calculated using the area bounded by the $M_{y'}$ vs. $\theta_{y'}$ hysteresis.

A significant scatter is shown for both viscous ξ from snap-back and equivalent ξ from cyclic tests. The value of equivalent ξ ranges from 8 to 30% for all cyclic tests as shown in Figures 5.14b, whereas the viscous ξ ranges from 10 to 35%. The values of viscous and equivalent ξ are similar when the footing rotation is about 6 to 10 mrad. It seems that the viscous ξ increases with increase in rotation in snap-back tests. In contrary to viscous ξ, the equivalent ξ decreases as footing rotation increases. This is attributed to the skinny moment-rotation hysteresis loops at the large amplitude of rotation as shown in Figure 5.12. The pattern and ranges of both viscous and equivalent ξ under oblique loading are fairly similar to the viscous and equivalent ξ of footing under orthogonal loading (Sharma and Deng 2019a and b).

5.5.3 Re-centering Ratio

In order to quantify the re-centering ability of a rocking system, the displacement re-centering ratio (R_d) is introduced as follows:

$$R_d = 1 - \frac{\theta_{y'res}}{\theta_{y'max}} \qquad\qquad [5.8]$$

where $\theta_{y'res}$ is the residual foot rotation about y' axis at zero moment. The re-centering characteristic of a rocking foundation is a result of the closure of the gap that forms between soil and footing. As the size of the gap is related to A/A_c, R_d was observed to correlate with the A/A_c ratio (Deng et al. 2014). Figure 5.15 depicts the distribution of R_d vs. A/A_c in the snap-back and cyclic tests. In cyclic loading tests, R_d was obtained at zero moment condition after each packet (i.e. three full cycles at a given drift ratio). From Figure 5.15, it is seen that R_d is relatively high, ranges from 0.7 to 1.0, for all the tests regardless the A/A_c, embedded depth, and test type. The value of R_d for snap-back tests is a little greater than R_d for cyclic tests, probably owing to the less number of full cycles in snap-back tests. The value of R_d for embedded footings is greater

than the footings on surface. The results indicate that a good potential for the rocking structure to return back its initial position given a reasonably-large FSv in cohesive soils. Furthermore, despite the large $\theta_{y'max}$ (up to 7%), $\theta_{y'res}$ may still be acceptable, due to the re-centering characteristic of the rocking foundations. The empirical equation of R_d vs. A/A_c curve of all points in the present study is regressed as follows:

$$R_d = \frac{1}{1.5\frac{A_c}{A}+1.0}$$
[5.9]

Figure 5.15 compares the R_d vs. A/A_c curve in the present study to the curve of footings subjected to orthogonal cyclic loading (Sharma and Deng 2019a). It is shown that when the cyclic loading is applied to the rocking system, irrespectively of the loading direction, the system performs similarly in terms of re-centering ability. However, R_d for oblique loading is greater than R_d for orthogonal loading, indicating an even better re-centering ability for foundations subjected to oblique loading.
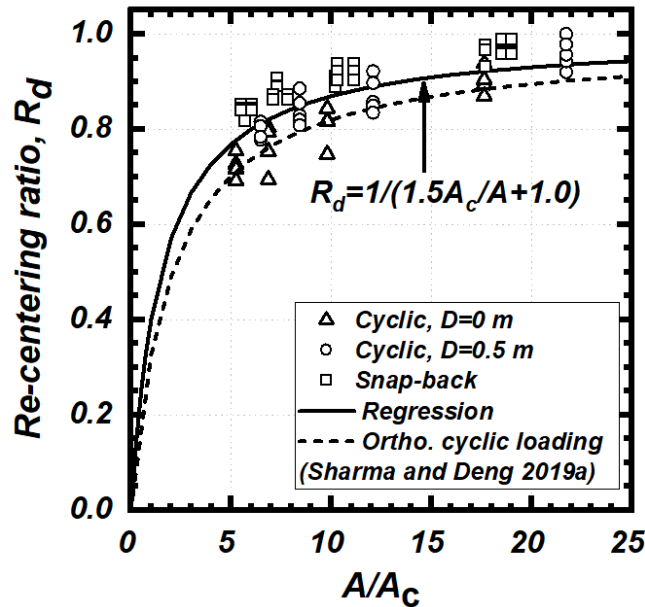
Figure 5.15. Effect of A/A_c on re-centering ratio. Residual rotation was assessed about y' axis.

115
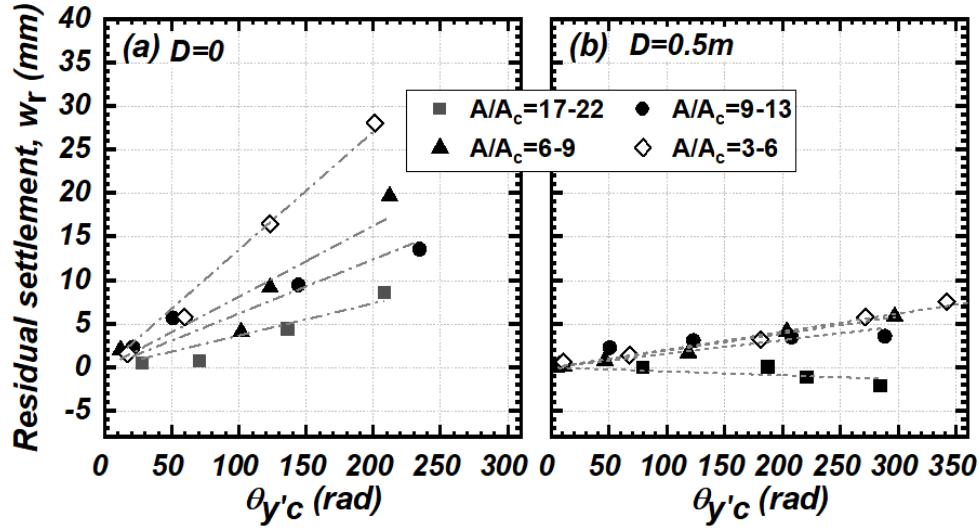
Figure 5.16. Residual settlement (w_r) vs. cumulative footing rotation ($\theta_{y'c}$) of the footings grouped by A/A_c ratios.

5.5.4 Residual Settlement

Figures 5.16 show the results of residual settlement (w_r) vs. cumulative footing rotation ($\theta_{y'c}$), where the residual settlement (w_r) was obtained after 4 packets of 3 to 4 cycles of similar drift amplitude to a drift ratio up to 7%. The residual settlement was calculated for all FSv at each station. The concept of cumulative footing rotation is explained in Deng et al. (2012a) and Hakhamaneshi and Kutter (2016). In general, it is shown that the results of w_r vs. $\theta_{y'c}$ are approximately linear. The results show that residual settlements can be significant if A/A_c is small. If A/A_c is large (e.g., > 10), w_r was deemed small even at $\theta_{y'c}$ of 200 mrad, which is seldom reached during a strong motion. Even for very large cumulative rotations (i.e., 250 mrad), w_r of the footing was about 17 mm which corresponds to only 1.7% of the narrow width of foundation. The settlement response is sinking dominated for the surface footing and uplift dominated for the embedded footing. The value of w_r of the embedded footing is minimal even

116

under the lowest A/A_c and at $\theta_{y'c}$ of 350 mrad (Figure 5.16). This is caused by the soil flowing into the gap from the backfill, which was observed after removing the footing.

Settlement of footings subjected to oblique loading was less than the settlement of footing subjected to orthogonal loading. The total settlement of the obliquely loaded footing for the same A/A_c group was about 66 % of the residual settlement of the footing under orthogonal (Sharma and Deng 2019a). More rounded soil surface was observed in oblique loading cases as compared to aligned loading. Rounding of soil surface decreases the area of footing in contact with the soil. Consequently a shallower stress bulb will be developed and evidently the settlements may be restricted.

5.5.5 Footing Normal Force and Critical Contact Area

Figure 5.17 shows the normal strain (ε) distribution in the footing, using the example of OS41 at $\theta_{y'}$ of 55 mrad. It is observed that ε in the central array, particularly near the column (L4 and T3), were greater than ε measured near the footing edge (L8 and T6) because of the stress concentration near the column. The strains at the top and bottom rebars may not be equal as a result of the effect of soil shear stress under the footing.

The critical contact area was observed approximately triangular. In order to elaborate the dimension of critical contact area, at the maximum drift of each cyclic packet, the test was paused and the critical contact length along y axis (m, Figure 5.17) was measured for all surface footings. The critical contact length (n) along x axis was not measured. However, n was estimated as $2A_{c\_ob}/m$, where A_{c_ob} follows Equation 5.1, given that the soil's bearing capacity (q_u) has been fully mobilized at $\theta_{y'} = 55$ mrad (i.e., factor of safety = 1). Because q_u changes with both the L'/B' ratio and s_u within contact area, an iterative process is needed until A_{c_ob} has converged into a constant.
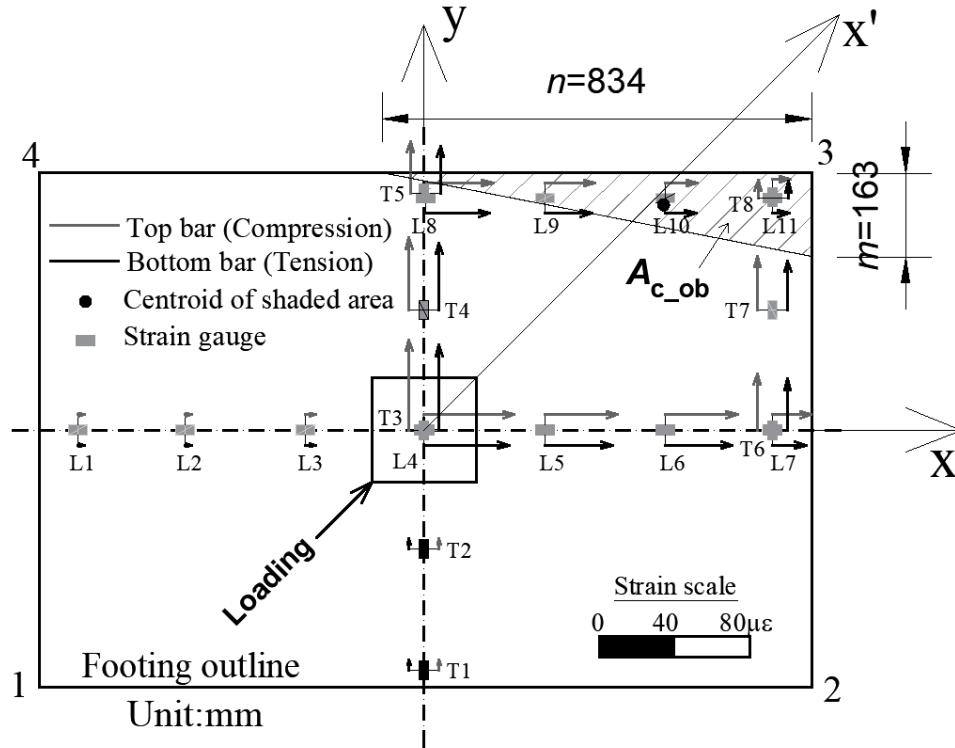
Figure 5.17. Strain distributions in the footing at $\theta_{y'}$ = 55 mrad and estimated critical contact area for test OS41.

Figure 5.17 also sketches A_{c_ob}, values of m and n, and the centroid of the critical contact area for test OS41. The centroid is very close to the x' axis, although there is still an offset from x'. The estimated A_{c_ob}, measured m, and estimated n for all surface footings are summarized in Table 5.3. The values of m and n indicate that the method of estimating A_{c_ob} works reasonably well; however, the values of m and n implied that the centroids were slightly offset from the x' axis, which can be explained by the error in Equation 5.1 and the out-of-plane rocking moment.

The readings of SG in the footing can be used to further verify the critical contact length. The normal strains at two adjacent SG stations should be the same if two SG stations are above the soil, because there is no soil shear stress along the uplift zone. Therefore, the edge of critical length should be within the SG stations where there is a significant change in normal strain (e.g.,

between T7 and L8 in Figure 5.17). Figure 5.18 shows the distribution of normal forces along the central and edge SG arrays along the *x* and *y* axis, for test OS41 for each cyclic packet. The normal force is calculated from the top and bottom strains (Figure 5.17) and the cross-sectional area at the SG station along the transverse direction. In Figure 5.18d, we take the distribution at the drift ratio of 4.2% for example. The normal force at T6 and T7 is almost the same but there was a sharp change from T7 to T8; this indicates that the footing segments from left edge to T7 were detached and the edge of the contact area should be between T7 and T8. In Figure 5.18c, the edge of the contact area should be between T4 and T5 following the same principle. The normal forces decreasing continuously from L8 to L11 at the edge imply that the footing from L8 to L11 was detached from the soil (Figure 5.18b), as also shown in Figure 5.17.
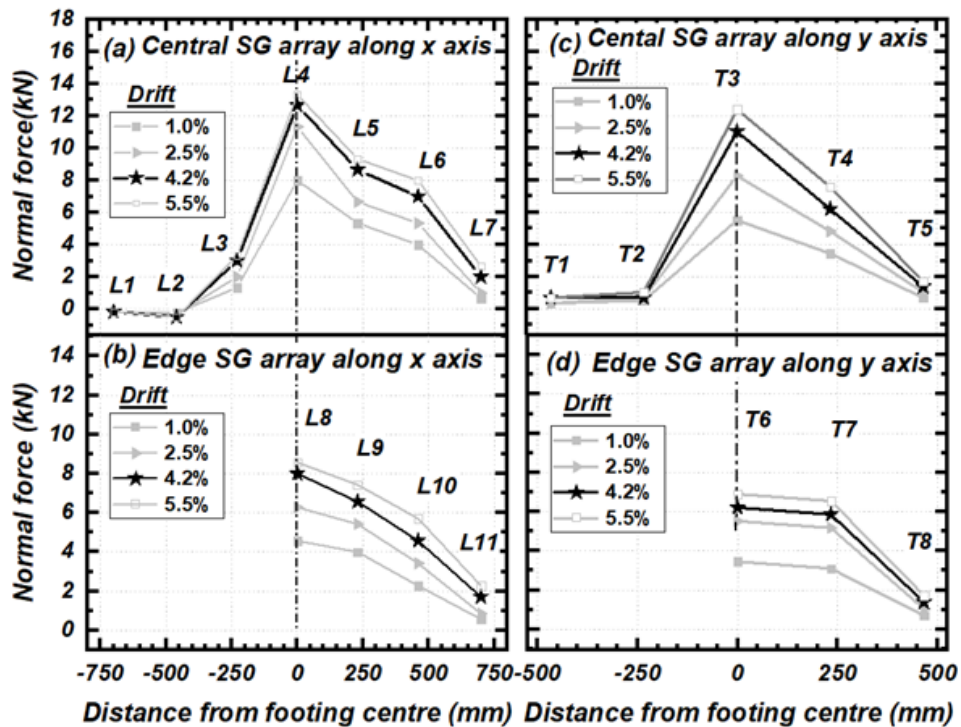
Figure 5.18. Normal force distributions calculated from for test OS41 (a) central SG array along *x* axis (b) normal edge SG array along *x* axis, (c) central SG array along *y* axis, and (d) normal edge SG array along *y* axis.

119

The footing uplift and plastic deformation of soil beneath the footing was observed during the field test. Out of 4 corners of the footing (Figure 5.4), three corners 1, 2, and 4 were detached from the soil and only corner 3 was in contact, when the footing was paused at the maximum rotation. This observation offers further evidence of the triangular critical contact area.

5.5.6 Deformed Soil Topography and Changed Soil Properties

Figure 5.19a shows the deformed soil surface beneath the footing after all four tests at Station 4 for "surface" footing. Significant rounding of soil surface along the loading direction can be seen in Figure 5.19a. Several tensile cracks which are fairly aligned to the critical contact area of the footing were observed. These cracks were caused by the transient contact length of the footing and the rounding of soil during cyclic loading. The pressure on the soil in contact area is very high whereas the pressure within the gap zone is zero; the differential pressure between two points crossing the contact area generated the soil cracks.

After the rocking system was removed from the station, the deformed soil topography was approximated by measuring the depth of soil at multiple points along the diagonal directions of the footing. The measured soil surface profiles along A-A and B-B sections at Station 4 are shown in Figure 5.19b and 5.19c. The total settlement of the surface footing at the center after four tests at Station 4 about 40.2 mm, while the settlement at corners along A-A section was about 90 mm. The differential settlement in Figure 5.19b clearly shows the soil rounding along A-A section. The soil rounding along B-B section (Figure 5.19c) was not as pronounced as in Figure 5.19b. The total settlement of the footing under orthogonal loading at a station next to Station 4 was about 1.5 times of the total settlement of the footing under oblique loading at Station 4 (Sharma and Deng 2019a). For embedded tests at Station 5, the total settlement at the

centre and corners of the embedded was about 22 mm and 40 mm. This might be attributed to the backfilled soil flowing into the gap formed during rocking.
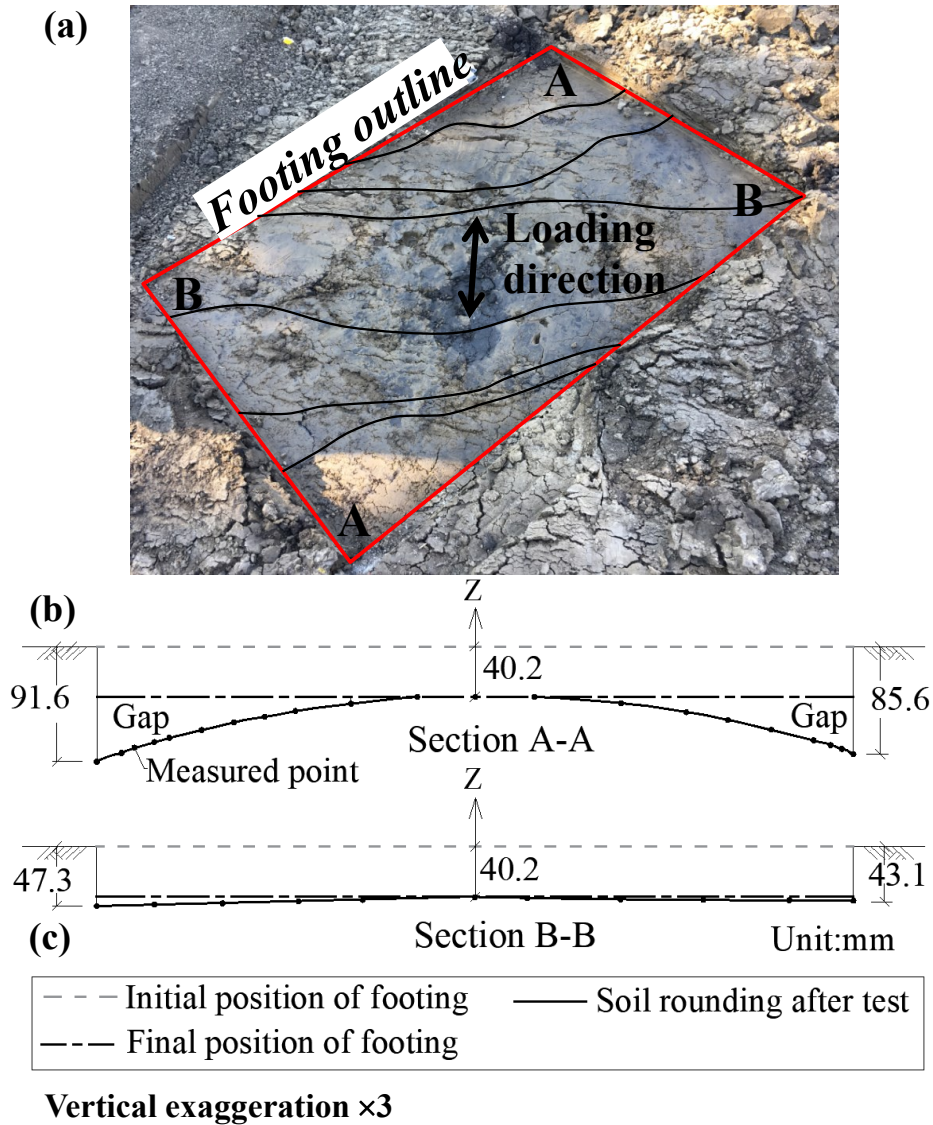
Figure 5.19. (a) Rounding of soil beneath the "surface" footing after all tests at Station 4, (b) measured profile along A-A section, and (c) measured profile along B-B section.

Shelby tube samples were obtained from a depth of 0 m to 1.0 m from the base of the footing, before and immediately after a test sequence as shown in Figure 5.1. Laboratory tests consisted of UCS and direct shear were carried out. The increase in both total density (ρ_t) and s_u

of soil is significant. It is seen that ρ_t of soil before tests was about 1.87 g/cm^3 and increased to about 1.91 g/cm^3 after all tests at Stations 4 and 5. The average s_u of soil from UCS tests before the test was about 70 kPa, which was increased to average s_u of 78 kPa at shallow depth (<0.45 m) at both Stations 4 and 5. However, we have not observed obvious changes in either ρ_t or s_u for soils deeper than approximately 0.45 m. The increased ρ_t and s_u of soil after the experiments should be attributed to the soil yielding and densification during the experiment.

5.6 Conclusions

The paper presents a series of oblique snap-back and cyclic loading tests of rocking foundations in cohesive soils. The following conclusions may be drawn:

1. The system rocked primarily along the plane of the oblique loading direction. The out-of-plane rocking moment was 6-15% of the in-plane moment and the out-of-plane footing rotation was 9.3-13.4% of the in-plane rotation.

2. In snap-back tests, the measured period of the rocking system was approximately 2-4 times of the periods of fixed-base system. The fundamental period of obliquely loaded rocking foundation increases as the initial *FSv* decreases.

3. A method to estimate moment capacity of the footing at any oblique angle is proposed and the method is validated by tests at 45° oblique angle in the present study.

4. A rotational stiffness reduction curve was established for the rocking system subjected to oblique loading on the clay. The equivalent damping ratio based on the moment-rotation hysteresis curve ranged from 8 to 30% while viscous damping ratio from snap-back tests ranged from 10 to 35%.

5. The rocking system exhibited a good re-centering ability along the oblique loading direction. The correlation of re-centering ratio vs. *A/Ac* was developed. The re-centering

ability of a rocking system subjected to oblique loading on clay is even better than that of footing subjected to orthogonal loading.

6. The value of w_r was less than 1.7% of the narrow width of footing even at $\theta_{y'c}$ of 250 mrad. As A/A_c increases, w_r reduces significantly. The settlement of footing subjected to oblique loading on clay was less than the values of aligned footing given the similar A/A_c range.

7. A method of estimating the critical contact area is developed based on the bearing capacity equations of footings subjected to two-way eccentricity. The method of estimating A_{c_ob} works reasonably well. The critical contact area is approximately triangular, which was observed from post-rocking inspection. The critical contact length can be approximately located using the readings of normal strain gauges in the footing.

8. Rounding of soil surface beneath the footing along the loading direction was observed, which is more significant in surface footing. An increase in the shear strength and density beneath the footing edges due to rocking cycles was observed.

6. Performance-Based Seismic Design of Rocking Shallow Foundations in Cohesive Soil: Methodology and Examples[4]

Abstract

This paper proposes a performance-based seismic design (PBSD) methodology for design of rocking shallow foundations for ordinary bridges in cohesive soils. The method is developed based on the existing displacement-based procedure where the expected performance is quantified by linking three performance indicators: maximum allowable drift, residual rotation and residual settlement. This study develops empirical correlations to obtain the secant stiffness and hysteresis damping ratios of rocking foundations as an input to the proposed PBSD guide. The empirical equations of re-centering ratio and residual settlement obtained from field testing program of rocking foundation were adopted to check the performance in terms of residual drift and residual settlement. In this design procedure, a bridge system consisting of a rocking foundation, a damped elastic column, and a deck mass is integrated into a single-degree-of-freedom system for which the system damping and period are calculated. The PBSD methodology is further illustrated with two examples. The shallow foundation of as-built Sanguinetti Bridge, Sonora County, California, was re-designed for assumed cohesive soil sites in British Columbia and California. Sensitivity analysis was carried out to understand the effects of normalized scant stiffness and hysteresis damping on the footing size and performance indicators. It is observed that the foundations of Sanguinetti Bridge can be designed reasonably

---

[4] This chapter is currently being prepared as a journal manuscript: Sharma, K. and Deng, L. 2019d. Performance-based seismic design of rocking shallow foundations in clay: methodology and examples, Canadian Geotechnical Journal.

well using the PBSD while satisfying the performance criteria for 2% maximum drift, residual drift, and residual settlement.

6.1 Introduction

Shallow foundation is commonly used to support bridges and building structures. Siddiquee and Alam (2017) reported that shallow foundation comprised of 36.4% and 40.3% of single and flared column bridge system respectively in BC, Canada. NCHRP (2010) reported that 17% of bridges in 39 states in the USA are supported by shallow foundations, including 30% in Washington and 25% in Nevada. Moreover, 6% and 3.75% of bridges that have shallow foundation are rested in clay in Washington and Nevada respectively.

Shallow foundations are conventionally designed as a fixed base. For this philosophy, the period of the structure is assumed relatively small, which leads to a large base shear and moment as the lengthening of period of system and increasing damping due to soil nonlinearity are not considered (AASHTO 2011; CSA 2014). A large footing size is required for large base shear and moment. An ultimate moment at the footing is calculated by multiplying the ultimate moment capacity of column by an overstrength factor greater than 1.3 (Gazetas 2019). Conventional footing design permits eccentricity due to seismic loading to fall within the middle two-third of the footing, which leads to excessively large footing.

As noted in Gazetas (2019), "adding extra capacity to a foundation-structure system can often reduce its seismic resilience". Rocking shallow foundations (with reduced capacity) have demonstrated advantages over conventional fixed-base foundation in seismic zones. The principle of rocking foundation has been adopted in the building codes of several countries. CSA (2014) states that soil nonlinearity (i.e. rocking foundation) can be considered and introduces the provisions of PBSD. EGBC (2018) allows the rocking foundation as a specialized seismic

system to enhance the post-seismic performance and accelerate the return to service of highway bridges in BC. NBCC (2005) added the provision of rocking shallow foundation and states that if the footings are larger than would be required for forces using a force reduction factor (R) value of 2.0, then their size can be reduced corresponding to R of 2.0. NZS (2004) states that rocking shallow foundation can be considered in the seismic design by a special study. A special study is defined as a non-linear time history analysis of a soil-foundation-structure system for several possible different earthquake motions which is frequently beyond the regular designer as it demands much time and effort with experts (Kelly 2009). In the USA, FEMA 440 (FEMA 2005) and ASCE 41-13 (ASCE 2014) incorporate nonlinear soil-foundation-structure interaction (i.e. rocking) effects by considering an increased period and a modified damping of the system. Rocking foundation may be permitted under seismic loading provided that foundation soils are not susceptible to loss of strength under the imposed cyclic loading (AASHTO 2011).

The performance-based seismic design (PBSD) specifies the tolerable displacement of earth structures and is commonly practiced in geotechnical earthquake engineering (Finn 2018). Various PBSD approaches were developed to control the lateral displacements of structures (Surez and Kowalsky 2011; Sadan et al. 2013). These approaches are based on the direct displacement-based design (DDBD) concept that designates a target performance level in term of displacement limits under a specified design earthquake (Priestley 2000; Malekpour and Dashti 2013; Billah and Alam 2016). Although PBSD can be potentially useful for foundations, very limited research is available for rocking foundation system.

Algie (2011) and Deng et al. (2014) proposed a DDBD methodology for the seismic design of rocking shallow foundations for shear wall and ordinary bridges respectively. Both of them defined the performance level of the structure in terms of drift limits and involved the

complicated process to calculate the initial stiffness, yield rotation, hysteresis, and radiation damping. Performance levels which are the backbone of the PBSD were not defined and checked in Algie (2011). More recently, the field behaviour of rocking foundations with large rotation (~7%) in cohesive soil was investigated (Sharma and Deng 2019a and 2019b). The empirical relationships for the performance indicators developed in field tests can be potentially implemented in the PBSD of rocking foundations.

The objective of present research is to develop a PBSD framework for rocking shallow foundation in cohesive soils. This PBSD framework considers three performance indicators: the maximum allowable drift, residual drift, and residual settlement. In this design procedure, a bridge system consisting of a rocking foundation, a damped elastic column, and a deck mass is integrated into a single-degree-of-freedom system for which the system damping and period are calculated. This study uses empirical relationships for the performance indicators. Two design examples are presented with realistic values to show the feasibility of PBSD. Sensitivity analysis is carried out to understand the effects of normalized scant stiffness and hysteresis damping on the footing size and performance indicators.

6.2   Input Parameters

6.2.1   Damping Ratio

The total damping of the soil-foundation-structure system can be split into structural damping, ξ_p and foundation damping, ξ_f. The foundation damping is the contribution of hysteresis damping, ξ_{hys} (i.e. material damping) and radiation damping, ξ_r. Ambrosini (2006) and Adamidis et al. (2014) revealed that ξ_r would rarely exceed 2%. The yielding of soil reduces the energy dissipation through the outgoing waves. As a result, ξ_r of nonlinear soil is significantly less than

that of elastic soil. As such, ξ_{hys} is taken as ξ_f. Then, the system damping (ξ_{sys}) can be calculated using Equation 6.1 (Sullivan et al. 2010; Algie 2011):

$$\xi_{sys} = \frac{\xi_{hys}\Delta_f + \xi_p\Delta_p}{\Delta_f + \Delta_p}$$
[6.1]

where Δ_f and Δ_p are the footing displacement due to rocking and sliding, and structural displacement of pier respectively.
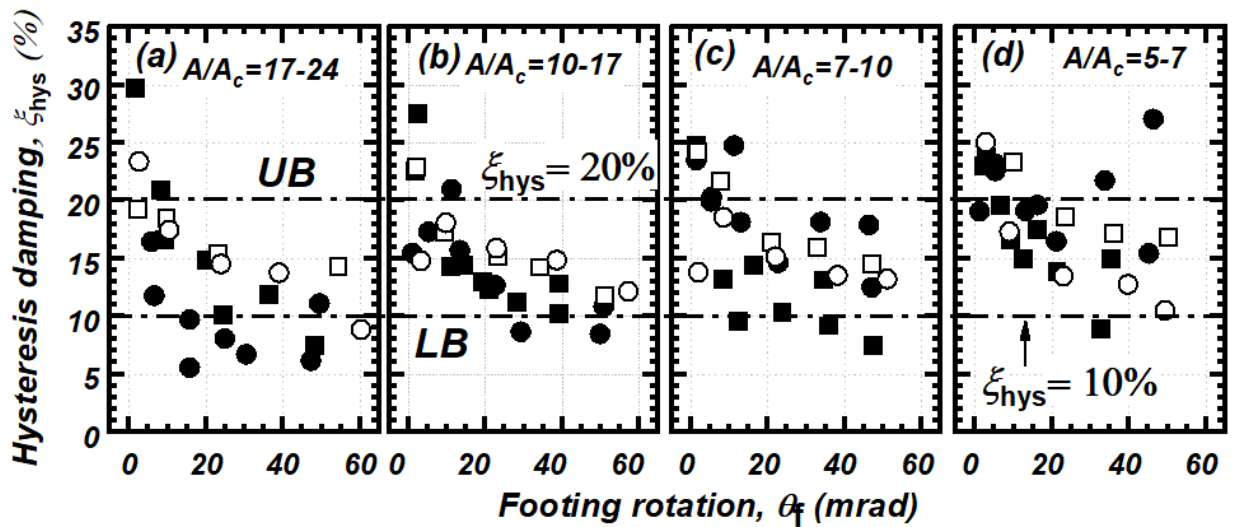
Figure 6.1. Equivalent damping ratio versus amplitude of rotation for all tests with different A/Ac ranges: (a) 17-24, (b) 10-17, (c) 7-10, and (d) 5-7.

CSA (2014) suggests that damping of the isolation system used in the design and analysis be based on field tests. The field tests of rocking shallow foundation in cohesive soil showed that the damping of the soil-foundation system was significantly greater than the 5% (Sharma and Deng 2019b) as shown in Figure 6.1. The damping throughout the field tests ranged from 8 to 30%. Field test results (Algie 2011; Phipps 2013) have observed similar outcomes.

6.2.2 Secant Stiffness

Since soil loses its stiffness with the increase in lateral load after yielding, effective secant stiffness (K_{sec}) is used in the design (Figure 6.2). In the DDBD, K_{sec} at the maximum displacement (Δ_d) is used rather than the initial stiffness (K_{ini}). The characterization of the structure by K_{sec} avoids many problems inherent in force-based design where K_{ini} is used to determine an elastic period (Priestley et al. 2007). An empirical relationship between K_{sec} and footing rotation was developed from lateral cyclic tests in cohesive soil, considering different loading direction, initial factor of safety (FSv), and embedded depth (D). The secant stiffness was calculated from moment vs. footing rotation hysteresis measured in the field under the cyclic loading (Figure 6.2b).
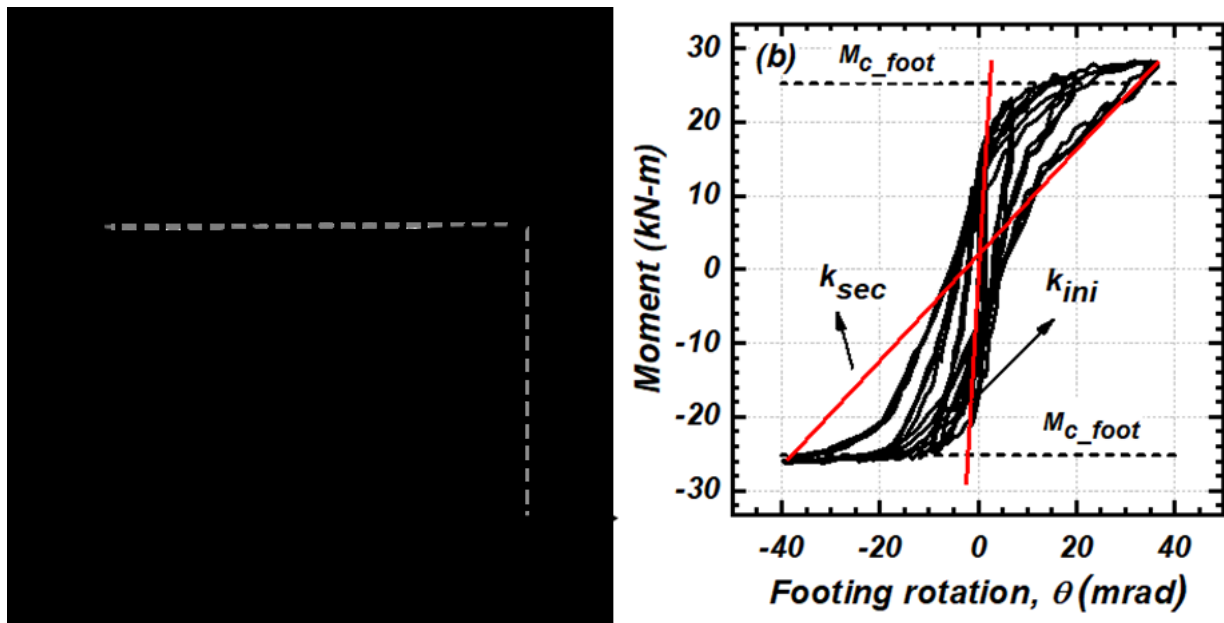
Figure 6.2. (a) Illustration of initial-stiffness and secant stiffness concepts related to a footing's nonlinear response and (b) nonlinear moment vs. rotation curves from a field test in cohesive soil in Edmonton, Canada.
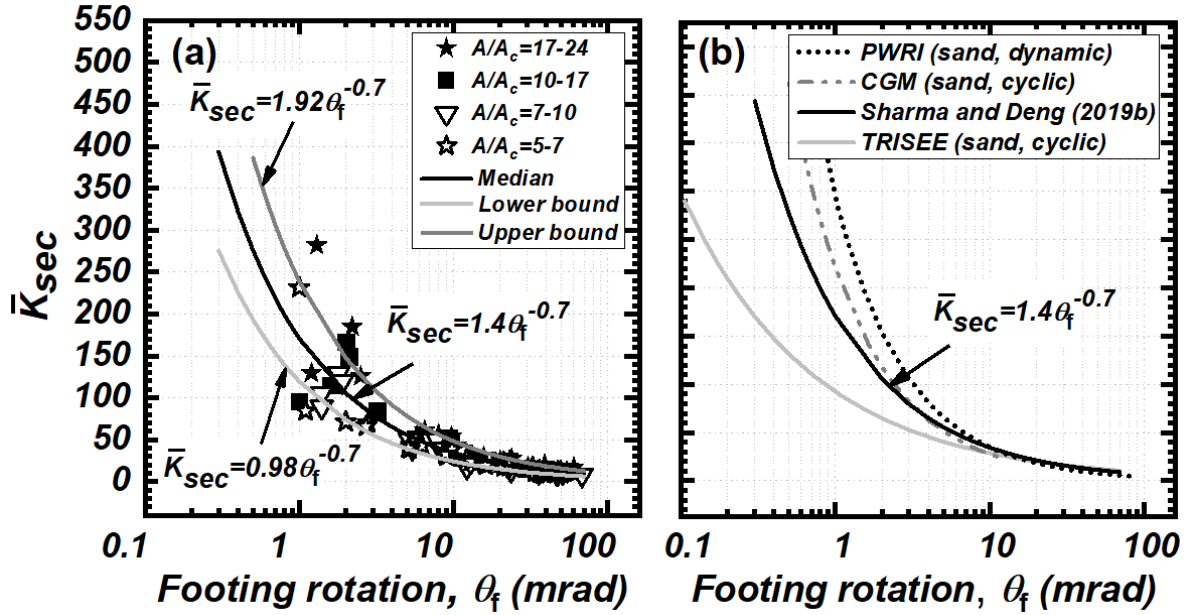
Figure 6.3. (a) normalized rocking stiffness degradation vs. maximum footing rotation and (b) normalized rocking stiffness degradation compared to results from the literature (Sharma and Deng 2019b).

In order to develop a rotational stiffness reduction trend, the normalized secant stiffness $\overline{K}_{sec}$ was introduced in Sharma and Deng (2019b), as defined in Equation 6.2:

$$\overline{K}_{sec} = \frac{M_{max}}{\theta_f \cdot Q \cdot L_f} = \frac{K_{sec}}{Q \cdot L_f} \qquad [6.2]$$

where M_{max} = maximum rocking moment; θ_f = maximum footing rotation due to design drift; Q = vertical load on the foundation; and L_f = footing length along the rocking direction.

Figure 6.3a shows the distribution of $\overline{K}_{sec}$ vs. θ_f. It is seen $\overline{K}_{sec}$ distribution becomes much more condensed and is almost unique at greater θ_f regardless of the A/A_c ratio or loading direction. The best estimate of $\overline{K}_{sec}$ vs. θ_f correlation of the present study is obtained as follows (Sharma and Deng 2019b):

$$\overline{K}_{sec} = 1.4\theta_f^{-0.7} \qquad [6.3]$$

130

The selection of $\bar{K}_{sec}$ empirical correlation affects the estimation of K_{sec} in Equation 6.2 and thus the subsequent design. The effect of $\bar{K}_{sec}$ on the foundation design will be further elucidated.

6.3   Performance Indicators

6.3.1   Maximum and Residual Rotation

PBSD approaches are adopted to control the maximum lateral displacements of structures, so the designer has to properly define a maximum design displacement (Δ_d) to achieve a target performance level (Sadan et al. 2013). The maximum lateral displacement could be the sum of structural displacement (Δp), footing sliding (Δ_{sl}) and rocking-induced displacement (Δ_r) as shown in Figure 6.4. Maximum design displacement could be a function of drift and P-Δ moment limit, performance level of the seismic hazards, space needed to avoid building pounding in case of buildings or minimum seating width of abutment for bridge, and importance of the structures. NBCC (2010) limits the drift to 2% for high-importance building and 2.5% for general buildings. AASHTO (2011) tolerates a maximum drift of 4%. For conventional pier system, both CSA (2014) and Caltrans (2012) limit the P-Δ moment to $0.2M_{c\_p}$, where M_{c_p} is the design moment capacity of the pier.

ASCE 41-13 (ASCE 2014) recommends to check the residual rotation of the structure to evaluate the performance level of bridges or buildings. Specifically, for highway bridges, residual rotation may affect the decision on the opening of bridge after the earthquake (Billah and Alam 2016). CSA (2014) defines the performance level in term of residual drift after a seismic event; for example, a lifeline bridge should be operational with limited service at the selected seismic hazard level to meet the performance requirement. For the considered damage

level, a target residual drift (Δ_{res}) of 0.6% is assumed to meet the performance objective of a lifeline bridge (Billah and Alam 2016).
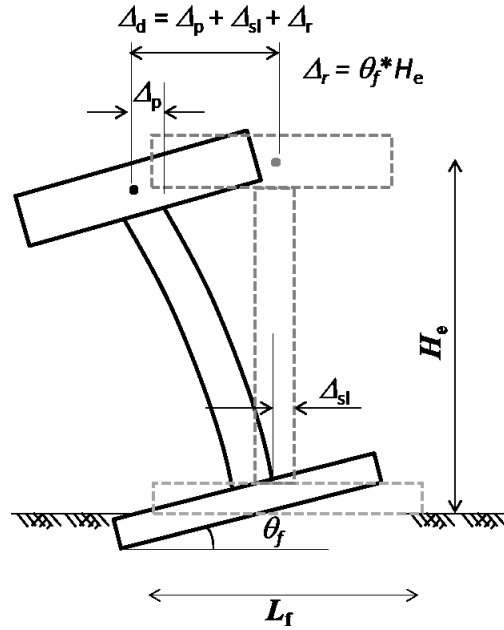
Figure 6.4. An SDOF structure showing three forms of displacement: structural (Δ_p), foundation sliding (Δ_{sl}), and rocking (Δ_r).

In the present research, the re-centering ratio is used to estimate the residual rotation and to evaluate the performance level of the bridge, which is defined as follows:

$$R_d = 1 - \frac{\theta_{res}}{\theta_f} \qquad [6.4]$$

where θ_{res} is the residual foot rotation at zero rocking moment and θ_f is the design footing rotation (i.e. maximum footing rotation).

The empirical equation of R_d vs. A/A_c curve (in Figure 6.5) developed from the field test in cohesive soil is followed (Sharma and Deng 2019b):

$$R_d = \frac{1}{2.055\frac{A_c}{A}+1.015} \qquad [6.5]$$

where A and A_c are the footing area and the critical contact area required to support the vertical load when the soil's ultimate bearing capacity is fully mobilized respectively. ASCE (2014) and Hakhamaneshi et al. (2016) adopted the R_d concept and defined the performance level of structures based on R_d.
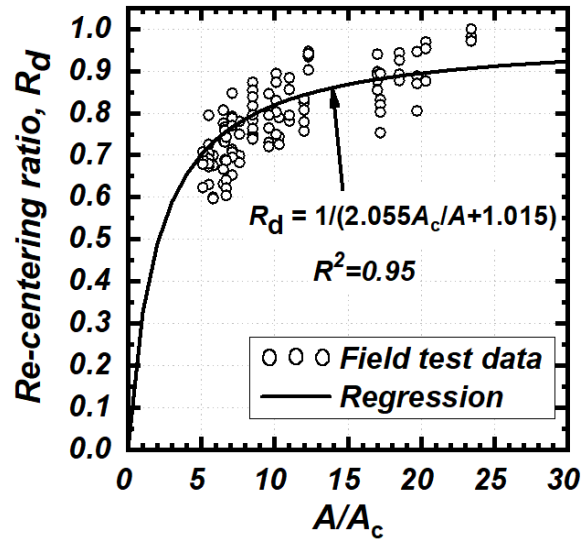
Figure 6.5. Empirical correlation between R_d and A/A_c

6.3.2   Rocking-induced Residual Settlement

The rocking-induced residual settlement w_r is one of the critical performance indicators considered in this PBSD approach, defined as:

$$w_r = C_{sett} L_f \theta_{cum} \qquad [6.6]$$

where C_{sett} and θ_{cum} is the settlement coefficient and cumulative footing rotation. The value of C_{sett} is empirically obtained from field tests in cohesive soil (Sharma and Deng 2019b).

The residual settlement using Equation 6.6 is an envelope that encloses most of the settlement data obtained from field test of rocking foundations under cyclic and snap-back tests in cohesive soil. Figure 6.6 show the C_{sett} vs. A/A_c correlation presented in Sharma and Deng (2019a and 2019b). Except in long-duration large earthquake, it is reasonable to consider that the

133

bridge or building experiences two full cycles of rotations equal to design footing rotation (Deng et al. 2014). Then, Equation 6.6 is rearranged to correlate the design rotation to the residual settlement:

$$w_r = 4C_{sett}L_f\theta_f \qquad [6.7]$$
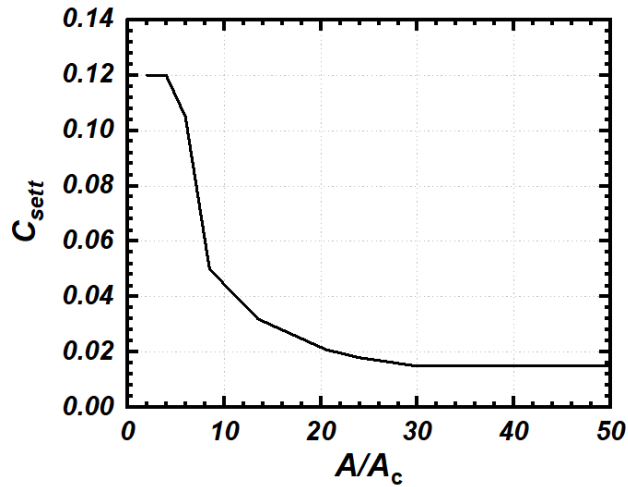
Figure 6.6. Dynamic settlement coefficient (C_{sett}) vs A/A_c (Adopted from Sharma and Deng (2019a and 2019b)

6.4   PBSD Procedure

This section briefly describes the proposed PBSD procedure. The procedure may be applied to standard ordinary bridges with seat type abutment having the following conditions: (1) the transverse resistance of shear keys is neglected; (2) for a single-column pier at the mid-span bridge, pier is assumed to be fixed to the bent cap beam; (3) for multiple-columns piers supporting at the mid-span bridge, the piers may be hinged at the top to the bent cap beam; and (4) considers elastic behaviour of the superstructure, not include inelastic effects of structural components. Figure 6.7 presents a flowchart of the PBSD procedure, which includes the following steps:
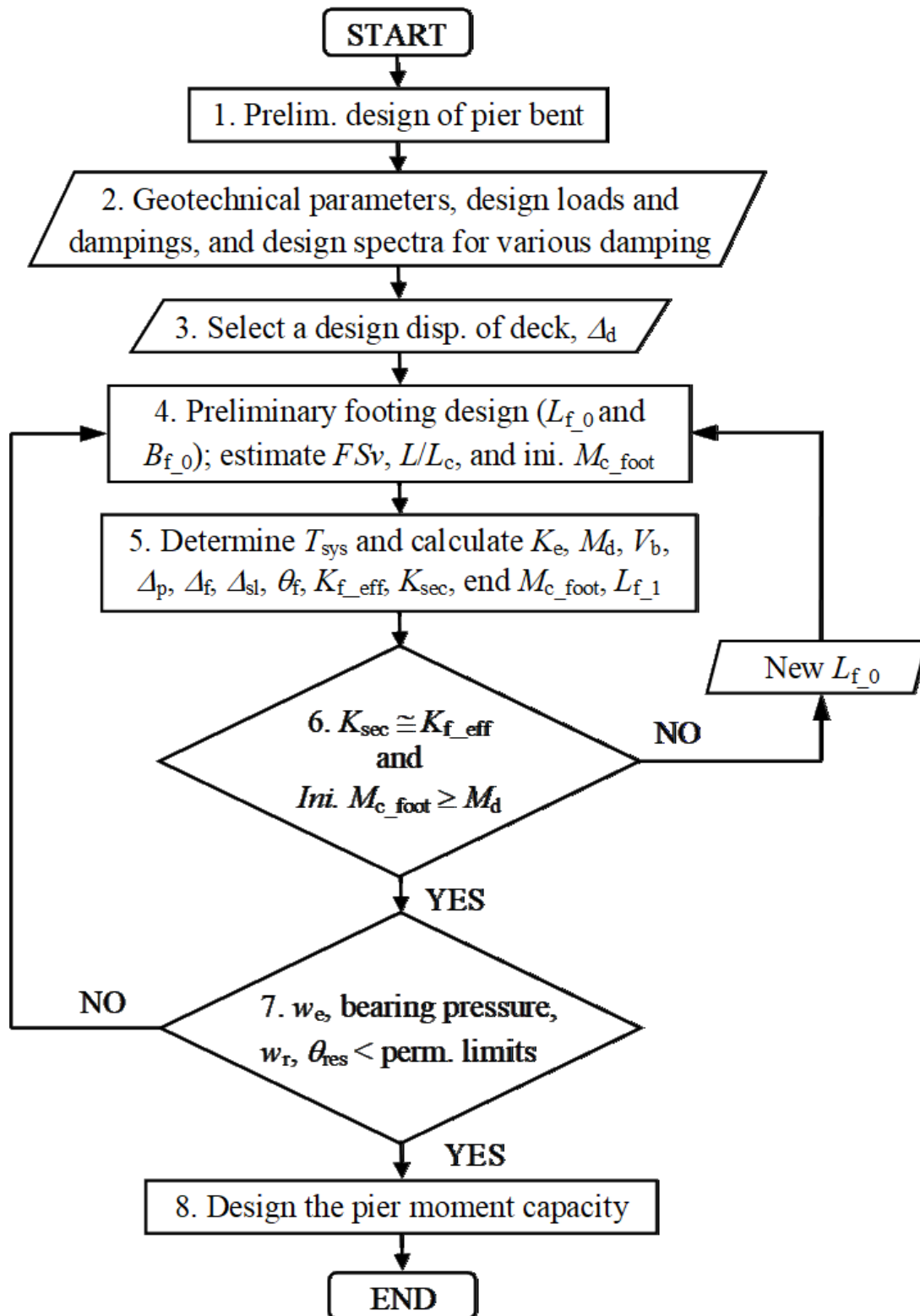
Figure 6.7. Flow chart of the PBSD procedure for rocking shallow foundation

1. Prepare a preliminary design of bridge bent. The detailed structural design is out of the scope of present research.

2. Geotechnical site characterization and design spectra for various damping ratios.

   For this study, design spectra obtained from CSA (2014) and Caltrans (2012) for 5% damping ratio are used for two different site-specific design examples. Equation 6.8 is used for adjusting the displacement spectra to account for a greater system damping (EC8 2003):

$$R_\xi = \left(\frac{0.1}{0.05+\xi}\right)^\alpha \qquad\qquad [6.8]$$

   where R_ξ is the damping modifier, α is a constant, $\alpha=0.5$ for far-field ordinary motions and $\alpha=0.25$ for near-field pulse motion, and ξ is the system damping ratio. The design displacement response spectra for any greater damping $S_{d,\xi}$ is equal to $S_{d,5\%} R_\xi$.

   A conservative ξ_{hys} of 10% is considered in the present study, towards the lower bound of damping ratio distribution. Previous research used equivalent hysteresis damping up to 20% (Algie 2011, Gajan et al. 2005). Initially, assume ξ_f equal to the system damping to start the design. Then ξ_{sys} can be checked later using Equation 6.1. For rocking foundation, ξ_{sys} is essentially close to the ξ_f as the footing rotation is significantly greater than the displacement of superstructure.

3. Select a design displacement (Δ_d) of the superstructure, the first performance indicator.

4. Conduct a preliminary design of the foundation based on CFEM (2006). Estimate A/A_c (or L_f/L_c) of the preliminary foundation design. An iterative process to account for the shape factor in soil bearing capacity may be required to improve L_c estimation. Calculate initial footing moment capacity (M_{c_foot}).

5. Design of rocking shallow foundation.

The objective of this step is to determine L_f, K_{sec} and moment capacity (M_{c_foot}) of the footing. The calculated K_{sec} and M_{c_foot} then shall be compared with the effective foundation stiffness, K_{f_eff} (in Step 5h) and design overturning moment (M_d) calculated in Step 5c. If they are considerably different, L_f in Step 5j can be used a preliminary length in Step 4 to the new iteration. Step 5 may be iterated until K_{sec} reasonably matches with K_{f_eff} and M_{c_foot} is greater than M_d.

a. Determine the equivalent period of the soil-foundation-structure system, T_{sys}, from a set of site-specific design displacement spectra for the given Δ_d and ξ_{sys}.

b. Calculate the effective system stiffness (K_e):

$$K_e = 4\pi^2 \frac{m}{T_{sys}^2} H_e^2 \qquad\qquad [6.9]$$

where m is the mass of superstructure.

c. Calculate the base shear (V_b) and M_d of the system

$$M_d = K_e \frac{\Delta_d}{H_e} \qquad\qquad [6.10a]$$

$$V_b = \frac{M_d}{H_e} \qquad\qquad [6.10b]$$

where H_e is the effective height of the pier (Figure 6.4).

d. Calculate Δ_p considering V_b and stiffness of the pier (K_p):

$$\Delta_p = \frac{V_b}{K_p} \qquad\qquad [6.11a]$$

e. Calculate the foundation displacement:

$$\Delta_f = \Delta_d - \Delta_p \qquad\qquad [6.11b]$$

f. Check ξ_{sys} using Equation 6.1. If the calculated ξ_{sys} is not close to the initial ξ_{sys}, then assume the calculated ξ_{sys} as an initial value and start from Step 5a.

g. Estimate the footing sliding displacement Δ_{sl} using:

$$\Delta_{sl} = \frac{V_b}{K_{fh}} \qquad\qquad [6.12]$$

where K_{fh} is horizontal stiffness of the footing using the equation developed in Gazetas (1991). Gajan and Kutter (2009) and others showed that Δ_{sl} is minimal when the moment to shear ratio (which is equal to H_e/L_f) is greater than 1. A designer may neglect Δ_{sl} because rocking is considered predominant displacement mode and the dominant mode of nonlinearity.

h. Calculate the maximum footing rotation (θ_f):

$$\theta_f = \frac{\Delta_r}{H_e} = \frac{\Delta d - \Delta sl - \Delta s}{H_e} \qquad\qquad [6.13]$$

where Δ_r is rocking-induced lateral displacement at the top of pier.

i. Calculate the effective foundation stiffness (K_{f_eff}):

$$K_{f\_eff} = \frac{M_{ini}}{\theta_f} \qquad\qquad [6.14]$$

j. Determine K_{sec} of the designed footing considering L_f, m, and θ_f, using Equations 6.2 and 6.3.

Determine M_{c_foot}:

$$M_{c\_foot} = K_{sec}\theta_f \qquad\qquad [6.15a]$$

Calculate the new L_f:

$$L_f = \frac{2M_{c\_foot}}{Q\left(1-\frac{L_c}{L}\right)} \qquad\qquad [6.15b]$$

6. A foundation must have adequate stiffness and overturning capacities. Check whether K_{sec} in Step 5i is close to K_{f_eff} in Step 5h and M_{c_foot} in Step 5j is greater than M_d in Step 5c. If yes, proceed to Step 7. If not, use L_f from Step 5j in Step 4 as the start point of the next iteration.

7. Check of performance of the design.

a. Check the elastic settlement (w_e) using existing methods (e.g. CSA 2014; CFEM 2006; AASHTO 2010).

b. Check the bearing capacity of the footing under the normal operation condition.

c. Check w_r using Equation 6.7. This is the 2nd performance indicator.

   The settlement criteria defined by AASHTO (2010) can also be applied to the rocking-induced settlement. The normalized rocking-induced settlement ($2w_r/L_f$) should be less than θ_f.

d. Check θ_{res} using:

$$\theta_{res} = (1 - R_d)\theta_f \qquad [6.16]$$

   which is the 3rd performance indicator.

e. Check Δ_{sl}. This is an optional check. The value of Δ_{sl} is estimated in Step 5f.

8. Design the bridge pier. This step is outside the scope of present research. In general, it is accepted that the bridge pier be designed with an over-strength factor (e.g., 1.3 in Gazetas 2019 and 1.2 in Deng et al. 2014) with regard to the foundation.

6.5 Design Examples

Sanguinetti Bridge located in Sonora County, CA, is redrawn in Figure 6.8 (State of California 1973). It is a 51.7 m long, 2-span continuous bridge with a single-pier-bent at the midspan. The details of the bridge are given in Table 6.1. The footing was designed conventionally as a fixed base with a transverse width of 6.7 m (Figure 6.8b). However, the footing dimension obtained through conventional design is much larger than required for bearing capacity of the underlying soil.
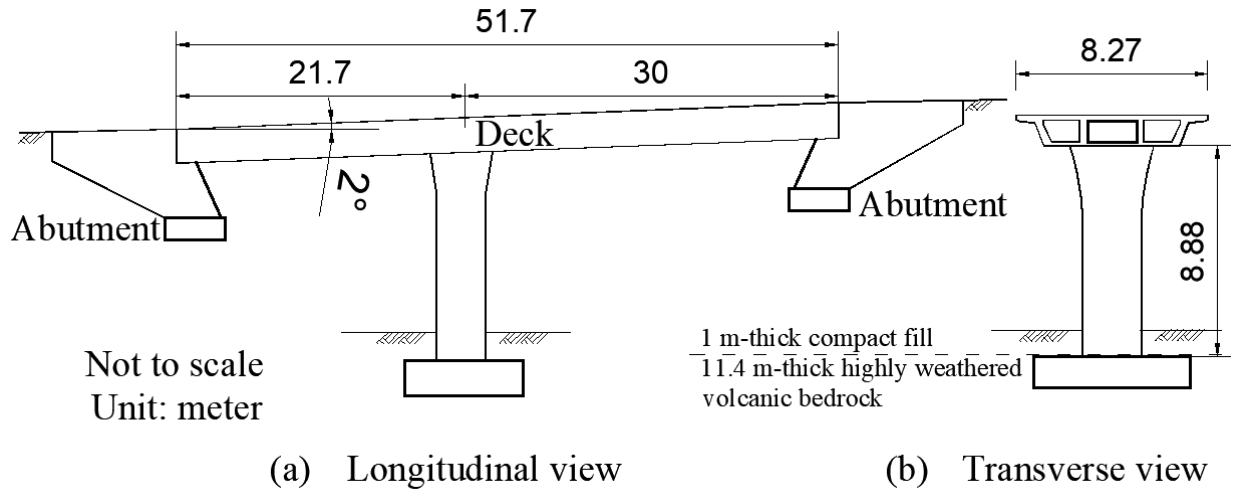
Figure 6.8. (a) Longitudinal; (b) transverse profiles of Sanguinetti Bridge.
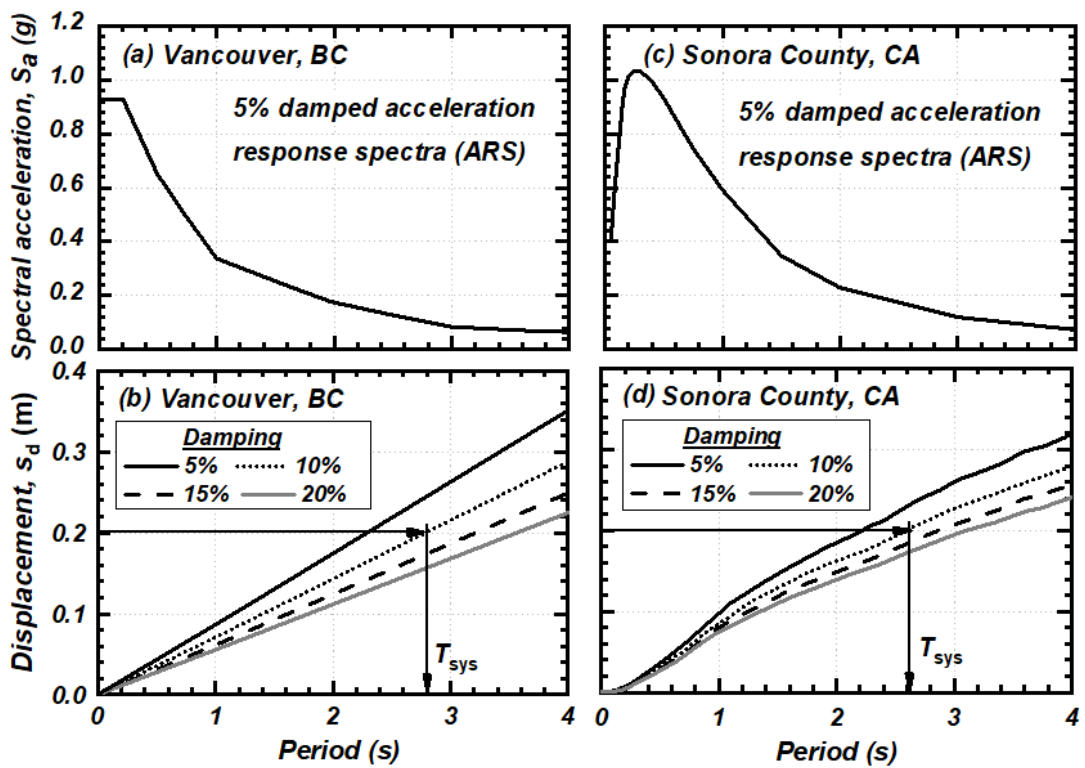
Figure 6.9. (a) 5% damped acceleration response spectra at a site in Vancouver, BC, (b) design displacement spectra for varying damping ratios for Vancouver, BC, (c) 5% damped acceleration response spectra at a site in Sonora County, CA, and (d) design displacement spectra for varying damping ratios for Sonora County.

This research conducted two re-design examples of the shallow foundations for Sanguinetti Bridge as if the bridge were located at Vancouver, BC, and Sonora County, CA. The difference between two examples is the design acceleration response spectra. For the present research, it is assumed that the foundations are in a cohesive soil layer with their bottoms resting on elastic silt (MH) with shear strength of 80 kPa and unit weight of 18.5 kN/m^3, because this MH soil was tested in the field by Sharma and Deng (2019a and 2019b). Foundation is assumed to be rocking along the transverse axis; the foundation length in the rocking direction will be redesigned following the proposed PBSD framework.

Table 6.1. Geotechnical and structural parameters of Sanguinetti bridge as built

Parameter	Value
Soil unit weight (kN/m^3)	16.4
Friction angle	35
Cohesion (kPa)	0
Site classification	C
Deck mass, m (kg)	5.05×10^5
Deck length (m)	51.7
Pier height (m)	8.88
Pier stiffness (kN/m)	8.32×10^4
Fixed-base period, T_0 (s)	0.49
Embedment depth, D (m)	2.0

6.5.1 Case Design in Vancouver, BC

The dimension and properties of the as-built superstructure are reused in this example. The step by step procedure produced the following results.

1. The moment-axial load diagram is used to estimate the yield moment capacity of the pier, which is M_{c_p} = 16.5 MN-m. The pier assumed 95.8 kN axial load, half of the total deadweight of the superstructures.

2. The bridge pier is assumed to be located in stiff clay. The medium to stiff clay is defined as Soil Profile Type III in CSA (2014). The spectral acceleration is selected according to CSA (2014) which corresponds to 2% probability of exceedance in 50 years with a return period of 2,475 years (Figure 6.9a). The displacement response spectra shown in Figure 6.9b were calculated from acceleration response spectra. Assume that the bridge is located far from any major faults, so the value of α=0.5 is used in Equation 6.8.

3. The design displacement (Δ_d) is assumed to be 0.20 m, which is less than the allowable drift recommendation by NBCC (2010) and CSA (2014). This is also less than $0.2M_{c\_p}/(m \cdot g)$ = 0.66 m and the minimum seating width recommended by CSA (2014). Considering the drift and P-Δ moment limits, a larger design displacement could be assumed, but a greater design displacement leads to unduly small footing length that would fail in the checks against bearing capacity and rocking-induced settlement.

4. Initially, a trial L_f=4.0 m is assumed and the ratio of L_f to B_f is considered 1.3. The trial values are based on the minimum FSv required for bearing capacity of the footing. The design is intended to maintain the critical contact area ratio, A/A_c of about 8 to 10 to have the improved performance in R_d and w_r (Gajan and Kutter 2008; Deng et al. 2014). Initial M_{c_foot} = 4.50 MN-m.

5. Assume ξ_p = 5% and ξ_f = 10%. The footing damping (ξ_f) is taken as ξ_{hys} for this design displacement.

   a. The design period of the system read from acceleration response spectra is: T_{sys} =2.8 s given Δ_d and ξ_{hys}.

   b. K_e = 200 MN-m (Equation 6.9)

   c. M_d = 4.52 MN-m and V_b = 509 kN (Equation 6.10).

      The stiffness of the pier is K_p = 83.2 MN/m. Then the structural deformation of pier from Equation 6.11a: Δ_p = 6.14 mm. The elastic deformation of the pier is almost insignificant compared to Δ_d. Then, the footing displacement:

      $\Delta_f = \Delta_d - \Delta_p$ =193.9 mm

   d. Check ξ_{sys} using Equation 6.1: ξ_{sys} =9.85 %, which is very close to the initial ξ_{sys} of 10%.

   e. Horizontal stiffness of footing is K_{fh} = 107×10^5 MN/m (Gazetas 1991). The sliding displacement is Δ_{sl} = 4.77 mm (Equation 6.12). The sliding displacement is minimal as the system is rocking dominated.

   f. Calculate rocking-induced displacement from Equation 6.13a: Δ_r = 189.1 mm. Then calculate the footing rotation (Equation 6.13b): θ_f = 0.021 rad.

   g. K_{f_eff} = 212 MN-m (Equation 6.14)

   h. The secant stiffness of the foundation given L_f, m, and θ_f ($=\theta_{max}$) is calculated from Equations 6.2 and 6.3: K_{sec} = 165 MN-m.

   i. The moment capacity of the footing from Equation 6.15a: final M_{c_foot} = 4.52 MN-m. The length of the footing is back-calculated using Equation 6.15b: L_f = 4.05 m.

6. The value of K_{sec} (in Step 5i) differs from K_{f_eff} (in Step 5h), and therefore iteration should be performed to satisfy the following condition: a. $K_{sec} \cong K_{f\_eff}$, b. Initial $M_{c\_foot} >$ M_d, and (c) L_f in Step 4 $\cong$ L_f in Step 5i. Table 6.2 shows that all three conditions are satisfied after 7 iterations. If the results of the successive iteration are not converging, the average L_f from the last two iterations can be used as the input for the next iteration to reduce the number of iterations.

7. Check of performance of the design.

   a. The elastic settlement based on the formulas in AASHTO (2010) is w_e = 2.4 cm. The allowable settlement recommended by AASHTO (2010) is 0.04×Deck length of bridge/2 = 10.3 cm.

   b. The factored vertical load is calculated considering a dead load factor = 1.5 and a live load factor = 1.5. The resistance factored for the ultimate bearing capacity is taken as 0.45. The ratio of the factored bearing capacity to the factored vertical load is 2.0, greater than the minimum threshold value (i.e. 1.0) recommended by AASHTO.

   c. The settlement coefficient for the given A/A_c = 8.6 (Table 6.2) is C_{sett} = 0.032. The rocking-induced settlement from Equation 6.6 is w_r = 1.14 cm. The normalized settlement (i.e. $2w_r/L_f$) is 0.55%. The normalized rocking-induced settlement meets the settlement criterion.

   d. As the moment-to-shear ratio (H_e/L_f) of 2.14 is greater than 1.0, the system will be rocking dominated. This indicates that sliding will be minimal. The sliding calculated in Step 5e normalized by L_f is only 0.12%.

   e. The re-centering ratio for the given A/A_c = 8.6 (Table 6.2) is R_d = 0.8. According to Hakhamaneshi et al. (2016), R_d = 0.8 for rectangular footing can satisfy the

immediate occupancy (IO) performance level. The residual rotation from Equation 6.16 is θ_{res} = 0.005 rad. The residual drift is 0.47%, less than allowable residual drift 0.6% for lifespan bridge (CSA 2014).

In summary, after seven iterations, the foundation design (i.e. L_f = 4.15 m, B_f = 5.40 m) meets the performance level for maximum drift (i.e. 2.5%), residual drift (0.47%), and rocking-induced settlement (1.14 cm). The design also meets the criteria for elastic settlement and bearing capacity at the normal operation condition.

Table 6.2. Iterative steps in the re-design of rocking foundation of Sanguinetti Bridge assumed to be located in Vancouver, BC

Parameters	Iterative steps						
	1	2	3	4	5	6	7
Initial L_{f_0} (m)	4	4.05	4.08	4.1	4.12	4.14	4.15
Initial B_{f_0} (m)	4.8	5.27	5.30	5.33	5.36	5.38	5.40
FSv	5.1	5.5	5.6	5.70	5.71	5.74	5.80
L/L_c	8.0	8.2	8.3	8.4	8.45	8.5	8.6
Init. M_{c_foot} (MN-m)	4.50	4.57	4.61	4.64	4.67	4.69	4.71
M_d (MN-m)	4.52	4.52	4.52	4.52	4.52	4.52	4.52
K_{f_eff} (MN-m)	212	212	212	212	212	212	212
K_{sec} (MN-m)	212	215	216	217	218	219	220
End M_{c_foot} (MN-m)	4.54	4.60	4.63	4.65	4.68	4.69	4.71
End L_{f_1} (m)	4.05	4.08	4.1	4.12	4.14	4.15	4.15
End B_{f_1} (m)	4.86	4.90	5.33	5.36	5.38	5.40	5.40

6.5.2 Case Design in Sonora County, CA

The footing of Sanguinetti Bridge is re-designed for Sonora County, CA, as another example of PBSD framework. The dimension and properties of the as-built superstructure are also reused. Following are the steps.

1. The bridge is assumed to be supported by a site with Soil Class C (stiff soil). The corresponding spectral acceleration (Figure 6.9c) is selected according to Caltrans (2010). The displacement spectra are calculated using $\alpha=0.5$.

2. Adopt $\Delta_d = 0.20$ m, which is less than the minimum seating width recommended by Caltrans (2010). This is also less than $0.2 \cdot M_{c\_col} / (m \cdot g) = 0.66$ m.

3. Initially a trial value of footing length $L_f = 4.0$ m is assumed for a square footing i.e. $B_f = 4.0$ m. and initial $M_{c\_foot} = 4.30$ MN-m.

4. $\xi_p = 5\%$ and $\xi_f = 10\%$. Assume $\xi_f \cong \xi_{hys}$.

   a. $T_{sys} = 2.64$ s (Figure 6.9d), given $\Delta_d=0.2$ m and $\xi_{hys} \cong 10\%$

   b. $K_e = 226$ MN-m (Equation 6.9)

   c. $M_d = 5.09$ MN-m and $V_b = 573$ kN (Equation 6.10)

   d. $\Delta_p = 6.9$ mm (Equation 6.11a) given $K_p = 8.32 \times 10^4$ kN-m and $V_b = 573$ kN. Footing displacement $\Delta_f = \Delta_d - \Delta_p = 193.86$ mm. Then check ξ_{sys} using Equation 6.1: $\xi_{sys} = 9.83$ %, which is very close to the initial ξ_{sys} of 10% considered in Step 5a.

   e. $K_{fh} = 107$ MN-m (Gazetas 1991) and $\Delta_{sl} = 4.77$ mm (Equation 6.12)

   f. $\Delta_r = \Delta_d - \Delta_p - \Delta_{sl} = 188.2$ mm (Equation 6.13a), and $\theta_f = 0.021$ rad (Equation 6.13b)

   g. $K_{f\_eff} = 240$ MN-m (Equation 6.14).

   h. $K_{sec} = 165.2$ MN-m given the L_f, m and θ_f (Equations 6.2 and 6.3)

i. Final M_{c_foot} = 4.53 MN-m (Equation 6.15a). The length of footing is back-calculated using Equation 15b: L_f = 4.22 m.

5. Since K_{sec} (in Step 5h) differs from the K_{f_eff} (in Step 5g), iterations are needed. Table 6.3 shows that all three conditions are satisfied after 8 iterations.

Table 6.3. Iterative steps in the re-design of rocking foundation of Sanguinetti Bridge located in Sonora County, CA

Parameters	Iterative steps							
	1	2	3	4	5	6	7	8
Initial L_{f_0} (m)	4	4.22	4.4	4.5	4.58	4.64	4.67	4.68
Initial B_{f_0} (m)	4	4.22	4.4	4.5	4.58	4.64	4.67	4.68
FSv	4.13	4.6	4.92	5.13	5.30	5.43	5.50	5.52
L/L_c	6.1	6.78	7.38	7.72	8.00	8.21	8.32	8.36
Init. M_{c_foot} (MN-m)	4.3	4.63	4.89	5.04	5.14	5.24	5.28	5.30
M_d (MN-m)	5.09	5.09	5.09	5.09	5.09	5.09	5.09	5.09
K_{f_eff} (MN-m)	240	240	240	240	240	240	240	240
K_{sec} (MN-m)	214	225	235	240	244	247	249	250
End M_{c_foot} (MN-m)	4.53	4.78	4.98	5.10	5.19	5.26	5.29	5.30
End L_{f_1} (m)	4.22	4.4	4.5	4.58	4.64	4.67	4.68	4.68
End B_{f_1} (m)	4.22	4.4	4.5	4.58	4.64	4.67	4.68	4.68

6. Check of performance of the design.

a. w_e = 2.40 cm, less than the allowable settlement (10.3 cm) recommended by AASHTO (2010).

b. The ratio of the factored bearing capacity to the factored vertical load is 1.88, greater than the minimum threshold value (i.e. 1.0).

c. Select $C_{sett} = 0.032$ for the given $A/A_c = 8.36$ (Table 6.3). Thus $w_r = 1.30$ cm (Equation 6.6). The normalized settlement (i.e. $2w_r/L_f$) is 0.54%. As the normalized settlement is less than θ_f, it meets the settlement criterion.

d. As the moment-to-shear ratio of 1.9 is greater than 1.0, the system will be rocking dominated. The sliding displacement calculated in Step 5e normalized by L_f is only 0.095%.

e. Select $R_d = 0.78$ for the given $A/A_c = 8.36$ (Table 6.3). According to Hakhamaneshi et al. (2016), $R_d = 0.78$ for rectangular footing can satisfy the immediate occupancy (IO) performance level. The residual rotation from Equation 6.16 is $\theta_{res} = 0.005$ rad. The residual drift is 0.467%, less than 0.6% (CSA 2014). The residual drift meets the residual drift criterion.

6.6 Sensitivity Analysis

The relationship between ξ_{hys} vs. θ_f and $\overline{K}_{sec}$ vs. θ_f may be not unique (Figures 6.1 and 6.3). Conservative $\overline{K}_{sec}$ and ξ_{hys} may be selected for the worst condition. If a design is sensitive to variations in the soil properties being considered, a sensitivity analysis should be carried out (Jia 2016). A sensitivity analysis in this section was intended to quantify the effects of selecting $\overline{K}_{sec}$ and ξ_{hys} on the footing dimensions considering the same Δ_d and corresponding site conditions as in previous examples.

6.6.1 Effect of Secant Stiffness

The benchmark design examples in previous section adopted Equation 6.3 as the best estimate of the correlation of $\overline{K}_{sec}$ vs. θ_f. This study considers lower bound (LB) and upper bound (UB) of

$\overline{K}_{sec}$ vs. θ_f correlations as shown Figure 6.3a and redesigns the foundation following the proposed PBSD framework. The LB and UB equations are followed:

$$\overline{K}_{sec} = 0.98\theta_f^{-0.7}, \quad \text{for LB} \qquad [6.17a]$$

$$\overline{K}_{sec} = 1.40\theta_f^{-0.7}, \quad \text{for UB} \qquad [6.17b]$$

As the design displacement and site conditions are the same as previous examples, corresponding K_{f_eff} and M_d remained unchanged regardless of $\overline{K}_{sec}$. Figures 6.10a and 6.10b show the effect of $\overline{K}_{sec}$ on L_f and performance indicators i.e. Δ_{res} and w_r. The LB $\overline{K}_{sec}$ decreases K_{sec} for given θ_f and Q. Given the lower value of $\overline{K}_{sec}$, L_f should be increased to achieve the secant stiffness criterion (i.e. $K_{f\_eff} \cong K_{sec}$; Step 6) with constant load on footing (see Equations 6.2 and 6.3 for details). As the design L_f increases, the Δ_{res} and w_r are improved significantly as shown in Figure 6.10b. In this case, as L_f becomes greater, M_{c_foot} easily meets M_d ($M_{c\_foot} > M_d$; Step 6). The results indicate that the design is governed by K_{sec} for LB $\overline{K}_{sec}$ case.

The UB $\overline{K}_{sec}$ increases K_{sec} for the given θ_f. Given the greater value of $\overline{K}_{sec}$, even the smaller L_f can achieve the stiffness conditions with constant load on footing. However, a decrease in L_f results in compromising M_{c_foot}. Then, L_f may need to be increased to meet the footing moment capacity criterion (i.e. $M_{c\_foot} > M_d$; Step 6). Eventually, L_f may not change significantly as shown in Figure 6.10a. As L_f remains the same, Δ_{res} and w_r do not change significantly as shown in Figure 6.10b. In this case, the moment capacity requirement governs the footing design rather than the secant stiffness. As A/A_c for both the benchmark and UB cases was around 8 and performances indicators are within limits with less footing size as compared to LB case, it appears that the benchmark case with average $\overline{K}_{sec}$ leads to a reasonable design for rocking foundation.
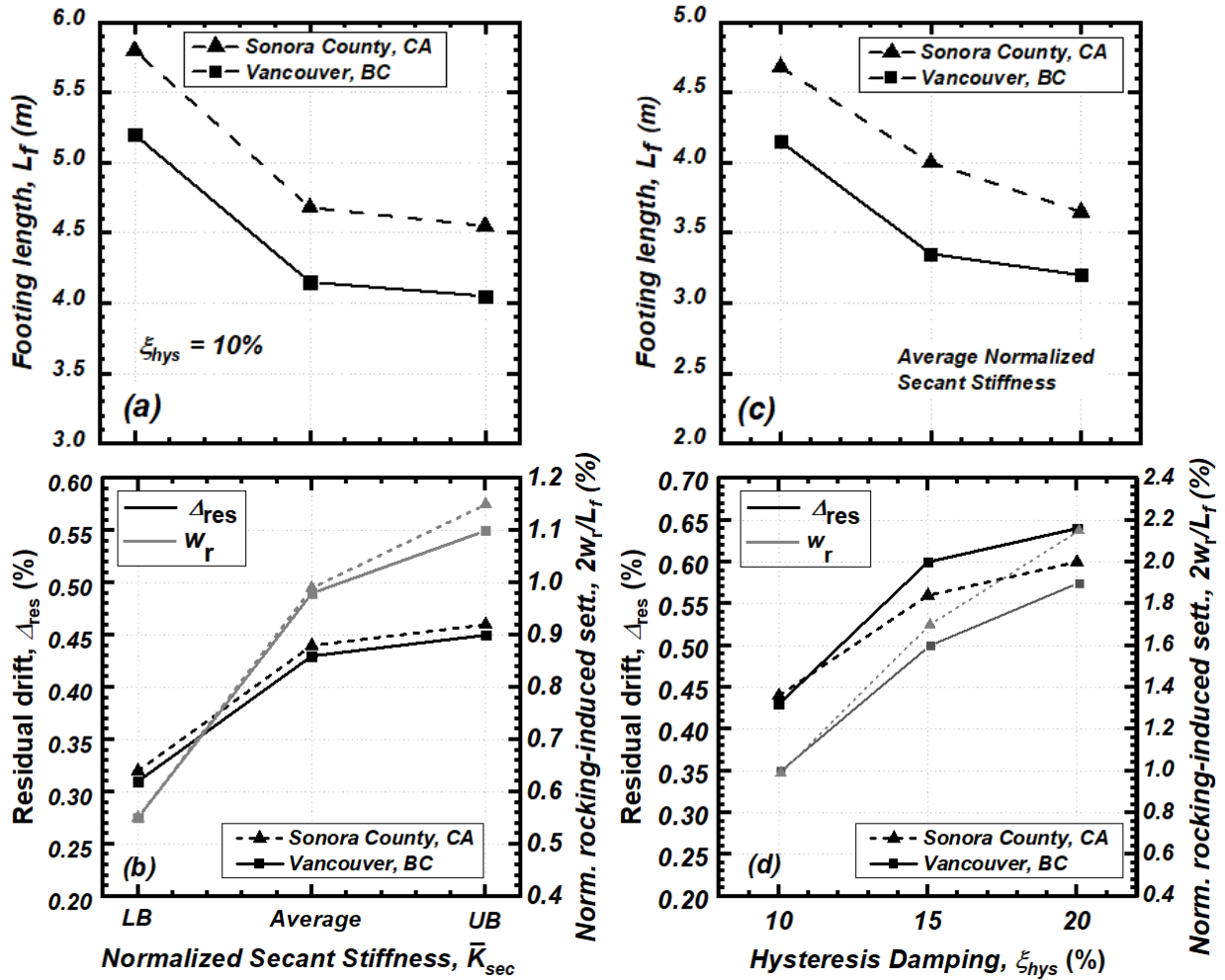
Figure 6.10. (a) Effect of normalized secant stiffness on footing length, (b)) effect of normalized secant stiffness on residual drift and normalized rocking-induced settlement, (c) effect of foundation damping on footing length, and (d) effect of foundation damping on residual drift and normalized rocking-induced settlement. UB: Upper bound and LB: Lower bound.

6.6.2 Effect of Hysteresis Damping Ratio

The hysteresis damping ratios were obtained from the field on rocking shallow foundation in cohesive soil, ranging from 8 to 30%. However, excluding some extreme values, for most cases, ξ_{hys} fell inside the range of 10 to 20%, particularly for the footing rotation less than 10 mard

(Figure 6.1). The benchmark design examples adopted a conservative ξ_{hys} of 10%. In this section, ξ_{hys} values of 15% and 20% were considered.

Figures 6.10c and d show the effect of ξ_{hys} value on L_f and performance indicators i.e. Δ_{res} and w_r. Increasing ξ_{hys} results in greater T_{sys}, and less K_e, M_d and V_b. The value of K_{f_eff} decreases as the M_d decreases with greater ξ_{sys}. Then a smaller footing can be used to achieve the value of M_d and K_{f_eff} for M_{c_foot} and K_{sec} respectively. When ξ_{hys} increases from 10% to 20%, L_f is decreased by about 22% for both examples as shown in Figure 6.10c. Decreased L_f with greater ξ_{hys} leads to increase in Δ_{res} and w_r as shown in Figure 6.10d. Figure 6.10c and d show that when ξ_{hys}= 15%, both Δ_{res} and w_r reach close to the limiting value. When ξ_{hys} is greater than 10%, A/A_c appears to be less than 8, so it is seen that the benchmark case leads to a reasonable design of rocking foundation.

6.7   Conclusions

This study presents a performance-based seismic design framework for rocking shallow foundations of ordinary bridges. The framework considers the performance level in maximum drift, residual drift, and rocking-induced settlement. Following conclusions may be drawn.

This study developed necessary empirical correlations to obtain the secant stiffness and hysteresis damping ratios of rocking foundations. These correlations are essentially needed as an input to the developed PBSD guide. The empirical relationships of re-centering ratio vs. footing rotation and dynamic settlement coefficient vs. A/A_c were adopted to check the performance in terms of residual drift and residual settlement.

The proposed PBSD methodology was illustrated with two examples. In these examples, Sanguinetti Bridge, a highway overpass, was re-designed with shallow foundations as if the

foundations are located in Vancouver, BC, or Sonora Country, CA, on a stiff clay (site Class C). The maximum drift of the examples were set as 2.25%, and the as-built bridge deck properties were used as the input. The redesign resulted in a footing dimension 4.15 m ×5.40 m in Vancouver, and 4.68 m ×4.68 m in Sonora County. The redesigned footing dimension was less than the as-built dimension by about 30% and still satisfied the performance criteria in the residual drift, residual settlement, elastic settlement, and bearing capacity.

The effects of secant stiffness and hysteresis damping on rocking shallow foundation were investigated in a sensitivity analysis. The average normalized secant stiffness was observed reasonable for rocking foundation design. The UB secant stiffness resulted in similar footing size as average normalized secant stiffness, while LB secant stiffness results the higher footing size with very high performances. A 10% hysteresis damping led to more reasonable footing dimension. As the hysteresis damping increases, the footing size decreases which may lead to exceeding performance indicators.

7. Conclusions and Recommendations

The present research project investigated the behaviour of rocking shallow foundations in cohesive soil in Edmonton, Alberta.

The research was conducted in two consecutive tracks. Firstly, series of field tests were carried on bridge systems with rocking foundation and elastic column. The experiments were done in two sets: snap-back tests and pseudo-static cyclic tests. The rocking system consisted of a 1.5 m by 1.0 m concrete footing, column, and deck. The footing was extensive instrumented to characterise mechanical response of the footing. The loading direction, depth of embedment, footing aspect ratio, and initial static factor of safety were systematically varied. Geotechnical investigation were carried prior to and during the tests. Geotechnical investigation consisted of pre-test CPT, Shelby tube sampling before and after rocking tests, and laboratory testing of undisturbed soil samples. Laboratory test program was carried out to determine the unconfined compressive strength (UCS), undrained shear strength (s_u) using direct shear under various normal stresses, Atterberg limits, and physical properties. The system performance indices, such as moment capacity, damping, stiffness, settlement and re-centering capability, were quantified and compared to the published literature. The empirical relationship between rocking amplitude vs. period, secant stiffness vs. footing ration, re-centering ration vs. critical contact area ratio, damping vs. footing rotation etc. were developed which can be used in the design of rocking foundation. The changes in soil properties and the footing mechanical response were characterized. Secondly, performance-based design guidelines of rocking foundations for ordinary bridges were proposed. Two design examples for an ordinary bridge located at two different sites were presented. The seismic design guidelines are proposed to support the

provision of PBSD that has recently added to many standards and guidelines (AASHTO 2011; CSA 2014; FHWA 2014; NZT 2014) and replace the conventional force-based design of conventional bridges.

Main conclusions of the present research and recommendations for future research are presented in this chapter.

7.1   Conclusions

7.1.1   Snap-back Tests

The nonlinear dynamic behaviour of a soil-footing-column-structure system designed with a rocking foundation was investigated using snap-back tests at a cohesive soil site. During the snap-back tests, an initial drift was applied to the deck and then the system was released to enable the free vibration. The snap-back tests allowed the structure to behave in a similar manner to that expected during ground shaking. The snap-back test method is relatively simple to perform, can be repeated easily, and simulate the behaviour of the structure during the earthquake. Main conclusions are:

a. The moment capacity of the footing correlated very well with the predicted values. The moment vs. rotation behaviour was observed highly non-linear. The footing rotation required to mobilize the moment capacity of footing on clay was about 0.012 rad. The shear capacity of footing did not significantly change with the number of trials or amplitude of horizontal displacement. The maximum sliding observed was about 0.18% of footing length, which is very small in general. Minimum sliding observed in the field test satisfied the statement that sliding is minimal when the moment to shear ratio (which is equal to H_e/L_f) is greater than 1. The shear capacity considering the soil-footing interface shear resistance underestimated the

measured shear capacity by 26% and the shear capacity considering statics equilibrium correlated well with the measured values.

b. The field experiments demonstrated a large amount of damping during the oscillations after snap-back release of the shallow foundations. The damping ratio observed during the oscillations of the shallow foundations ranged from 8 to 30%. High damping can be beneficial to a structure by reducing seismic forces. The damping ratio was insensitive to the amplitude of rotation when footing rotation exceeded 20 mrad, despite of scattered data. The trend of damping ratio with footing rotation on clay was observed slightly higher than footing on sand.

c. Lengthening of the period was observed in the field test. Average measured period of the rocking system was elongated by approximately 235% comparing with the period of fixed-base structure. Rounding of the soil surface due to rocking-induced plastic deformations was observed. Rounding of the soil surface beneath footing due to rocking-induced plastic deformations was observed which might be attributed to the lengthening of the period. The fundamental periods of the rocking system increase approximately linearly, as the initial FSv decreases.

d. Excessive settlement did not occur during snap-back tests. The residual settlement was less than 1% of the length of the foundation even at a cumulative footing rotation of 250 mrad. As critical contact area ratio increases, the residual settlement of the footing reduces significantly. The settlement of footing on clay was much less than the values on sand given the similar critical contact area ratio range. The rocking system exhibited a good recentering ability, even better than on sand.

e. The state of soil beneath the footing before and after rocking was examined. An increase in the density and shear strength beneath the critical contact area due to rocking cycles was observed. The depth of influence zone, where the soil properties changed significantly, was approximately two times the critical contact length of footing.

7.1.2 Cyclic Performance and Footing Mechanical Response

A series of field test on soil-footing-column-deck-abutment systems was designed to study how the systems perform and how is the mechanical response of the rocking foundations under cyclic loading. The footing was intensively instrumented with strain gauges to assist the estimation of transient soil-footing contact area during the cyclic loading tests. The cyclic loading consists of 5 packets of which each contain 3 to 4 cycles of similar displacement amplitude up to 7%. Thirty-eight strain gauge stations were attached onto the top and bottom rebars of the footing to monitor the normal strain in footing. Main conclusions are:

a. As observed in snap-back test, an increase in the unit weight and shear strength beneath the footing edges due to rocking cycles was observed. The influence depth was approximately two times the critical contact length of the footing same as the snap-back test.

b. The calculated footing moment capacity agreed very well with the experimental results. The results are similar to those reported by preceding researchers using the centrifuge and shake table test. The moment-rotation and settlement-rotation relationships of rocking footings during cyclic and seismic loading were further examined. The footing moment capacity increased slightly even after 7% of cyclic rotation possibly due to the increasing strength of soils in the critical contact area. This is advantageous over a concrete or steel column which typically exhibits degrading flexural moment capacity.

c. A degradation of rotational stiffness was observed as soil was strained due to increasing amplitudes of rotation. A rotational stiffness reduction curve was established for the rocking system on the clay. The normalized stiffness is almost unique at large footing rotation regardless of the critical contact area ratio, soil types, or test condition. The normalized stiffness vs. footing rotation equation was proposed for foundations in clay and used later in PBSD methodology as an input.

d. The results of field investigation generally supported the claim that energy may be dissipated at the soil-structure interface. Rounding of the soil surface due to rocking-induced plastic deformations was observed. The damping ratio based on the moment-rotation hysteresis curve ranged from 8 to 30%. High damping can be beneficial to a structure by reducing seismic forces. The damping ratio generally decreases as the amplitude of footing rotation increases. The hysteresis damping measured in the field was used as an input in PBSD methodology.

e. Excessive settlement did not occur during the cyclic loading tests. The value of rocking-induced settlement was less than 3% of the footing length even at cumulative footing rotation of 350 mrad. As critical contact area ratio increases, rocking-induced settlement reduces significantly. Footings with critical contact area ratio greater than 10 showed negligible rocking-induced settlement. The settlement of footing on clay was less than the values on sand given the similar rocking-induced settlement range. The empirical equation of rocking-induced residual settlement was adopted to check the performance in terms of residual settlement in PBSD methodology.

f. The rocking system exhibited a good re-centering ability. The correlation of re-centering ratio vs. critical contact area ratio was developed. The re-centering ability of a rocking

system on clay is slightly better than that of a footing on sand. A rocking footing with large critical contact area ratio has a good trade of energy dissipation and re-centering ability that will produce good seismic performance for soil-foundation-bridge systems. The empirical equation of re-centering ratio was adopted to check the performance in terms of residual drift in PBSD methodology.

g. The footing remained elastic during rocking. The transient soil-footing contact length can be estimated with the mechanical response of footing based on the strain gauge readings. The method suggests that the edge of the transient contact area should fall within the SG stations where there was a sharp change in the strain or normal force. Measured contact length of footing with soil agreed very well with the calculated contact length of footing and confirmed the validity of strain gauge-based estimation method.

7.1.3   Effects of Loading Obliquity on Rocking Foundation

This research evaluated the effects of loading obliquity on rocking foundation resting on cohesive soil. Lateral snap-back and cyclic loading tests at an oblique angle of 45° with respect to the footing axes were carried. During the snap-back tests, an initial drift was applied to the deck and then the system was released to enable the free vibration. The cyclic loading consists of 5 packets of which each contain 3 to 4 cycles of similar displacement amplitude. The footing was intensively instrumented with strain gauges in order to assist the estimating of the critical contact length of the footing. Natural periods, damping ratio, re-centering ratio, settlement, and stiffness degradation during the tests were discussed and compared with the results from previous studies with orthogonal loading. Main conclusions are:

a. The system rocked primarily along the plane of the oblique loading direction during the free vibration after releasing from initial position. The out-of-plane rocking moment was 6-15%

of the in-plane moment and the out-of-plane footing rotation was 9.3-13.4% of the in-plane rotation.

b. The lengthening of the period was observed. Measured period of the rocking system was approximately 2-4 times of the periods of fixed-base system. The fundamental period of obliquely loaded rocking foundation increases linearly as the initial *FSv* decreases. The fundamental period of obliquely loaded rocking foundation compared with the results from previous studies with orthogonal loading.

c. The oblique loading results in biaxial moments and two-way eccentricity, which may complicate the performance evaluation. There is no prediction method for determining the moment capacity of obliquely loaded foundations. An equation to estimate moment capacity of the footing at any oblique angle was proposed and the equation validated by field tests at 45° oblique angle in the present study.

d. Since soil loses its stiffness with the increase in lateral load after yielding, a rotational stiffness reduction curve was established for the rocking system subjected to oblique loading on the clay. A higher damping was observed in both snap-back and cyclic loading tests. The viscous damping ratio from snap-back tests ranged from 10 to 35% while equivalent damping ratio based on the moment-rotation hysteresis curve ranged from 8 to 30%.

e. The rocking system exhibited a good re-centering ability along the oblique loading direction. The correlation of re-centering ratio vs. critical contact area ratio was developed. The re-centering ability of a rocking system subjected to oblique loading on clay is even better than that of footing subjected to orthogonal loading.

f. The settlement of footing subjected to oblique loading on clay was less than the values of aligned footing given the similar critical contact area ratio range and loading condition. The

value of rocking-induced settlement was less than 1.7% of the narrow width of footing even at greater cumulative rotation of 250 mrad. As in aligned loading case, rocking induced settlement reduces significantly with increase in critical contact area ratio.

g. A method of estimating the critical contact area is developed based on the bearing capacity equations of footings subjected to two-way eccentricity. The method of estimating critical contact area worked reasonably well. The critical contact area was approximately triangular, which was observed from post-rocking inspection. The critical contact length can be approximately located using the readings of normal strain gauges in the footing.

h. Rounding of soil surface beneath the footing along the loading direction was observed, which is more significant in surface footing. The settlement at the edge of surface footing was greater than the embedded footing. This might be attributed to the backfilled soil flowing into the gap formed during rocking in embedded footing. As in orthogonal loading case, an increase in shear strength and density beneath the footing edges due to rocking cycles was observed.

7.1.4 Performance-based Seismic Design for Rocking Shallow Foundation

Procedure for performance-based seismic design of rocking foundation for ordinary bridges was developed and elaborated with two design example. PBSD methodology was developed based on the existing displacement-based procedure and expected performance level was checked considering three performance indicators: maximum design drift, residual settlement and residual rotation. Empirical correlations of the secant stiffness and hysteresis damping ratios of rocking foundations developed from field tests data considered as an input to the proposed PBSD guide. The empirical equations of re-centering ratio and residual settlement obtained from field testing program of rocking foundation were adopted to check the performance in terms of residual drift

and rocking-induced residual settlement. An ordinary bridge system consisting of a rocking foundation, an elastic column, and a deck mass was integrated into a single-degree-of-freedom system for which the system damping and period were calculated. The hysteresis damping obtained from the field test was considered as footing damping. The PBSD methodology was further illustrated with two examples. The shallow foundation of as-built Sanguinetti Bridge, Sonora County, California, was re-designed for assumed cohesive soil sites in Vancouver, British Columbia and Sonora County California to illustrate the application of the new design procedure. The difference between two examples is the design acceleration response spectra. Sensitivity analysis was carried out to understand the effects of normalized scant stiffness and hysteresis damping on the footing size and performance indicators.

Major steps in the design procedure are: (1) Prepare a preliminary design of bridge bent; (2) collect geotechnical information and design spectra for various damping ratios; (3) select a design displacement (Δ_d) of the superstructure; (4) conduct a preliminary design of the foundation; (5) Design of rocking shallow foundation: calculation of effective stiffness of footing, design moment and base shear, secant stiffness, and footing moment capacity etc.; (6) Check stiffness and overturning capacities. If the secant stiffness and footing moment capacity do not meet the effective stiffness of footing and design moment respectively, the foundation should be redesigned and iterated until secant stiffness reasonably matches with effective stiffness of footing and footing moment capacity is greater than design moment. The foundation design shall undergo performance checks in the elastic settlement, the bearing capacity, the rocking-induced settlement, the lateral sliding resistance and the residual rotation.

Observations from the design examples and sensitivity analysis are:

1. It took a few iterations before secant stiffness and footing moment capacity meet the effective stiffness of footing and design moment respectively.

2. It is likely that large design displacement results the smaller footing that may not meet the performance criteria. For instance, the first trial design with design displacement 300 mm, did not meet the criteria for rocking-induced settlement and residual rotation because critical contact area ratio of the design was relatively small.

3. A minimum critical contact area ratio 8.0 is suggested for the finalized design. If it is not satisfied, actions should be taken to increase the critical contact area ratio.

4. The dimension of designed rocking foundation was less than the as-built dimension by about 30% and still satisfied the performance criteria in the residual drift, residual settlement, elastic settlement, and bearing capacity.

5. The average normalized secant stiffness was observed reasonable for rocking foundation design considering reasonable critical contact area ratio (~8) and performance criteria in the residual drift, residual settlement, elastic settlement, and bearing capacity.

6. A 10% hysteresis damping led to more reasonable footing dimension. As the hysteresis damping increases, the footing size decreases which may lead to exceeding performance indicators.

7. The performance-based seismic design guidelines can practically be used for ordinary bridge systems with rocking shallow foundations. Design examples showed the feasibility of the design guidelines.

7.2 Recommendations

1. Additional field tests are required, on different soil types, to fully understand rocking shallow foundation behaviour. Rocking foundation system with different sizes, shapes and aspect ratio of footing should be tested. Rocking shallow foundation with various moment to shear ratios should be considered as well. Field should be primarily focused on low moment to shear ratio to determine the critical state from where rocking is dominated over sliding of footing. Large number of tests with various conditions will help to get a broad representation of potential rocking foundations for Canada and other countries.

2. Field tests on rocking shallow foundation with dense strain gauges mounted onto the rebars are required to properly characterise the mechanical response of the footing during rocking. Pressure sensors can also be used beneath the footing at small interval to predict the critical contact length fairly.

3. Additional field tests are required to evaluate the effect of obliquity on field performance of rocking shallow foundation. The load should be applied at a various arbitrary angle range from 0 to 90 degree with the orthogonal axis of the footing.

4. The empirical equations of secant stiffness, re-centering ratio, residual settlement and damping need further validation using data from more full-scale experiments with different parameters. Different types of clays, rotation amplitudes, footing sizes, and embedment configurations could be varied in these tests.

5. A three dimension numerical modeling, calibrated using field test data is required. Calibrated three dimension model then can used for parametric analysis considering different factor of safety, embedded depth, loading direction, moment-to-shear ratio etc.

The same model can be used for incremental dynamic analysis considering past earthquake.

6. An idealized single column bridge pier with deck mass supported by an isolated footing was considered in this research. Rocking footings are subjected to large and numerous impacts. Further studies should be extended to more complex structural systems with various foundation types.

7. Performance-based seismic design (PBSD) presented in this research is simple and quick to use for rocking shallow foundation for regular bridge. The proposed PBSD methodology should extended for multi-span and complex bridge system. This method can be verified by non-linear time history analysis.

8. Further research should be carried out on accelerated bridge construction using rocking shallow foundation. More specific attention should be given to footing-column and column-deck connections for rocking foundation bridge system.

References

AASHTO. 2010. Load and Resistance Factor Design (LRFD) bridge design specifications, 6th ed., American Association of State Highway and Transportation Officials Washington, DC.

AASHTO. 2011. Guide Specifications for LRFD Seismic Bridge Design, 2nd ed., American Association of State Highway and Transportation Officials: Washington, DC.

Acikgoz, S., and DeJong, M.J. 2014. The rocking response of large flexible structures to earthquakes. *Bulletin of Earthquake Engineering*, **12**(20): 875–908.

Acikgoz, S., Ma, Q., Palermo, A., and DeJong, M.J. 2016. Experimental Identification of the Dynamic Characteristics of a Flexible Rocking Structure. *Journal of Earthquake Engineering*, **20**: 1199–1221.

Adamidis, O., Gazetas, G., Anastasopoulos, I., and Argyrou, C. 2014. Equivalent-linear stiffness and damping in rocking of circular and strip foundations. *Bulletin of Earthquake Engineering*, **12**(3): 1177–1200.

Algie, T.B. 2011. Nonlinear rotational behaviour of shallow foundations on cohesive soil. PhD thesis, University of Auckland, New Zealand.

Algie, T.B., Henry, R.S., and Ma, Q.T. 2007. Insitu free vibration tests on a single degree of freedom structure with foundation uplift. *Proceedings of the NZSEE Conference* 2007, March 30- April 1, Auckland, New Zealand, paper no. **25**: 1–9.

Ambrosini, R.D. 2006. Material damping vs. radiation damping in soil–structure interaction analysis. *Computers and Geotechnics*, **33**(2): 86–92.

American Society of Civil Engineers (ASCE). 2014. Seismic Evaluation and Retrofit of Existing Buildings (ASCE/SEI 41-13), Reston, VA.

Anastasopoulos, I., Drosos, V., and Antonaki, N. 2015. Three-storey building retrofit: rocking isolation versus conventional design. *Earthquake Engineering and Structural Dynamics*, **44** (8): 1235-1254.

Anastasopoulos, I., Loli, M., Georgarakos, T., and Drosos, V. 2013. Shaking table testing on rocking-isolated bridge pier on sand. *Journal of Earthquake Engineering*, **17**: 1-32.

Anastasopoulos, I., Kourkoulis, R., Gelagoti, F., and Papadopoulos, E. 2012. Response of SDOF systems on shallow improved sand: an experimental study. *Soil Dynamics and Earthquake Engineering*, **40**: 15–33.

Antonellis, G., and Panagiotou, M. 2014. Seismic response of bridges with rocking foundations compared to fixed-base bridges at a near-fault site. *Journal of Bridge Engineering*, *ASCE,* **19**(5): 04014007.

Antonellis, G., Gavras, A.G., Panagiotou, M., Kutter, B.L., Guerrini, G., Sander A., Fox, P.J., Restrepo, R.I., and Mahin, S.A. 2014. *Shake-table test response of bridge columns supported on rocking shallow foundations*, Report No. UCB/SEMM-2014/07, Department of Civil and Environmental Engineering, University of California at Berkeley, Berkeley, CA, USA.

Antonellis, G., Gavras, A.G., Panagiotou, M., Kutter, B.L., Guerrini, G., Sander, A.C., and Fox, P.J. 2015. Shake table test of large-scale bridge columns supported on rocking shallow foundations. *Journal of Geotechnical and Geoenvironmental Engineering*, *ASCE*, **141**(5): 04015009.

Antonellis, G., Gavras, A.G., Panagiotou, M., Kutter, B.L., Sander, A., Guerrini, G., and Fox, P.J. 2014. Shake table test response of large-scale bridge columns supported on rocking shallow foundations. *Proc. of 10th U.S. National Conference on Earthquake Engineering, Frontiers of Earthquake Engineering*, July 21-24, Anchorage, Alaska, USA.

Apostolou, M., Gazetas, G., and Garini, E. 2007. Seismic response of slender rigid structures with foundation uplifting. *Soil Dynamics and Earthquake Engineering*, **27**: 642–654.

Applied Technology Council (ATC). 1992. Guidelines for Cyclic Seismic Testing of Components of Steel Structures for Buildings, Report No. ATC-24, Applied Technology Council, Redwood City, CA.

Ataei, H., Mamaghani, M., and Lui, E. 2017. Proposed framework for the performance-based seismic design of highway bridges. *Structures Congress*, pp. 240-53.

Barthes, C.B. 2012. *Design of earthquake resistant bridges using rocking columns*. PhD Thesis, UC Berkeley, USA.

Bartlett, P.E. 1976. *Foundation rocking on a clay soil*. ME thesis, University of Auckland, School of Engineering, Rep. No. 154, Auckland, New Zealand.

Billah, A., and Alam, M.S. 2016. Performance-Based Seismic Design of Shape Memory Alloy–Reinforced Concrete Bridge Piers. II: Methodology and Design Example. *Journal of Structural Engineering ASCE*, **142**(12): 04016141.

Brown, P.T. 1969. Numerical analyses of uniformly loaded circular rafts on deep elastic foundation. *Geotechnique*, **19**(3): 399–404.

Browne, M., Carr, A.J., and Bull, D. 2006. The analysis of reinforced concrete rocking wall behavior. *Proceedings of the 2006 NZSEE Conference*, Napier, New Zealand.

Caltrans. 2012. Caltrans ARS Online (v1.0.4). (http://dap3.dot.ca .gov/shake_stable).

Campbell, K.W. 1977. *The use of seismotectonics in the Bayesian estimation of seismic risk*, Report UCLA-ENG-7744, School of Engineering and Applied Science, University of California, Los Angeles, CA.

Canadian Standards Association (CSA). 2014. Canadian Highway Bridge Design Code, CAN/CSA-S6-14, Mississauga, ON.

Canadian Standards Association (CSA). 2014. Design of concrete structures. CSA A23.3-14, Rexdale, Ont., Canada.

CFEM. 2006. Canadian foundation engineering manual, 4th ed., Canadian Geotechnical Society, Richmond, British Columbia, Canada.

Chatzigogos, T.C., Pecker, A., Yilmaz, T.M., and Dietz, M. 2011. Seismic Engineering Research Infrastructures for European Synergies: *Report on Pseudo-dynamic test techniques with SSI*, WP14-JRA3.

Chiou, J., Chen, C., Huang, Y., and Chen, C. 2015. Shaking Table Testing on a Column-Footing Model. *Proc. of 6th International Conference on Earthquake Geotechnical Engineering,* Christchurch, New Zealand.

Chopra, A.K. 2007. Elastic response spectrum: A historical note. *Earthquake Engineering and Structural Dynamics*, **36**(1): 3–12.

Chopra, A.K., and Yim, C. 1985. Simplified earthquake analysis of structures with foundation uplift. *Journal of Structural Engineering, ASCE*, **111** (4): 906-930.

Combault, J. and Teyssandier, J.P. 2005. The Rion-Antirion bridge: concept, design and construction. *Proc. of the 2005 Structures Congress and the 2005 Forensic Engineering Symposium*, New York, pp. 149–158.

Combault, J., Pecker, A., Teyssandier, J.P., and Tourtois J.M. 2005. Rion-Antirion Bridge, Greece – concept, design, and construction. *Structural Engineering International, pp.* 22–27.

Das, B.M. 2016. *Principles of Foundation Engineering*. 8th ed. Cengage Learning, Boston, MA.

Deng, L., and Kutter, B.L. 2012. Characterization of rocking shallow foundation using centrifuge model tests. *Earthquake Engineering and Structure Dynamics*, **41**(5): 1043–1060.

Deng, L., Kutter, B. L., and Kunnath, S. K. 2012b. Probabilistic seismic performance of rocking-foundation and hinging-column bridges. *Earthquake Spectra*, **8**(2): 309-326.

Deng, L., Kutter, B.L., and Kunnath, S.K. 2012a. Centrifuge modeling of bridge systems designed for rocking foundations. *Journal of Geotechnical and Geoenvironmental Engineering, ASCE*, **138**(3): 335–344.

Deng, L., Kutter, B.L., and Kunnath, S.K. 2014. Seismic design of rocking shallow foundations: a displacement-based methodology. *Journal of Bridge Engineering, ASCE*, **19**(11): 1-11.

Drosos, V., Georgarakos, T., Loli, M., Anastasopoulos, I., Zarzouras, O., and Gazetas, G. 2012. Soil-Foundation-structure interaction with mobilization of bearing capacity: an experimental study on sand. *Journal of Geotechnical Geoenvironmental Engineering, ASCE*, **138**(11): 1369-1386.

Duncan, J.M., Wright, S.G., and Thomas, L.B. 2014. *Soil Strength and Slope Stability*, 2nd ed., Wiley, Hoboken, NJ.

EC8. 2003. *Design Provisions for Earthquake Resistance of Structures*. Pub. ENV-2003-2, Comite Europeaen de Normalization, Brussels.

EGBC. 2018. *Performance based seismic design of bridge in BC.* Engineers and Geoscientist British Columbia, Canada.

Elghazouli, A. Y. 2009. *Seismic design of buildings to Eurocode 8*, Spon Press.

Espinoza A.O. 2011. Seismic performance of reinforced concrete bridges allowed to uplift during multi-directional excitation. PhD thesis, University of California, Berkeley, CA.

Espinoza, A., and Mahin, S.A. 2008. Shaking table and analytical investigation of reinforced concrete bridge piers with foundations allowed to uplift during earthquakes. Report No. UCB/SEMM-08/03, Department of Civil and Environmental Engineering, University of California, Berkeley, CA, USA.

Faccioli, E., Paolucci, R., and Vivero, G. 2001. Investigation of seismic soil–footing interaction by large-scale cyclic tests and analytical models. *Proc.4th International Conference on Recent Advances in Geotechnical Earthquake Engineering and Soil Dynamics*, San Diego, CA, USA, Paper no. SPL-5.

FEMA. 2000. Prestandard and Commentary for the Seismic Rehabilitation of Buildings, FEMA 356. Washington D.C.: Federal Emergency Management Agency.

FEMA. 2005. Improvement of nonlinear static seismic analysis procedures. FEMA 440, Federal Emergency Management Agency, Washington, DC.

FEMA. 2007. Interim Protocols for Determining Seismic Performance Characteristics of Structural and Non-structural Components Through Laboratory Testing. FEMA 461, Federal Emergency Management Agency, Washington, DC.

FHWA. 2002. Geotechnical engineering circular No. 6, shallow foundation. U.S. Department of Transportation, Federal Highway Administration.

FHWA. 2014. LRFD Seismic analysis and design of bridges reference manual, Federal Highway Administration.

Finn, W.D.L. 2018. Performance based design in geotechnical earthquake engineering. *Soil Dynamics and Earthquake Engineering*, **114**: 326-332.

Gajan, S., and Kutter, B.L. 2008. Capacity, settlement, and energy dissipation of shallow footings subjected to rocking. *Journal of Geotechnical and Geoenvironmental Engineering, ASCE*, **134** (8): 1129–1141.

Gajan, S., Kutter, B.L., Phalen, J.D., Hutchinson, T.C., and Martin, G.R. 2005. Centrifuge modeling of load-deformation behavior of rocking shallow foundations. *Soil Dynamics and Earthquake Engineering*, **25**: 773–783.

Gajan, S., Phalen, J.D., Kutter, B.L., Hutchinson, T.C., and Martin, G. 2005. Centrifuge modeling of load-deformation behaviour of rocking shallow foundations. *Soil Dynamics and Earthquake Engineering*, **25** (7–10): 773-783.

Gaxiola-Camacho, J.R., Azizsoltani, H., Francisco, J.V., Haldar, A. 2017. A novel reliability technique for implementation of Performance-Based Seismic Design of structures. *Engineering Structure*, **142**: 137-147.

Gazetas, G. 1991a. Formulas and charts for impedances of surface and embedded foundations. *Journal of Geotechnical Engineering*, *ASCE.* **117** (9): 1363–1381.

Gazetas, G. 1991b. Foundation Vibrations. Foundation Engineering Handbook, Chapter 15 (2nd ed.), Fang, H-Y (ed.). V. N. Reinhold, New York, pp. 553–593.

Gazetas, G. 2019. Benefits of unconventional seismic foundation design. BGS 59th Rankine Lecturer, https://www.youtube.com/watch?reload=9&v=pOXzqjTo34o&feature=youtu.be.

Gazetas, G., Anastasopoulos, I., Adamidis, O., and Kontoroupi, T. 2013. Nonlinear rocking stiffness of foundations. *Soil Dynamic and Earthquake Engineering*, **47**:83–91.

Gazetas, G., and Apostolou, M. 2004. Nonlinear soil–structure interaction: foundation uplifting and soil yielding. In: Celebi M (ed) *Proceedings of the 3rd USA–Japan workshop on soil–structure interaction*, March 29-30, Menlo Park, California, USA.

Gazetas, G., Apostolou, M. and Anastasopoulos, J. 2003. Seismic uplifting of foundations on soft soil, with examples from Adapazari (Izmit 1999 earthquake). *Proc. of BGA International Conference on Foundations: Innovations, observations, design and practice,* Dundee. 37-49.

Gazetas, G., Dais, D., Gelagoti, F., and Kourkoulis R. 2018. Multistory building frames and shears walls founded on "Rocking" spread footings. In: Pitilakis K. (eds) Recent Advances in Earthquake Engineering in Europe. *ECEE 2018. Geotechnical, Geological and Earthquake Engineering*, 46: 309-322.

GEER. 2017. *Geotechnical Engineering Reconnaissance of the 19 September 2017 Mw 7.1 Puebla-Mexico City Earthquake*, DOI: 10.18118/G6JD46

Gelagoti, F., Kourkoulis, R., Anastasopoulos, I., and Gazetas, G. 2012. Rocking isolation of low-rise frame structures founded on isolated footings. *Earthquake Engineering and Structural Dynamics*, **41**(7): 1177–1197.

Guan, Z., Chen, X., and Li, J. 2018. Experimental investigation of the seismic performance of bridge models with conventional and rocking pile group foundations, *Engineering Structures*, **168**: 889–902.

Ha, J.G., Ko, K.W. Jo, S.B. Park, H.J., and Kim, D.S. 2019. Investigation of seismic performances of unconnected pile foundations using dynamic centrifuge tests. *Bulletin of Earthquake Engineering*. https://doi.org/10.1007/s10518-018-00530-y.

Hakhamaneshi, M. 2014. Rocking foundations for building systems, effect of footing shape, soil environment, embedment and normalized moment-to-shear ratio, PhD thesis, University of California, Davis, CA, USA.

Hakhamaneshi, M., and Kutter, B.L. 2016. Effect of footing shape and embedment on the settlement, re-centering and energy dissipation of shallow footings subjected to rocking. *Journal of Geotechnical and Geoenvironmental Engineering, ASCE*, **142**(12): 04016070.

Hakhamaneshi, M., Kutter, B.L., Moore, M., and Champion, C. 2016. Validation of ASCE 41-13 modeling parameters and acceptance criteria for rocking shallow foundations. *Earthquake Spectra*, **32**(2): 1121–1140

Hibbeler, R.C. 2015. Engineering Mechanics: Statics and Dynamics. 14th ed., Pearson Education, London, United Kingdom.

Higher, W.H., and Anders, J.C. 1985. Dimensioning footings subjected to eccentric loads. *Journal of Geotechnical Engineering*, *ASCE,* **111**(5): 659-663.

Housner, G.W. 1956. Limit Design of Structures to Resist Earthquakes. *Proc. of World Conference on Earthquake Engineering, Earthquake Engineering,* Research Institute, University of California, Berkeley.

Housner, G.W. 1963. The behavior of inverted pendulum structures during earthquakes. *Bulletin of the Seismological Society of America*, **52**: 2.

Ilki, A., and Fardis, M. 2014. *Seismic evaluation and rehabilitation of structures*. Springer.

Iwashita, K., and Taniguchi, H. 2000. Effect of uplift on earthquake response of building. *Proc. 12th world conference on earthquake engineering,* Auckland, New Zealand, paper no. 1328.

Jia, J. 2016. *Soil dynamics and foundation modeling: offshore and earthquake engineering*. Springer, Heidelberg

Kariuki, C. 2016. 1G shaking table tests on performance of rocking foundations. MSc Thesis, University of Tokyo, Tokyo, Japan.

Kelly, T.E. 2009. Tentative Seismic Design Guidelines for Rocking Structures. *Bulletin of the New Zealand National Society for Earthquake Engineering*, **42**(4): 239-274.

Kim, D.K., Lee, S.H., Kim, D.S., Choo, Y.W., and Park, H.G. 2015. Rocking effect of a mat foundation on the earthquake response of structures. *Journal of Geotechnical and Geoenvironmental Engineering, ASCE*, **141**(1): 04014085.

Ko, K.W., Ha, J.G., Park, H.J., and Kim, D.S. 2018a. Soil rounding effect on embedded rocking foundation via horizontal slow cyclic tests. *Journal of Geotechnical and Geoenvironmental Engineering, ASCE*, **144**(3): 04018004.

Ko, K.W., Ha, J.G., Park, H.J., and Kim, D.S. 2018b. Comparison between cyclic and dynamic rocking behavior for embedded shallow foundation using centrifuge tests. *Bulletin of Earthquake Engineering*, **16** (11): 1571-1593.

Kokkali, P., Abdoun, T., Anastasopoulos, I. et al. 2014. Experimental investigation of the rocking response of SDOF systems on sand. In ICPMG2014 – Physical Modeling in Geotechnics*: Proceedings of the 8th International Conference on Physical Modeling in Geotechnics*, January 14-17 (Gaudin C and White D (Eds)). CRC Press, Boca Raton, FL, USA, **1**:659–666.

Kourkoulis, R., Gelagoti, F., and Anastasopoulos, I. 2012. Rocking isolation of frames on isolated footings: design insights and limitations. *Journal of Earthquake Engineering*, **16**(3): 374–400.

Kramer, S.L. 2019. *Performance-based geotechnical seismic design*. 17th Gerald A. Leonards Lecture, Purdue University, IN.

Kutter, B.L., Martin, G., Hutchinson, T., Harden, C., Gajan, S., and Phalen, J. 2006. *Workshop on Modeling of Nonlinear Cyclic Load- Deformation Behavior of Shallow Foundations.* Peer

report 2005/14, Pacific Earthquake Engineering Research Centre, University of California, Berkeley, USA.

Liu, C. and Evett, J.B. 1997. *Soil Properties, Testing, Measurement, and Evaluation*, 3rd ed., New Jersey, Prentice Hall.

Liu, W., Hutchinson, T.C., Gavras, A.G., Kutter, B.L., and Hakhamaneshi, M. 2015b. Seismic behavior of frame-wall-rocking foundation systems. II: Dynamic test phase. *Journal of Structural Engineering, ASCE*, **141**(12): 04015060.

Liu, W., Hutchinson, T.C., Kutter, B. L., Gavras, A.G., and Hakhamaneshi, M., 2015a. Seismic behavior of frame-wall-rocking foundation systems-Part I: Test program and slow cyclic test results. *Journal of Structural Engineering*, ASCE, **141**(12): 04015059.

Liu, W., Hutchinson, T.C., Kutter, B.L., Hakhamaneshi, M., Aschheim, M., and Kunnath, S. 2012. Demonstration of compatible yielding between soil-foundation and superstructure components. *Journal of Structural Engineering, ASCE*, **139**: 1408-1420.

Loli, M., Knappett, J.A., Brown, M.J., Anastasopoulos, I., and Gazetas, G. 2014. Centrifuge modeling of rocking-isolated inelastic RC bridge piers. *Earthquake Engineering and Structural Dynamics*, **43**(15): 2341–2359.

Loli, M., Knappett, J.A., Brown, M.J., Anastasopoulos, I., and Gazetas, G. 2014. Centrifuge modeling of rocking-isolated inelastic RC bridge piers. *Earthquake Engineering and Structural Dynamics,* **43**(15): 2341–2359.

Lu, Y., Hajirasouliha, I., and Marshall, A.M. 2018. Direct displacement based seismic design of fexible-base structures subjected to pulse-like ground motions. *Engineering Structure,* **168**: 276–289.

Lu, Y., Marshall, A.M., and Hajirasouliha, I. 2016. A simplified Nonlinear Sway-Rocking model for evaluation of seismic response of structures on shallow foundations. *Soil Dynamics and Earthquake Engineering*, **81**:14–26.

Malekpour, S., and Dashti, F. 2013. Application of the Direct Displacement Based Design Methodology for Different Types of RC Structural Systems. *International Journal of Concrete Structures and Materials*, **7**(2): 135-153.

Marsh, L. K., and Stringer, S. J. 2013. Performance-based seismic bridge design, a synthesis of highway practice. *NCHRP Synthesis-440, TRB*, Washington, DC.

Mashal, M., Palermo, A., and Chegini, Z. 2014. Quasi-static cyclic tests of half-scale fully precast bridge bents incorporating emulative and posttensioned low damage solutions. *Proc. 2nd European Conf. of Earthquake Engineering and Seismology,* Turkish Earthquake Foundation, Istanbul, Turkey.

Mashal, M., Palermo, A., and Chegini, Z. 2014. Quasi-static cyclic tests of half-scale fully precast bridge bents incorporating emulative and posttensioned low damage solutions. *Proc. of 2nd European Conference of Earthquake Engineering and Seismology*, Turkish Earthquake Foundation, Istanbul, Turkey.

Meyerhof, G.G. 1953. The bearing capacity of foundations under eccentric and inclined loads. *Proc. of the Third International Conference on Soil Mechanics and Foundation Engineering*, **1**: 440-444.

Meyerhof, G.G. 1965. Shallow Foundations. *Journal of the Soil Mechanics and Foundation Division, ASCE*, **91**(SM2): 21-31.

Mitoulis, S.A., and Rodriguez, J.R. 2017. Seismic performance of novel resilient hinges for columns and application on irregular bridges. *Journal of Bridge Engineering, ASCE*, **22** (2): 04016114.

National Earthquake Hazards Reduction Program (NEHRP). 2004. *Recommended Seismic Design Criteria for New Steel Moment-frame Buildings*, FEMA-273, Federal Emergency Management Agency, Washington, DC, USA.

National Earthquake Hazards Reduction Program (NEHRP). 2009. *Recommended provisions for seismic regulations for new buildings.* Federal Emergency Management Agency, Washington, DC.

NBCC. 2010. National Building Code of Canada, 13th ed., National Research Council of Canada, Ottawa.

NCHRP. 2010. LRFD design and construction of shallow foundations for highway bridge structures, Report 651, Transportation Research Board, NRC, Washington, DC.

Negro, P., Paolucci, R., Pedretti, S., and Faccioli, E. 2000. Large-scale soil–structure interaction experiments on sand under cyclic load. *Proc. of the 12th world conference on earthquake engineering*, Auckland, New Zealand.

NZS. 2004. Structural Design Actions, Part 5: Earthquake actions New Zealand. NZS 1170.5, Standards New Zealand, Wellington, N.Z.

NZT. 2014. *New Zealand Bridge Manual: Transit New Zealand.* Auckland, New Zealand.

Ou, Y.-C., Wang, P.-H., Tsai, M.-S., Chang, K.-C., and Lee, G. C. 2010. Large-scale experimental study of precast segmental unbonded posttensioned concrete bridge columns for seismic regions. *Journal of Structural Engineering*, ASCE, **136**(3): 255-264.

Paolucci, R., Shirato, M., and Yilmaz M.T. 2008. Seismic behaviour of shallow foundations: Shaking table experiments vs numerical modeling. *Earthquake Engineering and Structural Dynamics*, **37**(4): 577–595.

Pecker, A. 2006. Enhanced seismic design of shallow foundations: Example of the Rion Antirion bridge. *4th Athenian Lecture on Geotechnical Engineering*, Hellenic Society of Soil Mechanics and Geotechnical Engineering, Athens, Greece.

Pecker, A., and Pender, M.J. 2000. Earthquake resistant design of foundations: New construction. *Proc., GeoEng200*, Melbourne, Australia, pp. 313–332.

Pelekis, I., Madabhushi, G.S., and DeJong, M.J. 2018. Seismic performance of buildings with structural and foundation rocking in centrifuge testing. *Earthquake Engineering and Structural Dynamics*, **47**(12): 2390-2409.

Pender, M.J., Algie, T.B., Orense, R.P., and Wotherspoon, L.M. 2011. Snap-back testing for estimation of nonlinear behaviour of shallow and pile foundations. *Proc. of the 9th Pacific Conference on Earthquake Engineering: Building an Earthquake Resilient Society*, Paper No. 20, Auckland, New Zealand.

Phipps, J.N. 2013. Experimental and numerical investigation of dynamic rocking foundation behavior, M.Sc. thesis, Iowa State University, USA.

Phipps, J.N., Ashlock J.C., and Sritharan, S. 2012. Experimental results of foundation rocking on a natural clay deposit. *Proc. of the 15th World Conference on Earthquake Engineering*, Lisbon, Portugal.

Priestley, M.J.N. 2000. Performance-Based Seismic Design. Keynote Address, *Proc. 12th World Conference on Earthquake Engineering*, Auckland, New Zealand.

Priestley, M.J.N., Calvi, G.M., and Kowalsky, M.J. 2007. Direct Displacement-Based Seismic Design of Structures. Pavia, Italy: IUSS Press.

Public Works Research Institute (PWRI). 1997. Report on the Disaster Caused by the 1995 Hyogoken Nanbu Earthquake. Reports for PWRI. vol. 33, Public Works Research Institute, Tsukuba, Japan.

Qiu, C.X., and Zhu, S. 2017. Performance-based seismic design of self-centering steel frames with SMA-based braces. *Engineering Structure*, **130**: 67–82.

Raychowdhury, P. 2008. Nonlinear Winkler-based Shallow Foundation Model for Performance Assessment of Seismically Loaded Structures. *PhD thesis*, Department of Structural Engineering, University of California, San Diego, USA.

Raychowdhury, P., and Hutchinson T. C. 2009. Performance evaluation of a nonlinear Winkler-based shallow foundation model using centrifuge test results. *Earthquake Engineering and Structural Dynamics*, **38** (5): 679-698.

Raychowdhury, P., and Hutchinson T. C. 2011. Performance of seismically loaded Shear walls on nonlinear shallow foundations. *International Journal for Numerical and Analytical Methods in Geomechanics*, **35** (7): 846-858.

Robertson P. K., and Cabal K. L. 2012. *Guide to Cone Penetration Testing for Geotechnical Engineering*, 5th ed., Gregg Drilling and Testing Inc., Signal Hills, Calif.

Rosebrook, K. 2001. Moment loading on shallow foundations: centrifuge test data archives, M.Sc. thesis, University of California, Davis, CA, USA.

Saad, A.S., Sanders, D.H., and Buckle, I.G. 2018. Experimental evaluation of bridge column foundation rocking behavior. *Journal of Bridge Engineering ASCE*, **23**(11): 04018088.

Sadan, O.B., Petrini, L., and Calvi, G.M. 2013. Direct displacement-based seismic assessment procedure for multi-span reinforced concrete bridges with single-column piers. *Earthquake Engineering and Structural Dynamics*, **42**: 1031–1051.

Sakellaraki, D., and Kawashima, K. 2006. Effectiveness of seismic rocking isolation of bridges based on shake table test. *Proc. of the First European Confrerence on Earthquake Engineering and Seismology, European Association for Earthquake Engineering*, Instanbul, Turkey.

Salimath, R., Pender M.J., and Algie T.B. 2017. Field snap-back testing of shallow surface foundations on stiff clay. *Proc. of the PBD III, Earthquake Geotechnical Engineering*, Vancouver, BC, Canada.

Sharma, K., and Deng, L. 2019a. Characterization of rocking shallow foundations on cohesive soil using field snap-back tests, *Journal of Geotechnical and Geoenvironmental Engineering, ASCE* (accepted).

Sharma, K. and Deng, L. 2019b. Field cyclic testing of rocking foundations in cohesive soils: foundation performance and footing internal behaviour. *Canadian Geotechnical Journal* (in revision).

Sharma, K., and Deng, L. 2017. Field investigation of rocking shallow foundations on cohesive soil subjected to lateral cyclic loads. *Proc. of GeoOttawa 2017*, Canadian Geotechnical Society.

Sharma, K., and Deng, L. 2018. Rocking foundation on a natural clay subjected to lateral cyclic loads. *Proc. of the 5th Geotechnical earthquake engineering and soil dynamics conference*, Austin, TX, USA.

Sharma, K., Deng, L. 2019c. Effects of loading obliquity on field performance of rocking shallow foundations in cohesive Soil. *Geotechnique* (in review).

Shirato, M., Nakatani, S., Fukui, J., and Paolucci, R. 2008. Large-scale experiments on nonlinear behaviour of shallow foundations subjected to strong earthquakes. *Soils and Foundations*, **48**(5): 673-692.

Siddiquee, K., and Alam, M.S. 2017. Highway Bridge Infrastructure in the Province of British Columbia (BC), Canada. *Infrastructures*, **2**(7): 1-18.

Sideris, P., Aref, A., and Filiatrault, A. 2014. Large-scale seismic testing of a hybrid sliding-rocking posttensioned segmental bridge system. *Journal of Structural Engineering*, *ASCE*, **140** (6): 04014025.

Sil, A., Gourab, D., and Pritam, H. (2019) Characteristics of FBD and DDBD techniques for SMRF buildings designed for seismic zone V in India. *Journal of Building Pathology and Rehabilitation*, **4**(1):1-18.

Speicher, M.S., DesRoches, R., and Leon, R.T. 2011. Experimental results of a NiTi shape memory alloy (SMA)-based recentering beam–column connection. *Engineering Structures*, **33**(9): 2448–57.

State of California. 1973. As built plans: U.C.D. cyclic overcrossing. Department of Transportation, State of California.

Stoer, J., and Bulirsch, R. 1992. *Introduction to Numerical Analysis*, Springer-Verlag, New York.

Storie, L., Pender, M., Clifton, G., and Wotherspoon, L. 2014. Soil foundation-structure interaction for buildings on shallow foundations in the Christchurch earthquake. *Proc, of 10th NCEE*, Anchorage, Alaska.

Suarez, V.A., and Kowalsky, M.J. 2011. A stability-based target displacement for direct displacement-based design of bridge piers. *Journal of Earthquake Engineering*, **15**(5): 754–774.

Sullivan, T.J., Salawdeh, S., Pecker, A., Corigliano, M. and Calvi, G.M. 2010. Soil foundation-structure interaction considerations for performance-based design of RC wall structures on shallow foundations, in *Soil-Foundation-Structure Interaction*, Orense, R. P., Chouw, N., and Pender, M. J. Leiden, The edited by Netherlands: CRC Press/Balkema. pp.193-200.

Tazarv, M., and Saiidi, M. 2016. Seismic design of bridge columns incorporating mechanical bar splices in plastic hinge regions. *Engineering Structures*, **124**: 507–520.

Terzaghi, K. 1943. *Theoretical Soil Mechanics*, J. Wiley and Sons, New York.

Tileylioglu, S., Stewart J.P., and Nigbor R.L. 2011. Dynamic stiffness and damping of a shallow foundation from forced vibration of a field test structure. *Journal of Geotechnical and Geoenvironmental Engineering*, *ASCE*, **137**(4): 344–53.

Trono, W., Jen, G., Panagiotou, M., Schoettler, M., and Ostertag, C. 2014. Seismic response of a damage-resistant recentering post tensioned HYFRC bridge column. *Journal of Bridge Engineering, ASCE*, **20** (7): 04014096.

Tsatsis, A., and Anastasopoulos, I. 2015. Performance of rocking systems on shallow improved sand: shaking table testing. *Frontiers in Built Environment,* **1**(9): 1–19.

Vivek, B., and Raychowdhury, P. 2017. Influence of SSI on Period and Damping of Buildings Supported by Shallow Foundations on Cohesionless Soil. *International Journal of Geomechanics*, *ASCE*, **17**(8): 04017030.

Wiessing, P.R. 1979. Foundation rocking on sand. *ME thesis*, University of Auckland, School of Engineering, Rep. No. 203, Auckland, New Zealand.

Yashinsky, M., and Karshenas, M.J. 2003. *Fundamentals of Seismic Protection for Bridges*. Earthquake Engineering Research Institute (EERI), Oakland, CA.

Zhang, Q., and Alam, S.M. 2019. Performance-based seismic design of bridges: a global perspective and critical review of past, present and future directions, *Structure and Infrastructure Engineering*. DOI: 10.1080/15732479.2018.1558269.

Zhao, L., Hao, H., Bi, K., and Li, X. 2018. Numerical study of the seismic responses of precast segmental column bridge under spatially varying ground motions. *Journal of Bridge Engineering*, 23(12): 04018096.

Appendix A: Site Investigation
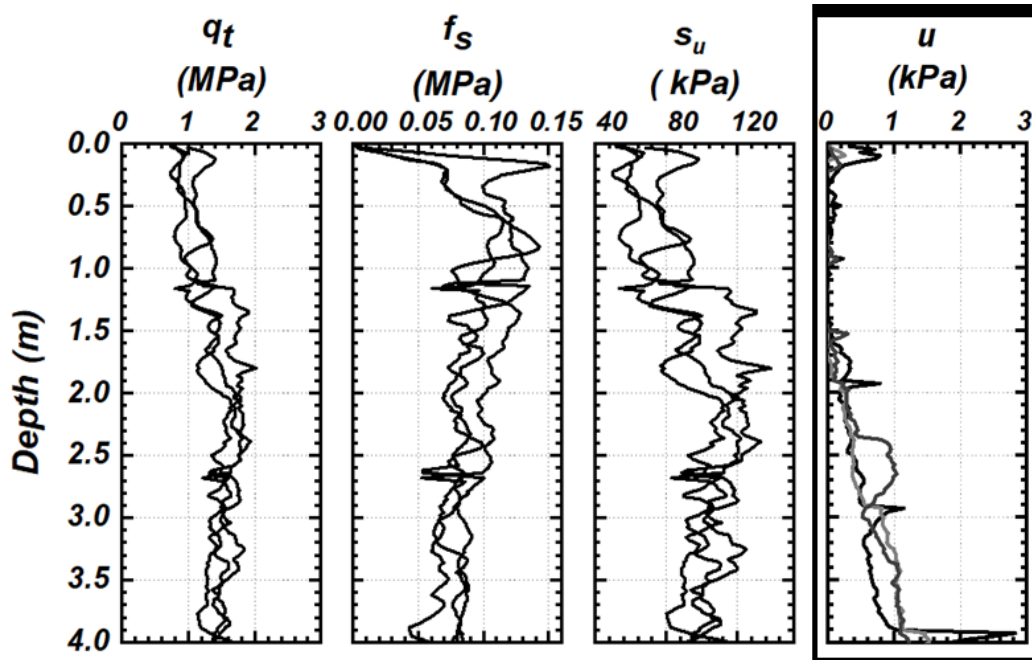
Figure A.1. CPT profile of test site

Figure A.2. Soil sample collection, sample preparation and testing
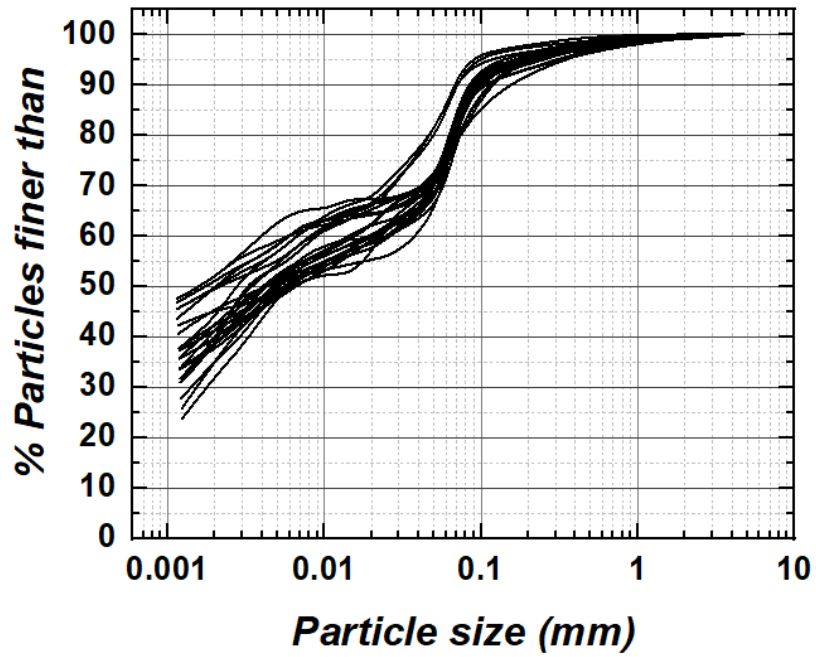
Figure A.3. Particle size distribution of the soil collected from site
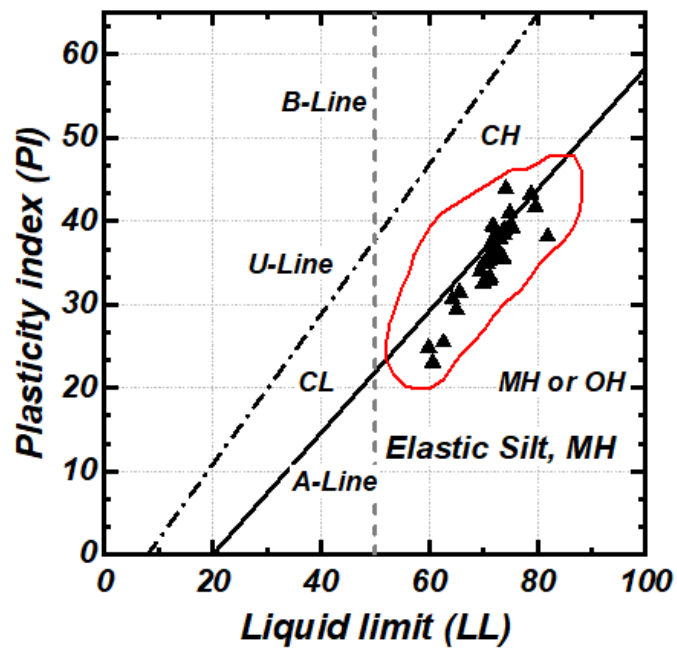
Figure A.4. Plasticity chart of the soil
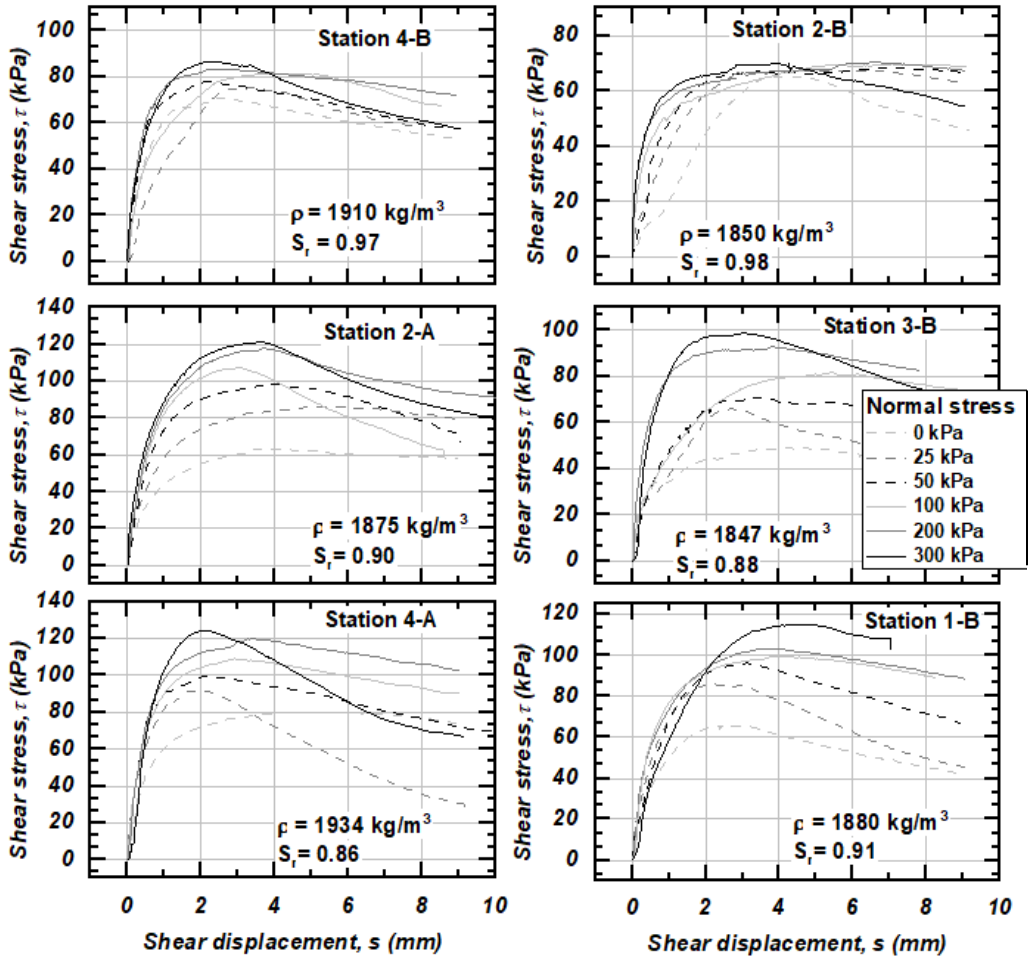
Figure A.5. Results from direct shear test of the undisturbed soil samples
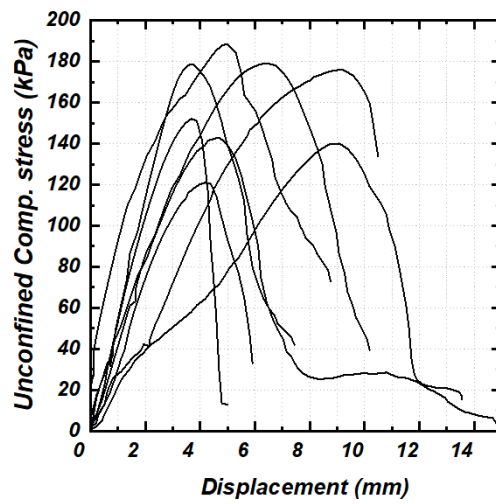
Figure A.6. Typical stress-strain relationships from UCS tests (Note: summary of all tests results are presented in Table A.1)

Table A.1. Unconfined compressive strength and other properties soil

Station	sample Depth (mm)	UCS (kPa)	Strain at Peak stress (%)	Density (kg/m3)	Water content (%)	Void ratio (e)	Remark
1	305	164	8.64	1910	31.46	0.89	Before test
	102	143	6.5	1902	31.02	0.89	Before test
	25	121	4.23	1887	31.54	0.92	Before test
	102	140	5.2	1897	31.07	0.90	Before test
	25	138	5.9	1891	30.95	0.90	Before test
	508	150	6.13	1906	31.08	0.89	Before test
	51	178	7.01	1933	31.89	0.88	After test
	305	165	4.88	1918	28.97	0.85	After test
	508	163	5.79	1915	29.56	0.86	After test
	305	169	6.09	1923	29.27	0.85	After test
	102	179	5.11	1934	29.01	0.83	After test
	0	190	5.87	1945	28.65	0.82	After test
4	330	201	6.25	1968	27.06	0.78	After test
	50	220	8.15	1980	27.63	0.77	After test
	635	188	3.33	1953	27.58	0.80	After test
	200	206	4.5	1958	27.53	0.79	After test
	762	190	6.4	1902	28.01	0.85	After test
	51	196	5.95	1894	27.94	0.86	After test
	250	204	5.25	1902	27.89	0.85	After test
	508	178	2.66	1933	27.84	0.82	After test
	762	162	3.33	1910	30.56	0.88	Before test
	300	158	4.53	1889	28.72	0.87	Before test
	50	145	4.03	1882	28.12	0.87	Before test
	200	160		1901	28.23	0.85	Before test
	25	159	5.02	1902	28.05	0.85	Before test
	300	155	4.9	1894	28.57	0.87	Before test
	635	162	6.85	1902	29.05	0.87	Before test
5	711	179	10.93	1931	29.72	0.85	After test
	102	183	8.78	1927	29.664	0.85	After test
	50	191		1956	29.43	0.82	After test
	457	184		1943	29.73	0.84	After test
	50	181	12.85	1946	28.62	0.82	After test
	381	168	2.91	1932	29.9	0.85	After test
	76	175		1931	29.85	0.85	After test
	660	167	11.05	1935	29.33	0.84	After test

	305	138	8.23	1912	30.93	0.88	Before test
	50	142		1914	30.07	0.87	Before test
	102	147		1916	30.15	0.87	Before test
	508	160		1919	30.57	0.87	Before test
	51	141	7.52	1913	30.24	0.87	Before test
	635	150	6.80	1891	32.09	0.92	Before test
	203	139		1899	31.15	0.90	Before test
	356	133	7.81	1931	28.79	0.83	Before test
	610	178	5.15	1927	29.06	0.84	After test
	254	188	6.325	1963	30.04	0.82	After test
	330	101	3.15	1874	29.43	0.90	After test
	0	186		1948	29.83	0.83	After test
	25	182	4.63	1925	29.76	0.85	After test
	635	175	5.17	1923	29.85	0.86	After test
4	254	178	5.93	1925	29.76	0.85	After test
	51	142	5.01	1915	30.77	0.88	Before test
	305	162	4.94	1919	31.00	0.88	Before test
	635	163	5.03	1920	30.94	0.88	Before test
	50	143	5.93	1904	31.21	0.90	Before test
	635	168	6.8	1901	30.90	0.89	Before test
	305	160	4.25	1899	31.25	0.90	Before test
	51	87	3.00	1911	29.0454	0.86	Before test
	279	106	4.55	1885	28.9905	0.88	Before test
	457	92	3.68	1892	30.7813	0.90	Before test
	686	177	8.20	1895	31.91	0.91	Before test
	254	117	4.20	1899	32.16	0.91	Before test
	737	124	4.34	1873	33.52	0.96	Before test
2	51	132		1898	32.52	0.92	Before test
	152	138	5.59	1939	27.96	0.82	After test
	81	160	6.50	1939	28.06	0.82	After test
	406	153	5.06	1908	33.3	0.92	After test
	330	194	8.08	1917	29.78	0.86	After test
	51	155	8.30	1959	28.56	0.81	After test
	25	147	6.79	1887	32.16	0.93	After test
	483	147	5.40	1905	32.25	0.91	Before test
	254	146	3.59	1899	31.34	0.90	Before test
6	51	127	7.99	1904	33.84	0.93	Before test
	635	181	8.13	1909	31.8	0.90	Before test
	102	189	7.18	1921	30.34	0.87	After test

	152	149	6.90	1925	29.54	0.85	After test
	254	162	4.90	1935	29.65	0.84	After test
	406	184	8.47	1946	32.18	0.87	After test
3	127	107	5.52	1934	31.37	0.87	Before test
	0	113		1902	30.85	0.89	Before test
	178	103	7.84	1891	31.24	0.91	After test
	508	168	7.05	1889	32.04	0.92	After test
9	508	135	7.01	1921	29.98	0.86	Before test
	51	121	7.57	1909	30.53	0.88	Before test
	25	155	6.11	1941	28.98	0.83	Before test
	635	142	7.07	1929	28.83	0.84	Before test
10	203	131	6.57	1902	30.056	0.88	Before test
	635	138	5.88	1909	30.51	0.88	Before test
	460	144	6.88	1933	29.056	0.84	Before test
11	0	160	6.12	1951	28.21	0.81	Before test
	25	175	5.95	1942	28.59	0.82	Before test
	610	149	4.94	1934	29.27	0.84	Before test
12	51	132	5.25	1909	30.35	0.88	Before test
	460	142	5.34	1902	30.89	0.89	Before test

Figure A.7. Vane shear test on undisturbed sample

189

Appendix B: Calibration of sensor
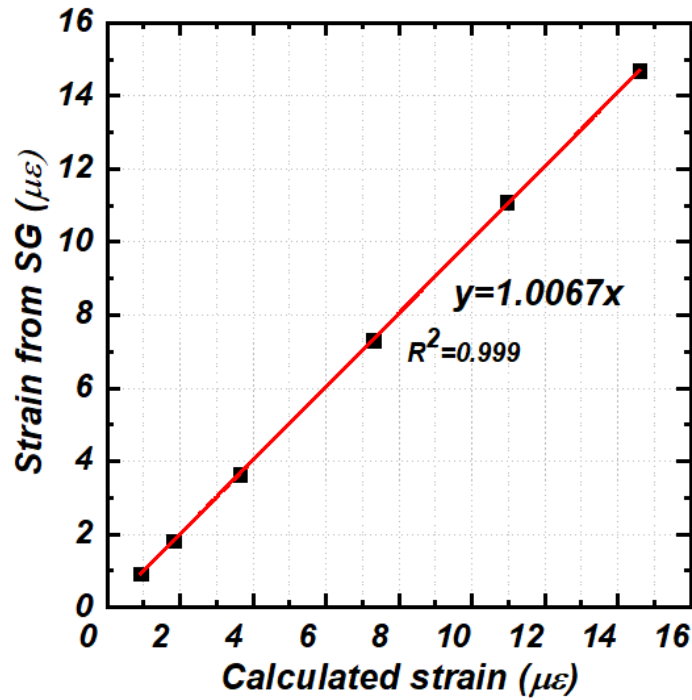
Figure B.1. Calibration of the strain gauges (Note: Three strain gauges were calibrated)
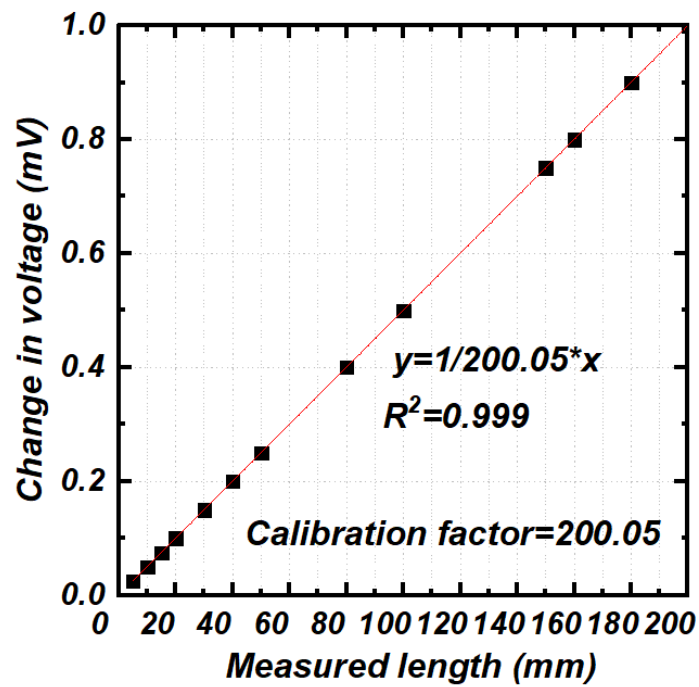
Figure B.2. Calibration of the linear potentiometer (LP) (Note: All nine LPs were calibrated before tests)

Appendix C: Soil-footing-structure design
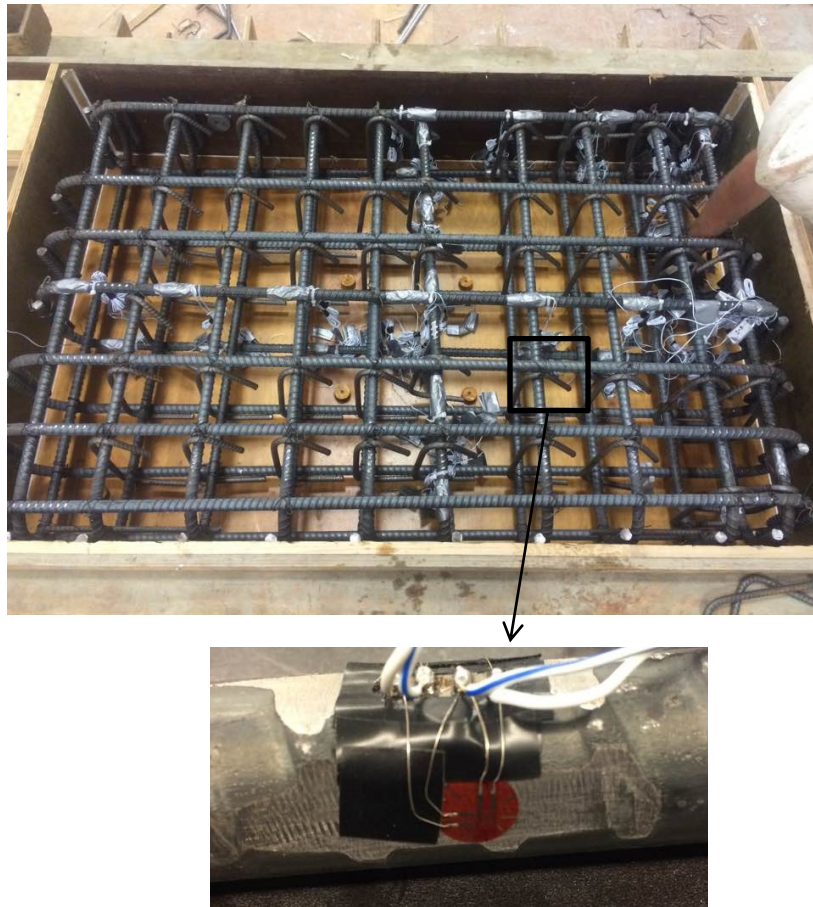
Figure C.1. Formwork for concrete foundation (pre-cast), mounted strain gauges and close-up view of strain gauges.

Calculation of factor of safety and critical contact length

1. Footing properties and Factor of safety calculation

Length   Width   Thickness

$L := 1.5 \ m$ $B := 1.0 \ m$ $D_f := 0.3 \ m$ $D_e := 0.0 \ m$ $h_c := 2.0 \ m$

Number of slabs $ns := 0$

size of the column- 8" (203 mm) square tube column

$a := 8 \ in = 0.203 \ m$ $t_{wall} := 0.50 \ in = 0.013 \ m$

Distance to cg from bottom of footing

$$h_{cg} := \left(0.3 + 2 + \frac{.45}{2}\right) m = 2.525 \ m$$

Calculation of weight

$W_{footing} := 1075 \ kg \cdot g = 10.542 \ kN$ $W_{deck} := 2462 \ kg \cdot g = 24.144 \ kN$

$W_{slab} := ns \ 2873 \ kg \cdot g = 0 \ kN$

$$W_{column} := h_c \cdot \left(a^2 - \left(a - t_{wall}\right)^2\right) \cdot 7850 \ \frac{kg}{m^3} \cdot g = 0.77 \ kN$$

Total weight of structures $W_{st} := W_{footing} + W_{deck} + W_{slab} + W_{column} = 35.456 \ kN$

     Weight of superstructure $W_{sp} := W_{deck} + W_{slab}$

Soil properties properties

     shear strength of soil $S_u := 75 \ \frac{kN}{m^2}$

     Unit of wt. of soil   Angle of int. friction   Cohesion

     $\gamma_s := 18 \ \frac{kN}{m^3}$ $\phi := 0 \ deg$ $C := S_u$

Weight of soil above footing $W_{soil} := \text{if}\left(D_e \le D_f, 0 \ \frac{kg \cdot m}{s^2}, \left(L \cdot B \cdot \left(D_e - D_f\right) \cdot \gamma_s\right)\right) = 0 \ N$

     Total weight $W_t := W_{st} + W_{soil} = \left(3.546 \cdot 10^4\right) N$

Calculation of soil paramter

$$N_q := e^{\pi \cdot \tan(\phi)} \cdot \frac{1 + \sin(\phi)}{1 - \sin(\phi)} = 1 \qquad\qquad N_c := (2 + \pi) = 5.142$$

$$N_\gamma := 2\,(N_q+1)\cdot\tan(\phi) = 0 \qquad\qquad s_q := 1+\frac{L}{B}\,\tan(\phi) = 1$$

$$s_c := 1+\frac{L}{B}\cdot\frac{N_q}{N_c} = 1.292$$

$$s_\gamma := 1-0.4\cdot\frac{L}{B} = 0.4$$

Since $\phi = 0$

$$d_q := 1+2.\,\tan(\phi)\cdot(1-\sin(\phi))^2\cdot\frac{D_e}{L} = 1 \qquad\qquad d_\gamma := 1$$

$$k := \mathrm{if}\left(\frac{D_e}{L}\le 1, \frac{D_e}{L}, \mathrm{atan}\left(\frac{D_e}{L}\right)\right)$$

$$d_c := 1+0.4\cdot k = 1$$

$$q_s := \gamma_s\cdot D_e$$

Bearing capacity of soil using conventional equation

$$q_u := C\cdot N_c\cdot s_c\cdot d_c + q_s\cdot N_q\cdot s_q\cdot d_q + \frac{1}{2}\cdot\gamma_s\cdot L\cdot N_\gamma\cdot s_\gamma\cdot d_\gamma = 498.119 \;\textit{kPa}$$

$$Fsv := \frac{q_u\cdot L\cdot B}{W_{st}+W_{soil}} \qquad Fsv = 21.073$$

Critical contact length

$$su := S_u \qquad \gamma := \gamma_s \qquad\qquad D := D_e$$

$$BearingCap(su,\phi,\gamma,D,L,B) := \left\| \begin{array}{l} N_q \leftarrow e^{\pi\cdot\tan(\phi)}\cdot\dfrac{1+\sin(\phi)}{1-\sin(\phi)} \\[2mm] N_c \leftarrow (2+\pi) \\[1mm] N_\gamma \leftarrow 2\,(N_q+1)\cdot\tan(\phi) \\[1mm] d_q \leftarrow 1+2.\,\tan(\phi)\cdot(1-\sin(\phi))^2\cdot\dfrac{D}{L} \\[2mm] d_\gamma \leftarrow 1 \\[1mm] \mathrm{if}\;\left(\dfrac{D}{L}\right)\le 1 \\[2mm] \qquad \left\| k\leftarrow\dfrac{D}{L} \right. \\[2mm] \mathrm{else} \\[1mm] \qquad \left\| k\leftarrow\mathrm{atan}\left(\dfrac{D}{L}\right) \right. \\[2mm] d_c \leftarrow 1+0.4\cdot k \\[1mm] s_c \leftarrow 1+\dfrac{L}{B}\cdot\dfrac{N_q}{N_c} \\[2mm] s_q \leftarrow 1+\dfrac{L}{B}\,\tan(\phi) \end{array} \right.$$

$$s_\gamma \leftarrow 1 - 0.4 \cdot \frac{L}{B}$$

$$\delta \leftarrow 0.04$$

$$i_c \leftarrow 1 - \frac{2\,\delta}{\pi + 2}$$

$$i_q \leftarrow \left(1 - \delta \cdot \tan(\phi)\right)^2$$

$$i_\gamma \leftarrow \left(1 - \delta \cdot \tan(\phi)\right)^2$$

$$q_n \leftarrow N_c \cdot d_c \cdot s_c \cdot i_c \cdot su + N_q \cdot d_q \cdot s_q \cdot i_q \cdot \gamma \cdot D + 0.5 \cdot N_\gamma \cdot \gamma \cdot L \cdot$$

Change in stress

$$changinstress\,(L,B,z,W_{st}) := \left\| m \leftarrow \frac{L}{2\,z} \right.$$

$$n \leftarrow \frac{B}{2 \cdot z}$$

$$Ir \leftarrow \frac{1}{4 \cdot \pi} \left(\frac{2 \cdot m \cdot n \cdot \sqrt{m^2 + n^2 + 1}}{m^2 + n^2 + m^2 \cdot n^2 + 1} \left(\frac{m^2 + n^2 + 2}{m^2 + n^2 + 1} \right) + \mathrm{atan} \left(\frac{2}{n} \right) \right.$$

$$\sigma \leftarrow \frac{W_{st}}{L \cdot B}$$

$$\Delta\sigma \leftarrow 4 \cdot Ir \cdot \sigma$$

Average stress $$avgstress\,(L,B) := \left\| \Delta\sigma_0 \leftarrow \frac{W_{st}}{L \cdot B} \right.$$

$$z \leftarrow L$$

$$\Delta\sigma_1 \leftarrow changinstress\,(L,B,z,W_{st})$$

$$z \leftarrow 2 \cdot L$$

$$\Delta\sigma_2 \leftarrow changinstress\,(L,B,z,W_{st})$$

$$\Delta\sigma_{avg} \leftarrow \frac{\Delta\sigma_0 + 4 \cdot \Delta\sigma_1 + \Delta\sigma_2}{6}$$

From direct shear tests

$$Sig := \begin{bmatrix} 0 \\ 25 \\ 50 \\ 100 \\ 200 \\ 300 \end{bmatrix} kPa \quad Tau := \begin{bmatrix} 49.72 \\ 65.88 \\ 73.52 \\ 81.81 \\ 93.04 \\ 98.933 \end{bmatrix} kPa$$

Trial 1

$$q_{no} := BearingCap\,(su, \phi, \gamma, D, L, B) = 490.369\ kPa$$

$$L := \frac{W_{st}}{} = 0.072\ m$$

$$\frac{}{q_{no} \cdot B}$$

$Sig1 := avgstress\left(L_c, B\right) = 259.594 \; kPa$

$nSu := \mathrm{linterp}\left(Sig, Tau, Sig1\right) = 96.552 \; kPa$

Trial 2

$q_{no} := BearingCap\left(nSu, \phi, \gamma, D, L_c, B\right) = 495.579 \; kPa$

$$L_c := \frac{W_{st}}{q_{no} \cdot B} = 0.072 \; m$$

$Sig1 := avgstress\left(L_c, B\right) = 262.339 \; kPa$

$nSu := \mathrm{linterp}\left(Sig, Tau, Sig1\right) = 96.714 \; kPa$

Trial 3

$q_{no} := BearingCap\left(nSu, \phi, \gamma, D, L_c, B\right) = 496.337 \; kPa$

$$L_c := \frac{W_{st}}{q_{no} \cdot B} = 0.071 \; m$$

$Sig1 := avgstress\left(L_c, B\right) = 262.738 \; kPa$

$nSu := \mathrm{linterp}\left(Sig, Tau, Sig1\right) = 96.737 \; kPa$

Trial 4

$q_{no} := BearingCap\left(nSu, \phi, \gamma, D, L_c, B\right) = 496.447 \; kPa$

$$L_c := \frac{W_{st}}{q_{no} \cdot B} = 0.071 \; m$$

$$\frac{L}{L_c} = 21.003$$

$Sig1 := avgstress\left(L_c, B\right) = 262.796 \; kPa$

$nSu := \mathrm{linterp}\left(Sig, Tau, Sig1\right) = 96.741 \; kPa$

$Shear\_Force := L_c \cdot B \cdot nSu = 6.909 \; kN$

Design of Rocking System

Length   Width   Thikness

$L := 1.5\ m$ $B := 1.0\ m$ $D_f := 0.3\ m$ $D_e := 0.0\ m$ $h_c := 2.0\ m$

$t_D := 0.45\ m$

Soil properties properties

shear strength of soil $S_u := 75\ \dfrac{kN}{m^2}$

Unit wt. of concrete   Unit of wt. of soil   Angle of int. friction   Cohesion

$\gamma_c := 25\ \dfrac{kN}{m^3}$ $\gamma_s := 18\ \dfrac{kN}{m^3}$ $\phi := 0\ deg$ $C := S_u$

$m_{rm} := 62\ \dfrac{kg}{m}$

Calculation of Load

Weight at the top of column $W_{bl} := 2462\ kg \cdot g = 24.144\ kN$

Weight of coumn $W_c := m_{rm} \cdot h_c \cdot g = 1.216\ kN$

Weight of footing $W_f := 1075\ kg \cdot g = 10.542\ kN$

Weight of soil above footing $W_s := 0\ kN = 0\ N$

RCC slabs on the top of deck (2.0 m*2.0 m* 0.3 m)

Number of slab $ns := 3$ $ts := 0.3\ m$

$W_{ext} := ns\ 2873\ kg \cdot g = 84.524\ kN$

Weight of deck $W_D := W_{bl} + W_{ext} = 108.667\ kN$

Total vertical load $Q_f := W_{bl} + (W_c + W_f + W_s + W_{ext}) = 120.426\ kN$

$P_u := W_D + W_c = 109.884\ kN$

Calculation of soil paramter

$N_q := e^{\pi \cdot \tan(\phi)} \cdot \dfrac{1 + \sin(\phi)}{1 - \sin(\phi)} = 1$ $N_c := (2 + \pi) = 5.142$

$N_\gamma := 2\ (N_q + 1) \cdot \tan(\phi) = 0$ $s_q := 1 + \dfrac{B}{L}\ \tan(\phi) = 1$

$s_c := 1 + \dfrac{B}{L} \cdot \dfrac{N_q}{N_c} = 1.13$ $s_\gamma := 1 - 0.4 \cdot \dfrac{B}{L} = 0.733$

Since $\phi = 0$

$$d_q := 1 + 2. \tan(\phi) \cdot (1 - \sin(\phi))^2 \cdot \frac{D_e}{B} = 1 \qquad\qquad d_\gamma := 1$$

$$d_c := 1 + 0.4 \cdot \frac{D_e}{B} = 1$$

$$q_s := \gamma_s \cdot D_e$$

Bearing capacity of soil using conventional equation

$$q_u := C \cdot N_c \cdot s_c \cdot d_c + q_s \cdot N_q \cdot s_q \cdot d_q + \frac{1}{2} \cdot \gamma_s \cdot B \cdot N_\gamma \cdot s_\gamma \cdot d_\gamma = (4.356 \cdot 10^5)\ Pa$$

$$Fsv := \frac{q_u \cdot L \cdot B}{Q_f} \qquad Fsv = 5.426$$

Calculation of moment capacity and base shear coefficient
Details of 203*203*12.7 steel tube column

$$b_f := 203\ mm \qquad d_f := 203\ mm \qquad t_f := \frac{25.4}{2}\ mm$$

$$a := 41047\ mm^2 \quad I_{xx} := 14.1 \cdot 10^7\ mm^4 \quad I_{yy} := 14.1 \cdot 10^7\ mm^4 \quad f_y := 350 \cdot 10^6\ \frac{N}{m^2}$$

2.1 Moment capacity of Column

$$M_{c\_col\_y} := \frac{f_y}{\frac{b_f}{2}} \cdot I_{yy} = (4.862 \cdot 10^5)\ J \qquad\qquad M_{c\_col\_x} := \frac{f_y}{\frac{d_f}{2}} \cdot I_{xx} = (4.862 \cdot 10^5)\ J$$

2.2 Moment capacity of the foundation

$$L_c := \frac{L}{Fsv} = 0.276\ m \qquad M_{cap\_foot} := \frac{Q_f \cdot L}{2} \left(1 - \frac{L_c}{L}\right) = (7.367 \cdot 10^4)\ J$$

$$B_c := \frac{B}{Fsv} = 0.184\ m \qquad M_{cap\_foot} := \frac{Q_f \cdot B}{2} \left(1 - \frac{B_c}{L}\right) = (5.281 \cdot 10^4)\ J$$

$$H_{ccg} := h_c + \frac{(0.45\ m + ns \cdot 0.3\ m)}{2} + 0.3\ m = 2.975\ m \qquad\qquad h_{ccg} := H_{ccg}$$

2.3 Calculate base shear coefficient of rocking foundation

$$C_{rx} := \frac{L}{2 \cdot H_{ccg}} \cdot \left(1 - \frac{L_c}{L}\right) = 0.206 \qquad\qquad C_{ry} := \frac{B}{2 \cdot H_{ccg}} \cdot \left(1 - \frac{B_c}{B}\right) = 0.137$$

2.4 Calculate base shear coefficient of hinging column

$$C_{y\_x} := \frac{M_{c\_col\_x}}{H_{ccg} \cdot W_D} = 1.504 \qquad\qquad C_{y\_y} := \frac{M_{c\_col\_y}}{H_{ccg} \cdot W_D} = 1.504$$

Shear load (at top of column)

$$H_x := W_D \cdot C_{rx} = (2.235 \cdot 10^4)\ N \qquad\qquad H_y := W_D \cdot C_{ry} = (1.49 \cdot 10^4)\ N$$

Moment at Column (Mcol)

$$h_{cd} := h_c + \frac{(t_D + ns \cdot ts)}{2}$$

$$M_{col\_x} := H_x \cdot h_{cd} = (5.978 \cdot 10^4) \; J \qquad\qquad M_{col\_y} := H_y \cdot h_{cd} = (3.985 \cdot 10^4) \; J$$

$$FOS\_m\_x := \frac{M_{c\_col\_x}}{M_{col\_x}} = 8.134 \qquad\qquad FOS\_m\_y := \frac{M_{c\_col\_y}}{M_{col\_y}} = 12.201$$

2.4 Calculation of period and frequency

$$M := \frac{W_D}{g} = (1.108 \cdot 10^4) \; kg$$

$$E := 200 \; GPa$$

$$K_x := \frac{12 \cdot E \cdot I_{xx}}{h_{ccg}^{\;3}} = (1.285 \cdot 10^7) \; \frac{kg}{s^2} \qquad\qquad K_y := \frac{12 \cdot E \cdot I_{yy}}{h_{ccg}^{\;3}} = (1.285 \cdot 10^7) \; \frac{kg}{s^2}$$

$$w_{nx} := \sqrt{\left(\frac{K_x}{M}\right)} = 34.056 \; \frac{1}{s} \qquad\qquad w_{ny} := \sqrt{\left(\frac{K_y}{M}\right)} = 34.056 \; \frac{1}{s}$$

$$T_{fx} := 2 \cdot \pi \cdot \sqrt{\left(\frac{M}{K_x}\right)} = 0.184 \; s \qquad\qquad T_{fy} := 2 \cdot \pi \cdot \sqrt{\left(\frac{M}{K_y}\right)} = 0.184 \; s$$

2.5 Calculation of rocking period and frequency

$$\nu := 0.5 \qquad\qquad H_c := h_{ccg}$$
$$\qquad\qquad\qquad\qquad\qquad\qquad\qquad\qquad M = (1.108 \cdot 10^4) \; kg$$

$$v_s := 150 \; \frac{m}{s} \qquad\qquad E_{ms} := 200 \cdot S_u = (1.5 \cdot 10^7) \; Pa$$

$$G := \gamma_s \cdot \frac{v_s^{\;2}}{g} = (4.13 \cdot 10^7) \; Pa$$

$$G := \frac{E_{ms}}{2 \, (1+\nu)} = (5 \cdot 10^6) \; Pa$$

$$K_{xx} := \frac{G \cdot B^3}{1-\nu} \cdot \left(0.4 \cdot \frac{L}{B} + .1\right) = (7 \cdot 10^6) \; J$$

$$K_{yy} := \frac{G \cdot B^3}{1-\nu} \cdot \left(0.47 \cdot \left(\frac{L}{B}\right)^{2.4} + 0.034\right) = (1.278 \cdot 10^7) \; J$$

$$T_{rocking\_x} := 2 \cdot \pi \cdot \sqrt{\frac{M \cdot H_c^{\;2}}{K_{xx}}} = 0.744 \; s \qquad\qquad T_{rocking\_y} := 2 \cdot \pi \cdot \sqrt{\frac{M \cdot H_c^{\;2}}{K_{yy}}} = 0.55 \; s$$

$$T_x := \sqrt{T_{fx}^{\;2} + T_{rocking\_x}^{\;2}} = 0.766 \; s \qquad\qquad T_y := \sqrt{T_{fy}^{\;2} + T_{rocking\_y}^{\;2}} = 0.581 \; s$$

Design for flexural reinforcement

Check the eccentricity for concrete block

$$Mu := H_x \cdot h_{ccg} = 66.48 \ kN \cdot m$$

$$e := \frac{Mu}{P_u} = 0.605 \ m$$

$$q_{max} := \frac{P_u}{L \cdot B} \left(1 + 6 \cdot \frac{e}{L}\right) = \left(2.505 \cdot 10^5\right) \ Pa$$

$$q_{min} := \frac{P_u}{L \cdot B} \left(1 - 6 \cdot \frac{e}{L}\right) = -1.04 \cdot 10^5 \ Pa$$

$$a := \frac{q_{max} \cdot L}{3 \cdot \left(q_{max} + \text{abs}\left(q_{min}\right)\right)} = 0.353 \ m \qquad\qquad P_u = \left(1.099 \cdot 10^5\right) \ N$$

$$q_{fmax} := \frac{2 \cdot P_u}{3 \cdot a \cdot B} = \left(2.073 \cdot 10^5\right) \ Pa$$

$$\text{con} := \text{if}\left(q_{fmax} < q_u, \text{``Okay''}, \text{``Increase footing size''}\right) = \text{``Okay''}$$

$$FSV := \frac{q_u}{q_{fmax}} = 2.101$$

Flexural moment Mf

$$D := 300 \ mm$$

$$a_b := \frac{L}{2} = 0.75 \ m$$

$$M_f := q_{fmax} \cdot 1 \ m \cdot \frac{a_b^2}{2} = \left(5.832 \cdot 10^4\right) \ J$$

$$d_f := D - 40 \ mm - \frac{20}{2} \ mm = 0.25 \ m$$

$$k_r := \frac{M_f}{1 \ m \cdot d_f^2} = 0.933 \ MPa$$

From the chart/table for given kr

$$\rho := 0.15\%$$

$$A_{srequired} := \rho \cdot 1000 \ mm \cdot d_f = 375 \ mm^2$$

Select 20 M reinforcement (i.e. 19.5 mm diameter)

$$d_r := 19.5 \ mm$$

$$A_r := \pi \cdot \frac{d_r^2}{4} = 298.648 \ mm^2$$

$$a := \text{round}\left(\frac{A_{srequired}}{A_r}, 0\right) = 1$$

$$Numbers\_bar := \text{if}\left(a < \frac{A_{srequired}}{A_r}, a+1, a\right) = 2$$

$$Spacing\_of\_Bar := \text{round}\left(\frac{1000}{Numbers\_bar}, 0\right) = 500$$

Provide 20 M bar @150 mm not to have concrete in the crack during the test. Similary, provide reinforcement equally on transverse direction.

Shear design

$$A := L \cdot B \quad d := D - 2 \cdot 0.05 \ m \qquad \lambda := 1 \qquad\qquad \text{Factor for concrete density}$$
$$\qquad\qquad\qquad\qquad\qquad\qquad \phi_c := 0.65 \qquad\qquad \text{Resistance factor for concrete}$$
$$q_{sf} := \frac{P_u}{A} \text{ Factored stress on soil} \quad f'_c := 30 \ MPa \qquad \text{Specified comp. strength @ 28 days}$$

$$q_{sf} = 73.256 \ kPa$$

Shear stress at critical section at d/2 distance from column face
$$N := 400 \ mm$$

$$V_f := q_{sf} \cdot B \cdot \left(L - N - \frac{d}{2}\right) = 73.256 \ kN \qquad\qquad Q_f = \left(1.204 \cdot 10^5\right) N$$

Shear resistance by concrete is assumed equal to zero.
Use 1-legged 10 mm dia stirrups

$$A_v := \pi \cdot 2 \cdot \frac{(10. \ mm)^2}{4} = \left(1.571 \cdot 10^{-4}\right) m^2$$

Spacing of stirrups

$$S := 1.43 \cdot 0.85 \cdot \frac{A_v}{V_f} \cdot f_y \cdot d = 0.182 \ m \qquad\qquad V_f = 73.256 \ kN$$

Provide stirrups @ 150 mm $\qquad\qquad d_{pr} := 150 \ mm$

$$V_{fs} := 1.43 \cdot 0.85 \cdot A_v \cdot f_y \cdot \frac{d}{d_{pr}} = 89.101 \ kN$$